ISTANBUL TECHNICAL UNIVERSITY ★ GRADUATE SCHOOL

INVESTIGATION OF VIBRATIONS CREATED DURING TBM EXCAVATION AND ROCK CUTTING

Ph.D. THESIS

Uğur ATEŞ

Department of Mining Engineering

Mining Engineering Programme

JUNE 2024

ISTANBUL TECHNICAL UNIVERSITY ★ GRADUATE SCHOOL

INVESTIGATION OF VIBRATIONS CREATED DURING TBM EXCAVATION AND ROCK CUTTING

Ph.D. THESIS

Uğur ATEŞ
(505132005)

Department of Mining Engineering

Mining Engineering Programme

Thesis Advisor: Prof. Dr. Hanifi ÇOPUR

JUNE 2024

ISTANBUL TEKNİK ÜNİVERSİTESİ ★ LİSANSÜSTÜ EĞİTİM ENSTİTÜSÜ

TBM KAZISI VE KAYA KESME DENEYLERİ SIRASINDA OLUŞAN TİTREŞİMLERİN İNCELENMESİ

DOKTORA TEZİ

Uğur ATEŞ
(505132005)

Maden Mühendisliği Anabilim Dalı

Maden Mühendisliği Programı

Tez Danışmanı: Prof. Dr. Hanifi ÇOPUR

HAZİRAN 2024

Uğur Ateş, a Ph.D. student of ITU Graduate School student ID 505132005 successfully defended the thesis/dissertation entitled "INVESTIGATION OF VIBRATIONS CREATED DURING TBM EXCAVATION AND ROCK CUTTING", which he prepared after fulfilling the requirements specified in the associated legislations, before the jury whose signatures are below.

Thesis Advisor :	**Prof. Dr. Hanifi ÇOPUR** İstanbul Technical University	.....
Jury Members :	**Prof. Dr. Cemal BALCI** Istanbul Technical University	.....
	Prof. Dr. Nuray TOKGÖZ Istanbul University - Cerrahpasa	.....
	Prof. Dr. Abdullah KARAMAN Istanbul Technical University	.....
	Prof. Dr. Ümit ÖZER Istanbul University - Cerrahpasa	.....

Date of Submission : 03 May 2024
Date of Defense : 11 June 2024

To my beloved family,

FOREWORD

I would like to express my sincere gratitude to my thesis advisor Prof. Dr. Hanifi COPUR for his guidance and support throughout my studies. I am deeply appreciative of the invaluable insights and direction he has provided. I would also like to thank the members of my thesis steering committee, Prof. Dr. Cemal BALCI, Prof. Dr. Alaettin KILIC, and Prof. Dr. Nuray TOKGOZ, for their insightful suggestions and guidance during the course of my study. I would like to thank Prof. Dr. Nuh BILGIN for his support and encouragement, Prof. Dr. Deniz TUMAC, Dr. Emre AVUNDUK and Dr. Aydın SHATERPOUR-MAMAGHANI for their assistance during the laboratory experiments. Prof. Dr. Serdar AKYUZ is also acknowledged for analyzing the thin sections of the rocks samples.

I am deeply grateful for the help and support provided by my managers and colleagues at Gulermak Heavy Industries Construction & Contracting Co. Inc., Gulermak-Kolin-Kalyon Metro Construction JV, Statkraft, TunnelConsult Engineering and Pini Engineering companies throughout my studies.

I gratefully acknowledge the contributions of Gulermak-Kolin-Kalyon Metro Construction JV, Gulermak-Nurol-Makyol Metro Construction JV and Kalyon Construction Group for permitting the installation of accelerometers on their TBMs, providing TBM excavation data and muck samples, and assisting with the various stages of this study. Gulermak-Nurol-Makyol Metro Construction JV is also acknowledged for providing rock samples for the laboratory experiments, and Trakkom Engineering & Industries for fabricating the casings of the accelerometers. I would like to extend my sincere gratitude to Mr. Sinan ACUN, Mr. Mesut Emre AYMIR, Mr. Ihsan YAGCIOGLU, Mr. Muammer CINAR and Mr. Fatih KARA for their invaluable help and support during the site experiments. I would like to thank Dr. Nicola DELLA VALLE and Mr. Ignacio SAENZ DE SANTA MARIA GATON for their support during my studies. Mr. Irfan Serkan BINEN is acknowledged for his generous assistance during the various stages of this thesis. Without their help, this study would not have been possible.

I would like to thank the Scientific Research Projects Department of Istanbul Technical University (Project Number: MDK-2017-40698) for providing financial support.

Last but not least I would like to express my deepest gratitude to my family and my wife, Özge, for their patience, encouragement and continuous support during my studies.

May 2024

Ugur ATES
(M.Sc. Mining Engineer)

TABLE OF CONTENTS

Page

FOREWORD ..... **ix**
TABLE OF CONTENTS ..... **xi**
ABBREVIATIONS ..... **xiii**
SYMBOLS ..... **xv**
LIST OF TABLES ..... **xvii**
LIST OF FIGURES ..... **xix**
SUMMARY ..... **xxv**
ÖZET ..... **xxix**
1. INTRODUCTION **1**
1.1 Objectives of the Thesis 2
1.2 Literature Review 3
1.2.1 Tunnel boring machines 4
1.2.2 Laboratory studies 5
1.2.3 Field studies 7
1.3 Research Methodology and Framework 14
1.3.1 Recording system development 14
1.3.2 Field studies 14
1.3.3 Laboratory studies 15
1.4 Limiting Factors 15
2. INFORMATION ON THE TBM PROJECTS **17**
2.1 Mecidiyekoy-Mahmutbey Metro Line 17
2.1.1 TBM specifications 18
2.1.2 Geological conditions of the studied section 18
2.1.3 Accelerometer setup 20
2.2 Umraniye-Atasehir-Goztepe Metro Line 20
2.2.1 TBM specifications 21
2.2.2 Geological conditions of the studied section 21
2.2.3 Accelerometer setup 24
2.3 European Region Potable Water Transmission Tunnel Project 25
2.3.1 TBM specifications 26
2.3.2 Geological conditions of the studied section 26
2.3.3 Accelerometer setup 28
3. VIBRATION RECORDING SYSTEM, METHOLODOGY AND ANALYSIS TECHNIQUES **31**
3.1 Vibration Monitoring System Composition 31
3.1.1 Accelerometers 31
3.1.2 Analog to digital converters 35
3.1.3 Selection of data sampling rate 35
3.1.4 Data recording software and computers 36
3.2 Analysing Methods and Data Processing 38
3.2.1 Time domain analyses 41
3.2.1.1 Statistical analyses 41

3.2.1.2 Probability analyses 45
3.2.2 Frequency-domain analyses 48
4. ANALYSIS OF SITE DATA AND INVESTIGATION OF THE VARIABLES AFFECTING TBM VIBRATIONS 53
4.1 Mecidiyekoy-Mahmutbey Metro Line (TBM 1) 54
4.2 Umraniye-Atasehir-Metro Line (TBM 2 and 3) 59
4.2.1 Analysis of the vibration data obtained from TBM 2 61
4.2.1.1 Probability analyses 70
4.2.2 Analysis of the vibration data obtained from TBM 3 74
4.2.2.1 Probability analyses 83
4.3 European Region Potable Water Transmission Tunnel Project (TBM 4) 87
4.3.1 Probability analyses 95
4.4 Investigation of Variables affecting Vibrations based on Field Measurements 99
4.4.1 Effect of geological / lithological changes on TBM vibrations 99
4.4.2 Effect of TBM operational and performance parameters on vibration 117
4.4.3 Effect of cutter conditions on TBM vibrations 121
4.4.4 Effect of accelerometer positions on vibration 126
4.4.5 Effect of accelerometer types on vibration 128
4.4.6 Effect of EPB TBM diameter on vibration 128
5. LABORATORY EXPERIMENTS 131
5.1 Equipment, Procedures and Parameters 131
5.1.1 Physical and geomechanical property test equipment and procedures 131
5.1.2 Full-scale linear rock cutting test equipment and accelerometers 132
5.2 Rock Samples used During the FLCM Experiments 135
5.2.1 Pendik Formation (mudstone) 135
5.2.2 Kurtkoy Formation (siltstone) 135
5.2.3 Beige marble 136
5.2.3.1 Difficult cuttability section (DC) 137
5.2.3.2 Easy cuttability section (EC) 137
5.2.4 Physical and geomechanical properties of the rock samples 137
5.3 Full-Scale Linear Cutting Test Procedures and Parameters 138
5.4 Experimental Results 141
5.5 Investigation of Variables Affecting Vibrations Based on FLCM Tests 145
5.5.1 Effect of mineralogical and geomechanical properties on vibrations 145
5.5.2 Effect of rock cutting parameters on vibrations 155
5.5.3 Frequency analyses of FLCM vibration data 163
6. DISCUSSION 167
7. CONCLUSIONS 177
REFERENCES 183
APPENDICES 191
APPENDIX A 192
APPENDIX B 203
CURRICULUM VITAE 207

ABBREVIATIONS

BDV : Boulder Detection Variable
CC : Cutting Coefficient
CCS : Constant Cross Section
CNN : Convolutional Neural Networks
CWT : Continuous Wavelet Transform
DC : Difficult Cuttability
EC : Easy Cuttability
EPB : Earth Pressure Balance
FFT : Fast Fourier Transform
FLCM : Full-Scale Linear Rock Cutting Machine
GSI : Geological Strength Index
MBTS : Multi-Mode Boring Test System
MEMS : Micro-Electro-Mechanical System
NATM : New Austrian Tunneling Method
PLC : Programmable Logic Controller
PLT : Point Load Test
PSD : Power Spectral Density
RPM : Revolutions per Minute
RNN : Recurrent Neural Networks
RQD : Rock Quality Designation
SRMBI : Specific Rock Mass Boreability Index
TBM : Tunnel Boring Machine
UCS : Uniaxial Compressive Strength
VFD : Variable Frequency Drive

SYMBOLS

CI	**:** Coarseness index
FN	**:** Mean (average) normal force
F'N	**:** Peak (maximum) normal force
FR	**:** Mean (average) rolling force
F'R	**:** Peak (maximum) rolling force
FS	**:** Side force
g	**:** Earth gravity (9.82 m/s^2)
Hz	**:** Hertz
Is	**:** Point load strength index
k	**:** Kurtosis
kS	: Kilosamples
N	: Window length
n	**:** Data number in a ring
p	**:** Penetration (mm)
RMS	**:** Root mean square
RMS_{int}	**:** Interval RMS
SL	**:** Line spacing (mm)
SE	**:** Specific energy
Q	: Rock volume cut in unit cutting length (m^3/km)
α	**:** Weibull distribution shape parameter
β	**:** Weibull distribution scale parameter
$\propto$	**:** Acceleration amplitude in g per axis
μ	**:** Mean acceleration
μ_3	**:** Skewness
γ	**:** Weibull distribution location parameter
σ	**:** Standard deviation
σ^2	**:** Variance
σ_c	**:** Uniaxial compressive strength
σ_t	**:** Tensile strength

LIST OF TABLES

Page

Table 2.1 : Specifications of the TBM 1. ..... **18**
Table 2.2 : Properties of the rocks encountered along the Mecidiyekoy-Mahmutbey Metro Line (Artson Geoteknik, 2014). **19**
Table 2.3 : Lithological units and Schmidt hammer test results (Mecidiyekoy-Mahmutbey Metro Line). **19**
Table 2.4 : Specifications of the TBM 2 and 3. ..... **21**
Table 2.5 : Rock mass properties of Umraniye-Atasehir-Goztepe Metro Line (Yuksel Proje, 2017; Palakci and Ugur, 2021). **22**
Table 2.6 : Lithology and borehole information for TBM 2 and TBM 3 (Geodata Engineering S.p.A., 2016; Yüksel Proje, 2017). **23**
Table 2.7 : Specifications of the TBM 4. ..... **26**
Table 2.8 : Rock and soil properties of the lithological units encountered in European Region Drinking Water Transfer Tunnel Project (EMAY Uluslararası Mühendislik ve Müsavirlik A.S., 2018). **27**
Table 2.9 : Litological unit starting and ending locations according to site logs obtained from European Region Potable Water Transmission Tunnel Project site. **28**
Table 2.10 : Point Load Test results of the muck samples obtained from European Region Potable Water Transmission Tunnel Project site. **28**
Table 3.1 : Accelerometers used in during the study. **34**
Table 4.1 : Vibration data lengths recorded during the site experiments. **53**
Table 4.2 : Geological units seen on the alignment with identification numbers for both TBMs in Umraniye-Atasehir-Goztepe Metro Line. **60**
Table 4.3 : Average TBM operational parameters for TBM 2 ..... **62**
Table 4.4 : Average Weibull parameters per lithological units (TBM 2). **72**
Table 4.5 : Average TBM operational parameters for TBM 3 ..... **75**
Table 4.6 : Average Weibull parameters per lithological unit (TBM 3). **84**
Table 4.7 : Geological units seen on the alignment with identification numbers and TBM 4's operational parameters. **88**
Table 4.8 : Average Weibull parameters per lithological unit (TBM 4). **96**
Table 4.9 : Average RMS vibration ratios of top to bottom accelerometers for all TBMs and measurement axes. **127**
Table 5.1 : Physical and geomechanical properties of the rock samples used in linear cutting experiments. **138**
Table 5.2 : Rock cutting configuration (experimental matrix) **139**
Table 5.3 : Results of full-scale linear rock cutting tests. **142**
Table 5.4 : Average Weibull parameters obtained from laboratory experiments for Accelerometer 3 and 4. ..... **149**

LIST OF FIGURES

Page

Figure 1.1 : TBM types. **4**
Figure 1.2 : Cross-section of an EPB TBM (courtesy of Herrenknecht). **5**
Figure 1.3 : Multi-Mode Boring Test System. **6**
Figure 1.4 : An example power spectral density (top) and frequency spectrogram (bottom) from Walter (2012). **11**
Figure 1.5 : Impacts shown on the frequency spectrum (numbered 3 to 5) and calculated boulder detection values (Buckley, 2015). **12**
Figure 1.6 : An impact seen on the time domain and frequency spectrum (Liu et al., 2022). **13**
Figure 2.1 : Location of the Mecidiyekoy-Mahmutbey Metro Line. **17**
Figure 2.2 : Geological profile of the section where vibration recording was performed in Mecidiyekoy – Mahmutbey Metro Line Construction Site (Artson Geoteknik, 2014). **19**
Figure 2.3 : Approximate accelerometer locations on TBM 1 and cutterhead photo. **20**
Figure 2.4 : Installed accelerometers with their protective cases (TBM 1). **20**
Figure 2.5 : Location of the Umraniye-Atasehir-Goztepe Metro Line. **21**
Figure 2.6 : Geological profile of the section where vibration recording was performed in Umraniye-Atasehir-Goztepe Metro Line Construction Site (Yüksel Proje, 2017). **23**
Figure 2.7 : Approximate accelerometer placement on TBM 2 and TBM 3. ..... **24**
Figure 2.8 : Accelerometer bases and steel cover (TBM 2) **24**
Figure 2.9 : Installed accelerometers (TBM 2). **25**
Figure 2.10 : Location of the European Region Potable Water Transfer Tunnel. **26**
Figure 2.11 : Geological profile of the section where vibration recording was performed in European Drinking Water Transmission Project Construction Site (EMAY Uluslararası Mühendislik ve Müsavirlik A.S., 2018). **27**
Figure 2.12 : Approximate accelerometer locations on the TBM 4 ..... **29**
Figure 2.13 : Installed accelerometers (TBM 4). **29**
Figure 3.1 : Dimension Engineering DE-ACCM3D (left) and Analog Devices ADXL354BZ (right) accelerometer. **32**
Figure 3.2 : Waterproof accelerometer housing. **32**
Figure 3.3 : Sensing elements of MEMS-type accelerometers. **33**
Figure 3.4 : 356A17 model piezoelectric accelerometer, (a) sensing elements of piezoelectric type accelerometers (b) (Sinha et al., 2014; Harris & Piersol, 2002). **33**
Figure 3.5 : Piezoelectric accelerometer saturation problem. **34**
Figure 3.6 : National Instruments USB-6009 (on left) and 9230 BNC (on right) type analog to digital converters. **35**
Figure 3.7 : A view of the software interface during vibration recording. **36**

Figure 3.8 : Waterproof computer cabinets in TBMs (TBM 2 on left, TBM 4 on right)..... **38**
Figure 3.9 : A view of the data merging software..... **39**
Figure 3.10 : Calculation flowchart of the Matlab script. **40**
Figure 3.11 : The noise before and after the excavation, recorded on the ring 2064 of TBM 2 (z-axis)..... **41**
Figure 3.12 : An example illustration of acceleration percentage graph and acceleration-time graph for a detailed inspection of vibration data..... **42**
Figure 3.13 : An example of averaging the statistical data according to lithological units..... **42**
Figure 3.14 : Changes in the cumulative probability curves depending on the Weibull shape and scale parameters. **46**
Figure 3.15 : Cumulative histogram of vibration data recorded on the excavation of ring 2445 of TBM 2, together with Weibull and Normal distribution fits. **48**
Figure 3.16 : Raw vibration data (top), frequency spectrogram (middle) and power spectral density (bottom) belongs to ring 2008 recorded on TBM 2 (z axis)..... **50**
Figure 3.17 : Frequency spectrogram of vibrations recorded during the excavation of ring 2449 on the x, y and z axes of bottom accelerometer of TBM 2. ... **51**
Figure 4.1 : Calcite vein at the excavation face. **55**
Figure 4.2 : Cutterhead acceleration measured by bottom z-axis on a face with hard calcite vein. **55**
Figure 4.3 : Vibration recordings of bottom z-axis of ring 1657 during cutterhead rotating with 2.1 RPM. **55**
Figure 4.4 : TBM 1 top accelerometer data between rings 1426 and 1769 (Mecidiyekoy-Mahmutbey Metro Line). **57**
Figure 4.5 : TBM 1 bottom accelerometer data between rings 1426 and 1769 (Mecidiyekoy-Mahmutbey Metro Line). **58**
Figure 4.6 : TBM 2 top accelerometer data between rings 1400 and 2100 (Umraniye-Atasehir-Goztepe Metro Line). **63**
Figure 4.7 : TBM 2 top accelerometer data between rings 2100 and 2930 (Umraniye-Atasehir-Goztepe Metro Line) **64**
Figure 4.8 : TBM 2 bottom accelerometer data between rings 1400 and 2100 (Umraniye-Atasehir-Goztepe Metro Line). **65**
Figure 4.9 : TBM 2 bottom accelerometer data between rings 2100 and 2930 (Umraniye-Atasehir-Goztepe Metro Line) **66**
Figure 4.10 : Vibration data of the rings 1560 to 1564 of TBM 2 for z-axes (Sandstone-Limestone #3). **67**
Figure 4.11 : Vibration data of the rings 2300 to 2304 of TBM 2 for z-axes (Siltstone-Claystone #16 and #18)..... **68**
Figure 4.12 : Vibration data of the ring 1510 of TBM 2 (z-axis of top accelerometer)..... **69**
Figure 4.13 : Vibration data and photos taken from the cutterhead of the rings between 1800 and 2040 belong to top accelerometer (TBM 2). **71**
Figure 4.14 : Cumulative probability graphs obtained by using Weibull distribution for top and bottom accelerometers of TBM 2..... **73**
Figure 4.15 : Weibull probability distributions for andesite dykes with different weathering degrees (z-axis of the top accelerometer of TBM 2). **74**

Figure 4.16 : TBM 3 top accelerometer data between rings 1500 and 2100 (Umraniye-Atasehir-Goztepe Metro Line). **76**
Figure 4.17 : TBM 3 top accelerometer data between rings 2100 and 2630 (Umraniye-Atasehir-Goztepe Metro Line). **77**
Figure 4.18 : TBM 3 bottom accelerometer data between rings 1500 and 2100 (Umraniye-Atasehir-Goztepe Metro Line). **78**
Figure 4.19 : TBM 3 bottom accelerometer data between rings 2100 and 2630 (Umraniye-Atasehir-Goztepe Metro Line). **79**
Figure 4.20 : Vibration data of ring 1860 of TBM 3 (Bottom accelerometer, z-axis). **81**
Figure 4.21 : Vibration data of ring 1861 to 1865 of TBM 3 (z-axes). **82**
Figure 4.22 : Probability graphs obtained by using Weibull distribution for top and bottom accelerometers for TBM 3. ..... **85**
Figure 4.23 : Weibull probability distributions for dykes with different weathering degrees (TBM 3, top accelerometer z-axis). **86**
Figure 4.24 : Weibull probability distributions for siltstone-claystone and sandstone-claystone units (TBM 3, top accelerometer z-axis). **86**
Figure 4.25 : TBM 4 top accelerometer data between rings 1 and 1100 (European Region Potable Water Transmission Tunnel Project). **90**
Figure 4.26 : TBM 4 top accelerometer data between rings 1100 and 2000 (European Region Potable Water Transmission Tunnel Project). **91**
Figure 4.27 : TBM 4 bottom accelerometer data between rings 1 and 1100 (European Region Potable Water Transmission Tunnel Project). **92**
Figure 4.28 : TBM 4 bottom accelerometer data between rings 1100 and 2000 (European Region Potable Water Transmission Tunnel Project). **93**
Figure 4.29 : Vibration data of rings 1575 (#25), 1614 (#26) and 1700 (#27) for TBM 4. ..... **94**
Figure 4.30 : Probability graphs obtained by using Weibull distribution for top and bottom accelerometer for TBM 4. ..... **98**
Figure 4.31 : Weibull probability distributions graphs showing siltstone, siltstone-sandstone and sandstone units (TBM 4, bottom accelerometer, z-axis). **99**
Figure 4.32 : Percentage of acceleration data higher than 1g per lithological section for bottom accelerometers of (a) TBM 2, (b) TBM 3 and (c) TBM 4.. **101**
Figure 4.33 : RMS vibration data per lithological section for bottom accelerometers of (a) TBM 2, (b) TBM 3 and (c) TBM 4. ..... **102**
Figure 4.34 : The relationships between RMS vibration data and RQD for top accelerometers of (a) TBM 2, (b) TBM 3. ..... **103**
Figure 4.35 : The relationships between RMS vibration data and GSI for top accelerometers of (a) TBM 2, (b) TBM 3. ..... **103**
Figure 4.36 : The relationships between RMS vibration data and UCS for bottom accelerometers of (a) TBM 2, (b) TBM 3. ..... **104**
Figure 4.37 : Interval RMS vibration data per lithological section for bottom accelerometers of (a) TBM 2, (b) TBM 3 and (c) TBM 4. ..... **105**
Figure 4.38 : Relationships between interval RMS vibrations and RQD for TBM 2 and TBM 3. ..... **106**
Figure 4.39 : Relationships between interval RMS vibrations and GSI for TBM 2 and TBM 3. ..... **106**
Figure 4.40 : Relationships between interval RMS vibrations and UCS for TBM 2 and TBM 3. ..... **107**

Figure 4.41 : Relationships between interval RMS vibrations and PLI for TBM 4. ..... **107**
Figure 4.42 : Crest factor per lithological section for bottom accelerometers of (a) TBM 2, (b) TBM 3 and (c) TBM 4. ..... **109**
Figure 4.43 : Vibration data of the z-axes for the top and bottom accelerometers on TBM 2 belonging to the rings 1561 (top) and 2303 (bottom). **110**
Figure 4.44 : Skewness of the data per lithological section for bottom accelerometers of (a) TBM 2, (b) TBM 3 and (c) TBM 4. ..... **111**
Figure 4.45 : Saturation seen on piezoelectric accelerometers of TBM 2. ..... **111**
Figure 4.46 : Kurtosis of the data per lithological section for bottom accelerometers of (a) TBM 2, (b) TBM 3 and (c) TBM 4. ..... **112**
Figure 4.47 : Relationships between interval RMS acceleration and Boreability Index for TBM 2, 3 and 4. ..... **113**
Figure 4.48 : The relationships between RQD and Weibull parameters for bottom accelerometers, (a) and (b) for TBM 2, (c) and (d) for TBM 3. ..... **114**
Figure 4.49 : The relationships between GSI and Weibull parameters for bottom accelerometers, (a) and (b) for TBM 2, (c) and (d) for TBM 3. ..... **115**
Figure 4.50 : The relationships between PLI and Weibull parameters for bottom accelerometer of TBM 4. ..... **116**
Figure 4.51 : Power spectral densities for fresh and weathered dykes obtained from the data of TBM 2 (bottom accelerometer, z-axis). **117**
Figure 4.52 : Relationships between interval RMS acceleration and thrust for TBM 2, 3 and 4. ..... **118**
Figure 4.53 : Relationships between interval RMS acceleration and cutterhead speed for TBM 2, 3 and 4. ..... **119**
Figure 4.54 : Power spectral densities for consecutive rings with different cutterhead speeds obtained from TBM 2 (bottom accelerometer, z-axis). **119**
Figure 4.55 : Relationships between interval RMS acceleration and penetration for TBM 2, 3 and 4. ..... **120**
Figure 4.56 : Relationships between interval RMS acceleration and specific energy for TBM 2, 3 and 4. ..... **121**
Figure 4.57 : Vibration data of the ring 1886 (x, y and z-axes, top and bottom accelerometers, TBM 2). **123**
Figure 4.58 : Vibration data of the ring 1895 and the broken disc ring (x, y and z-axes, top and bottom accelerometers, TBM 2). **123**
Figure 4.59 : Waterfall FFT graph of the ring 1895 (z-axis of bottom accelerometer). **124**
Figure 4.60 : Vibration data of the rings 2329 to 2331 (z-axes, top and bottom accelerometers, TBM 2). **125**
Figure 4.61 : Waterfall FFT graphs of the of rings 2330 (top) and 2331 (bottom) of TBM 2 (z-axis of bottom accelerometer). **126**
Figure 4.62 : Accelerometer installation positions in TBMs. **127**
Figure 5.1 : Schematic view of full-scale linear cutting machine. **133**
Figure 5.2 : Forces acting on a CCS disc cutter. **133**
Figure 5.3 : Accelerometer numbers (#) and placements on FLCM. **134**
Figure 5.4 : The view of the concreted mudstone sample in the FCLM box. **135**
Figure 5.5 : The view of the concreted siltstone sample in the FCLM box. **136**
Figure 5.6 : The view of the concreted marble sample in the FCLM box. **136**
Figure 5.7 : Rock cutting paths (Siltstone of Kurtkoy Formation). **139**
Figure 5.8 : Bedding planes (a for siltstone and b for mudstone). **139**

Figure 5.9 : Force and vibration data recorded during one of the cutting tests. **141**
Figure 5.10 : Variations of average normal force (a) and average rolling force (b) with penetration. **143**
Figure 5.11 : Variations of specific energy with S_L/p ratio. **144**
Figure 5.12 : Variations of peak normal force (a) and peak rolling force (b) with penetration. **144**
Figure 5.13 : Variations of peak to average normal force (a) and peak to average rolling force (b) with penetration..... **145**
Figure 5.14 : An example representation of the relationships between vibrations and rocks geomechanical properties..... **146**
Figure 5.15 : Variations of interval RMS acceleration and maximum acceleration with uniaxial compressive strength (a,b), tensile strength (c,d), Schmidt Hammer hardness (e,f), Shore Sclerescope hardness (g,h). **148**
Figure 5.16 : Weibull distribution for siltstone calculated from accelerometer 3. . **151**
Figure 5.17 : Weibull distribution for mudstone calculated from accelerometer 3. **152**
Figure 5.18 : Weibull distribution for all rock samples calculated from z-axis of accelerometer 4 for different penetration values (a) 4 mm, b) 6 mm and c) 8 mm)..... **153**
Figure 5.19 : Variations of Weibull parameters with uniaxial compressive strength for x, y and z-axis of accelerometer 4..... **154**
Figure 5.20 : Variation of interval RMS acceleration with normal force (a), rolling force (b), penetration (c) and cutting coefficient (d). **156**
Figure 5.21 : Variation of interval RMS acceleration with peak normal force (a) and peak rolling force (b). **157**
Figure 5.22 : Variation of interval RMS acceleration with ratio of peak normal force to average normal force (a) and peak rolling force to average rolling force (b). **158**
Figure 5.23 : Variation of interval RMS acceleration with coarseness index (a) and sieve size (>25 mm) (b). **158**
Figure 5.24 : Interval RMS acceleration versus normalized optimum normal force (a), normalized optimum rolling force (b), optimum specific energy (c), normalized optimum coarseness index (d). **159**
Figure 5.25 : Variation of maximum acceleration with peak normal force (a), peak rolling force (b), penetration (c) and cutting coefficient (d)..... **160**
Figure 5.26 : The variations on the Weibull parameters with normal forces obtained from accelerometer 4 during laboratory experiments..... **161**
Figure 5.27 : The variations on the Weibull parameters with peak forces obtained from accelerometer 4 during laboratory experiments..... **162**
Figure 5.28 : The variations on the Weibull parameters with optimum normal forces obtained from accelerometer 4 during laboratory experiments..... **163**
Figure 5.29 : The variations on the Weibull parameters with peak optimum forces obtained from accelerometer 4 during laboratory experiments..... **164**
Figure 5.30 : Raw acceleration data from z-axis of accelerometer 3, cutting force data, spectrogram and PSD of the vibration data. **165**
Figure A.1 : Percentage of acceleration data higher than 1g per lithological section for top accelerometers of (a) TBM 2, (b) TBM 3 and (c) TBM 4……**192**
Figure A.2 : RMS vibration data per lithological section for top accelerometers of (a) TBM 2, (b) TBM 3 and (c) TBM 4. ……...**193**
Figure A.3 : The relation between RMS vibration data and RQD for bottom accelerometers of (a) TBM 2, (b) TBM 3. ……...**194**

Figure A.4 : The relation between RMS vibration data and GSI for bottom accelerometers of (a) TBM 2, (b) TBM 3 ...……**194**
Figure A.5 : The relation between RMS vibration data and UCS for top accelerometers of (a) TBM 2, (b) TBM 3 ...……**195**
Figure A.6 : Interval RMS vibration data per lithological section for top accelerometers of (a) TBM 2, (b) TBM 3 and (c) TBM 4 ...……**196**
Figure A.7 : Crest factor per lithological section for top accelerometers of (a) TBM 2, (b) TBM 3 and (c) TBM 4. ……..……..**197**
Figure A.8 : Skewness of the data per lithological section for top accelerometers of (a) TBM 2, (b) TBM 3 and (c) TBM 4 ……**198**
Figure A.9 : Kurtosis of the data per lithological section for top accelerometers of (a) TBM 2, (b) TBM 3 and (c) TBM 4 ……**199**
Figure A.10 : The relationships between RQD and Weibull parameters for top accelerometers, (a) and (b) for TBM 2, (c) and (d) for TBM 3 ……**200**
Figure A.11 : The relationships between GSI and Weibull parameters for top accelerometers, (a) and (b) for TBM 2, (c) and (d) for TBM 3. ……..**201**
Figure A.12 : The relationships between PLI and Weibull parameters for top accelerometer of TBM 4……...**202**
Figure B.1 : Variations of interval RMS acceleration and maximum acceleration with static Poisson's ratio (a,b), dynamic Poisson's ratio (c,d), static elasticity modulus (e,f), dynamic elasticity modulus (g,h). ..…….….**203**
Figure B.2 : Variations of interval RMS acceleration and maximum acceleration with P wave velocity (a,b), S wave velocity (c,d), brittleness (B1) (e,f), brittleness (B2) (g,h)… ……..……..……...**204**
Figure B.3 : Weibull distribution for beige marble (EC) calculated from accelerometer 3 ……**205**
Figure B.4 : Weibull distribution for beige marble (DC) calculated from accelerometer 3 ……**206**

INVESTIGATION OF VIBRATIONS CREATED DURING TBM EXCAVATION AND ROCK CUTTING

SUMMARY

Tunnel Boring Machines (TBMs) are widely employed in infrastructure projects due to their high advance rates and providing a safe working environment. The TBMs should be operated in accordance with the geological conditions to achieve optimal excavation rates. The majority of contractors, especially the ones working in remote locations, predominantly depend on the geological information provided during the tender phase or undertake a limited number of supplementary geotechnical investigations prior to starting projects. Especially in remote locations that characterized by a limited geological data, the expertise of the crew becomes highly significant. Although the most effective way of assessing geological conditions during tunnel excavation involves examining the excavation face, contractors often hesitate to halt excavation for face inspections unless deemed necessary or forced by contractual obligations. Furthermore, the application of closed-face soft ground TBMs often renders face inspections impractical. Although alternative techniques such as probe drilling or geophysical methods could be applied in the TBMs, these approaches require considerable amount of time, with some geophysical methods still undergoing development.

Given the reluctance of contractors to allocate resources towards new geological studies and the necessity for continuous geological information it becomes evident that a system capable of providing real-time information to the TBM crew regarding the encountered geological conditions is required. Since the TBMs vibrate during excavation, utilizing vibrations to understand the geological conditions ahead seems practical.

In this context, field measurements of the vibrations generated during excavation by TBMs have been investigated for ground identification in various studies. However, TBMs include too many influential factors and noise sources that impact the vibrations (e.g., multiple cutters on the cutterhead, motors and other parts in shield and backup area, etc.), requiring a deeper understanding of vibrations specifically arising from the rock cutting process within a more controlled environment. Even some authors focused laboratory analyses and investigated the vibrations generated during rock cutting tests, these experiments remain fairly limited.

The principal objective of this study is to understand the vibrations generated during the TBM excavation and provide a system that could give information to the site crew regarding the geological conditions on the excavation face. To reach this goal, a special vibration data recording system has been developed and installed onto four Earth Pressure Balance Tunnel Boring Machines (EPB TBMs), excavating in three different project sites; that are Mecidiyeköy-Mahmutbey Metro Line, Umraniye-Atasehir-Goztepe Metro Line and European Region Potable Water Transmission Tunnel.

The employed vibration recording system comprises accelerometers, analog-digital converters, and a dedicated computer running custom-designed data recording software tailored for the purpose of this project.

Initial deployment and testing of the system took place at the Mecidiyekoy-Mahmutbey Metro Line project site. Following this initial implementation, the system underwent further refinement, with the addition of new features and hardware enhancements. A total of 6 km tunnel excavation was monitored, and vibration data continuously recorded in three orthogonal directions (x, y, and z). The influence of geological conditions including soils and hard rocks, EPB TBM operating parameters (thrust, torque, face pressure, cutterhead rotational speed, penetration rate), cutter damages/breakages, positions and types of accelerometers, and TBM diameters on vibration were investigated. During vibration analysis, primarily Root Mean Square (RMS) and interval RMS vibrations, together with different vibration statistics were used.

A comprehensive analysis was conducted on the collected TBM vibration data, incorporating geological information, site shift reports, and disc changing logs. This analysis revealed a significant influence of geological and lithological variations on the vibration patterns generated during excavation. In particular, moderately strong to strong correlations were observed between interval RMS acceleration values and rock mass parameters such as Rock Quality Designation (RQD) and Geological Strength Index (GSI). The analysis yielded a clear trend, an increase in rock strength corresponds to rise in TBM vibrations, while vibrations greatly reduced in the case of weathered rocks and soils. The presence of short weathered zones was distinguishable in the vibration data. This characteristic suggests that the measurement has the potential to serve as an early warning system for detecting geological transitions during TBM excavation. Furthermore, an acceleration threshold value of 1g, representing the percentage of data points surpassing this limit, is established as an effective marker for distinguishing between different lithological units. It is observed that the vibrations recorded in TBMs could exceed 10g.

The analysis also revealed an influence by the operational parameters of TBMs and conditions of the cutters on the vibrations. Notably, it was observed that broken disc cutters produce distinct high-amplitude vibrations.

Considering the noise sources in TBMs, it is acknowledged that there is a need for a better understanding of vibrations created during the rock cutting process under more controlled environment. With this objective, laboratory rock cutting tests were conducted using a Full-Scale Linear Rock Cutting Machine (FLCM) equipped a 17-inch constant cross section (CCS) disc cutter. To record vibrations, FLCM was equipped with five accelerometers. Three different rock samples were used (siltstone, mudstone and beige marble) having uniaxial compressive strength values ranging from 21 to 82 MPa. During the experiments, it was discovered that the beige marble sample exhibited two distinct mineralogical characteristics on its left and right sides. As a result, vibration data belong to these different parts analyzed separately.

Installing accelerometers to a FLCM and recording vibrations during the rock cutting has not been performed previously, which makes this research unique. A modified version of the vibration data recording software was used during the laboratory experiments, and the tests were conducted using varying line spacing (distance between the cutters) and penetration values, while maintaining a constant cutting speed throughout. Forces acting on the cutting tool (average and maximum normal, rolling

and side forces) and vibrations generated during cutting tests were simultaneously recorded in three orthogonal directions. The raw vibration data was processed to extract key statistical parameters for further analysis. These parameters included peak acceleration, RMS acceleration, and interval RMS acceleration. The relations between vibration statistical parameters and cutting performance parameters (average and maximum normal, rolling and side forces), cutting geometry (line spacing and penetration), specific energy, coarseness index and mechanical properties of rocks (uniaxial compressive strength (UCS), point load strength index (PLI), RQD and GSI) were analyzed.

Following the analyses, it was observed that vibrations tend to rise together with increased tool forces, penetration depth, and chip size. Notably, a moderately strong, directly proportional relationship was observed between normal force and vibration, particularly under optimal cutting conditions. Furthermore, moderately strong to strong correlations were identified between peak normal force, average normal force, specific energy at optimum cutting conditions, and interval RMS acceleration. Another strong correlation was found between maximum acceleration and peak normal force. Preliminary equations were developed for predicting tool forces and rock strength based on vibration measurements. The impact of rock geomechanical properties and mineral composition on vibrations were substantial, with a general trend of increasing vibrations as rock strength rises. The observations indicated that accelerations exceeding 20g could arise during the rock cutting process.

The vibrations generated in both rock cutting experiments and TBM excavation exhibit non-stationary random characteristics. This kind of data is best represented by Weibull distribution and using this distribution type cumulative probability graphs were prepared. The relationships between Weibull parameters (shape "α" and scale "β") and various factors influencing vibration were investigated. These analyses effectively highlighted the effect of various geological conditions on the vibrations.

Given the random nature of the vibration data, spectrograms and power spectral density (PSD) analyses were employed to investigate the data in the frequency domain. These analyses revealed that the vibrations recorded during both the laboratory experiments and TBM excavations exhibited broadband frequency characteristics. Furthermore, no statistically significant relationships were observed between the identified dominant frequencies and the properties of the rock formations or the excavation parameters. These findings were limited the usability of the frequency domain data for differentiating the geological conditions.

This research successfully bridges the gap between field studies and controlled laboratory experiments, contributing to a deeper understanding of the factors influencing vibrations generated during TBM excavation and rock cutting experiments. The results of laboratory analyses and TBM vibration analyses exhibited consistent findings, verifying each other. The study's outcomes suggest that utilizing real-time vibration monitoring holds potential for anticipating geological conditions ahead of TBMs. This capability could significantly enhance TBM performance by helping to select optimum operational parameters on time in accordance with the geological conditions. The information obtained from the laboratory experiments regarding vibrations can serve as valuable input for TBM component design by guiding the engineers regarding the expected vibrations. While the vibration recording system may necessitate further enhancements for practical site application, this study can serve as a crucial information source for future investigations in this field.

TBM KAZISI VE KAYA KESME DENEYLERİ SIRASINDA OLUŞAN TİTREŞİMLERİN İNCELENMESİ

ÖZET

Tünel Açma Makineleri (TBM'ler) altyapı projelerinde geniş uygulama alanı bulmaktadır ve optimum kazı hızlarına ulaşmak için jeolojik koşullara uygun olarak kullanılmaları yapmaları gerekmektedir. Yüklenicilerin çoğunluğu, özellikle dağlık bölgelerde faaliyet gösterenler, genellikle ihale aşamasında sağlanan jeolojik bilgilere güvenmekte veya projelere başlamadan önce kısıtlı miktarda ek jeolojik araştırma yapmaktadır. Jeolojik verilerin sınırlı olduğu bölgelerde, kazı hızının planlanan düzeyde olması ve TBM sıkışması gibi problemler ile karşılaşılmaması için saha ekibinin uzmanlığı ile jeolojik ve TBM operasyonel parametrelerinin (itme ve döndürme kuvveti vb.) doğru yorumlanması oldukça önemlidir. Tünel kazısı sırasında jeolojik koşulları anlamanın en etkili yolu kazı aynasının incelenmesi olsa da, yükleniciler zorunda kalmadıkça veya sözleşmeden doğan yükümlülük bulunmadıkça aynanın incelenmesi için kazıyı durdurmak konusunda genellikle isteksizdir. Ayrıca zemin TBM'lerinde (pasa basınçlı -EPB TBM- veya çamur basınçlı -SPB TBM-) ayna basıncı uygulanan bölgelerde ayna incelemesi imkanı bulunmamaktadır. Aynadaki ve daha sonra karşılaşılacak jeolojik koşulların incelenmesi amacıyla araştırma delgileri açılabilmekte veya farklı TBM'lerde kullanılmak üzere geliştirilmiş jeofizik yöntemler (TSP ve BEAM gibi) kullanılabilmektedir, fakat bu alternatiflerin uygulanması önemli miktarda zaman gerektirmektedir. Ek olarak bu jeofizik yöntemlerden bazıları henüz geliştirilme aşamasında olup her zaman başarılı sonuçlar vermemektedir.

Yüklenicilerin ek jeolojik çalışmalar için kaynak ayırma konusundaki isteksizliği ve ekibin TBM'in optimum koşullarda kazı yapmasını sağlama amaçlı karşılaşılan jeolojik değişimler ile ilgili sürekli olarak bilgiye ihtiyaç duyması göz önüne alındığında, gerçek zamanlı jeolojik veri sağlayan bir sisteme olan ihtiyaç görülmektedir. TBM kazısı sırasında kaya kesme işlemi nedeniyle sürekli olarak titreşimlerin oluştuğu bilgisinden yola çıkılarak, bu titreşimlerin gerçek zamanlı jeolojik veri elde etme amaçlı olarak kullanılması fikri ortaya çıkmıştır.

Bu kapsamda literatürde farklı araştırmacılar tarafından TBM kazısı sırasında oluşan titreşimler (ivmeler) incelenmiştir. Fakat bu çalışmalarda oldukça küçük bir veri seti kullanıldığından, jeolojik koşulların TBM titreşimleri üzerine etkileri sadece genel hatlarıyla anlaşılabilmiş, kaya dayanımı ile oluşan titreşimlerin büyüklüğü arasında bir bağlantı kurulamamıştır. Önceki çalışmalarda kullanılan veri setlerinin kısıtlı olması yanında, TBM'lerde komplike yapıları nedeniyle çok fazla gürültü kaynağı bulunması (motor, pompa vb. ekipmanlar) ve TBM işletme parametrelerinin de oluşan titreşimler üzerinde etkisinin olması bu çalışmalarda kesin bulgular elde edilememesinin diğer nedenleri olarak sıralanabilir. Dolayısıyla titreşimler ile jeolojik koşullar arasında bağlantı kurabilmek için farklı koşullarda kazı yapan TBM'lerden veri alınması ve

değerlendirme yapılırken kaya/zemin özelliklerinin yanında TBM işletme parametrelerinin de değerlendirilmesi gerekmektedir.

Bu çalışmanın ana hedefi TBM kazısı sırasında oluşan titreşimlerin nedenlerini anlamak ve saha ekibine kazı aynasındaki jeolojik koşullar hakkında bilgi verebilecek bir sistemin oluşturulmasıdır. Bu amaçla tez kapsamında bir titreşim kayıt sistemi geliştirilmiş, geliştirilen bu sistem Mecidiyeköy-Mahmutbey Metro Projesi, Ümraniye-Ataşehir-Göztepe Metro Projesi ve Avrupa Bölgesi İçme Suyu Transfer Projesi'nde kazı yapmakta olan dört adet TBM'e monte edilerek kazı sırasında oluşan ivmeler kaydedilerek analiz edilmiştir.

Kullanılan titreşim kayıt sistemi ivmeölçerler, analog-dijital dönüştürücü ve bu sistem için özel olarak hazırlanmış kayıt yazılımını çalıştıran bir bilgisayardan oluşmaktadır. Sistemin internet bağlantısı sağlanması durumunda uzaktan kontrol edilmesi de mümkündür.

Sistemin ilk denemesi Mecidiyeköy-Mahmutbey Metro Hattı Projesi'nde yapılmış olup, buradan elde edilen bilgiler ışığında kayıt sisteminde donanımsal geliştirmeler yapılarak daha yüksek ölçüm aralığına sahip ivmeölçerler kullanılmaya başlanılmıştır. Ayrıca kayıt yazılımına da yeni özellikler eklenilerek güncelleştirmeler yapılmıştır. Tez çalışması kapsamında toplamda 6 km'lik tünel kazısı sırasında oluşan ivmeler birbirine dik üç eksende kaydedilmiştir. Zemin ve kaya ortamlarının jeolojik özellikleri, EPB TBM işletme parametreleri (itme kuvveti, döndürme kuvveti, ayna basıncı, kesici kafa dönüş hızı ve penetrasyon), kesici hasarları, ivmeölçer pozisyon ve türü, TBM çapı gibi değişkenlerin kazı sırasında oluşan ivmeler üzerindeki etkileri incelenmiştir. Analizler sırasında genellikle ortalama karekök (RMS) ve bileşke ortalama karekök (RMS_{int}) değerleri ile farklı istatistiksel veriler kullanılmıştır.

TBM'lerde bulunan diğer bileşenlerin oluşturduğu titreşimler, gürültü kaynakları ve kazı sırasında birden fazla diskten gelen titreşim sinyallerinin süperpoze olduğu düşünüldüğünde, direkt olarak kaya özellikleri ile titreşimler arasındaki ilişkilerin anlaşılması için kontrollü şekilde laboratuvar ortamında deneylerin yapılması gerektiği de görülmüştür. Bu amaçla, günümüz TBM'lerinde sıklıkla kullanılan 17 inç çaplı bir disk keski ile tam boyutlu doğrusal kaya kesme makinesinde (FLCM), kesme deneyleri yapılmış ve oluşan titreşimlerin kaydedilmesi amacıyla FLCM'ye beş adet ivmeölçer yerleştirilmiştir. Deney için tek eksenli basınç dayanımları 21 ile 82 MPa arasında değişen 3 adet kaya örneği (silttaşı, çamurtaşı ve bej mermer) kullanılmıştır. İlerleyen aşamalarda bej mermerin sağ ve sol bölümlerinin birbirinden farklı özellikler gösterdiği fark edilmiş ve bu iki taraf birbirinden ayrı analiz edilmiştir. Sahada elde edilen TBM titreşim verisinin kullanılmasına ek olarak doğrusal kaya kesme makinesinin ivmeölçerler ile donatılarak kaya kesme deneylerinin yapılmış olması, bu çalışmayı önceki çalışmalardan ayrılmaktadır.

Deneyler sırasında veri kaydı için TBM'lerde kullanılan kayıt sistemindeki yazılım bazı değişiklikler yapılarak kullanılmıştır. İvme ölçümleri ile keskiye etkiyen kuvvetlerin ölçümü eşzamanlı olarak yapılmıştır. Deneyler farklı kesme aralığı (keskiler arası mesafe) ve kesme derinliği (penetrasyon) değerleri kullanılarak tekrar edilmiş olup, kesme hızı sabit tutulmuştur. Kaya kesme sırasında oluşan kuvvetler ile üç eksende kaydedilen ivmeler daha sonra beraber analiz edilmiştir. Maksimum, ortalama karekök (RMS) ve bileşke ortalama karekök (RMS_{int}) ivme değerleri TBM'lerden elde edilen verilere benzer olarak analizlerde kullanılmıştır. Bu değerler, kaya kesme parametreleri (ortalama ve maksimum itme kuvveti – normal kuvvet ile döndürme kuvveti – yuvarlanma kuvveti ve yanal kuvvetler), kesme geometrisi

(keskiler arası mesafe ve kesme derinliği – penetrasyon, spesifik enerji, pasa irilik katsayısı ve kayaların mekanik ve kütlesel özellikleri (tek eksenli basınç dayanımı, nokta yük dayanım indeksi, RQD, GSI) ile karşılaştırılmıştır.

Ayrıca hem saha hem de laboratuvar deneylerinde elde edilen ivme verilerinin kümülatif olasılık dağılımları da yapılmıştır. Saha ve laboratuvarda kaydedilen titreşim verilerinin rasgele dağılıma ve sivri basıklığa (leptocurtic) sahip olduğu görülmüştür, dolayısıyla olasılık dağılımlarında bu tür verileri en iyi ifade eden dağılım türü olan Weibull dağılımı kullanılmıştır.

Çalışma süresince zaman ortamındaki analizlere ek olarak frekans ortamında da ivme sinyallerinin frekans bileşenlerinin belirlenmesi amacıyla spektrogram ve güç spektral yoğunluk (PSD) analizleri yapılmıştır. Frekans ortamındaki analizlerde hem laboratuvar deneyleri hem de sahada TBM kazısı sırasında elde edilen ivmelerin genişbant dağılıma sahip olduğu, baskın frekansların farklı jeolojik ortamlarda oldukça az değişim gösterdiği belirlenmiştir. Bu nedenle frekans ortamındaki analizlerin çalışma süresince kullanılabilirliği kısıtlı kalmış ve zaman ortamındaki analizlere odaklanılmıştır.

TBM'lerden elde edilen titreşim verilerinin analiz edilmesi sonucunda kazı sırasında oluşan titreşimlerin jeolojik koşullardan etkilendiği ve litolojideki değişimlerin titreşim kayıtlarında fark edilebilir olduğu görülmüştür. Özellikle bileşke ortalama karekök (RMS_{int}) ivme değerleri ile RQD ve GSI arasında orta-kuvvetli ve kuvvetli bağıntılar olduğu görülmüştür. Genel olarak laboratuvarda elde edilen sonuçları doğrular nitelikte, kaya dayanımının artması ile ivme genliklerinde artış olduğu görülmüş, zemin ortamlarında ise ivmelerin çok düşük seviyelere indiği gözlenmiştir. Sağlam kaya ortamlar arasındaki kısa zayıf zonlar titreşim kayıtlarında belirgin olarak görülmekte olup, bu da titreşim kayıt sistemini zayıf bölgelerin tespiti için ve ekibin bu bölgelerde kazı yapıldığı ile ilgili hızlı şekilde bilgilendirilmesi amacıyla kullanılabilir kılmaktadır. Analizler sırasında 1g'nin sınır değeri olarak kabul edilmesi ve bu değerin üzerinde kalan noktaların toplam kayıt içerisindeki yüzdesinin kullanılmasının litolojik birimler arasındaki ayrımların belirlenmesinde etkili bir yöntem olduğu görülmüştür. Ek olarak TBM'lerde oluşan ivmelerin 10g'nin üzerine çıkabildiği belirlenmiştir.

Kazı sırasında oluşan titreşimlerin TBM operasyonel parametrelerinden ve keskilerin durumundan da etkilendiği görülmüştür. Özellikle bazı bölgelerde disk kırılmalarını takiben belirgin yüksek genlikli titreşimler oluştuğu belirlenmiştir. Titreşimlerde oluşan bu değişimlerin, sistemin disk kırılmalarının tespitinde kullanılabileceğini de göstermektedir.

Laboratuvar analizleri sonucunda ise titreşimlerin, artan keski kuvvetleri, penetrasyon ve pasa parça büyüklüğü ile beraber arttığı görülmüştür. Özellikle, normal kuvvet ile ivme arasında orta-kuvvetli doğrusal bağıntılar olduğu görülmüştür. Optimum keskiler arası mesafe, kesme derinliği, maksimum normal kuvvet, ortalama normal kuvvet ve spesifik enerji ile bileşke ortalama karekök ivme değerleri arasında orta-kuvvetli ve kuvvetli korelasyonlar mevcuttur. Diğer bir kuvvetli korelasyon ise maksimum ivme ile maksimum normal kuvvet arasında bulunmuştur. Bu veriler ışığında, kesme kuvvetleri ve kaya dayanımının, kazı sırasında oluşan ivmeler kullanılarak tahmin edilmesini sağlayacak eşitlikler ortaya konulmuştur. Elde edilen bu eşitliklerin, çalışmanın genişletilmesi ve daha büyük bir veri tabanı kullanılması ile TBM'lerde gerçek zamanlı tahminlerde kullanılabileceği düşünülmektedir. Deneyler sırasında kayanın mekanik özelliklerinin ve mineral bileşiminin titreşimler üzerinde büyük

etkisi olduğu ve kaya dayanımı arttıkça titreşimlerin arttığı gözlenmiştir. Ayrıca, kaya kesme deneyleri sırasında oluşan ivmelerin 20g'nin üzerine çıkabildiği görülmüştür.

Bu çalışma TBM kazısı ve kaya kesme deneyleri esnasında oluşan titreşimler ile ilgili bugüne kadar yapılan çalışmaların en önemli eksikliklerinden biri olan saha ve laboratuvar verisinin birlikte değerlendirilmesi konusundaki boşluğu doldurmaktadır. Çalışma sonucunda TBM kazısı ve kaya kesme sırasında oluşan titreşimleri etkileyen faktörler belirlenmiş olup, sahada ve laboratuvarda elde edilen sonuçların tutarlı olduğu ve birbirini tamamladığı görülmüştür. Ayrıca 6 km tünel kazısı boyunca saha verisi toplanmış olması da bu çalışmayı öncekilerden ayırmaktadır. Analiz ve değerlendirmeler sonucunda kazı sırasında oluşan titreşimleri kullanarak, jeolojik koşulların gerçek zamanlı olarak tahmin edilebileceği görülmüştür. Ayrıca, tam ölçekli doğrusal kaya kesme deneyinin bir bileşeni olarak titreşim ölçümlerinin de yapılması ve bu verilerin TBM kazısı sırasında oluşan titreşimler ile karşılaştırılması sonucunda sonraki çalışmalarda bir veri tabanı oluşturulabileceği, bu veri tabanının da TBM üreticilerine ve tasarımcılara kazı sırasında beklenecek titreşimler ile ilgili bilgi sağlayabileceği düşünülmektedir. Geliştirilen kayıt sisteminin sahada uygulanması mevcut hali ile mümkün olmasa da yapılacak geliştirmeler sonucunda sahada uygulanabilir hale getirilmesi mümkün olup, bu tezin daha sonra yapılacak çalışmalar için yol gösterici olacağı düşünülmektedir.

1. INTRODUCTION

Tunnel boring machines (TBMs) are widely utilized for infrastructure projects and the performance of TBMs is heavily influenced by the ground conditions and geological variations encountered during excavation. Insufficient understanding of geological conditions during excavation significantly reduces the TBM advance rate, results in high energy consumption, cutter damages, and in the worst case, may lead to TBM entrapment. Therefore, it is crucial to promptly and accurately identify any deviations in geological conditions and respond accordingly.

Contractors, especially those working in remote locations, typically rely on the geological information provided to them during the tendering process, or they conduct a few additional geotechnical investigations at the beginning of the project. The most reliable and effective way to assess geological conditions during excavation is by inspecting the excavation face, however, many contractors are reluctant to halt TBM excavation for face inspections unless it is deemed necessary or mandated by the contract. Furthermore, in the case of closed face soft ground TBMs, it is often not possible to visually observe the face in the majority of situations.

Other alternatives to face inspection for evaluating the geological conditions include probe drilling and geophysical methods. However, probe drilling requires a considerable amount of time, reducing TBM utilization. The geophysical methods that are specifically adopted for TBM applications (e.g., TSP or BEAM etc.), are mostly still in development phase and rarely used. Given the drawbacks of these current alternatives, there is a clear need for a non-disruptive ground identification system.

Since vibrations generated during rock cutting are closely linked to applied cutting forces and geological conditions, utilizing vibration data which is measured as acceleration, for detecting lithological changes appears to be a practical approach. The vibrations had been used in the earlier days of tunneling subconsciously, as it was common for the TBM operator's cabin to be positioned in front of the TBM, typically within the shield. This placement had allowed operators to directly perceive vibrations during the excavation and understand changes in excavation characteristics related to

geological conditions. Being in close proximity to the cutterhead, operators could promptly respond by adjusting TBM operating parameters as needed. However, in many modern TBMs, operator's cabin is situated at the gantries, which is located at a considerable distance from the cutterhead, creating a need for a vibration detection system to re-utilize the vibrations occurred during excavation.

Valuable insights into the encountered geological conditions can be gained, by monitoring the vibrations produced during TBM excavation. Variations in vibration patterns can indicate changes in rock properties, the presence of fractures or some mechanical failures in the machinery. These indicators help in identifying anomalies in lithology or unexpected ground conditions that may pose challenges to the TBM's progress.

1.1 Objectives of the Thesis

While there is a growing interest in studying TBM vibrations, a comprehensive understanding of how geological conditions and rock strength influence TBM vibration characteristics is still lacking. With this study it is aimed to establish correlations between TBM vibration characteristics, various geological conditions (such as different lithological units and transition zones), TBM operational parameters, and cutter conditions to provide real-time information on the lithology and cutter problems to the operators and engineers. By utilizing this information, excavation parameters (cutterhead speed, thrust, torque etc.) could be adjusted quickly in response to geological changes, which will increase TBM performance, and reduce downtimes.

To provide better correlations, a deeper understanding of the vibrations related directly to the rock cutting process should be gained which is another goal of this study. As there are additional vibration and noise sources present in the TBMs such as multiple cutters, motors, bearings and pumps, their effect should be eliminated. A full-scale linear rock cutting machine equipped with accelerometers was used to fulfil this need, and rock cutting tests were conducted using a constant cross section (CCS) 17" disc cutter. The focus of the laboratory experiments is to investigate the relationships between cutting parameters, rock mechanical properties, and vibrations to gain a comprehensive understanding of the vibrations that occur during rock cutting under controlled conditions.

This study intends to contribute to the existing knowledge base and fill the gaps in understanding TBM vibrations, by combining the information obtained during the site and laboratory experiments.

The findings of this research can potentially lead to improved TBM performance by providing insights into geological conditions, enhancing the selection of suitable TBM operational parameters, and potentially mitigating the further damages to the cutting tools. Furthermore, as the vibrations can be used to identify soil transition zones or short faults that are not envisioned on the geological reports, ground settlements related with these unstable zones could be reduced.

1.2 Literature Review

The vibrations produced during rock cutting are primarily influenced by the applied cutting forces and geomechanical properties of the rock. Consequently, numerous studies have been carried out to investigate the relationships between these variables. Some of the researchers have conducted laboratory experiments to capture vibrations while others have measured vibrations directly in the TBMs, during excavation. It is possible to say that in the recent years, vibration research, especially the ones executed at site by utilizing TBMs, attracted attention of many researchers.

Laboratory and site studies differs significantly, since in the laboratory vibrations recorded in an isolated environment under more controlled conditions (e.g., homogenous rock surface, pre-set cutting parameters). However, TBMs include lots of noise sources, have a very large excavation face and multiple cutters. Thus, in this section, the relevant literature will be separately presented. It should be emphasized that, previous investigations were conducted either on-site or in laboratory, and none of the prior research covers both aspects, as this study does.

In addition, as the present study investigates vibrations generated during TBM excavation, a brief overview of TBM types, components, and main working principles will be given before presenting the information on existing research related to vibrations.

1.2.1 Tunnel boring machines

Tunnel boring machines can achieve high advance rates with minimal ground disturbance while providing a safe working area for the crew. Thus, utilization of TBMs for underground construction has been increasing steadily. It is possible to classify TBMs into two main categories, namely, soft ground TBMs and hard rock TBMs (Figure 1.1). Recent technological advancements have also introduced hybrid types, which combines two different types.

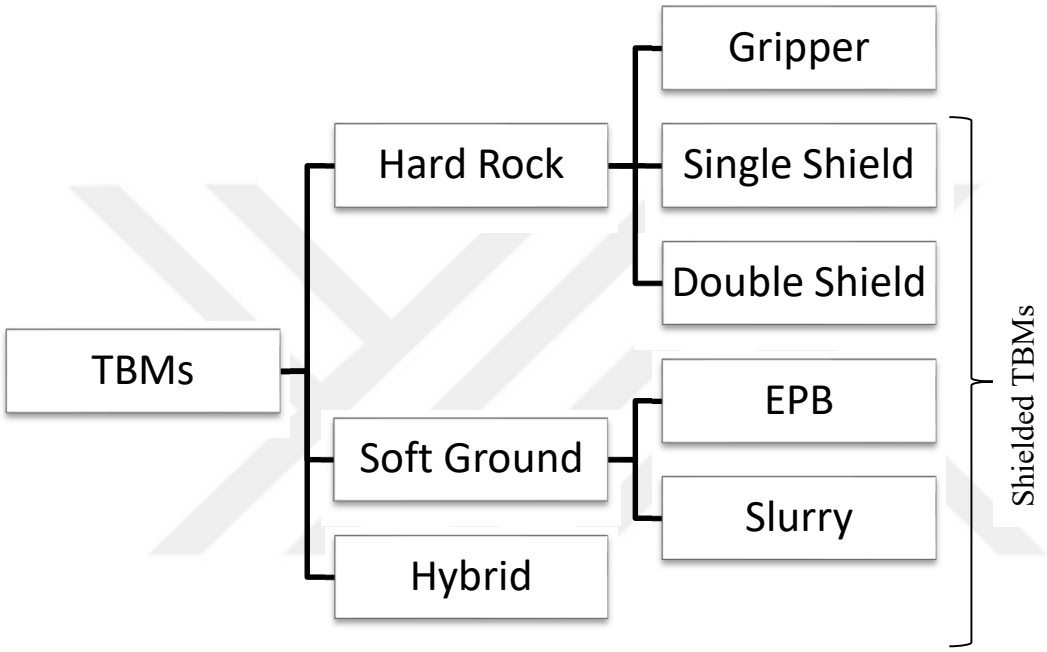

Figure 1.1 : TBM types.

Precast segments are used as the permanent lining with shielded TBMs. This support system involves segment pieces erected by the TBM to form a ring. The number and size of the segment pieces are determined by project specific requirements. Shielded TBMs are composed of a shield, which protects the equipment and workers while providing temporary support to the ground until the precast segments are installed. Within the shielded area, essential components such as the main bearing, cutterhead motors, gear reducers, conveyor, and various equipment are placed. During the excavation, the cutterhead is rotated and the TBM propels itself forward by thrusting against the segments using thrust cylinders. Once there is sufficient space available for ring installation (generally 1 to 2 meters depending on the project), excavation is halted, and precast segments are erected.

As the field studies are conducted on EPB (Earth pressure balance) TBMs, a general information on this type will be provided in this section and a general view of an EPB TBM is provided in Figure 1.2.

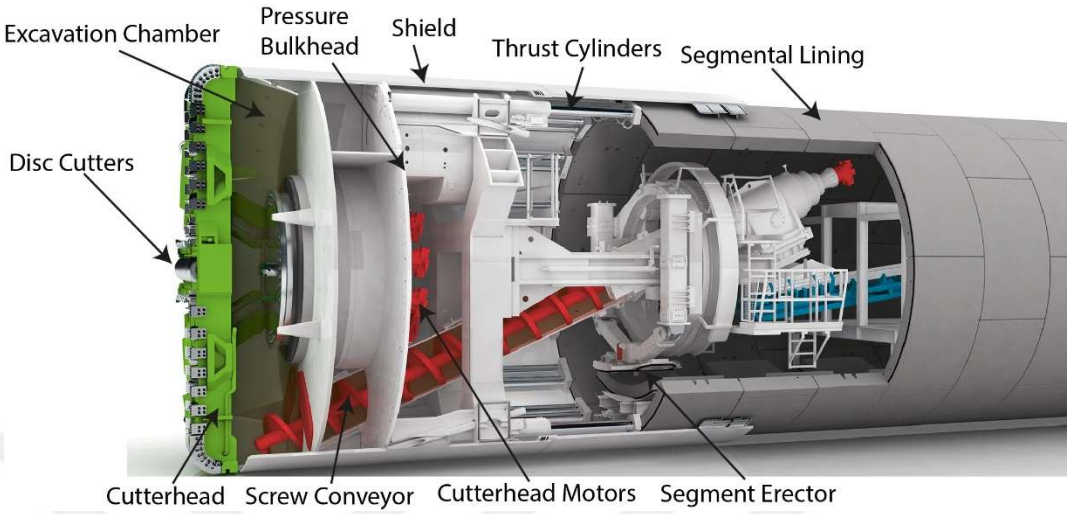

Figure 1.2 : Cross-section of an EPB TBM (courtesy of Herrenknecht).

EPB TBMs provide support at the face with excavated soil. The excavation chamber is filled with the excavated soil and a pressure bulkhead (where the accelerometers were installed during the present study) separates it from the rest of the TBM. During the excavation a pressure tight screw conveyor removes the soil from excavation chamber while discharges it to tunnel under atmospheric pressure. The support pressure is regulated by screw conveyor's rotation speed and the TBM's advance speed. Muck transport out of the tunnel is usually carried out as dry mucking.

1.2.2 Laboratory studies

The laboratory studies conducted to understand the vibrations occurred during rock cutting are very limited and only one of them utilizes accelerometers similar to present study. Limited access to full-scale linear rock cutting machines (FLCMs) might be a contributing factor to the relatively low number of laboratory experiments investigating rock cutting vibrations.

Huo et al. (2015) developed a dynamic multi-degree-of-freedom model for disc cutters to provide a better understanding of the vibration characteristics and load transmission of the cutters, which might be used to reduce cutter damages on TBMs caused by vibrations. The study shows that when subjected to shock excitation during tunneling operations, TBM disc cutters exhibit complex mechanical behavior among joint

interfaces. Effective anti-vibration design strategies that can be implemented in the disc cutter system to reduce excessive vibration and cutter damages that might occur during TBM tunneling were also discussed.

Yang et al. (2020) investigated the vibration characteristics of the cutterhead in soft-hard mixed strata using a Multi-Mode Boring Test System (MBTS). Except the utilization of the multiple cutters in the test system, the study is similar to the laboratory tests undertaken for the present research. The authors used the Su'ai Tunnel as the case and, geological conditions were modelled in the laboratory conditions. To facilitate data collection, accelerometers strategically placed within the cutterhead of the MBTS.

Different from an FLCM, MTBS composed of a cutterhead equipped with multiple disc cutters with adjustable saddles, making tests with different cutting radiuses possible (Figure 1.3). Similar to FLCMs, the rock samples fixed to the saddle with concrete and rock cutting is realized.

Figure 1.3 : Multi-Mode Boring Test System.

In the study, Yang et al. (2020) replicated three distinct geological scenarios, including soft-hard mixed stratum with different strength; as well as tunnel faces with varying proportions of hard rock and soil. The experiment investigated the impact of various geological conditions on the vibration of the cutterhead and the distribution pattern of acceleration amplitudes at distinct locations. The research was concluded that, different rock to soil ratios at the tested strata affected vibration characteristics, the

vibration frequency of the rock was less than 5 Hz, and vibration amplitudes of the cutterhead changed with rock strength.

1.2.3 Field studies

A significant number of authors have directed their research towards studying vibrations occurred during TBM excavation and have investigated the relationships between the TBM vibrations and geological conditions as well as TBM operational parameters.

Samuel and Seow (1984) were one of the first researchers who investigated the force components acting on a disc cutter with the strain gauges that were attached to the discs' shafts of a 4.1m diameter hard rock TBM. It was determined that there was no correlation between disc cutter rotational speed and chip formation frequency and the force signals were random with no apparent fundamental frequencies. Researchers also indicated a correlation between cutter loads and TBM operational parameters.

TBM manufacturers have been focused their attention in measuring forces and vibrations acting on cutters for cutter monitoring purposes and one of these systems is named as SmartCutter by the Robbins Company (Shanahan, 2010; Mosavat, 2017). The system is still in the development phase and the major focus of this system is to inform TBM operators regarding the state of the cutters. In this kind of cutter monitoring systems, which gets information from multiple cutters, it is generally preferred to use wireless devices, that are installed to the cutter holders, specifically wedge bolt of the cutter housing. It is acknowledged by the authors (Shanahan, 2010; Mosavat, 2017), tracking the changes in vibration of the cutters could reveal a variety of information, including variations in the geological conditions or a potential cutter failure issue. Shanahan (2010) indicated that to produce a useful dataset, extensive filtering and large amounts of data are required. Mosavat (2017) found that the peak acceleration reduces with increasing cutter wear, however, without frequency analyses it was not possible to give information on the geological conditions and since their priority was cutter monitoring these analyses were not utilized. As the system is a commercial one, the authors also did not provide too much information on the calculation methodology.

Huang et al. (2018) monitored the cutterhead vibrations and the rock pressure acting on the shield of a TBM for understanding the interaction between the shield and the

surrounding rock in Lanzhou Water Resource Diversion Project in China. The cutterhead of a 5.8m double shield TBM was equipped with a set of accelerometers having a measurement range of ±10g and obtained vibration data were analyzed in both time and frequency domains. Fast Fourier Transform (FFT) was used for the conversion of time domain data to frequency domain. The authors observed a significant correlation between the cutterhead vibrations and the TBM advance parameters, as well as the geological conditions encountered during excavation. They found that the acceleration amplitudes increased with higher cutterhead rotational speed and penetration rate. The vibrations perpendicular to the cutterhead were the most intense. During the normal excavation, the dominant frequency ranges were 40–45 Hz, 80–85 Hz, 120–130 Hz, 165–170 Hz, 205–210 Hz and 220–225 Hz. It is also reported that, following a TBM entrapment the cutterhead vibrates intensely and observed vibration amplitudes were 2-3 times higher than the normal operation. On frequency domain, the peaks on 50–55 Hz and 95–100 Hz were also seen following an entrapment in addition to the ones during normal operation. The authors concluded that by monitoring cutterhead vibrations, the state of the cutterhead could be predicted, for instance, a notable increase in cutterhead vibration amplitude might indicate blocked cutters, while an unexpected peak acceleration could suggest damaged cutters. In addition, the measured cutterhead vibration could play an essential role in the detection of mixed face conditions and geological mapping. Considering the difficulties during sensor installation and reliability problems during operation, the authors proposed that installing the sensors during manufacturing stages would be beneficial.

Wu et al. (2021) monitored the vibration data of a dual mode (EPB-Hard rock) TBM by placing accelerometers having ±16g measurement range on the cutterhead. The authors selected to monitor vibrations for a couple of minutes during the excavation of each ring and indicated that since the difference in the geological conditions between the rings will be small, continuous monitoring was not necessary. Furthermore, continuous monitoring would increase the power consumption which was a concern since the system was battery powered and would cause data transmission problems. For time domain analyses, average peak acceleration data which is the average of the absolute acceleration values of 20 peak points of each ring, and signal energy, which is the sum of the squares of acceleration values for 6 consecutive minutes were used.

Conversation to frequency domain was undertaken by FFT. The system was installed to the TBM excavating Shenzhen Metro Line 12, in China from Huaide station to Fuyong station and the tunnel alignment included soft soil, hard rock, mixed ground and fault zones. The study reported that the vibration amplitudes decreased significantly in the fault zones and increased with increasing rock compressive strength. A correlation between vibrations and boreability index was also detected. These results showed that there is a relationship between rock strength and TBM vibrations. The acceleration values were higher in axis at the direction of excavation. In the same study, the TBM vibrations were recorded with changing cutterhead speeds and thrust levels while keeping the other variables constant to understand the effect of TBM operational parameters on vibrations. During each test, muck samples were taken and each testing step was lasted around 10 minutes. With increasing penetration rate, the accelerations measured on the axis of the excavation direction increased almost linearly, and the vibration amplitudes significantly increased with increasing cutterhead rotational speed, remaining unchanged once the cutterhead rotational speed exceeded 3.5 RPM. It is also reported that dominant frequencies were concentrated in the range of 50-200 Hz, however, no further information on the frequency domain was provided. The study concluded that the vibrations can be used for determining the geological conditions on the tunnel face as the cutters broke the rock easily, the vibrations become weaker.

In most of the previously discussed studies, the data was transmitted wirelessly and the data monitoring was not performed continuously. The authors of these studies acknowledged the challenges associated with data transmission problems and the harsh environment of the cutterhead. In contrast to this attitude, some researches were performed vibration recordings by locating accelerometers behind the cutterhead, which can be considered as a more practical approach. However, it should be noted that, placing accelerometers behind the cutterhead introduces additional noise as the other equipment of the TBM (e.g., cutterhead motors, pumps, screw conveyor etc.) becomes closer and the vibration signals are passed through the main bearing before reaching the bulkhead.

A boulder detection system utilizing accelerometers developed by Walter (2012), and the system was installed onto two EPB TBMs having diameters of 6.20m and 6.44m (Walter et al., 2012; Walter, 2013 and Mooney et al., 2014). The first system which

can also be recognized as the trial test system, included one accelerometer and was installed to the TBM excavating Link Light Rail Tunnel project (U230) in Seattle, Washington. The system combined two dual-axis ±18g accelerometers with 100mV/g sensitivity. A custom application was written and it alerted the operator in case the vibration levels exceed the programmed threshold. With the knowledge obtained from the system, it was updated two times and on the latest system four ±5g accelerometers with 400mV/g sensitivity were used. The updated system was installed to a TBM excavating Toronto-York Spadina Subway Extension. It was hypothesized that the measured vibrations will correlate with the cutting head striking fixed objects, like boulders, during excavation. The vibration recording systems were installed behind the pressure bulkhead (Figure 1.2) and recorded vibrations continuously, different from most of the previous studies explained in this section. Both time domain and frequency domain analyses were conducted on the recorded data. While the time domain analyses focused on RMS vibrations, spectrograms and power spectral density were used for frequency domain analyses.

Walter (2013) reported that the vibration levels varied considerably along the alignment, but correlated strongly with ground conditions, especially when soil types changed. The observations were further verified by classical comparison of operational parameters with changing soil conditions and the findings offered an insight into machine/soil interaction. The accelerations also correlate well with specific energy (SE). These results illustrate the complex TBM-environment relationship, and the outcomes could allow operators to make decisions based on the provided real-time ground data. Frequency data was found to be broadband, having energy present between 100 and 600 Hz (Figure 1.4). The dominant frequencies were strongly related with the cutterhead rotation speed.

Buckley (2015) with the objective of improving Walter's (2013) findings continued to analyze the data with a specific focus on detecting and characterizing impacts to the TBM and finding the main ambient frequency components together with their relationship to cutterhead rotation speed. An enhanced system was installed to a 6.44m EPB TBM excavating N125 tunneling project in Seattle. The system included 4 tri-axial and 4 uniaxial accelerometers with ±10g measurement range and 400 mV/g sensitivity.

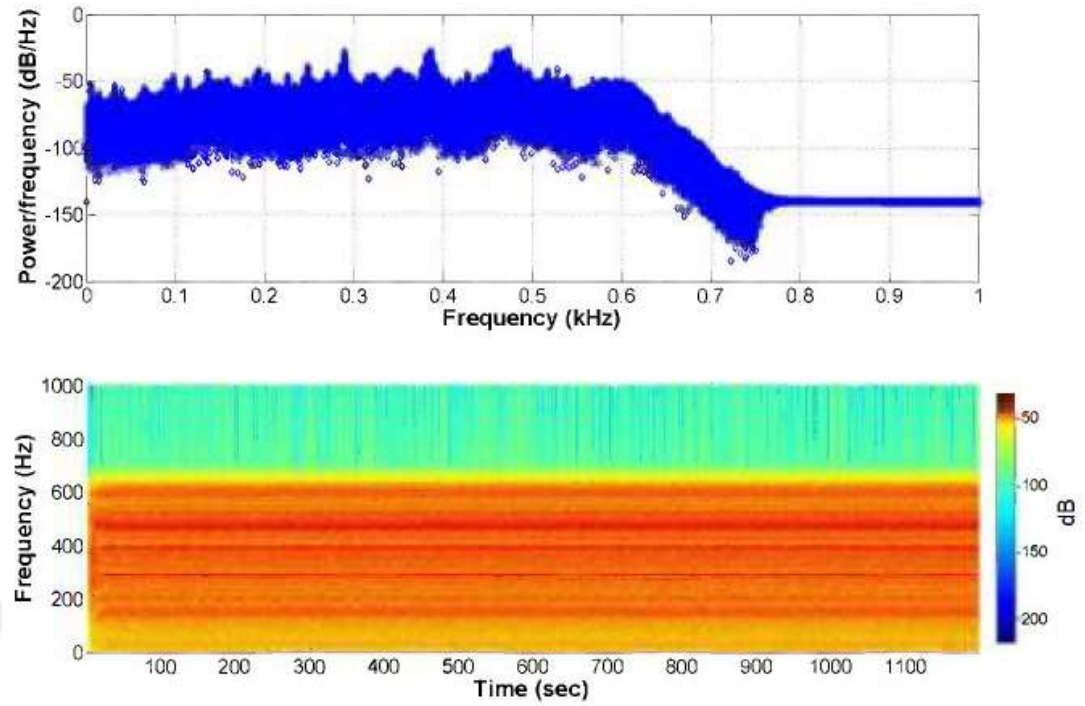

Figure 1.4 : An example power spectral density (top) and frequency spectrogram (bottom) from Walter (2012).

The study mainly focused informing TBM operator on boulder impacts, and this required obtaining a boolean or numeric value, which lead to creating a boulder detection variable (BDV) by Buckley (2015). Vibrations were recorded while TBM was at the station before starting the tunnel excavation by rotating the cutterhead to understand the effect of vibrations introduced by the TBM components and, it was seen that gearbox and motors create considerable noise, however, hitting the cutterhead with a hammer created broadband peaks in frequency spectrogram. Taking this information to the consideration the author decided to define the BDV value, as the summation of PSD frequency components, especially in the frequency ranges that are less effected by the ambient noise. As the peaks in the frequency range increases on impacts, BDV is also increases (Figure 1.5), alerting the operator. In addition to frequency analyses, time-domain analyses were also provided in the study.

The research concluded that the number of impacts were directly proportional to the percent of till-like deposits in the area which the cobbles mostly present and system worked as expected. Moreover, it was found that cutterhead rotational speed and earth pressure, respectively, had the two highest influences on ambient vibration apart from the geology. One of the major limitations mentioned by the author was the availability of the real ground condition data, since the developed systems required a good baseline

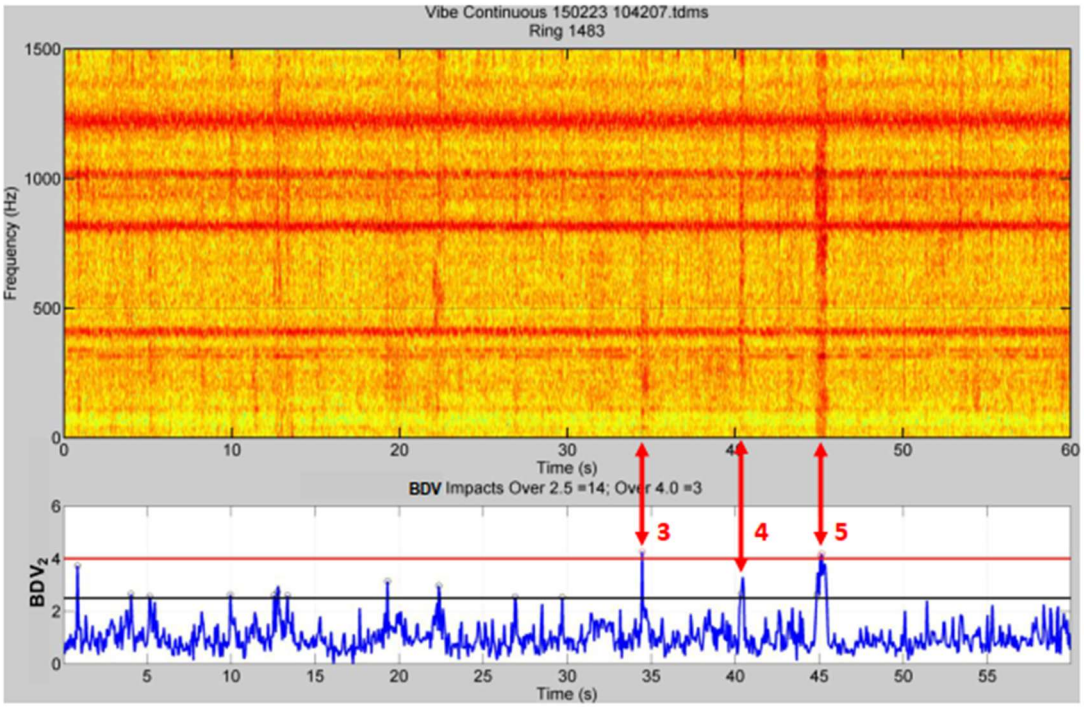

Figure 1.5 : Impacts shown on the frequency spectrum (numbered 3 to 5) and calculated boulder detection values (Buckley, 2015).

and further calibration for better predictions. Most of the researchers rely on project/tender geological data or the contractors' site crew for providing the in-situ geological condition data, which is not always available. As understanding the geological conditions is very important for tunneling, the contractors involved with the boulder detection system are also planning to utilize the system for their next project (Hunt and Frank, 2021).

Recently, Liu et al. (2022) installed accelerometers on back of the pressure bulkhead of a 6.68m EPB TBM and, investigated the vibration characteristics and patterns under different ground conditions. Even though the measurements were only performed at eight rings (12 meters), which can be considered as a quite limited dataset, the authors reported that vibration characteristics were sensitive to changes in excavation face conditions. During the study, acceleration magnitude, peak acceleration and RMS acceleration were utilized for time domain analyses and, FFT and continuous wavelet transform (CWT) were utilized for frequency domain analyses. The authors used FFT for understanding the frequency content of ambient noise, while CWT was used for analyzing the excavation vibration data. CWT is similar to short-time Fourier transform that is used for spectrograms but differs by having variable window length for different frequency contents (Liu et al., 2022). The authors reported that maximum

acceleration magnitudes were 0.25g and 5g for soil and hard rock, respectively. Furthermore, it was observed that as the hard rock ratio increased, the vibration amplitudes also increased. In soil conditions the peak frequencies were concentrated between 650 to 750 Hz, in contrast, during the excavation of hard rock the peaks were observed in a broader frequency range. It is also noted that, impacts on the cutterhead observed as broadband peaks in the frequency spectrum (Figure 1.6).

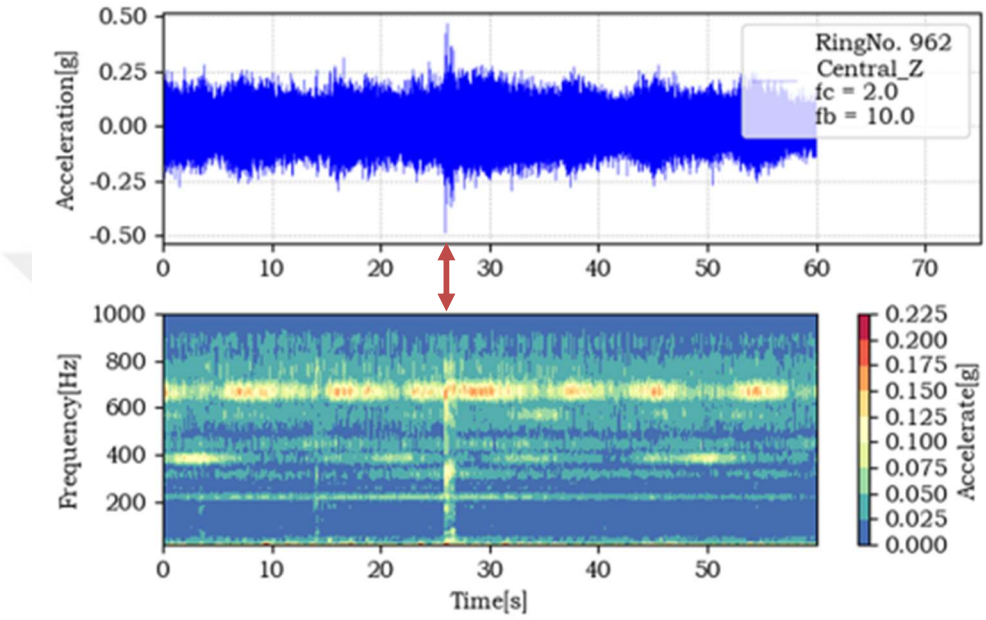

Figure 1.6 : An impact seen on the time domain and frequency spectrum (Liu et al., 2022).

Vibration patterns at different points of the bulkhead showed similar tendencies but with different amplitudes according to Liu et al. (2022). It is also seen that acceleration patterns matched at the hard rock sections of the excavation face in the mixed face conditions. Every time a disc group comes into contact with the hard rock section of the face, vibration amplitudes increased. The same dataset used by Liu et al. (2021) to investigate the usability of deep recurrent neural networks (RNNs) and convolutional neural networks (CNNs) for vibration-based ground identification. A real-time analysis framework was developed for identifying the ground type from vibration signals and the results were validated. The authors concluded that, models are capable of on predicting the ground conditions with different accuracies, however, the data length was quite limited and further studies are required for better prediction.

Huang et al. (2008) investigated the feasibility of utilizing vibration data within a multi-point detection system for condition monitoring of a TBM's main bearing. Data

was collected from different operating conditions such as normal operation, lubrication failure, defect etc. and it was analyzed using fuzzy logic. The authors concluded that their method was effective in diagnosing different types of faults in the main bearing.

1.3 Research Methodology and Framework

To achieve the research objectives, the study is divided into three main parts; recording system development, field studies and lastly, laboratory studies.

1.3.1 Recording system development

A custom vibration recording system was developed, consisting of accelerometers, digital-to-analog converters, and a data recording computer running dedicated software to record vibrations occurred during TBM excavation and laboratory studies. This phase of the study focused on hardware selection and the development of the data recording software with essential features. Throughout the research, the recording system was progressively upgraded with new software functionalities.

1.3.2 Field studies

The vibration monitoring system was installed to four EPB TBMs in three project sites; Mecidiyekoy-Mahmutbey Metro Line, Umraniye-Atasehir-Goztepe Metro Line, European Region Potable Water Transmission Tunnel Project. The details of these projects are presented in the Section 2.

The acceleration data (in three axes, x, y, z) recorded for over 6 km of TBM excavation in different geological conditions, which is the largest dataset in the literature. In addition to the vibration data, TBM operational parameter data (thrust, torque, cutterhead speed, penetration), shift reports, cutter change logs were obtained from the sites. Muck samples were taken from the conveyor belt for better understanding the geological conditions. Then, the vibration data, together with the other information, sorted and analyzed with custom Matlab scripts.

The relationships between the vibrations occurred during TBM excavation (RMS and RMS_{int} vibrations), geological conditions and variations (lithological changes, mechanical properties of the rocks and the presence of soils), TBM operational parameters (thrust, torque, cutterhead speed, penetration) and cutter conditions (disc changing locations) were investigated. In addition, the effects of EPB TBM diameter

and accelerometer positions and types on the vibration characteristics were also evaluated.

1.3.3 Laboratory studies

The laboratory investigations conducted in this study can be divided into two parts. The first part involves the full-scale linear rock cutting experiments to record the vibrations occurred during the rock cutting together with applied tool forces to the rock. This experiment was realized using the full-scale linear rock cutting machine (FLCM) located in Istanbul Technical University, Mining Engineering Department laboratories. The machine was equipped with accelerometers, and rock cutting experiments were realized using three different rock samples. The vibration monitoring system developed for TBMs was slightly modified to enable the recording of vibrations in the FLCM experiments. The acquired data analyzed using customized Excel and Matlab scripts.

In the second part of the laboratory studies, the physical and mechanical properties of the rock samples used for FLCM experiments were determined. The tests were also applied to the muck samples obtained during the field studies where possible. Uniaxial compressive strength, point load strength, indirect tensile strength, elasticity modulus, seismic P and S-wave velocities, Schmidt hammer hardness, and Shore sclerescope hardness tests were performed on at least three core samples for each sample for obtaining consistent results.

The acquired information from the physical and mechanical tests, as well as the vibration data obtained from the FLCM tests, were used to investigate the relationships between vibrations generated during rock cutting, tool force data, rock properties, and cutting geometry.

1.4 Limiting Factors

Several limitations were identified during the study that should be acknowledged. One of them was insufficient information regarding the in-situ geological conditions. In all three projects where TBM vibrations were recorded within the scope of this study, provided geological reports did not accurately reflect the precise geological conditions. Moreover, lithological changes occurring over short distances often remain undetectable on geological profiles. To mitigate this limitation, attempts were made to

obtain muck samples with the help of the site crews of the projects. However, the success of this process was only moderate due to the workload of the personnel.

Conducting full-scale rock cutting tests entails a substantial amount of work, involving sample acquisition, preparation, and execution of the tests. Due to the large sample sizes required for the tests, it was not always possible to find suitable sample. Consequently, only three rock samples were tested. Although some relationships between vibrations and other variables were identified, increasing the number of tests is essential to enhance statistical accuracy.

Financial considerations also impacted the project, as the equipment required a significant investment. At the beginning, the accelerometers and data recording system used in the study were basic, which restricted the amount of information that could be gathered from the first site. Even though later on the system was upgraded and improved, the limited budget of the project restrained the purchases, resulting in accelerometers with lower measurement ranges for some of the TBMs.

2. INFORMATION ON THE TBM PROJECTS

During the course of this research, the vibration recording systems were employed in three different tunnel construction projects. In this section, detailed information is provided about these projects, along with a description of the installation process for the accelerometers at each site.

2.1 Mecidiyekoy-Mahmutbey Metro Line

Mecidiyekoy – Mahmutbey Metro Line is an 18.5 km metro line that was excavated with a combination of NATM and EPB TBMs, in Istanbul. The metro line traverses a densely populated area with older buildings predominating. Furthermore, specific sections of the tunnel alignment encounter challenges due to problematic sandy soil conditions (Figure 2.1).

Figure 2.1 : Location of the Mecidiyekoy-Mahmutbey Metro Line.

In this project, the proof-of-concept TBM vibration recording system was initially installed on a TBM. The primary objective was to investigate the feasibility of employing vibration measurements for real-time detection of geological variations during tunneling operations.

2.1.1 TBM specifications

During the excavation of the metro line, three TBMs were employed, however, the vibration data recording system was installed to only one of them. Consequently, the information solely for this individual TBM will be presented. The TBM was Lovat branded 6.56m EPB TBM and it will be referred as TBM 1 throughout the study. The specifications of the TBM 1 are given in Table 2.1.

Table 2.1 : Specifications of the TBM 1.

Manufacturer and model of TBM	Lovat - RME257SE Series 18000
Excavation diameter	6.56 m
Number, diameter and type of disc cutters	#46 – 15.5" V type
Torque capacity	4500 kNm at 2.5 rpm
Cutterhead power (motor type)	8 x 137.5 = 1100 kW (hydraulic)
Thrust capacity	55000 kN
Segment length	1.4m

It is worth noting that during the excavation process, the cutterhead of TBM 1 sustained extensive damages, leading to a cutterhead maintenance on ring 1580 (Ates et al., 2016; 2017). This maintenance involved replacing damaged disc cutters and ripper housings, resulting in a notable difference in vibration characteristics before and after the intervention.

2.1.2 Geological conditions of the studied section

The studied section in this project was between Karadeniz Mahallesi and Tekstilkent Stations, and characterized by alteration of sandstone, claystone, and siltstone with varying strengths (Polat, 2014; 2015). Table 2.2 provides a summary of the physical-mechanical and rock mass properties of the encountered lithological units, and Figure 2.2 shows the geological profile of the section. Due to the limitations of the vibration recording system employed at this site, only a select portion of the acquired data will be presented in this study.

Table 2.2 : Properties of the rocks encountered along the Mecidiyekoy-Mahmutbey Metro Line (Artson Geoteknik, 2014).

Lithology	Sandstone (w1-2)	Sandstone (w3-4)
Unit weight (g/cm^3)	2.60	2.60
Cohesion (kPa)	150	110
Friction angle (°)	36	33
Elastic modulus (MPa)	1860	1325
Poisson's ratio (-)	0.30	0.30
Uniaxial compressive strength (MPa)	21	12
Average RQD (%)	25	13
Average GSI (-)	50	40
Average Q (-)	1.25	0.50
Average RMR (-)	42	35

w1-2: Slight alteration, w3-4: Moderate/High alteration

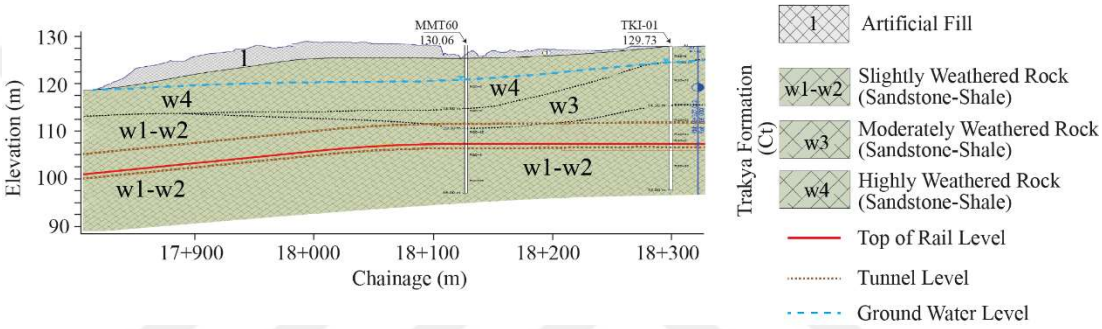

Figure 2.2 : Geological profile of the section where vibration recording was performed in Mecidiyekoy – Mahmutbey Metro Line Construction Site (Artson Geoteknik, 2014).

During the excavation, rock samples were collected from the belt conveyor and Schmidt hammer tests conducted on these samples. Even though the tender geological profile shows fresh sandstone-shale units along the studied section, it was seen that the area was composed of sandstone units from fresh to highly weathered states. The result of the Schmidt hammer tests and excavated lithological units are presented in Table 2.3.

Table 2.3 : Lithological units and Schmidt hammer test results (Mecidiyekoy-Mahmutbey Metro Line).

Ring No (Start)	Ring No (End)	Unit No	Lithological Unit (Excavated)	Schmidt Hammer Test Result (Converted to UCS)[1]
1426	1520	1	Sandstone (w3-w4)	43 (±21)
1521	1769	2	Sandstone (w1-w2)	72 (±15)

[1]Schmidt hammer tests were performed in accordance with ISRM (2007) suggestions.

2.1.3 Accelerometer setup

A very basic data recording system and software were utilized including two DE-ACCM3D model accelerometers coupled with a NI USB-6009 analog-digital converter, which were mounted behind the pressure bulkhead of the TBM, and vibrations were recorded continuously for 326 rings. Figure 2.3 and Figure 2.4 show the protective cases, locations of the accelerometers in the TBM, as well as directions of axes used during analyses.

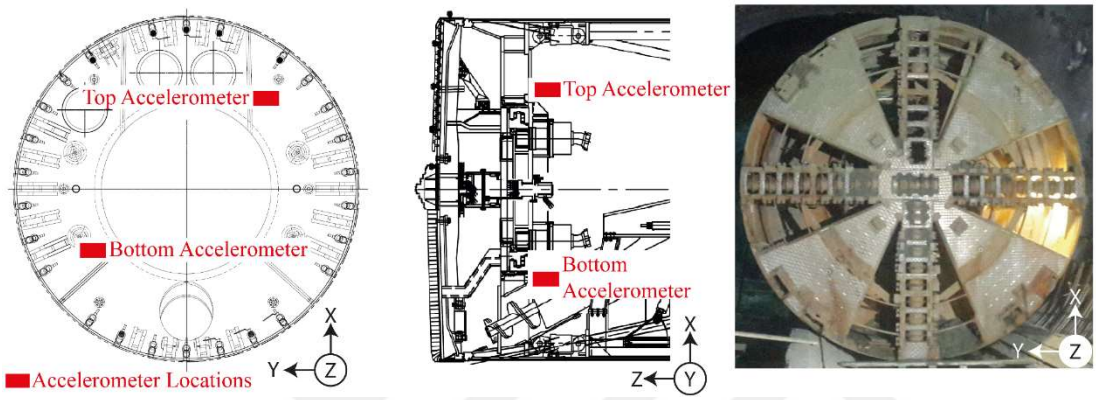

Figure 2.3 : Approximate accelerometer locations on TBM 1 and cutterhead photo.

Figure 2.4 : Installed accelerometers with their protective cases (TBM 1).

2.2 Umraniye-Atasehir-Goztepe Metro Line

Umraniye-Atasehir-Goztepe Metro Line is a 10.4 km line with 9 stations, which was constructed by four EPB TBMs with a diameter of 6.56 m, in Istanbul. The line starts from Goztepe Station at Goztepe Parki at a depth of 20m and then reaches Sahrayi-Cedid Station. From there, the line continues to climb towards north, reaching; Yeni Sahra Station, Atasehir Station, Finans Merkezi and Soyak Yenisehir Station. After this point, the line slightly curves to the west and reaches Atakent Station (Geodata Engineering, 2016). The line, running to the north again, arrives at Umraniye (renamed

as Carsi) Station and ends at Kazim Karabekir Station (Figure 2.5). Internal diameter of the tunnel is 5.7 meters.

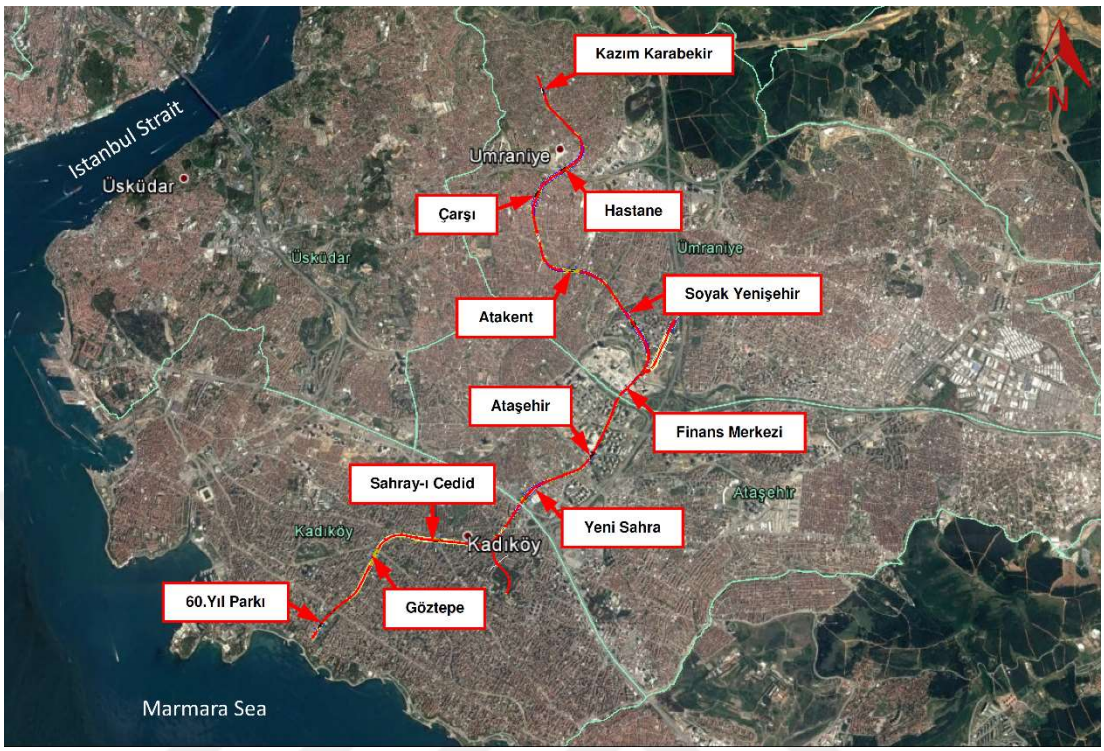

Figure 2.5 : Location of the Umraniye-Atasehir-Goztepe Metro Line.

2.2.1 TBM specifications

The accelerometers were installed to the TBMs excavating Northwards direction, and they will be mentioned as TBM 2 and TBM 3, respectively. All TBMs used in this line had the same specifications, which are listed in Table 2.4.

Table 2.4 : Specifications of the TBM 2 and 3.

Manufacturer and model of TBMs	TBM 2: Terratec - S67 TBM 3: Terratec - S68
Excavation diameter	6.56 m
Number, diameter and type of disc cutters	#47 - 17” CCS type
Torque capacity	5459 kNm (@1.68 RPM)
Cutterhead power (motor type)	6 x 160 = 960 kW (VFD)
Thrust capacity	40000 kN
Segment length	1.5 m

2.2.2 Geological conditions of the studied section

The studied section consisted of Pelitli and Pendik Formations in addition to some dykes and crushed zones. Pelitli Formation in the area of interest was composed of claystone and sandy-limestone with slight to medium weathering (w1-2). There were

also andesite and diabase dykes, which were generally crushed (w4-5). In the sections where Pendik Formation existed, the tunnel alignment was composed of claystone, siltstone-claystone, and claystone-limestone units. However, in addition to the weathered dykes, this section also had fresh dykes (w1-2) with very high uniaxial compressive strength of 210 MPa (Geodata Engineering S.p.A., 2016; Yuksel Proje, 2017). The presence of fresh dykes was not clear in the geological reports; however, they were confirmed during the excavation.

Similar to the TBM 1's project site, during the excavation of this line, rock samples were taken from the belt conveyor and laboratory analyses of the samples for the andesite dykes were performed (Palakci and Ugur, 2021). The physical-mechanical and rock mass properties of the units encountered in the excavated section are summarized in Table 2.5.

Table 2.5 : Rock mass properties of Umraniye-Atasehir-Goztepe Metro Line (Yuksel Proje, 2017; Palakci and Ugur, 2021).

	Pelitli Formation (SDp)	Pendik Formation (Dpk/ Dpkz)	Volcanic Dykes (w1-w2)	Volcanic Dykes (w4-w5)
Unit weight (g/cm^3)	26	26	27[1]	25
Elasticity modulus (MPa)	9000	6000	15000	8000
Uniaxial compressive strength (MPa)	30	25	210[1]	15
Average RQD (%)	13	13	-	3
Average GSI (-)	50	46	-	27
Average RMR (-)	55	51	-	32

[1] Values are taken from Palakci and Ugur (2021).
Note: Uniaxial compressive strength and elasticity modulus tests were performed according to TS EN 1900 (Turkish Standards Institution, 2006a,b,c) and TS 2030 (Turkish Standards Institution, 1975), respectively by Yuksel Proje (2017) and according to TS 1900 (Turkish Standards Institution, 2006a,b,c) by Palakci & Ugur (2021).

The lithological units excavated by the TBM 2 and 3 in addition to the information obtained from the boreholes in the area, are presented in Table 2.6. The boundaries of these lithological units determined by combining the project geotechnical report, TBM operational and performance parameters and the in-situ geological data recorded by the TBM crew during the excavation. The geological profile of the alignment where vibration data was recorded can be seen in Figure 2.6.

Table 2.6 : Lithology and borehole information for TBM 2 and TBM 3 (Geodata Engineering S.p.A., 2016; Yüksel Proje, 2017).

Lithological Units		Borehole Information					
Unit No	Lithological Unit (Excavated)	Borehole Chainage (km)	Borehole No	Crown Depth (m)	UCS (MPa)	RQD (%)	GSI (-)
1	Siltstone-Claystone	9+250	GU-33	35	56	61	40
2	Dyke (w4-w5)	9+450	GAU-33	43	-	15	15
3	Sandstone-Limestone	9+450	GAU-33	45	37	82	-
4	No Data	-	-	-	-	-	-
5	N5 Crossover	-	-	-	-	-	-
6	Claystone	10+060	GU-35	51	90	79	70
7	Claystone-Dyke (w1-w2)	-	-	-	-	-	-
8	Claystone	-	-	-	-	-	-
9	Dyke (w1-w2)	-	-	-	-	-	-
10	No Data	10+490	GAU-35[1]	-	21	56	-
		10+515	GAU-36[1]	-	34	15	-
11	Claystone	-	-	-	-	-	-
12	Carsi Station	10+525	GU-36[1]	-	6	25	15
13	Dyke (w4-w5)	10+580	GAU-37	35	90	22	20
		10+750	GAU-38	42	62	25	20
		10+780	GU-38[2]	45	15	10	30
14	Siltstone-Claystone	-	-	-	-	-	-
15	Dyke (w4-w5)	-	-	-	-	-	-
16	Siltstone-Claystone	-	-	-	-	-	-
17	Hastane Station	-	-	-	-	-	-
18	Siltstone-Claystone	11+090	GAU-39[1]	-	18	37	-
		11+160	GAU-40	37,5	14	47	-
		11+170	GU-40	37,5	71	68	55
19	Sandstone-Claystone	-	-	-	-	-	-
		11+280	GU-41	34	85	80	55
20	Claystone	11+470	GAU-42	31	50	89	-
		11+650	GU-42	35	60	77	40
21	Dyke (w1-w2)	11+850	GAU-43	37,5	100	80	60
22	Sandstone-Claystone	12+010	GU-43	46	60	80	60
23	Dyke (w4-w5)	-	-	-	-	-	-

[1] Borehole is in station.
[2] Borehole does not reach the tunnel level.
Note: The data on boreholes numbered as "GU" were obtained by Geodata Engineering S.p.A. (2016) according to ISRM 1979 (Bieniawski & Bernede, 1979) and numbered as "GAU" obtained by Yuksel Proje (2017) according to TS EN 1926 (Turkish Standards Institution, 2007)

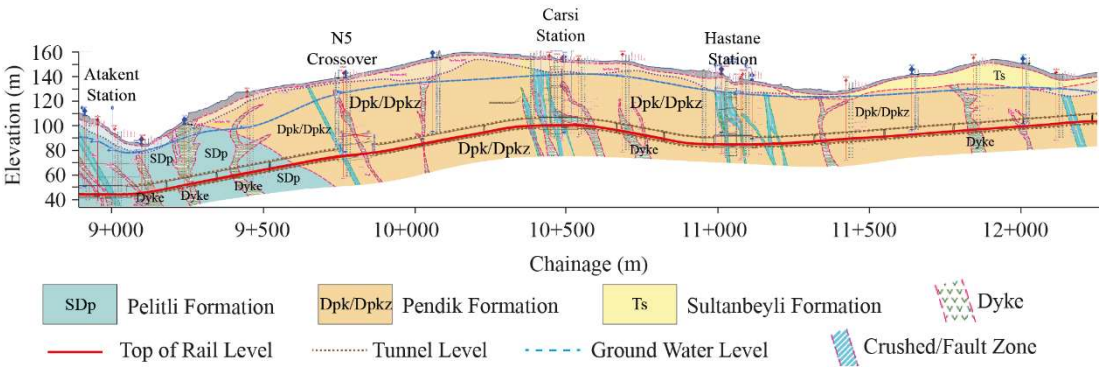

Figure 2.6 : Geological profile of the section where vibration recording was performed in Umraniye-Atasehir-Goztepe Metro Line Construction Site (Yüksel Proje, 2017).

2.2.3 Accelerometer setup

Piezoelectric accelerometers from PCB Electronics (model no: 356A17) were used on TBM 2, while MEMS type accelerometers (model no: ADXL354BZ) from Analog Devices were used on TBM 3. The use of different accelerometer types in TBMs excavating in parallel (twin tube) tunnels allowed to understand the effect of accelerometer types on the data quality. The placement of the accelerometers, which were very similar on both TBMs, can be seen in Figure 2.7 (as well as directions of axes used during analyses), while the photographs of the installed system on TBM 2 can be seen in Figure 2.8 and Figure 2.9.

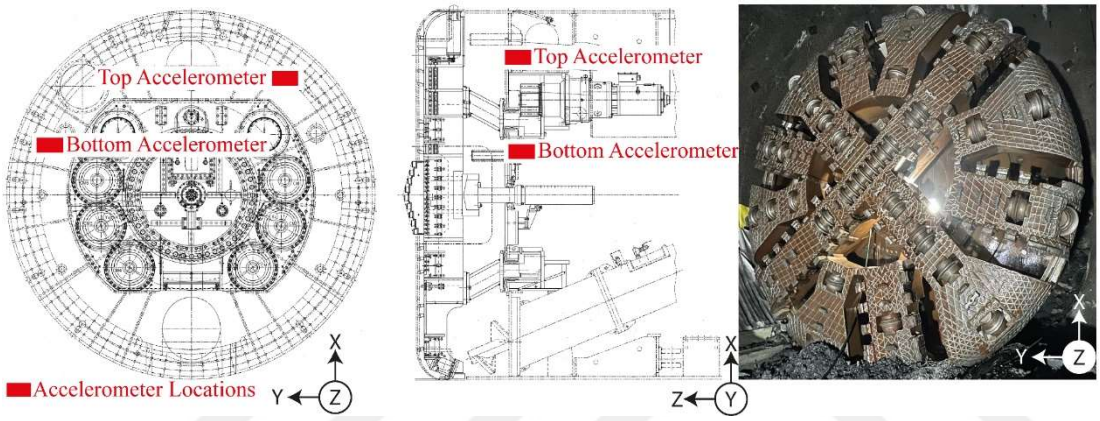

Figure 2.7 : Approximate accelerometer placement on TBM 2 and TBM 3.

Figure 2.8 : Accelerometer bases and steel cover (TBM 2).

Figure 2.9 : Installed accelerometers (TBM 2).

2.3 European Region Potable Water Transmission Tunnel Project

European Region Potable Water Transfer Tunnel passes from Kagithane, Gaziosmanpasa, Bayrampasa, Gungoren, Bahcelievler, Kücükcekmece municipalities and has a length of 20.8km (Figure 2.10). 19.5 km of the total tunnel length had been excavated with two TBMs and will have 4 m internal diameter (EMAY Uluslararası Mühendislik ve Müsavirlik A.S., 2018).

Figure 2.10 : Location of the European Region Potable Water Transfer Tunnel.

2.3.1 TBM specifications

Different from the other projects, the excavation diameter is 4.8m which allows making a comparison between the vibration patterns of EPB TBMs having different excavation diameters. The specifications of the TBM used in the project are given in Table 2.7 and the TBM will be mentioned as TBM 4 throughout the study.

Table 2.7 : Specifications of the TBM 4.

Manufacturer and model of TBM	Lovsuns - RME188SE Series 45300
Excavation diameter	4.8 m
Number, diameter and type of disc cutters	#31 - 17” CCS type
Torque capacity	4017 kNm (@1.90 RPM) 2181 kNm (@3.50 RPM)
Cutterhead power (motor type)	4 x 200 = 800 kW (VFD)
Thrust capacity	28480 kN
Segment length	1.5 m

2.3.2 Geological conditions of the studied section

The tunnel route mainly passes from slight to medium weathered siltstone-shale formation while alluvium, clay, and sandstone-shale formations were also present (EMAY Uluslararası Mühendislik ve Müsavirlik A.S., 2018). The geological report indicated the presence of crushed or completely weathered zones and fault zones along the line. The physical-mechanical and rock mass properties of the encountered lithological units in the excavated section are given in Table 2.8, while the geological profile from the tender stage is given in Figure 2.11.

Table 2.8 : Rock and soil properties of the lithological units encountered in European Region Drinking Water Transfer Tunnel Project (EMAY Uluslararası Mühendislik ve Müsavirlik A.S., 2018).

Lithology	Siltstone – Shale (w2-3)	Sandstone – Shale (w3-4)	Clay
Unit weight (g/cm^3)	2.60	2.50	1.90
Cohesion (kPa)	500	121	150
Friction angle (°)	44	34.8	-
Elastic modulus (MPa)	2420	386	31.5
Poisson's ratio (-)	0.24	0.28	-
Uniaxial compressive strength (MPa)	48	28	-
RQD (%)	39	12	-
GSI (-)	50.7	30.6	-
Q (-)	0.858	0.038	-
RMR (-)	41	25.6	-
SPT (N60)	-	-	12

Note: The tests were performed in accordance with TS 1900-1 and 2 (Turkish Standards Institution, 2006b,c) by Analiz Engineering and Cons. (2018).

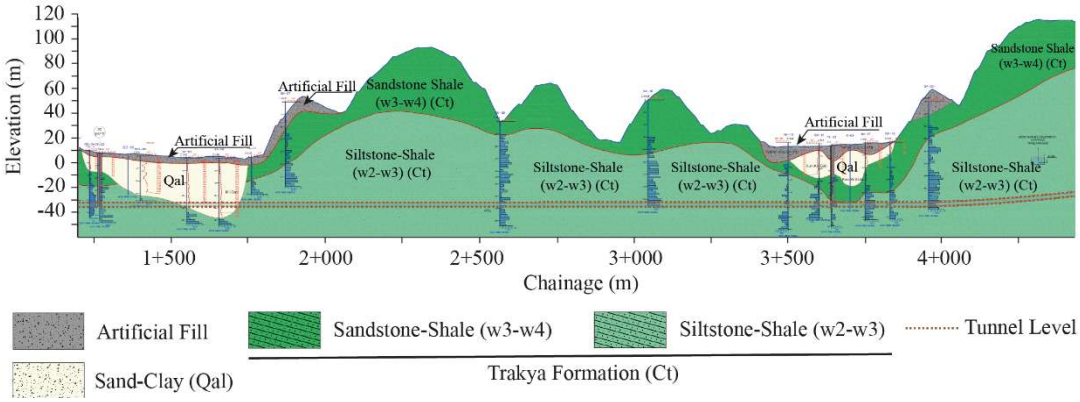

Figure 2.11 : Geological profile of the section where vibration recording was performed in European Drinking Water Transmission Project Construction Site (EMAY Uluslararası Mühendislik ve Müsavirlik A.S., 2018).

In addition to the tender geological data, a detailed in-situ geological information was provided by the site crew according to the logs taken during the excavation. Table 2.9 summarizes the lithological units and their starting and ending points in terms of ring numbers. Unique numbers to these lithological units are also provided in the table.

By using the vibration recording system's trigger and e-mail functions rock samples were taken during excavation from the belt conveyor on the locations with high acceleration, and point load tests were conducted on these samples based on ASTM D5731-02 (ASTM, 2016). The results of these point load tests are presented in Table 2.10.

Table 2.9 : Lithological unit starting and ending locations according to site logs obtained from European Region Potable Water Transmission Tunnel Project site.

Ring No (Start)	Ring No (End)	No	Lithological Unit	Ring No (Start)	Ring No (End)	No	Lithological Unit
0	23	1	Sandstone	1029	1220	18	Siltstone
24	37	2	Sandstone-Claystone	1221	1230	19	Alluvium
38	70	3	Sandstone	1231	1313	20	Siltstone-Claystone
70	220	4	No Data	1314	1325	21	Sandstone-Siltstone
221	265	5	Alluvium	1326	1400	22	Siltstone-Claystone
266	440	6	Alluvium-Siltstone	1401	1502	23	Sandstone-Siltstone
441	573	7	Claystone-Siltstone	1503	1514	24	S3 Shaft
574	618	8	Sandstone	1515	1600	25	Siltstone-Claystone
619	645	9	Sandstone-Siltstone	1601	1652	26	Sandstone-Siltstone
646	673	10	Sandstone	1653	1737	27	Siltstone-Claystone
674	683	11	Siltstone	1738	1760	28	Sandstone-Siltstone
684	755	12	Sandstone	1761	1800	29	Siltstone-Claystone
756	860	13	Sandstone-Siltstone	1800	1849	30	Alluvium
861	914	14	Sandstone	1850	1961	31	Siltstone-Claystone
915	928	15	Siltstone	1962	1965	32	Sandstone-Siltstone
929	975	16	Sandstone	1966	1999	33	Siltstone-Claystone
976	1028	17	Sandstone-Siltstone				

Table 2.10 : Point Load Test results of the muck samples obtained from European Region Potable Water Transmission Tunnel Project site.

Ring No	Lithological Unit	Point Load Index (Is_{50})
700	(12) Sandstone	10.44
1058	(18) Siltstone	5.62
1116	(18) Siltstone	3.91
1406	(23) Sandstone-Siltstone	8.86
1490	(23) Sandstone-Siltstone	8.76
1652	(27) Siltstone-Claystone	7.16
1758	(28) Sandstone-Siltstone	9.18

2.3.3 Accelerometer setup

TBM 4 was fitted with two ADXL354BZ model accelerometers coupled with a NI USB-6009 analog-digital converter. Figure 2.12 shows the locations of the accelerometers in TBM 4, as well as the directions of axes used during analyses. Installed accelerometers are shown in Figure 2.13.

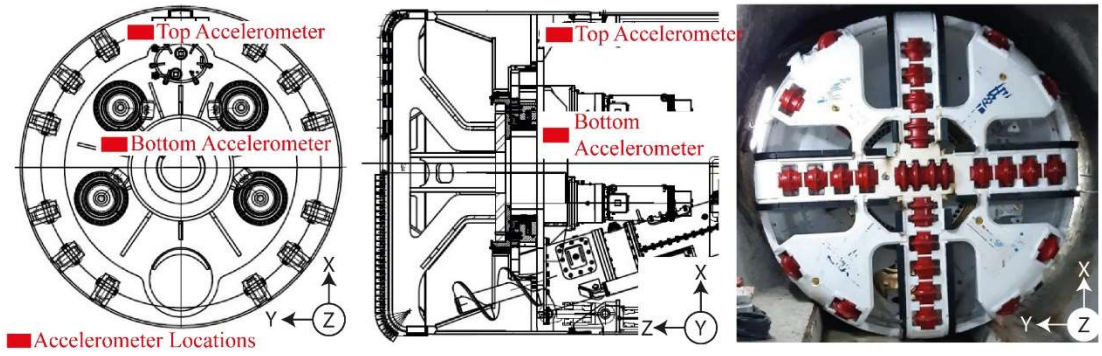

Figure 2.12 : Approximate accelerometer locations on the TBM 4.

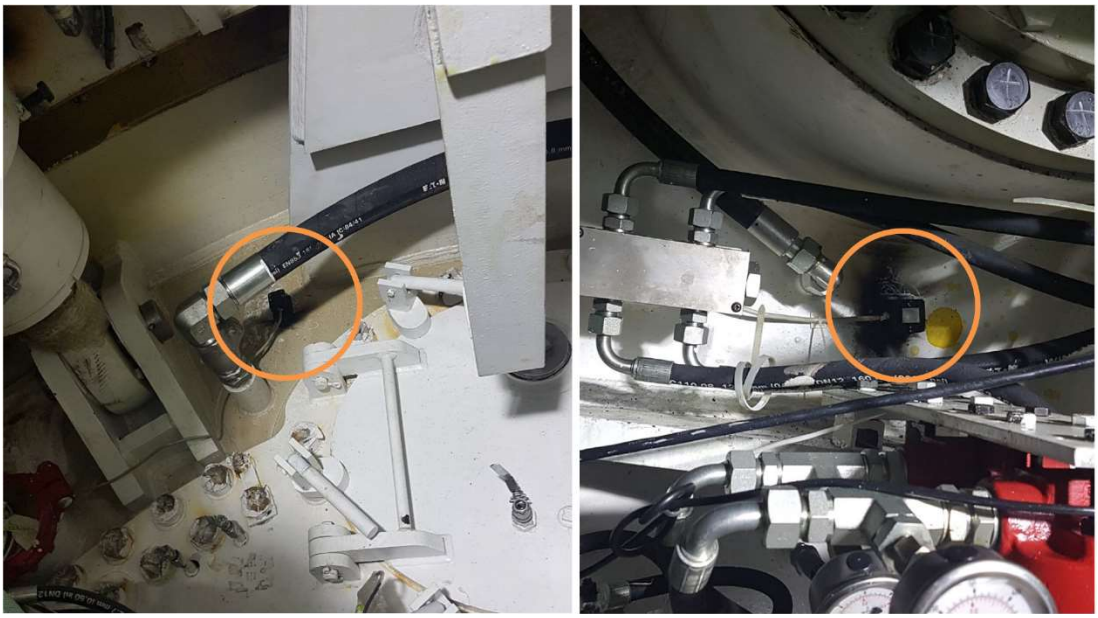

Figure 2.13 : Installed accelerometers (TBM 4).

3. VIBRATION RECORDING SYSTEM, METHODOLOGY AND ANALYSIS TECHNIQUES

In this section a comprehensive overview of the vibration recording software and hardware composition, as well as the data recording and processing methodology, including the analysis techniques employed in the study will be presented.

3.1 Vibration Monitoring System Composition

The vibration monitoring system consisted of three main parts: triaxial analog accelerometers, analog to digital converter and a data recording computer. Different systems had been used throughout the study starting with a very basic one with only data recording function; later on, it turned into a complete system with multiple functions like e-mail warnings on the detection of accelerations higher than set thresholds. The data was analyzed on later stages using Matlab software with custom-made scripts.

3.1.1 Accelerometers

Various types of triaxial analog accelerometers and analog to digital converters had been used throughout the study for measuring the vibrations. As the study evolved, better specified accelerometers started to be used.

The first set of accelerometers used for TBM vibration recording was DE-ACCM3D (Dimension Engineering, 2011) which has 3g measurement range, followed by ADXL354BZ (Analog Devices, 2017) with a 4g measurement range (Figure 3.1). In addition, during the laboratory experiments, ADXL356CZ (Analog Devices, 2020) with 40g measurement range was also used. These accelerometers are Micro-Electro-Mechanical Systems (MEMS) type, which is a fabrication technology that has been used to manufacture accelerometers and other sensors. This manufacturing method has reduced the production costs and made the smaller accelerometers possible. Owing to their cost-effectiveness and relatively small dimensions, capacitive MEMS accelerometers are frequently available as surface-mount components, facilitating

direct installation onto printed circuit boards. However, this type of accelerometers generally suffers from a poor signal to noise ratio and limited bandwidth (Hanly, 2016).

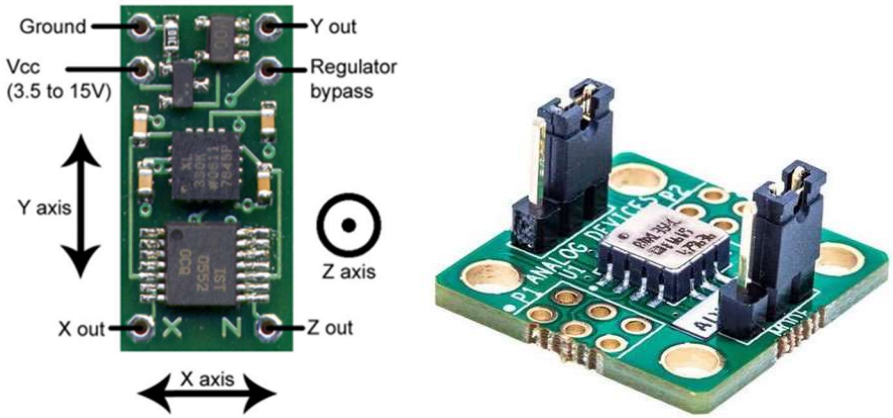

Figure 3.1 : Dimension Engineering DE-ACCM3D (left) and Analog Devices ADXL354BZ (right) accelerometer.

Since these accelerometers did not come with an enclosure, custom-made waterproof enclosures were produced for protection against water and impacts (Figure 3.2).

Figure 3.2 : Waterproof accelerometer housing.

MEMS type accelerometers have a sensing element mass that is suspended on flexures attached to a frame. This configuration forms two air gap capacitors between the mass and the upper/lower plates (Figure 3.3). As the mass moves with the application of acceleration, one air gap decreases and the other increases, creating a change in capacitance proportional to acceleration (Sinha et al., 2014; Harris & Piersol, 2002).

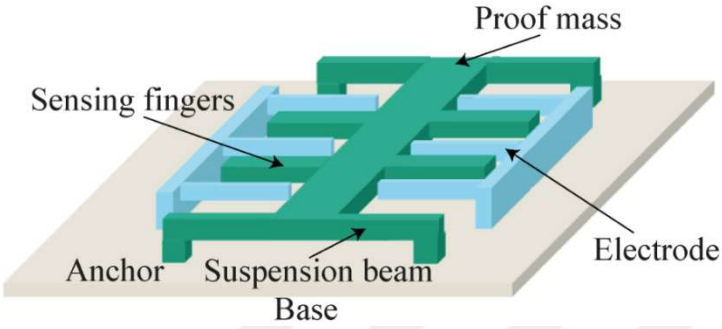

Figure 3.3 : Sensing elements of MEMS-type accelerometers.

MEMS type accelerometers record static acceleration in addition to dynamic one, which is the acceleration induced by Earth's gravity. Normally it is possible to eliminate this acceleration during post-processing; however, with the addition of the calibration function to the software used in the present study, static acceleration on all channels was set to 0g, which reduced post-processing time.

As the study progressed, more durable and industrial type piezoelectric accelerometers from PCB Electronics, model 356A17, were utilized (PCB Electronics, 2008) (Figure 3.4a). These accelerometers were ceramic shear type piezoelectric accelerometers that utilize flat plate shear sensing elements which have a 10g measurement range. Cross section of a typical shear-type piezoelectric accelerometer can be seen in Figure 3.4b (Hanly, 2016).

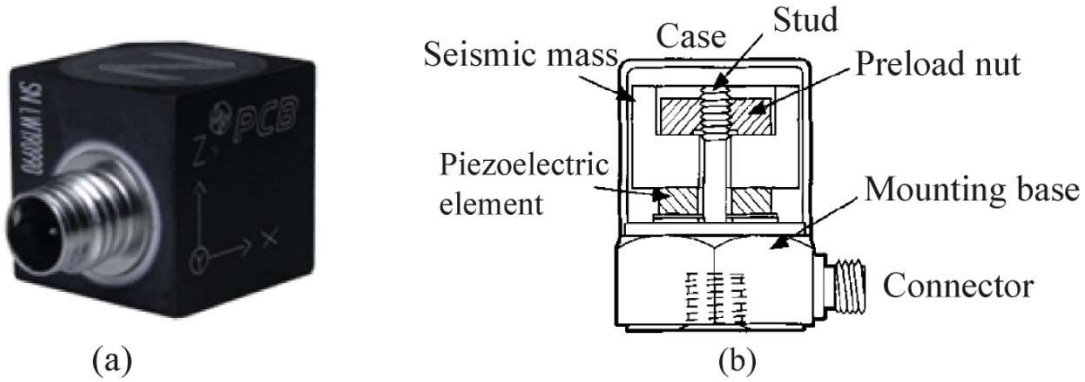

Figure 3.4 : 356A17 model piezoelectric accelerometer, (a) sensing elements of piezoelectric type accelerometers (b) (Sinha et al., 2014; Harris & Piersol, 2002).

Piezoelectric accelerometers use a polarized ceramic sensing element, lead zirconate titanate, producing a proportional electric charge or output under acceleration. Their sensitivity and frequency ranges are higher than the other accelerometers used in this study, in addition to their lower noise characteristics (Sinha et al., 2014; Harris & Piersol, 2002).

It is very important to select a suitable accelerometer for the signal in the case of using piezoelectric accelerometers. If input amplitudes and input frequencies are higher than the piezoelectric accelerometer's capacity, this input causes saturation on the accelerometer's amplifier, which causes the sensor to enter an overload recovery state, and no meaningful data can be acquired during the reset (Lindstrom, 2019) (Figure 3.5).

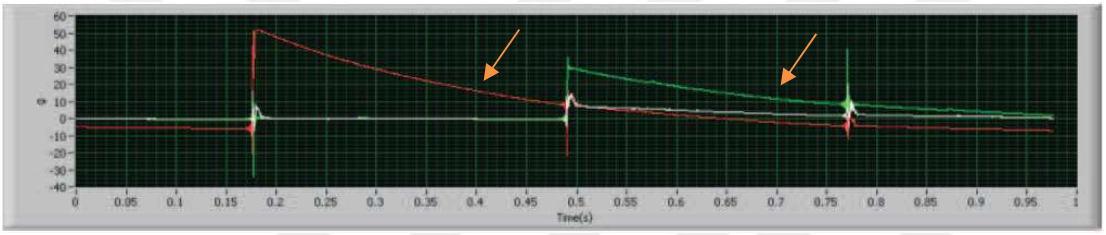

Figure 3.5 : Piezoelectric accelerometer saturation problem.

MEMS type accelerometers do not have this issue. The problem of overload recovery state was seen in this study during data recording from time to time, especially in very hard rock conditions.

The accelerometers used for vibration measurements/recordings during the study, and their specifications are given in Table 3.1.

Table 3.1 : Accelerometers used in during the study.

Manufacturer	Dimension Engineering	Analog Devices	Analog Devices	PCB Electronics
Model	DEACCM 3D	ADXL354BZ	ADXL356CZ	356A17
Type	MEMS	MEMS	MEMS	Piezoelectric
Number of accelerometers	2	4	1	2
Axes	x,y,z	x,y,z	x,y,z	x,y,z
Sensitivity (mV/g)	333	200	20	500
Measurement range (±g)	3	4	40	10
Frequency range (Hz)	0-500	0-1500	1500	0.5-3000
Internal analog LP filter (Hz)	500	1500	1500	N/A
Used in	TBM 1	TBM 3, 4, Lab.	Lab.	TBM 2, Lab.

3.1.2 Analog to digital converters

USB-6009 and 9230 BNC model analog-digital converters from National Instruments were used for digitizing the signals coming from analog accelerometers. NI USB-6009 is a 14-bit, 48kS/s (total) converter with 8 analog input channels (National Instruments, 2008) used with MEMS-type accelerometers, and NI 9230 BNC is a 24-bit, 12.8kS/s/channel converter with 3 analog input channels (National Instruments, 2015) that was used with piezoelectric accelerometers. (Figure 3.6). Shielded cables were used for reducing the noise between the accelerometers and analog-digital converters.

Figure 3.6 : National Instruments USB-6009 (on left) and 9230 BNC (on right) type analog to digital converters.

Two accelerometers per TBM were used and installed to different locations on the bulkhead. There were multiple reasons for this configuration. First of them was to understand the effect of the installation locations on the vibration. Secondly, it was possible to connect only two accelerometers per NI USB-6009 analog-digital converter, and using more accelerometers would increase the project cost considerably. Using two accelerometers was also proven to be useful during the data recording, as in some cases one of them had malfunctions, and data recording was continued with the working one.

3.1.3 Selection of data sampling rate

It is a known fact that choosing a suitable sampling rate for the signal in interest is crucial for proper digitizing. The Nyquist Theorem (Nyquist, 1928) explains the relationship between the sample rate and the frequency of the measured signal, and it indicates that the sample rate must be greater than twice of the highest frequency

component of interest in the measured signal. This frequency is often referred to as the Nyquist frequency and sampling below this rate causes aliasing (National Instruments, 2016). In addition, National Instruments (2016) recommends to select a sampling rate five times of the highest frequency of interest in the signal.

To mitigate the aliasing problem, four times of the maximum frequency range of the accelerometers was selected as the data sampling rate; which was for ADXL354BZ accelerometers 6000 Hz and for 356A17 accelerometers 12800 Hz. These sampling rates were the highest ones that could be selected with the analog to digital converters used in the study. The only exception from this rule was on the first system that utilizes DE-ACCM3D accelerometers due to the very limited hard drive space of the computer used.

3.1.4 Data recording software and computers

The analog to digital converters were connected to computers placed in the EPB TBMs, and a custom-made data recording software written in LabVIEW, a visual programming language from National Instruments, was used (Figure 3.7) for data recording. Since the system worked continuously and unattended, the computers were selected accordingly with the capacity of keeping recorded data for at least one month. The computers were connected to the internet to allow for controlling and updating remotely.

Figure 3.7 : A view of the software interface during vibration recording.

The software has signal filtering and compression capabilities as well as a triggering system, which shows a warning if a set percentage of the signals in the set time frame passes a threshold value, e.g., if 5% of the signals in the last 5 minutes passes ±1g in our case.

To enhance the monitoring, an e-mail warning system was implemented, which sends e-mail notifications if any of the accelerometer channels exceeded a predetermined threshold level. All software problems were recorded, and the log of the software was e-mailed daily. In the event of critical errors that disrupted data recording, the software was capable of restarting the computer automatically and subsequently resume data recording.

The integration of an e-mail warning system allowed for immediate notifications regarding changes in vibration data. This feature proved highly beneficial during the study, enabling prompt investigation of reasons of vibration variations and facilitating targeted ground sampling. Collaborating closely with the Contractors of the projects, the system helped proper geological sampling and timely identification of damaged cutter tools.

Before starting the data recording, the software records the static gravity and subtracts it from the signal during the recording for MEMS type accelerometers, making the data obtained free from the gravity.

For preventing data losses due to power failures, the vibration data files were split into 15 minutes and named as 'TBM number + Date + Time' which makes them easily recognizable. The sections which TBM was on standstill, were removed later on via remote connection for reducing the hard drive usage.

Due to the file sizes, it was not possible to transfer data via the internet. The recorded vibration data was transferred from the computers in the TBMs with hard drives on monthly basis. In addition to the vibration data, TBM excavation data (operational and performance data), shift reports, geological monitoring data, and disc replacement logs were also obtained.

The data recording computers, placed into waterproof cabinets in the TBMs (Figure 3.8).

Figure 3.8 : Waterproof computer cabinets in TBMs (TBM 2 on left, TBM 4 on right).

During the laboratory analyses 5 accelerometers were utilized, which required a slight modification in the software to allow increased accelerometer number to be recorded. However, main functionality was kept the same.

3.2 Analyzing Methods and Data Processing

Noise and vibrations are often produced by sources exhibiting random behavior. The vibrations resulting from a road surface interacting with the tires of a car, or vibrations caused by turbulence around an airplane wing can be given as examples for random vibrations (Brandt, 2011). During the TBM excavation or rock cutting, the interaction between disc cutters and rock surface creates vibrations. Since the rock surface is not homogeneous or flat, the discs that are contact with this surface continuously create a different vibration patterns. Furthermore, the signals coming from multiple disc cutters are superimposed. Thus, the vibration signals generated during excavation can be classified as non-stationary vibration. Even though they include stationary - deterministic parts created by motors, gearboxes and pumps working on specific frequencies, vibrations created during rock excavation are mainly nonstationary - random. Hence, random vibration analysis techniques are followed in this study.

Unlike stationary vibrations, the properties of nonstationary vibrations must be described as a function of time, which requires averages computed over an ensemble of sample records, acquired under statistically similar conditions (Bendat & Piersol, 2011). During the computations, each data segment should be sufficiently short not to smooth out the nonstationary characteristics of the data (Harris & Piersol, 2002). Throughout the data analysis, the excavation of one ring (1.4 meter for TBM 1, and 1.5 meter for TBM 2-4) was selected as one segment of data, and the calculations were performed ring by ring. Hence, the 15-minute vibration files recorded in TBMs were combined and a vibration file was created for each ring. This task was accomplished by using another custom written software in LabVIEW (Figure 3.9). Since the laboratory rock cutting experiments only takes a couple of seconds this process was not required for FLCM vibration data.

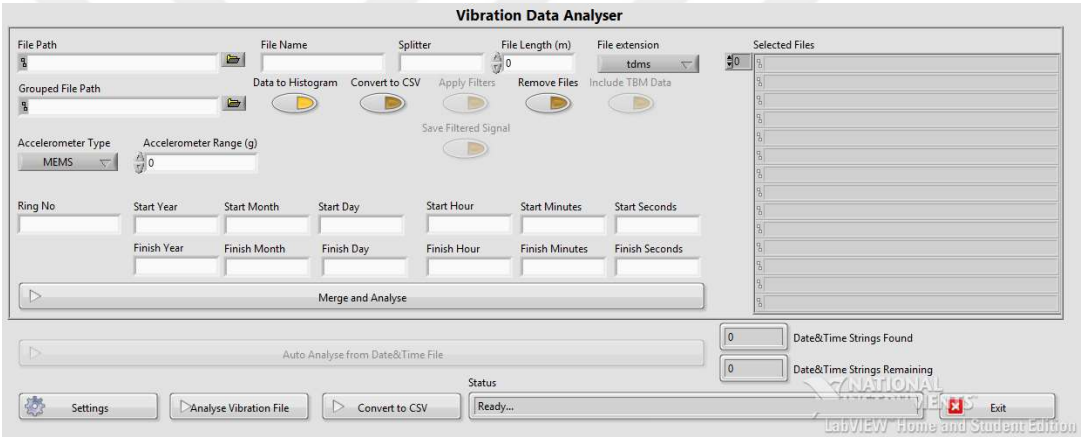

Figure 3.9 : A view of the data merging software.

Then, by using custom Matlab scripts, the following operations were applied to each ring;

- Removal of empty sections (TBM standstills) from the vibration data,
- Finding the percentage of acceleration amplitudes exceeding pre-set thresholds (e.g., 0.5g, 1g, 2g etc.),
- Statistical analyses (calculation of peak acceleration, RMS acceleration, interval RMS acceleration, standard deviation, variance, crest factor, skewness, kurtosis),
- Weibull analyses (obtaining α and β parameters by curve fitting),
- Calculation of spectrograms and power spectral density.

Calculation flowchart of the Matlab script is presented on Figure 3.10 and the details of these analyses will be provided on the following sections.

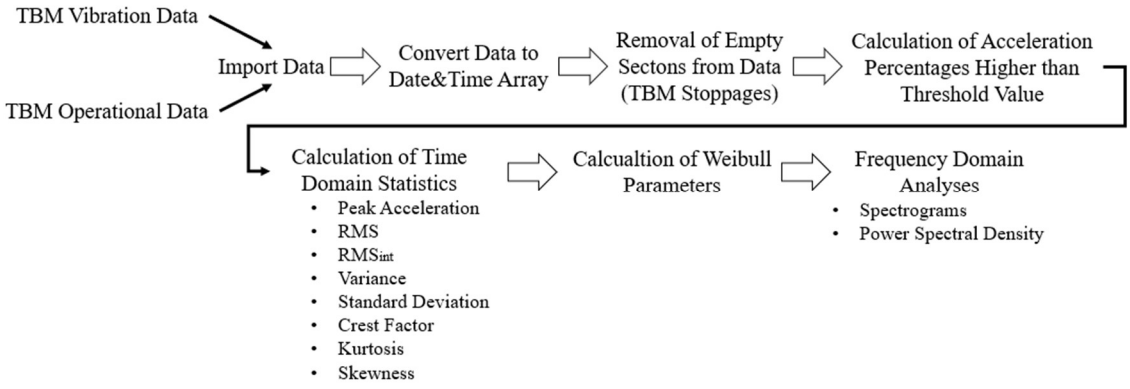

Figure 3.10 : Calculation flowchart of the Matlab script.

Vibration data is collected in the time domain; however, sometimes it is advantageous to transform the data into frequency domain for understanding the frequency components of the signals. Converting the vibration signals into frequency domain and analyzing them revealed that, the TBM vibrations and the vibrations occurred during rock cutting with FLCM were broadband signals and due to the contributing factors, it was very hard to get any meaningful interpretations in the frequency domain. Even though the analyses were done on both domains, this study will mainly focus on the time domain analyses.

Considering the complexity of the TBMs, environmental noise was a concern at the beginning of the project and the data was analyzed thoroughly to understand its effects on the excavation data. Following these preliminary analyses, it was seen that the noise is very minimal compared with the vibration caused by the excavation. Figure 3.11 shows a sample vibration data from one of the TBMs, which presents vibration data together with pre and post excavation data. The time where excavation start, and finish are also marked. As it is clear from the figure, the vibration amplitudes before and after the excavation are minimal in comparison with the ones recorded during excavation and it is possible to say that the environmental noise has a very limited influence on the data.

Throughout the study, the strengths of the relationships (R^2) are categorized as moderately strong between 50 and 69%, strong between 70 and 89%, and very strong if it is greater than or equal to 90%. However, it should be noted that in some instances, just two data points are available, making classification impossible.

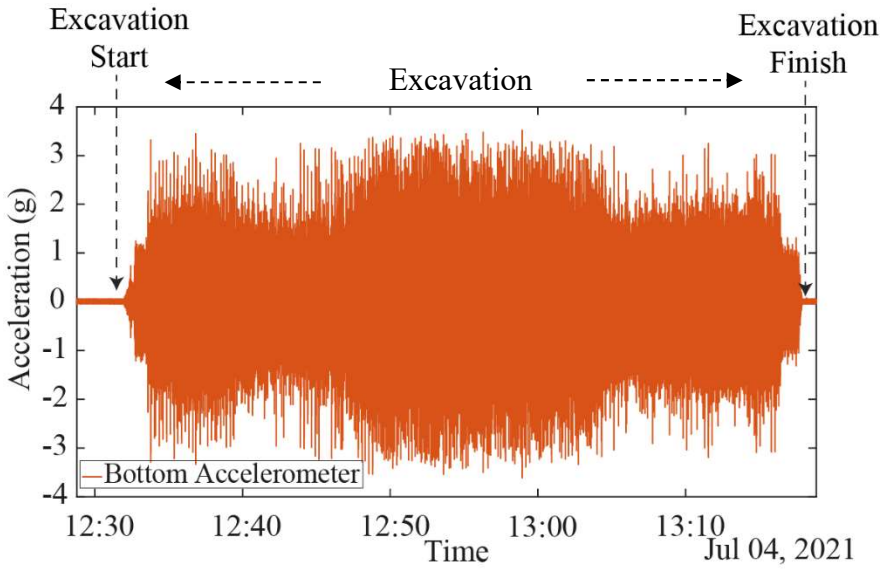

Figure 3.11 : The noise before and after the excavation, recorded on the ring 2064 of TBM 2 (z-axis).

3.2.1 Time domain analyses

3.2.1.1 Statistical analyses

The time domain data analysis is mainly based on the quantitative statistical methods. Analyzed vibration data was first inspected by using a plot showing the percentage of the acceleration signals passing a selected threshold, which is ±1g in this study. Average TBM operational and performance data, geological information, and disc cutter replacement logs were also taken into consideration during this analysis.

If there is an anomaly, the data belonging to that ring was analyzed further by using acceleration versus time plots. The recording time of the vibration patterns different from the general were correlated with TBM operational parameters and the shift reports taken from the engineers at site (Figure 3.12). If available, excavation face photos were also inspected for pinpointing the geological differences causing the vibration anomalies.

It is worth noting that the data acquisition system of the TBMs had a lower sampling rate, typically 0.1 or 0.2 Hz, in contrast to the higher sampling rate of the vibration recording system. This difference poses challenges when comparing data, particularly for shocks, as no anomalies were observed in the TBM operational data due to low sampling rate. The higher sampling rate (2 kHz) of the force data obtained during laboratory experiments facilitated easier and better comparisons than the TBM data.

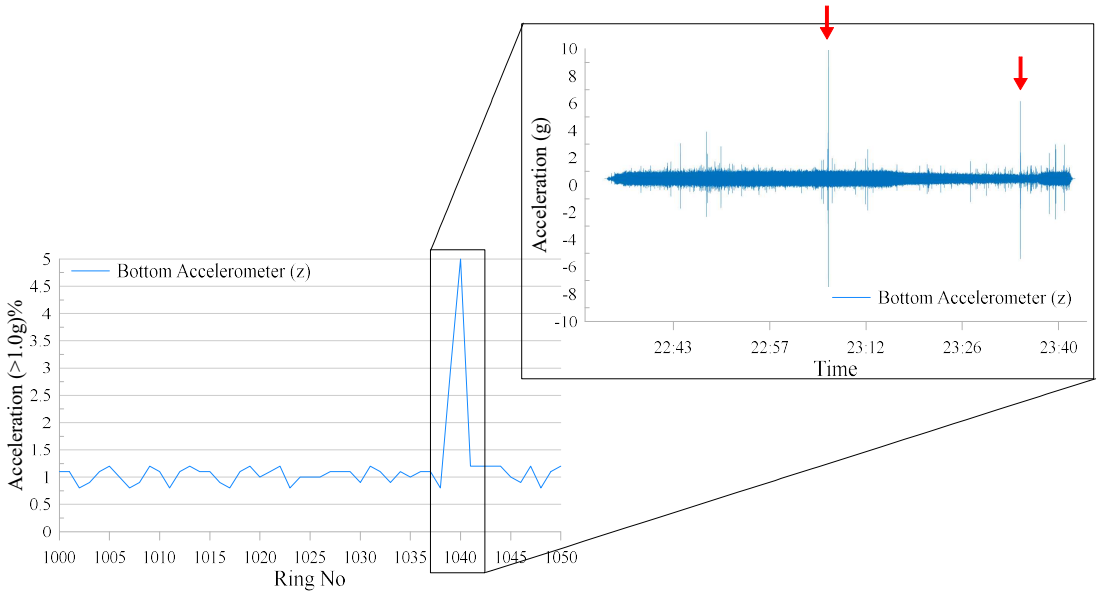

Figure 3.12 : An example illustration of acceleration percentage graph and acceleration-time graph for a detailed inspection of vibration data.

The statistical data for each ring was calculated including standard deviation, peak acceleration, RMS and interval RMS acceleration, crest factor, skewness and kurtosis. Subsequently, for each distinct lithological unit as exemplified Figure 3.13, the corresponding statistical vibration data were averaged. With this process, a representative data for different lithological units were obtained and this data were used to understand effect of geological conditions on TBM vibrations. For the laboratory experiments the statistical data was averaged for the repetitive line spacing and penetration values.

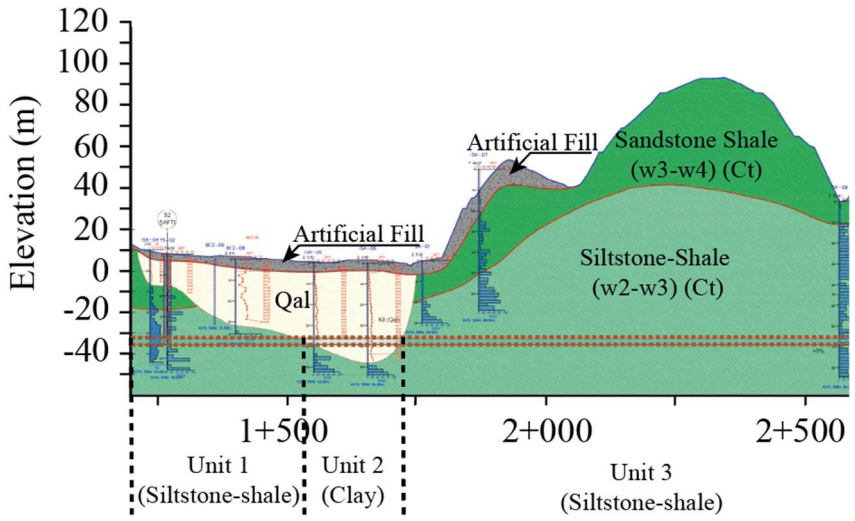

Figure 3.13 : An example of averaging the statistical data according to lithological units.

The main statistical parameters that were used during the analyses can be detailed as follows;

The standard deviation (equation 3.1) is a statistical metric defining the amount of variation in the signal and it shows the dispersion of the vibrations (Harris & Piersol, 2002). The variance (equations 3.2) is the mean of the squares of the deviations from the mean value of a vibrating signal (Harris & Piersol, 2002). These two parameters were also used for the calculation of other statistical parameters.

$$\sigma = \sqrt{\frac{1}{n}\sum_{i=1}^{n}(\propto_i - \mu)^2} \tag{3.1}$$

$$\sigma^2 = \frac{1}{n}\sum_{i=1}^{n}(\propto_i - \mu)^2 \tag{3.2}$$

where, $\propto$ is acceleration data, μ is mean acceleration and n is the data number in a ring.

Peak acceleration (equation 3.3) is the highest recorded acceleration value within a designated time window (corresponding to a single ring in the present study). Analysis of the data revealed that peak acceleration values can be useful for discriminating between soil and rock formations.

$$peak = \max(|\propto|) \tag{3.3}$$

The properties of dynamic signals in general cannot be summarized by a single value, however, in engineering it is often required to compare the two dynamic signals and understand which has higher energy content. The most common measure used in this respect is the root mean square, or RMS value, which is calculated as shown in equation 3.4 (Brandt, 2011). While peak acceleration shows highest instantaneous measurement in a ring, the RMS values are average measures of one ring.

$$RMS = \sqrt{\frac{1}{n}\sum_{i=1}^{n}(\propto_i)^2} \tag{3.4}$$

Interval RMS acceleration (equation 3.5) is a measure of the oscillatory content in the acceleration data and all axes are combined to form the interval RMS acceleration

(Rogers et al, 1997). Alongside RMS values, the interval RMS was also directly utilized for comparing vibration characteristics under varying geological conditions.

$$RMS_{int} = \sqrt{x_{RMS}^2 + y_{RMS}^2 + z_{RMS}^2} \tag{3.5}$$

where, x, y and z are the individual axes.

The crest factor (equation 3.6) is a common statistical metric in signal analysis, and it is defined as the ratio of the peak absolute value to the RMS value of the signal (Brandt, 2011). The results show how peaky the data is, and crest factor found useful for detecting the face homogeneity during the present study.

$$Crest = {|\propto_{peak}|}/{\propto_{RMS}} \tag{3.6}$$

Skewness is a dimensionless parameter and quantifies the asymmetry of a probability distribution relative to its mean. (equation 3.7). If the signal is symmetric, the skewness is zero, whereas positive or negative skewness signifies a rightward or leftward leaning distribution. For many random vibration signals, the probability distribution is expected to be symmetric around the mean (Brandt, 2011).

$$s = \frac{1}{n}\sum_{i=1}^{n}\left[\frac{\propto_i - \mu}{\sigma}\right]^3 \tag{3.7}$$

where, s is skewness.

Kurtosis is a measure of the "tailedness" of the histogram and calculated as shown in equation 3.8 (Irvine, 2019). For a normally distributed dataset, the kurtosis is exactly 3. If the kurtosis is larger, the distribution has ‘higher tails’ than the normal distribution, and vice versa if the kurtosis is smaller than 3 (Brandt, 2011).

$$k = \frac{1}{n}\sum_{i=1}^{n}\left[\frac{\propto_i - \mu}{\sigma}\right]^4 \tag{3.8}$$

where, k is kurtosis.

Skewness and kurtosis values were used to get information on distribution type of the vibration data.

3.2.1.2 Probability analyses

It is not possible to predict precise acceleration magnitude at a specific instant if the acceleration is random, however, a knowledge of the history of random acceleration is adequate to predict the probability of occurrence of various acceleration magnitudes (Steinberg, 2000). Recognizing the random nature of TBM vibrations, probability analyses utilized to investigate the key parameters that influence these vibrations.

As previously discussed, the vibration data related to excavation of rocks occurs in the contribution of many independent factors. Even though many naturally occurring, and artificially produced processes can be adequately characterized by the Gaussian (normal) distribution (Rouillard & Sek, 2010), statistical analyses revealed that TBM and rock cutting vibration data exhibit a leptokurtic distribution, which means there are more extreme values in the data compared to a normal distribution. This characteristic of the data prevents a full representation by using Gaussian model and for this kind of data, it is advised to use Weibull distribution (Rouillard, 2007; Garcia-Romeu-Martinez et al., 2007; Karadeniz et al., 2013 and Fei et al., 2014). This distribution type is related to extreme value analysis and mostly used in failure analysis, survival analysis, industrial engineering, mechanical engineering, weather forecasting, and extreme value theory (Harris & Piersol, 2002). The Weibull distribution has also found application in predicting vibrations (measured as peak particle velocity) induced by surface and underground blasting. The distribution is able to effectively model the relationship between peak particle velocity and scaled distance, as demonstrated in several studies (Ray & Dauji, 2019; Iwano et al., 2020; Yu et al., 2020).

The two parameter Weibull cumulative distribution function is defined by equation 3.9 (Rinne, 2008; Montgomery & Runger, 2018);

$$Weibull\ CDF: F_x(x) = 1 - exp\left[-\left(\frac{x}{\beta}\right)^{a}\right]\ for\ (a > 0, \beta > 0) \qquad (3.9)$$

where, x is the variable (acceleration in this study), α is the shape parameter, β is the scale parameter.

It is believed that the cumulative distribution better represents the findings of this study then the probability density, thus, Weibull cumulative distribution function will used during the analyses.

The Weibull distribution originally developed for failure analysis and survival analysis; hence, the input variable is lifetime (the duration between the failures) which is a non-negative value (Rinne, 2008). While a three-parameter variant exists that incorporates a location parameter, often called "delay" or "threshold" in failure context, this form of the distribution does not suit to vibration data and two-parameter distribution will be used. From a statistical point of view adjusting the location parameter while the others are held constant will result in a parallel movement of the density curve over the horizontal axis (Rinne, 2008). Figure 3.14 illustrates the influence of variations in the Weibull shape ("α") and scale ("β") parameters on the cumulative probability distributions, while holding the other parameter constant. A decrease in the "α" parameter confines the distribution to a narrower band in horizontal axis. For instance, when "α" is 3, the probability of accelerations exceeding 1.6g is nearly 0, conversely, when "α" is 0.5, the probability surpasses 30%. In contrast, an increase in the "β" parameter shifts the distribution curve along the vertical axis, resulting in a higher likelihood of observing a specific acceleration value. With a "β" parameter of 0.5, the probability of vibrations exceeding 1g is approximately 15%, whereas it increases to nearly 70% for a "β" parameter of 3.

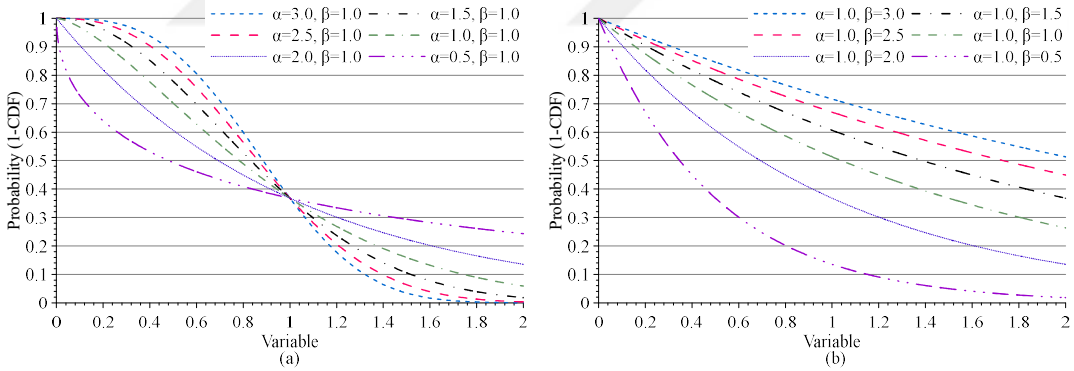

Figure 3.14 : Changes in the cumulative probability curves depending on the Weibull shape and scale parameters.

The acceleration values during the excavation constantly changing between positive and negative, thus, it is required to convert these negative values to the positive before creating Weibull distribution. As the polarity is not significant for the TBM and rock cutting vibration data, absolute values or moving RMS data can be used for creating the Weibull distribution.

The moving RMS is (equation 3.10) different from the single RMS value (equation 3.4) that was used to quantify the signal's energy content with one value. Moving RMS

calculates the RMS within a predefined window that slides along the entire signal. This sliding window essentially acts as a filter, smoothing out the signal's fluctuations. Furthermore, as the values are squared during the calculation, the negative ones are converted to the positive. The smoothness obtained by this filter depends on the window length, as the window length increases the signal becomes smoother.

$$RMS[j] = \sqrt{\frac{1}{N}\sum_{i=j-N+1}^{j}(\propto_i)^2} \tag{3.10}$$

where, N is the window length.

Since the objective was only the conversation from negative to the positive, a 10-point window length was used. Subsequently, employing the absolute values and moving RMS calculation, two datasets were created. The Weibull parameters (α and β) for each ring were obtained using the Matlab distribution fitter (fitdist) for both datasets. These parameters were then averaged to establish representative data for each lithological unit.

A comparison of the moving RMS filtered dataset and the absolute dataset revealed no significant difference in their usability for highlighting variations between lithological units. To illustrate, cumulative histograms were generated for absolute and moving RMS filtered vibration data collected during the excavation of ring 2445 with TBM 2. Then, Weibull cumulative distributions were fitted to both histograms. Additionally, a Normal distribution was included for the histogram derived from the absolute vibration data (Figure 3.15) for comparison.

As previously noted, the Normal distribution does not fully represent the vibration data, whereas Weibull distributions exhibit a good fit with both histograms. There is a difference present between two Weibull distributions calculated from the RMS and absolute datasets. A similar comparison of Weibull distributions created from both datasets (absolute and RMS) were done for multiple rings, and it was seen that difference between the probability curves changes ring to ring. However, this difference can be considered as minimal and, as the datasets with absolute values or moving RMS provide similar results, only the ones with absolute values will be used in this dissertation. The results of analysis using the RMS values can be found in Ates and Copur (2023).

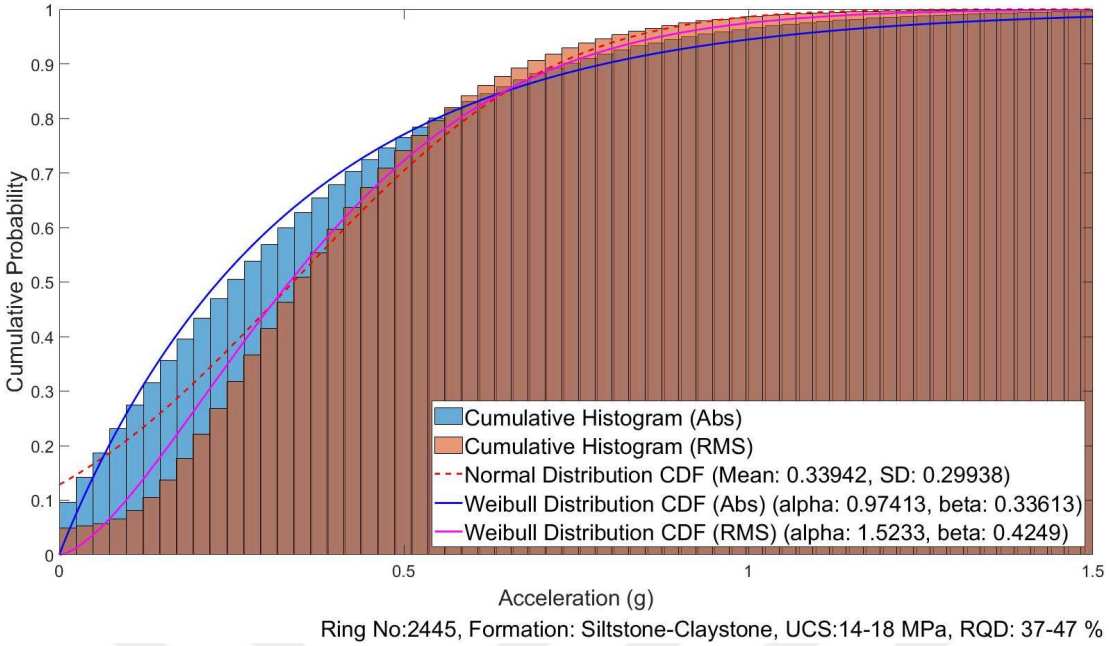

Figure 3.15 : Cumulative histogram of vibration data recorded on the excavation of ring 2445 of TBM 2, together with Weibull and Normal distribution fits.

Consistent with the methodology employed for the statistical parameters, representative α and β parameters were calculated for each lithological unit. This process involved averaging the parameters obtained from ring-by-ring distribution fits.

3.2.2 Frequency-domain analyses

Although the vibration data was initially acquired in the time domain, frequency domain analysis might offer valuable insights into the cutting process. Given the random nature of the TBM vibration data, the frequency spectrum can be represented through either by spectrograms or power spectral density (PSD) calculation as discussed by Brandt (2011).

For spectrogram calculation, the time domain data is segmented into short windows, and FFT is then applied to each segment with an overlap between consecutive FFTs. Spectrograms visually represent how acceleration signals vary over time and frequency, making them particularly useful in identifying when certain activities begin and end (Rogers et al., 1997; Hanly, 2016). Waterfall plots, which are basically frequency spectrograms represented as 3D graphs, were also utilized during the study to present the frequency content of the data. These plots showing time, frequency, and amplitudes, offering a comprehensive visualization of how spectral peak frequencies and amplitudes change over time.

Unlike periodic signals with discrete spectral lines, random signals exhibit continuous spectra, where the power is distributed across a range of frequencies rather than concentrated at specific points (Brandt, 2011). By calculating the average power at different frequencies over multiple signal periods, PSD provides an accurate representation of the energy distribution throughout the entire frequency range, particularly for random vibrations. Additionally, PSD normalization by frequency bandwidth allows for the comparison of signals with different durations.

The calculations were performed using Matlab and, spectrograms were generated using the "spectrogram" function, while power spectral densities were estimated using the "pwelch" function. A window size of 1 second with 50% overlap were employed for both calculations.

Figure 3.16 presents the raw vibration data acquired by the bottom accelerometer (z-axis) of TBM 2 during the excavation of ring 2008. The figure also includes a frequency spectrogram and the corresponding power spectral density of the data. For improved visualization, both magnitude and power values are represented on a logarithmic scale (dB).

Consistent with previous research by Walter (2013), the frequency spectrogram and power spectral density plots reveal broadband characteristics of the vibrations generated during TBM excavation. The signal exhibits distinct peaks at approximately 280 Hz, 700 Hz, 1300 Hz, 2200 Hz, and 2800 Hz. Notably, the spectrogram suggests that these dominant frequencies persist throughout the excavation process.

Additionally, to investigate potential variations in frequency content across the accelerometer axes (x, y, and z), respective power spectral densities were calculated, and the results are presented in Figure 3.17. The plot shows that all axes share similar dominant frequencies across the entire frequency range. The z-axis exhibits the highest power across most frequencies, with the exception observed at approximately 1250 Hz.

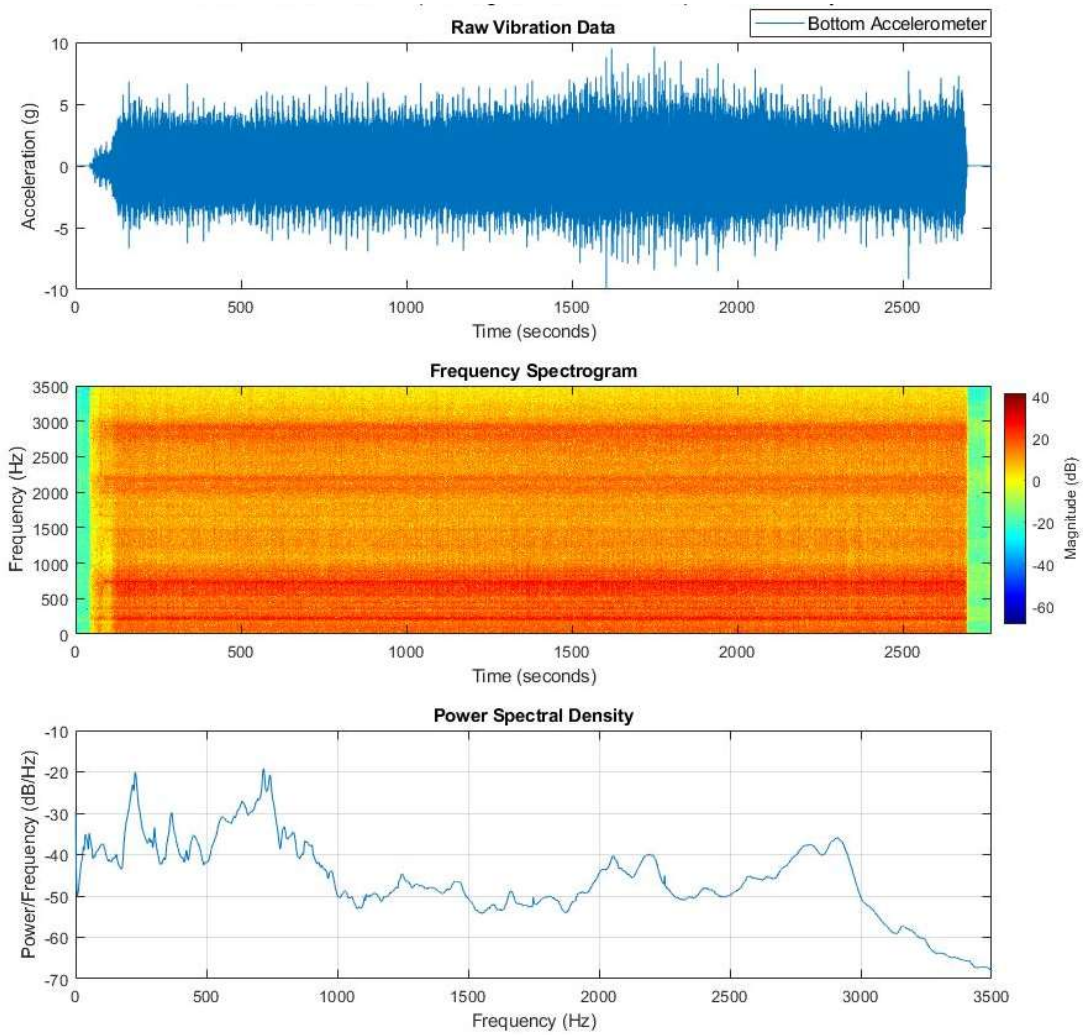

Figure 3.16 : Raw vibration data (top), frequency spectrogram (middle) and power spectral density (bottom) belongs to ring 2008 recorded on TBM 2 (z axis).

To understand frequency content of the signals in the various geological conditions, these analyses were replicated across multiple rings situated within different lithological units. It was observed that the vibration spectra maintain broadband characteristics and exhibits multiple dominant frequencies, similar to the observations presented in Figure 3.16 and Figure 3.17. Due to the complexity of the TBM itself and excavation process, definitively pinpointing the exact sources of the observed peak frequencies remains challenging. However, several factors, including cutterhead rotational speed and geological conditions, have been identified as potentially influencing variations in the peak values. While this research primarily focuses on the analyses in the time domain, these factors will be discussed in the following sections.

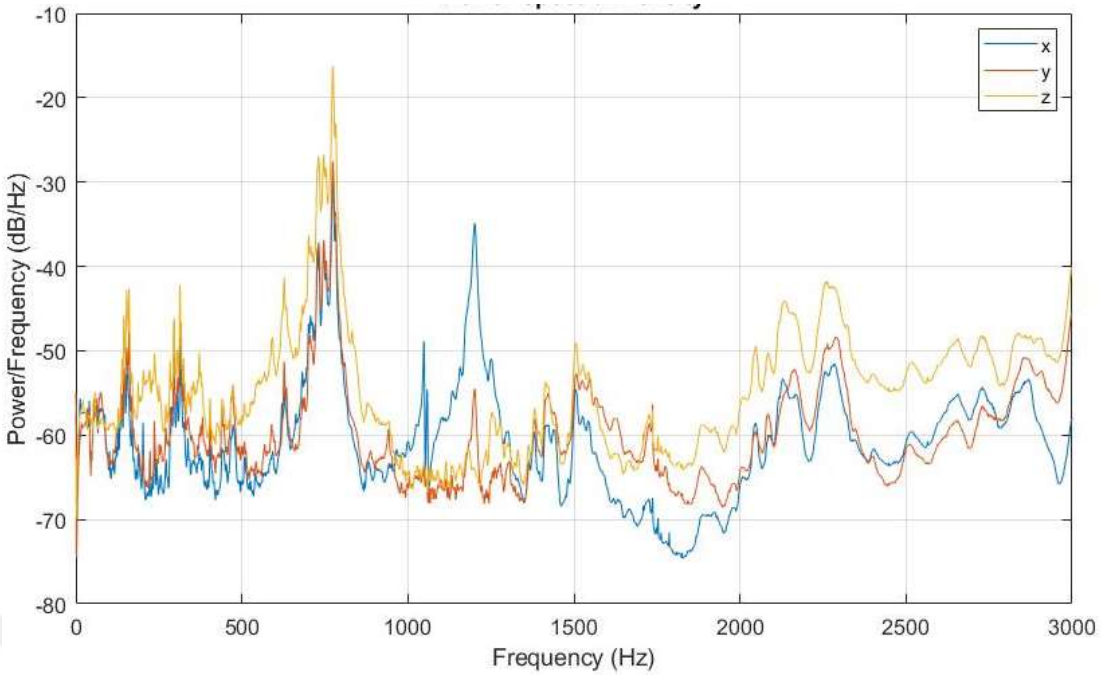

Figure 3.17 : Frequency spectrogram of vibrations recorded during the excavation of ring 2449 on the x, y and z axes of bottom accelerometer of TBM 2.

4. ANALYSIS OF SITE DATA AND INVESTIGATION OF THE VARIABLES AFFECTING TBM VIBRATIONS

This section presents a comprehensive analysis of the TBM vibration data obtained from the three projects. The analysis is structured in two phases. The initial phase involves a detailed examination of the vibration data for each TBM individually. Subsequently, the second phase focuses on combined analyses of the data from different TBMs to identify the different variables affecting the TBM vibrations.

The vibration data acquired from the TBMs were grouped according to the identified lithological units, as explained in the previous section. Following ring-by-ring data processing, the data belonging to each lithological section were averaged to create a characteristic vibration profile for each section. These characteristic vibration profiles were then utilized to analyze the impact of various factors on EPB TBM vibrations, including geological conditions (geological changes), TBM operational and performance parameters, cutter breakages/damages, accelerometer types/positions, and excavation diameters. Table 4.1 summarizes the lengths of the recorded and processed vibration data for each TBM.

Table 4.1 : Vibration data lengths recorded during the site experiments.

TBM No	Vibration Data Length (rings)	Vibration Data Length (m)
TBM 1	326	456
TBM 2	1082	1623
TBM 3	992	1488
TBM 4	1686	2529
	Total	6096

Analysis of the acceleration data revealed that the z-axis, which is the axis on the excavation direction, consistently exhibited the highest magnitude across all accelerometer axes for each TBM. Consequently, in the subsequent sections, the figures primarily derived from the z-axis will be presented, unless indicated otherwise. During the data processing, it was observed that the vibration amplitudes recorded on

a 6.5m EPB TBM could exceed 10g, especially in areas characterized by high-strength lithological units.

It is important to acknowledge that, similar to vibrations, TBM operating parameters are influenced by geological conditions and are tuned by operators to align with these specific conditions. Addressing the impact of changing operational parameters on vibrations necessitates conducting excavations within a controlled environment and in a controlled way (same geological conditions, different excavation parameters). However, this opportunity is very difficult to find considering that the majority of the contractors are reluctant to interrupt their operations for scientific research. Furthermore, it is also not easy to find a completely homogenous excavation face. Thus, within this study, changes on the vibrations are explained with their possible reasons considering the variations on TBM operational parameters and geological conditions.

4.1 Mecidiyekoy-Mahmutbey Metro Line (TBM 1)

The vibration data acquired from the first site was quite limited in terms of data length, vibration recording system's measurement range and sampling frequency. However, some distinct patterns connected to the geological conditions were discovered during the processing of the data from TBM 1.

The first one of the observed patterns was associated with a hard calcite vein having an approximate thickness of 30 cm on one side of the excavation face as shown in Figure 4.1. The vibration data belongs to this section from the z-axis of the bottom accelerometer is presented in Figure 4.2. The data was recorded when the cutterhead rotational speed was 3 RPM, and distinguishable peaks around every five seconds can easily be seen. The four-arm disc cutter placement on the cutterhead, as illustrated in Figure 2.3, results in each cutter arm passing the calcite vein location every five seconds at a cutterhead rotational speed of 3 RPM. In contrast with the other disc distributions, (+) shaped distribution allowed to see this pattern, corroborating the findings of previous studies by Walter et al. (2012), Walter (2013) and Liu et al. (2022).

Figure 4.1 : Calcite vein at the excavation face.

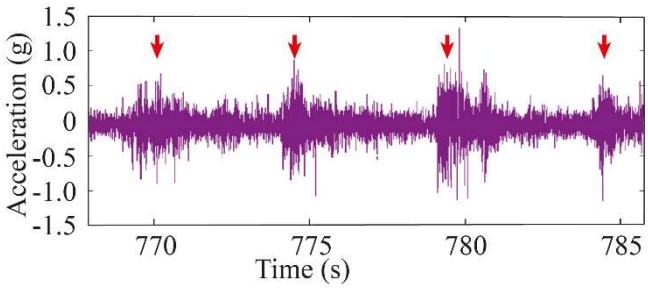

Figure 4.2 : Cutterhead acceleration measured by bottom z-axis on a face with hard calcite vein.

A similar observation of this pattern on a different ring is illustrated in Figure 4.3, which presents vibration recording in time domain when the cutterhead was turning with 2.1 RPM. At this speed, an arm of the cutterhead passes same location in every 7.2 seconds and the figure shows that peaks recorded in every 7 to 7.5 seconds. However, it is important to note that these peaks are not as distinguishable as in the previous case.

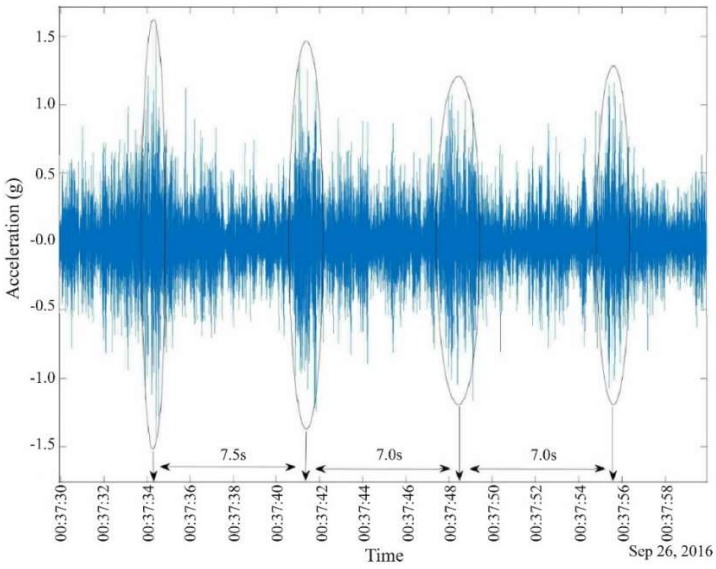

Figure 4.3 : Vibration recordings of bottom z-axis of ring 1657 during cutterhead rotating with 2.1 RPM.

This distinction could only exist when a small portion of the face has harder material than other part. As the disc cutters traverse this area, they create higher amplitude

vibrations compared to those produced by cutting through softer rock. In other cases, when the face is homogenous, discs will continuously chip the rock resulting in continuous high amplitude vibrations.

Figure 4.4 and Figure 4.5 provide a comprehensive visualization of the processed vibration data, incorporating lithological units identified by their respective numbers as outlined in Table 2.3, rock uniaxial compressive strength data converted from Schmidt hammer tests, top and bottom accelerometer data indicating the percentage of the points per ring above ±1g threshold, including their average per lithological unit, disc replacement locations, and selected TBM operational parameters. The threshold level of ±1g was chosen after testing various values and shown to be effective in differentiating the geological conditions. The figure also shows the location of the cutterhead maintenance which was explained in Section 2.1. Data recording interruptions occurred in certain sections of the dataset due to technical malfunctions, which are denoted by the "No Data" in the figures.

Despite the utilization of a very basic vibration recording system in this project, it was still possible to distinguish the difference between fresh and weathered sections. Particularly, between rings 1470 and 1510, where the excavated material was weak and face pressure was increased due to stability concerns, the percentage of points passing 1g were found to be very low. Following this section, there was an increase in vibration levels, aligning with the rise in rock strength.

The top accelerometer exhibited a higher percentage of accelerations exceeding the ±1g threshold on the z-axis, whereas the bottom accelerometer demonstrated a higher percentage on the x-axis.

This project further unveiled that vibration levels undergo alterations in the presence of disc cutter damages, and subsequent to disc replacements, a tendency for decreased vibration levels was observed. However, due to the limited amount of data, clear relationships could not be established.

Acknowledging the potential of utilizing vibrations to detect geological changes, the study continued, and in response to the limitations of the recording system, necessary modifications were implemented. Following this project, the upgraded TBM vibration recording system was deployed in two additional tunnel projects for further investigation.

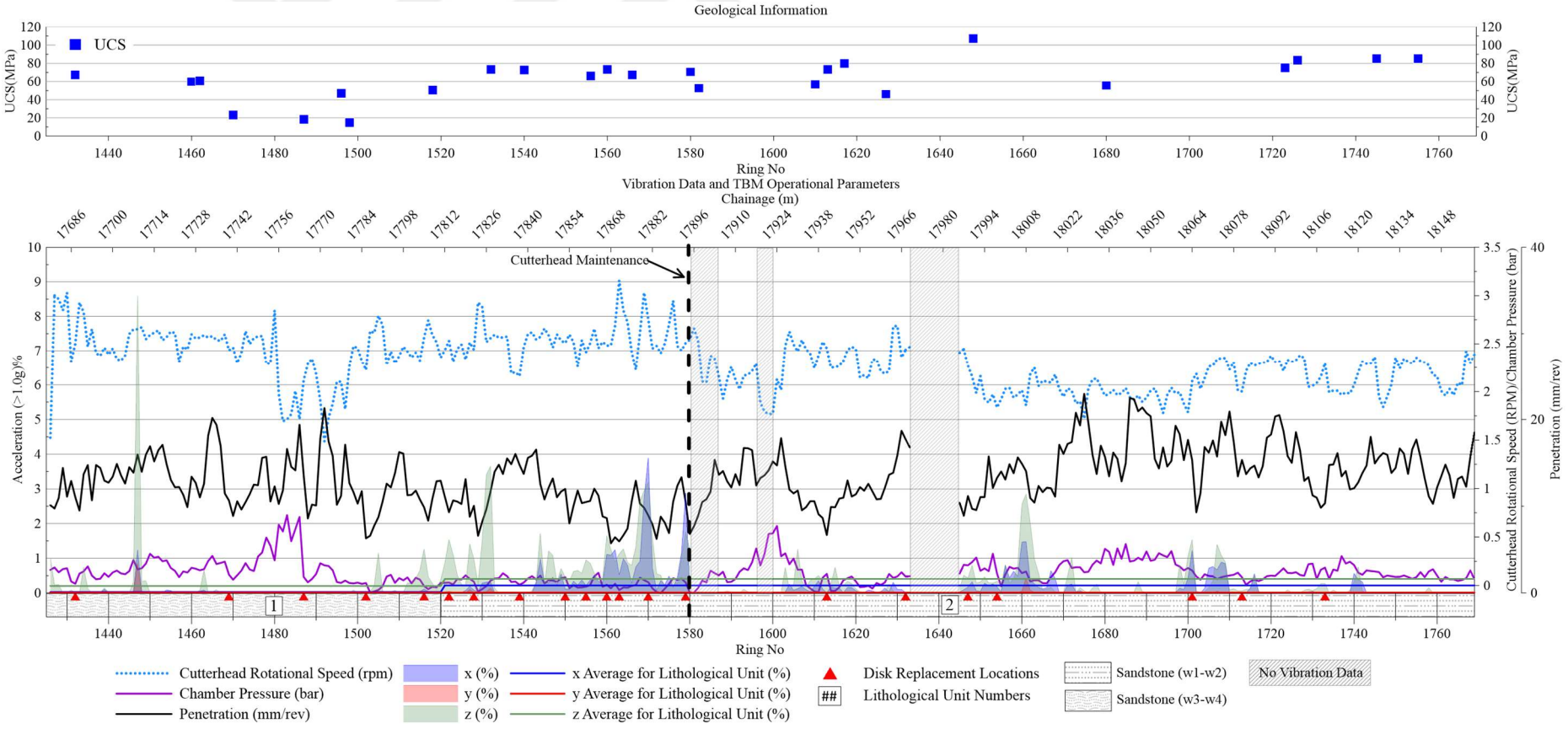

Figure 4.4 : TBM 1 top accelerometer data between rings 1426 and 1769 (Mecidiyekoy-Mahmutbey Metro Line).

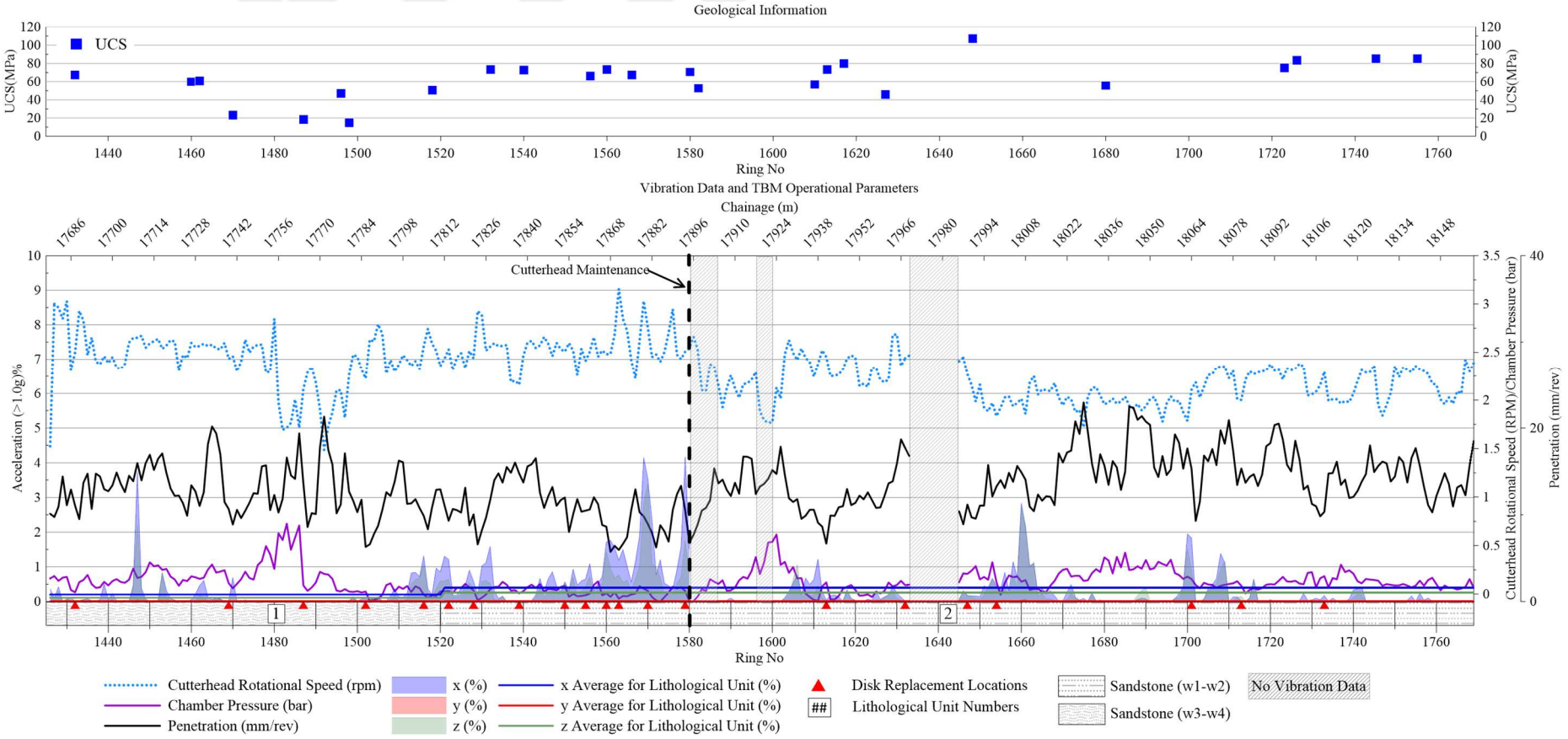

Figure 4.5 : TBM 1 bottom accelerometer data between rings 1426 and 1769 (Mecidiyekoy-Mahmutbey Metro Line).

4.2 Umraniye-Atasehir-Metro Line (TBM 2 and 3)

With the knowledge and experience acquired from TBM 1, together with enhanced data recording systems, a more comprehensive data was obtained from the TBMs in this project.

The project involved the side-by-side excavation of two identical TBMs. Despite the tunnels being in close proximity to each other, there were notable differences in the locations of the lithological units encountered during the excavation process. These lithological variations provided a unique opportunity to conduct an analysis of vibration patterns and characteristics between the two identical TBMs by eliminating the potential variations arising from differences in the machines themselves.

Simultaneously, it became possible to investigate the vibration patterns during the excavation of same lithological units by identical TBMs and to cross-validate the obtained vibration patterns with the other TBM.

For a better comparison between the two TBMs, Table 4.2 presents the starting and ending ring numbers for each lithological unit encountered by both machines. Red arrows in the table highlight the corresponding lithological units between the two tunnels. These units have been assigned unique numbers for a consistent reference throughout the study. For instance, the Sandstone-Limestone unit designated as "#3" in TBM 2 (rings 1551-1641) corresponds to the same unit excavated by TBM 3 between rings 1541 and 1580. The lithological unit numbers are also provided in the respective figures for an easy identification.

It should be noted that, on Terratec S68 (TBM 3), #19.1 and #19.2 are the same lithological units separated with a dyke.

Table 4.2 : Geological units seen on the alignment with identification numbers for both TBMs in Umraniye-Atasehir-Goztepe Metro Line.

Terratec S67 (TBM 2)				Terratec S68 (TBM 3)			
Ring No (Start)	Ring No (End)	No	Lithological Unit	Ring No (Start)	Ring No (End)	No	Lithological Unit
1410	1498	1	Siltstone-Claystone	-	-	-	-
1499	1550	2	Dyke (w4-w5)	1505	1540	2	Dyke (w4-w5)
1551	1641	3	Sandstone-Limestone	1541	1580	3	Sandstone-Limestone
		4	No Data	1581	1657	4	Claystone
		5	N5 Crossover			5	N5 Crossover
1722	1840	6	Claystone	1706	1800	6	Claystone
1841	1930	7	Claystone-Dyke (w1-w2)			-	No Data
1931	1990	8	Claystone	1821	1905	7	Claystone-Dyke (w1-w2)
1991	2030	9	Dyke (w1-w2)			-	No Data
		10	No Data	1993	2024	9	Dyke (w1-w2)
2075	2090	11	Claystone	2025	2060	10	Dyke (w4-w5)
		12	Carsi Station	2061	2081	11	Claystone
2100	2150	13	Dyke (w4-w5)			12	Carsi Station
2151	2223	14	Siltstone-Claystone	2103	2126	13	Dyke (w4-w5)
2224	2240	15	Dyke (w4-w5)	2127	2229	14	Siltstone-Claystone
2241	2390	16	Siltstone-Claystone	2230	2238	15	Dyke (w4-w5)
		17	Hastane Station	2239	2405	16	Siltstone-Claystone
2410	2457	18	Siltstone-Claystone			17	Hastane Station
2458	2760	19	Sandstone-Claystone	2416	2438	18	Siltstone-Claystone
2761	2850	20	Claystone	2439	2517	19.1	Sandstone-Claystone
2851	2910	21	Dyke (w1-w2)	2518	2532	23	Dyke (w4-w5)
2911	2930	22	Sandstone-Claystone	2533	2629	19.2	Sandstone-Claystone

4.2.1 Analysis of the vibration data obtained from TBM 2

Acceleration threshold graphs were generated to visualize differences in vibration levels as shown in Figure 4.6 to Figure 4.9 for TBM 2. Maximum accelerations also included into these figures. The average TBM operational parameters are outlined in Table 4.3.

In the majority of the recorded sections, the cutterhead speed remained within a narrow range, typically between 3.5 and 4 RPM. The limited variability in cutterhead speed poses a statistical challenge in interpreting its direct influence on vibrations. Chamber pressure and penetration per revolution of the cutterhead strongly follow the geological conditions; increasing in soils as cutterhead speed decreases slightly and decreasing in rocks with a slight increase in cutterhead speed. Figure 4.6 to Figure 4.9 effectively illustrate how these geological variations impacted vibration levels. The average acceleration lines provide a clear representation of the varying vibration levels corresponding to different geological units.

The examination of Figure 4.6 through Figure 4.9 reveals several significant observations, which can be listed as;

- The most substantial vibrations are observed along the z-axis which is in the excavation direction.
- Shocks are more distinguishable at the bottom accelerometer, whereas the overall percentage of accelerations exceeding 1g is higher for the top accelerometer in each lithological unit. This observation contrasts with the trends observed in the TBM 1. A potential explanation for this difference lies in the relative positioning of the accelerometers on TBM 2. Compared to TBM 1, the vertical distance between the accelerometers on TBM 2 was smaller and the accelerometers were situated closer to the machine's center (Figure 2.7).

Table 4.3 : Average TBM operational parameters for TBM 2.

Ring No (Start)	Ring No (End)	Lithological Unit	Cutter Speed (RPM)	Cutter Torque (kNm)	Average Face Pressure (bar)	Total Thrust (kN)	Penetration Rate (mm/rev)	Thrust / Cutter (kN)	Boreability Index (kN/cutter)/(mm/rev)	P (kW)	SE (kWh/m^3)	ICR (m^3/h)
1410	1498	(1) Siltstone-Claystone	3.71	709	0.79	10200	10.82	217	20.45	276	3.42	80.90
1499	1550	(2) Dyke (w4-w5)	3.54	681	0.97	9946	11.97	212	17.92	253	2.99	85.50
1551	1641	(3) Sandstone-Limestone	3.92	823	0.48	10959	9.41	233	25.73	338	4.57	74.37
		(4) No Data										
		(5) N5 Crossover										
1722	1850	(6) Claystone	3.73	776	0.25	10854	9.5	231	26.31	303	4.38	70.92
1851	1930	(7) Claystone-Dyke (w1-w2)	4.02	625	0.07	12405	6.64	264	44.48	263	5.05	53.43
1931	1990	(8) Claystone	3.65	642	0.39	10911	10.57	232	23.48	244	3.25	77.39
1991	2030	(9) Dyke (w1-w2)	3.64	562	0.29	11820	8.2	251	36.22	212	3.86	59.14
		(10) No Data										
2075	2090	(11) Claystone	3.57	688	0.46	9720	10.51	207	21.23	260	3.45	75.07
		(12) Carsi Station										
2100	2150	(13) Dyke (w4-w5)	3.51	643	0.66	7706	11.03	164	15.14	237	3.11	78.15
2151	2223	(14) Siltstone-Claystone	3.8	651	0.66	9911	10.78	211	20.10	259	3.15	82.46
2224	2240	(15) Dyke (w4-w5)	3.79	681	0.53	10058	10.24	214	21.35	270	3.49	77.94
2241	2390	(16) Siltstone-Claystone	3.76	649	0.60	10513	9.77	224	23.79	257	3.54	73.69
		(17) Hastane Station										
2410	2457	(18) Siltstone-Claystone	3.37	825	0.47	10381	9.61	221	24.07	295	4.64	65.18
2458	2760	(19) Sandstone-Claystone	3.8	722	0.27	12756	8.43	271	34.68	287	4.61	64.42
2761	2850	(20) Claystone	3.74	785	0.39	11863	9.19	252	28.96	307	4.61	69.26
2850	2910	(21) Dyke (w1-w2)	3.83	832	0.33	11493	9.74	245	25.98	334	4.55	75.18
2910	2930	(22) Sandstone-Claystone	3.82	817	0.19	9136	10.21	194	19.64	327	4.25	78.74
		Average	3.72	712	0.46	10625	9.80	226	25.27	278	3.94	73.04
		Minimum	3.37	562	0.07	7706	6.64	164	15.14	212	2.99	53.43
		Maximum	4.02	832	0.97	12756	11.97	271	44.48	338	5.05	85.50

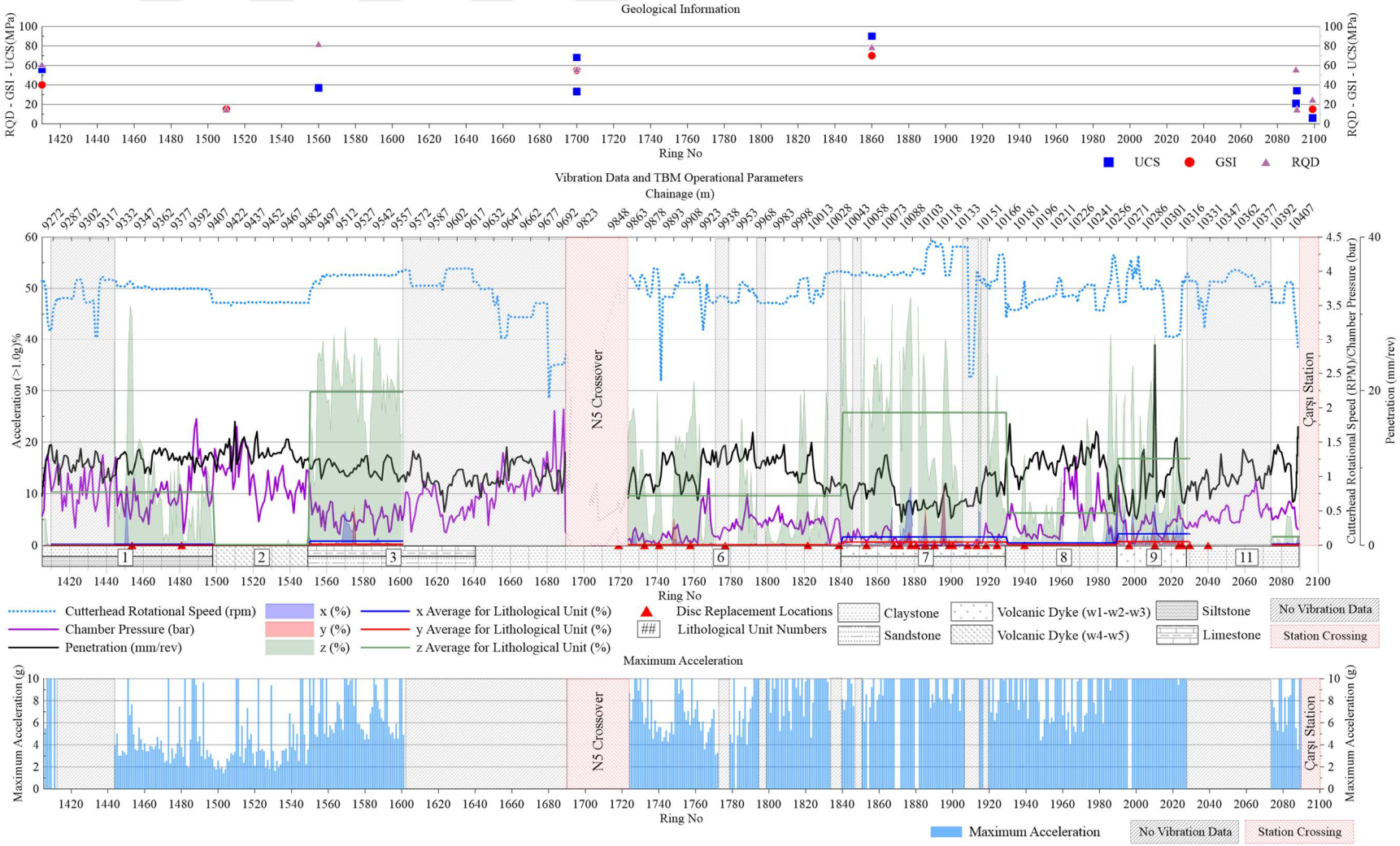

Figure 4.6 : TBM 2 top accelerometer data between rings 1400 and 2100 (Umraniye-Atasehir-Goztepe Metro Line).

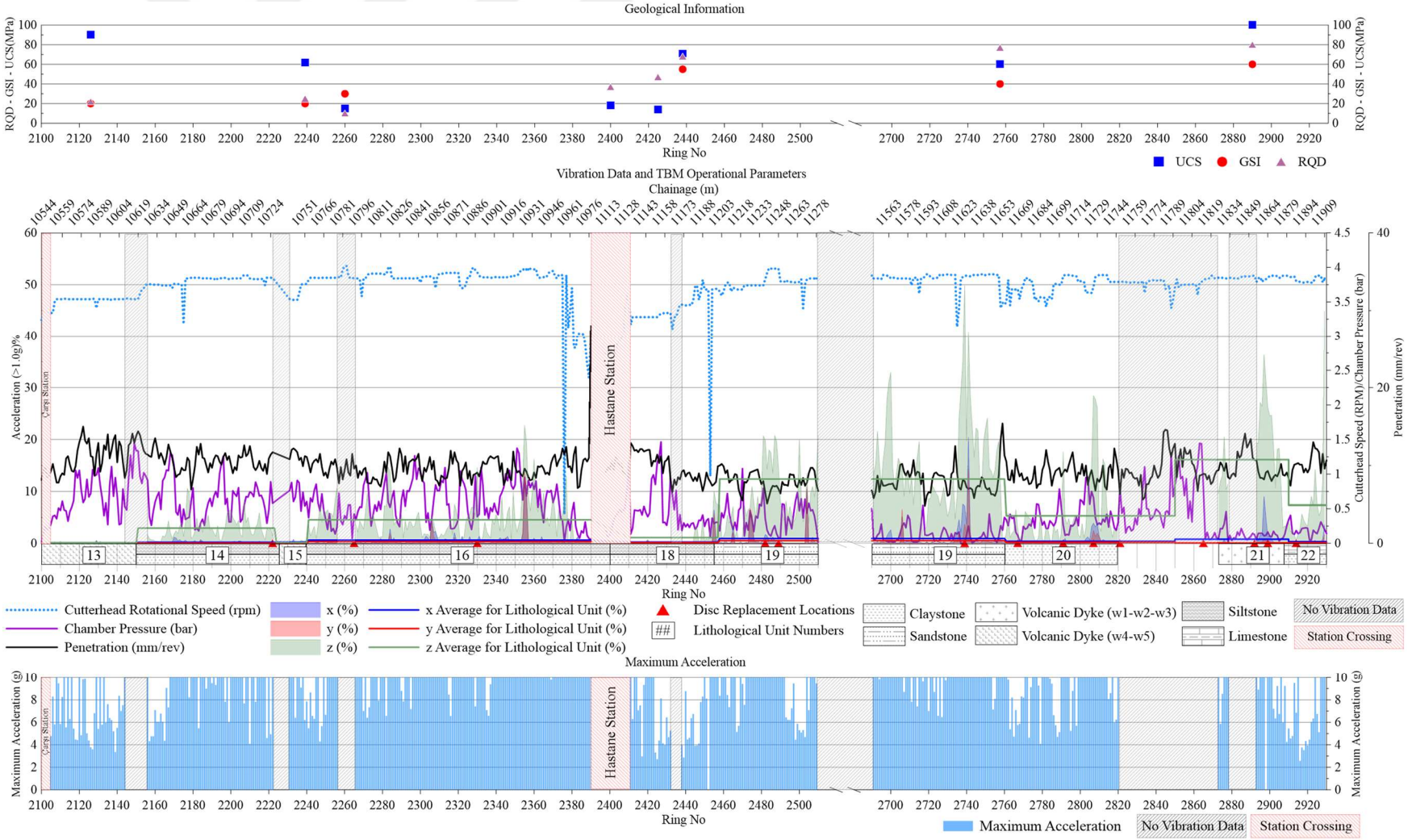

Figure 4.7 : TBM 2 top accelerometer data between rings 2100 and 2930 (Umraniye-Atasehir-Goztepe Metro Line).

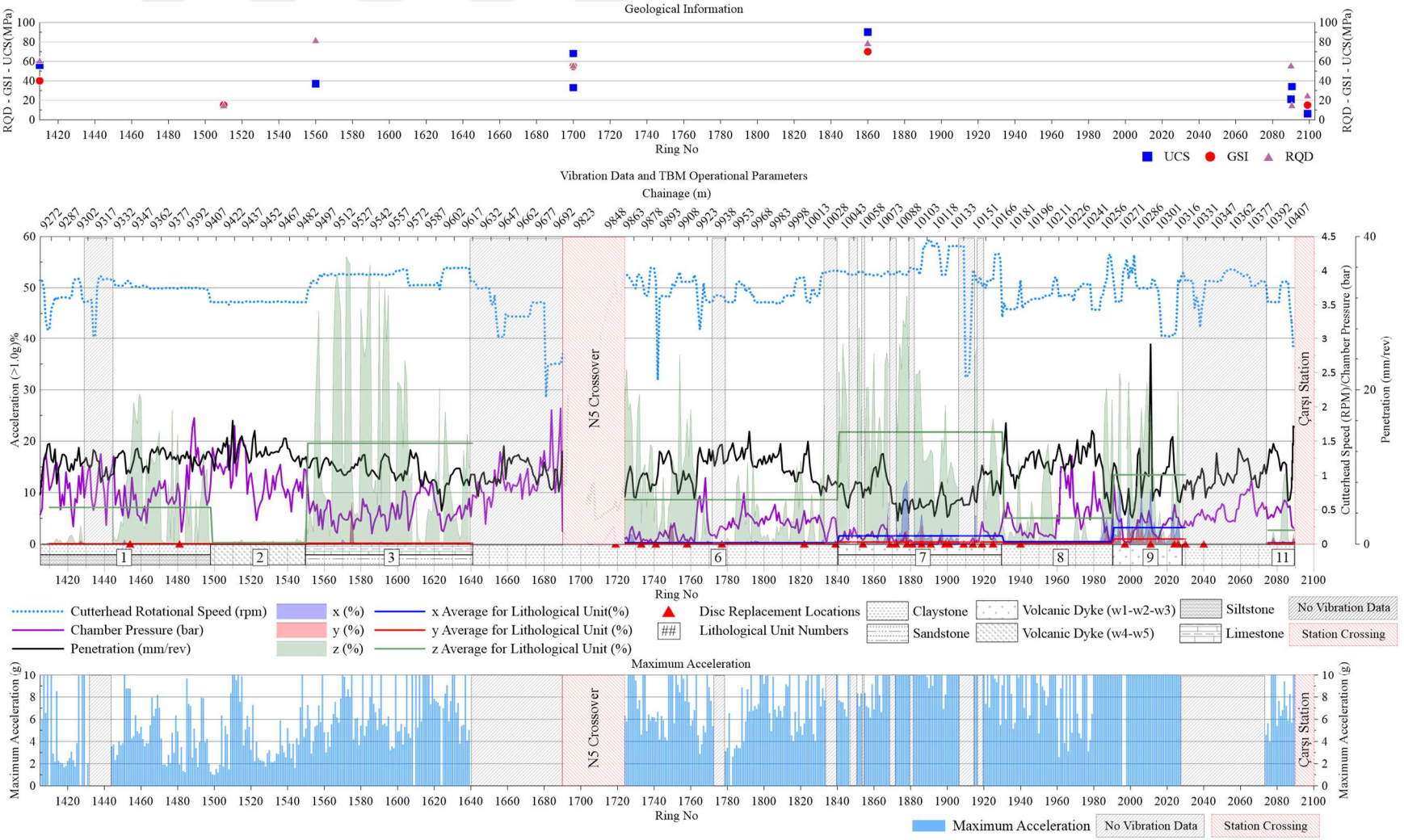

Figure 4.8 : TBM 2 bottom accelerometer data between rings 1400 and 2100 (Umraniye-Atasehir-Goztepe Metro Line).

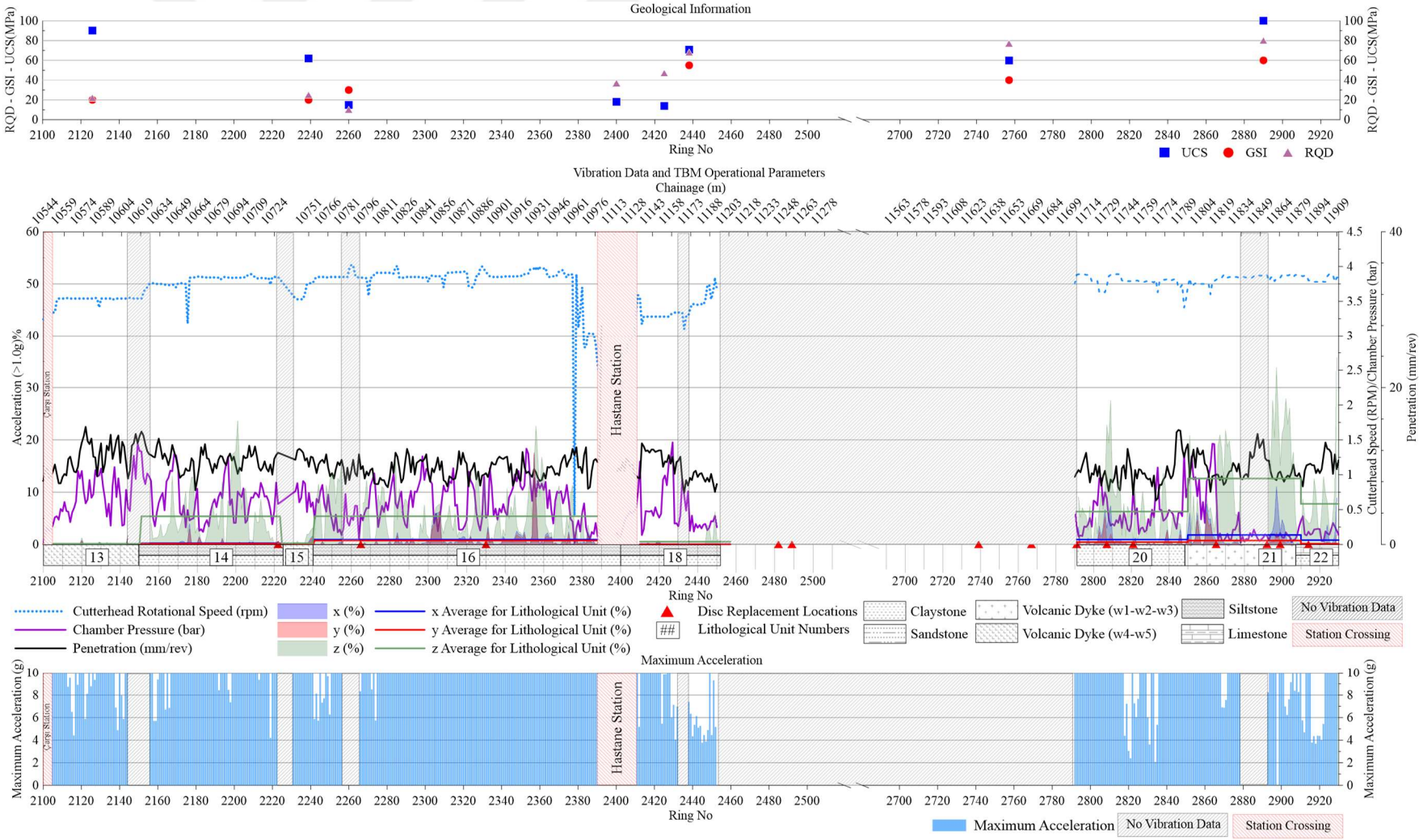

Figure 4.9 : TBM 2 bottom accelerometer data between rings 2100 and 2930 (Umraniye-Atasehir-Goztepe Metro Line).

- The relationship between vibration levels and alterations in geological conditions is apparent, as seen by the varying levels of average acceleration observed throughout different geological units. The vibration differences between the lithological units can be summarized as;
    - The highest vibration levels were recorded during the excavation of fresh andesite dykes (#7, #9 and #21), while the lowest ones were observed during the excavation of highly weathered dykes (#2 and #13).
    - The sandstone-limestone unit spanning between rings 1550 and 1640 (#3) exhibited significant incidence of accelerations exceeding the 1g threshold. However, the maximum acceleration levels rarely reached ±10g, showing that almost no shocks were observed. An example of this finding can be seen on Figure 4.10, which presents the vibration data of the five consecutive rings, showing consistent measurements during the excavation without any immediate peaks.

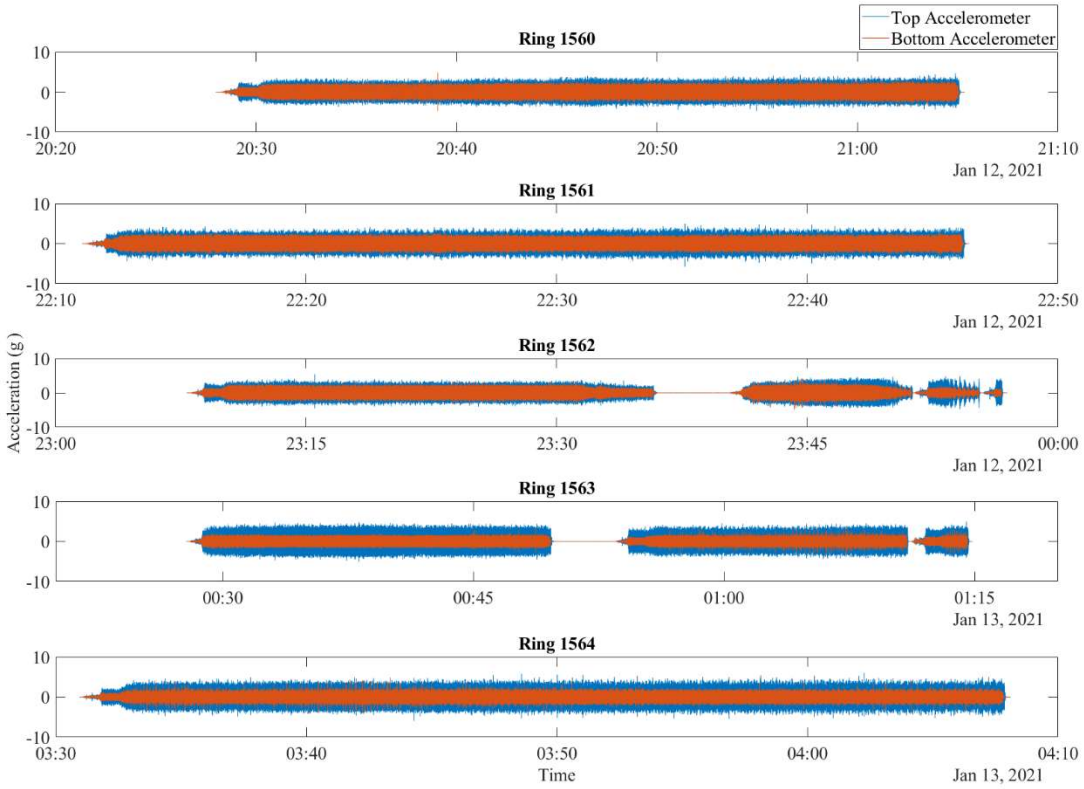

Figure 4.10 : Vibration data of the rings 1560 to 1564 of TBM 2 for z-axes (Sandstone-Limestone #3).

- In contrast to the previously discussed observation, during the excavation of siltstone-claystone units (#16 and #18) between rings 2240 and 2460, the overall percentage of acceleration levels exceeding the ±1g threshold remained low, while the maximum levels consistently reached ±10g. This behavior is believed to be influenced by alterations at the face. Figure 4.11 presents five consecutive rings in the area, showing the consistent occurrence of the shocks. It is noteworthy that a similar pattern was observed in TBM 3 as well, which eliminates the theory of these shocks being caused solely by damaged cutterhead components.

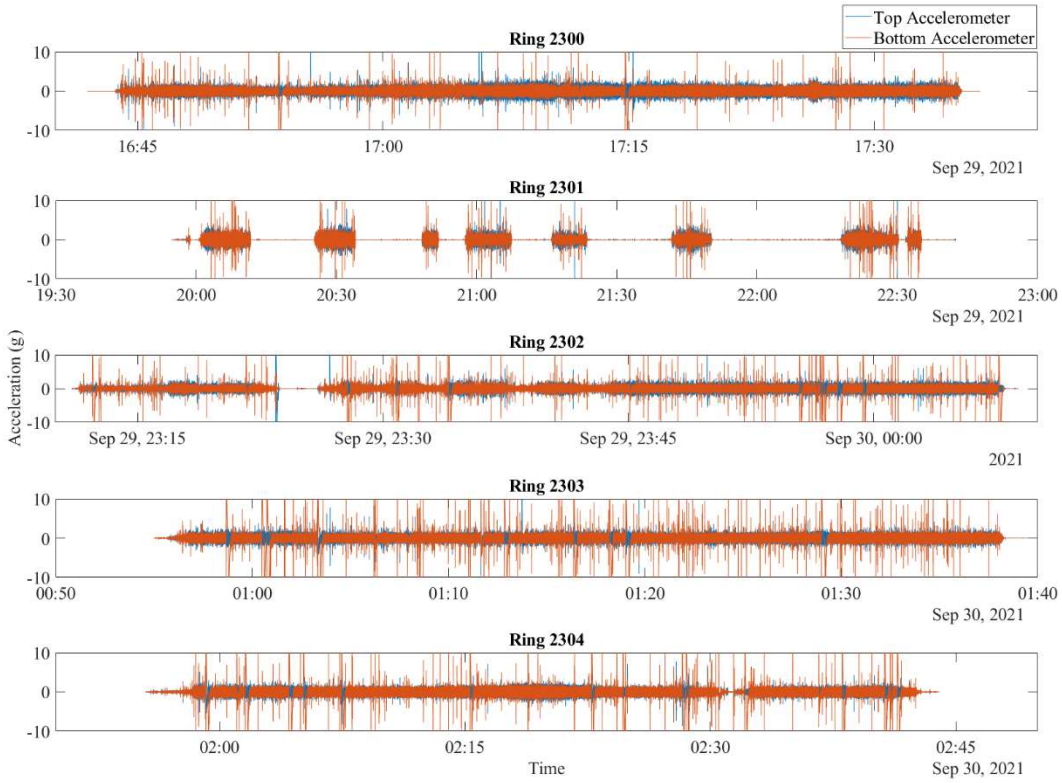

Figure 4.11 : Vibration data of the rings 2300 to 2304 of TBM 2 for z-axes (Siltstone-Claystone #16 and #18).

- In the local crushed or very weak zones, accelerations consistently remained below 1g. A good example of this observation can be seen between rings 1960 and 1970 (Claystone (#8), Figure 4.6 and Figure 4.8). Despite the absence of direct muck samples from this section, the observed elevation in chamber pressure serves as an indicative marker of a weak zone. This observation shows the potential applicability of the vibration monitoring system for identifying such weak zones.

Similar zones were also encountered in the vibration data of TBM 3, as elaborated in the subsequent section.

- A distinct correlation exists between the condition of cutting tools and vibration levels, particularly observable during hard rock excavation. When a cutter is damaged, it creates high amplitude shocks that is detectable in all accelerometer axes. The sections between the rings 1840 and 1930 where fresh claystone-andesite dyke (#7) was present, and between the rings 1990 and 2030 composed of a fresh andesite dyke (#9), serve as a good example of this phenomenon. Within these sections, a substantial number of broken cutting tools were identified and subsequently replaced. An in-depth analysis between the cutter conditions and vibrations will be presented in the following section.
- The analysis of vibration data identified high amplitude shocks exceeding 10g within low-strength geological units, such as the claystone unit (#2) encountered between rings 1500 and 1540 (Figure 4.12). However, pinpointing the exact origin of these shocks remains challenging due to the relatively low sampling rate (0.1 Hz) of the TBMs' data acquisition systems.

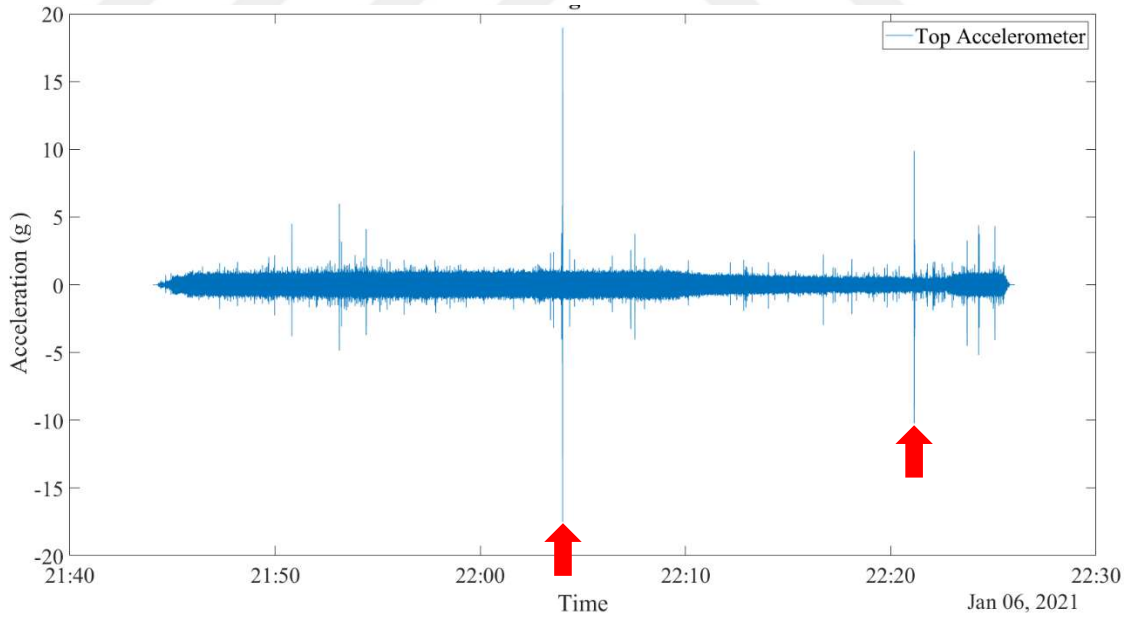

Figure 4.12 : Vibration data of the ring 1510 of TBM 2 (z-axis of top accelerometer).

Figure 4.13 illustrates the significant influence of the geological conditions on the vibrations. This figure presents the acceleration data between ring numbers 1800 and 2040, including the excavation face photos taken from the cutterhead and TBM operating parameters, together with geological information.

Between rings 1800 and 1820 the geological composition primarily consisted of very weak claystone, followed by a transition zone consisting of a stronger claystone which correspondingly led to an increase in vibration levels. Claystone and fresh andesite dykes (#7) were present together at the excavation face between rings 1840 and 1930, where the acceleration amplitudes increased. A significant number of broken cutting tools were also reported in this area, which notably influenced this increase. Following ring 1930, the TBM encountered claystone (#8) once more, leading to a reduction in vibrations until ring 1990, where a fresh andesite dyke (#9) was encountered.

4.2.1.1 Probability analyses

The Weibull parameters have been obtained through distribution fitting individually for each ring, and subsequently, the obtained α and β parameters have been averaged for each lithological unit to create a characteristic distribution, as detailed in the calculation methodology section.

The average Weibull parameters for the lithological units are presented in Table 4.4 and Figure 4.14. illustrates the corresponding Weibull cumulative distributions for the top and bottom accelerometers of each lithological unit. For ease of reference, both the table and legend of figure incorporates the unique number of each lithological unit as defined in Table 4.2. The figure effectively illustrates the variation in acceleration amplitudes across different lithological units. The data suggests a unique probability distribution of vibrations for different units, potentially enabling their identification based on vibration characteristics. Moreover, a greater likelihood of experiencing high amplitude vibrations within high strength rock formations was also observed.

To further explore this relationship, Figure 4.15 illustrates Weibull cumulative distributions for fresh (#9 and #21) and weathered (#2 and #13) dyke units. The difference between the probability distributions is clear and, this observation can be directly attributed to the changes in the geomechanical properties of the rocks due to weathering.

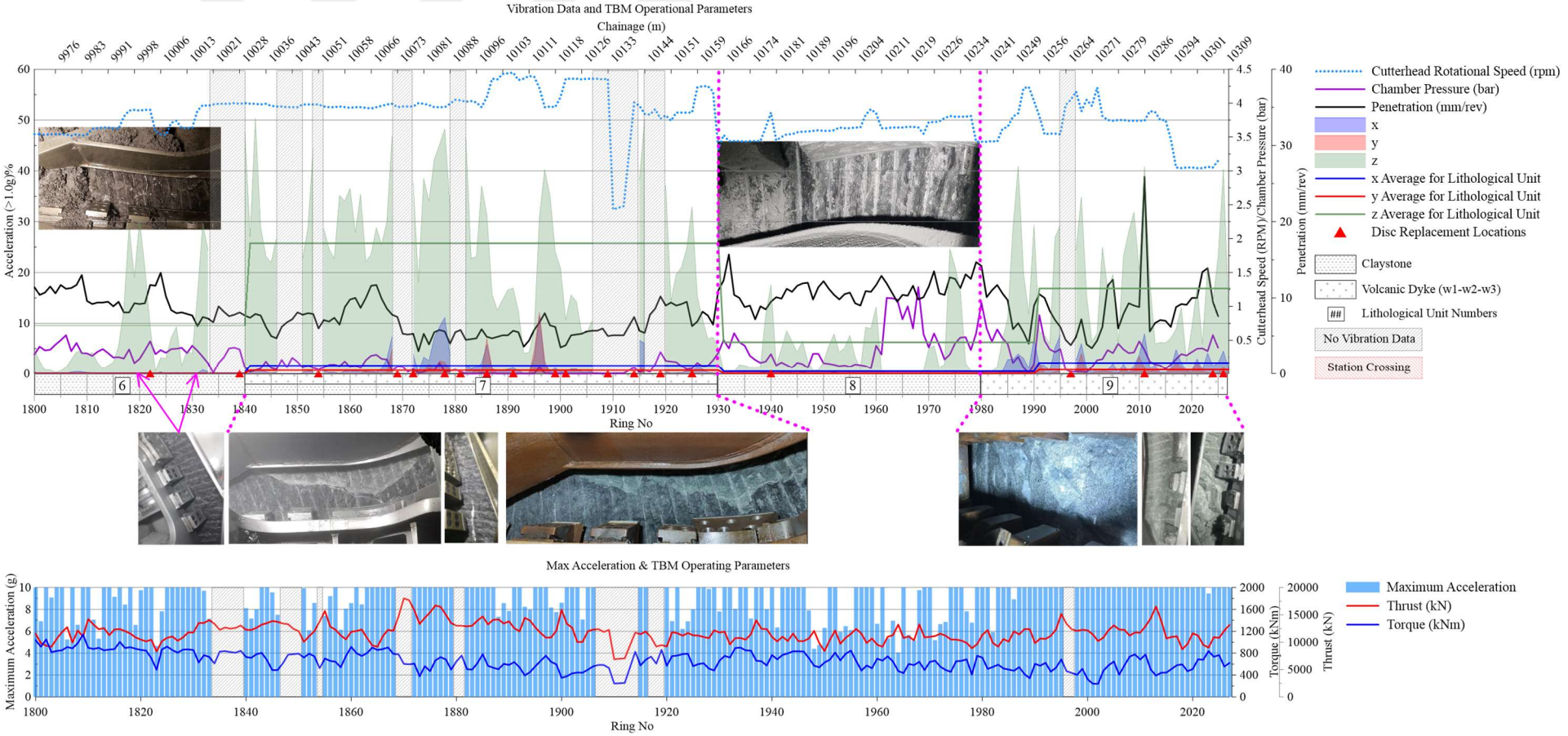

Figure 4.13 : Vibration data and photos taken from the cutterhead of the rings between 1800 and 2040 belong to top accelerometer (TBM 2).

Table 4.4 : Average Weibull parameters per lithological units (TBM 2).

Ring No (Start)	Ring No (End)	Lithological Unit	Top Accelerometer						Bottom Accelerometer					
			x		y		z		x		y		z	
			α	β	α	β	α	β	α	β	α	β	α	β
1410	1498	(1) Siltstone-Claystone	1.07	0.09	1.08	0.08	1.03	0.38	1.08	0.12	1.03	0.08	1.06	0.46
1499	1550	(2) Dyke (w4-w5)	1.10	0.07	1.12	0.05	1.10	0.22	1.10	0.11	1.06	0.04	1.10	0.19
1551	1641	(3) Sandstone-Limestone	1.10	0.14	1.11	0.14	1.11	0.64	1.11	0.24	1.08	0.11	1.12	0.79
		(4) No Data												
		(5) N5 Crossover												
1722	1850	(6) Claystone	0.86	0.12	0.89	0.10	0.81	0.37	0.91	0.12	0.81	0.08	0.86	0.40
1851	1930	(7) Claystone-Dyke (w1-w2)	0.90	0.22	0.92	0.18	0.87	0.60	0.92	0.23	0.85	0.15	0.90	0.67
1931	1990	(8) Claystone	0.92	0.12	0.94	0.09	0.89	0.30	0.96	0.12	0.89	0.08	0.92	0.33
1991	2030	(9) Dyke (w1-w2)	0.80	0.23	0.83	0.15	0.80	0.44	0.83	0.21	0.77	0.13	0.82	0.50
		(10) No Data												
2075	2090	(11) Claystone	0.89	0.08	0.90	0.07	0.86	0.22	0.92	0.08	0.86	0.06	0.89	0.21
		(12) Carsi Station												
2100	2150	(13) Dyke (w4-w5)	1.00	0.07	1.04	0.05	1.00	0.16	1.05	0.06	1.03	0.05	1.06	0.15
2151	2223	(14) Siltstone-Claystone	0.93	0.10	0.94	0.10	0.88	0.33	0.94	0.08	0.91	0.08	0.96	0.32
2224	2260	(15) Dyke (w4-w5)	0.89	0.11	0.88	0.10	0.85	0.34	0.94	0.09	0.89	0.07	0.92	0.29
2261	2390	(16) Siltstone-Claystone	0.82	0.13	0.84	0.11	0.84	0.32	0.87	0.11	0.89	0.08	0.93	0.34
		(17) Hastane Station												
2410	2457	(18) Siltstone-Claystone	0.98	0.09	1.02	0.06	0.95	0.18	1.00	0.09	0.96	0.06	1.00	0.20
2458	2760	(19) Sandstone-Claystone							0.92	0.16	0.91	0.12	0.93	0.47
2761	2850	(20) Claystone	0.88	0.13	0.92	0.13	0.89	0.37	0.96	0.12	0.89	0.10	0.94	0.35
2850	2910	(21) Dyke (w1-w2)	0.84	0.18	0.88	0.16	0.85	0.46	0.96	0.17	0.91	0.14	0.93	0.53
2910	2930	(22) Sandstone-Claystone	0.97	0.14	0.99	0.14	0.94	0.41	1.01	0.12	0.94	0.11	0.98	0.41

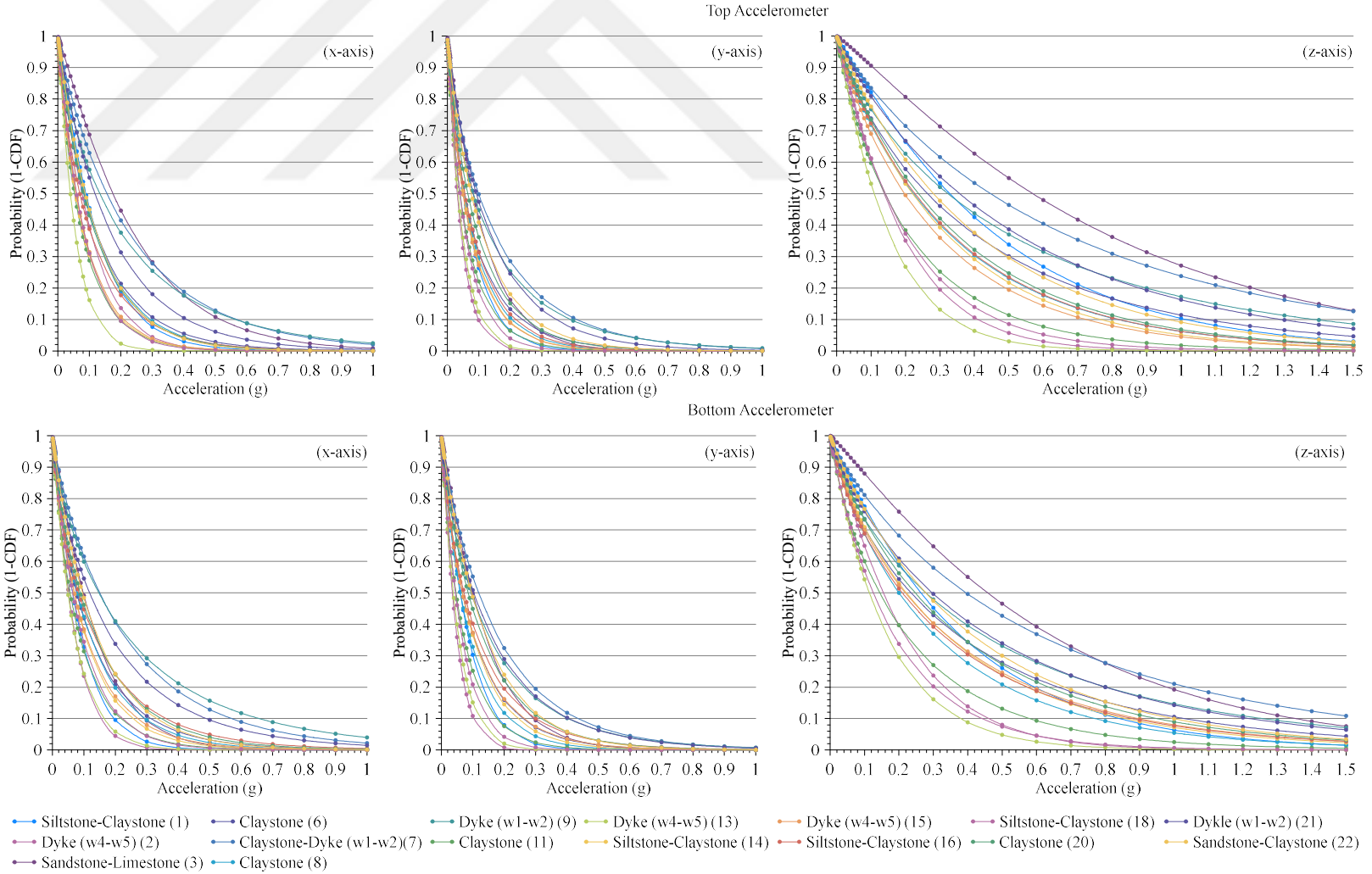

Figure 4.14 : Cumulative probability graphs obtained by using Weibull distribution for top and bottom accelerometers of TBM 2.

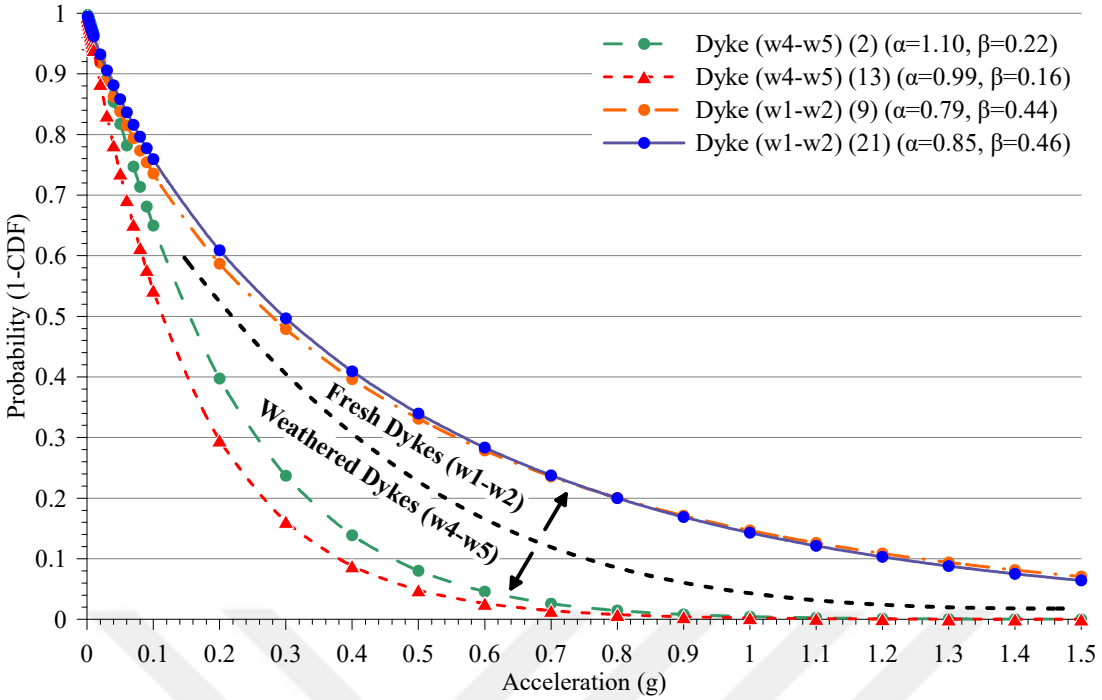

Figure 4.15 : Weibull probability distributions for andesite dykes with different weathering degrees (z-axis of the top accelerometer of TBM 2).

4.2.2 Analysis of the vibration data obtained from TBM 3

TBM 3 shares the same specifications with TBM 2, and they excavated side by side. The presence of two TBMs (TBM 2 and 3) provided the opportunity to compare vibrations under similar conditions, to demonstrate the reproducibility of results. It is important to acknowledge that the accelerometers on TBM 3 had a measurement range of 4g, whereas on TBM 2 the measurement range was 10g. Following the comparison of vibration data between TBM 2 and 3 in similar conditions, it has been realized that, the peak values in some sections might not accurately represent the actual acceleration amplitudes that TBM 3 experienced, due to the limited accelerometer measurement range.

The average TBM operational data for TBM 3 are presented on Table 4.5. Figure 4.16 to Figure 4.19 illustrate rock properties obtained from the boreholes, lithological units, top and bottom accelerometer data (indicated the percentage of data points per ring exceeding the ±1g threshold and their averages per lithological unit), disc replacement locations, selected TBM operating parameters, and the maximum acceleration amplitudes.

Table 4.5 : Average TBM operational parameters for TBM 3.

Ring No (Start)	Ring No (End)	Lithological Unit	Cutter Speed (RPM)	Cutter Torque (kNm)	Average Face Pressure (bar)	Total Thrust (kN)	Penetration Rate (mm/rev)	Thrust / Cutter (kN)	Boreability Index (kN/cutter)/(mm/rev)	P (kW)	SE (kWh/m^3)	ICR (m^3/h)
1505	1540	(2) Dyke (w4-w5)	3.74	842	0.67	8700	12.57	185	14.98	330	3.56	94.35
1541	1580	(3) Sandstone-Limestone	3.98	855	0.35	9399	9.98	200	20.38	355	4.52	79.42
1581	1657	(4) Claystone	3.80	853	0.54	10363	11.43	220	19.84	339	3.99	87.1
1706	1800	(5) N5 Crossover (6) Claystone	3.74	725	0.32	9569	8.53	204	24.96	283	4.50	63.73
1821	1905	(-) No Data (7) Claystone-Dyke (w1-w2)	3.86	639	0.08	12421	6.04	264	45.57	256	5.54	46.66
1993	2024	(-) No Data (9) Dyke (w1-w2)	3.99	499	0.10	12135	6.03	258	44.35	209	4.32	48.26
2025	2060	(10) Dyke (w4-w5)	3.64	654	0.30	11278	8.24	240	30.52	249	4.18	60.15
2061	2081	(11) Claystone	3.94	674	0.21	8669	9.91	184	19.03	278	3.59	78.23
2103	2126	(12) Carsi Station (13) Dyke (w4-w5)	3.41	548	0.27	7548	10.11	161	16.11	195	2.84	69.07
2127	2229	(14) Siltstone-Claystone	3.77	546	0.30	9101	9.050	194	22.12	216	3.21	68.02
2230	2238	(15) Dyke (w4-w5)	3.67	722	0.27	8044	10.91	171	15.87	277	3.47	80.02
2239	2405	(16) Siltstone-Claystone	3.26	602	0.26	9588	11.43	204	19.08	202	2.84	72.26
2416	2438	(17) Hastane Station (18) Siltstone-Claystone	3.53	546	0.02	6843	7.57	146	19.38	202	3.72	53.75
2439	2517	(19.1) Sandstone-Claystone	4.01	529	0.03	8836	7.76	188	25.26	222	3.61	62.20
2518	2532	(23) Dyke (w4-w5)	3.62	495	0.29	6707	10.35	143	14.26	182	2.54	75.06
2533	2629	(19.2) Sandstone-Claystone	4.02	534	0.07	10368	7.56	221	30.66	225	3.78	60.67
		Average	3.75	641	0.26	9348	9.22	199	23.90	251	3.76	68.68
		Minimum	3.26	495	0.02	6707	6.03	143	14.26	182	2.54	46.66
		Maximum	4.02	855	0.67	12421	12.57	264	45.57	355	5.54	94.35

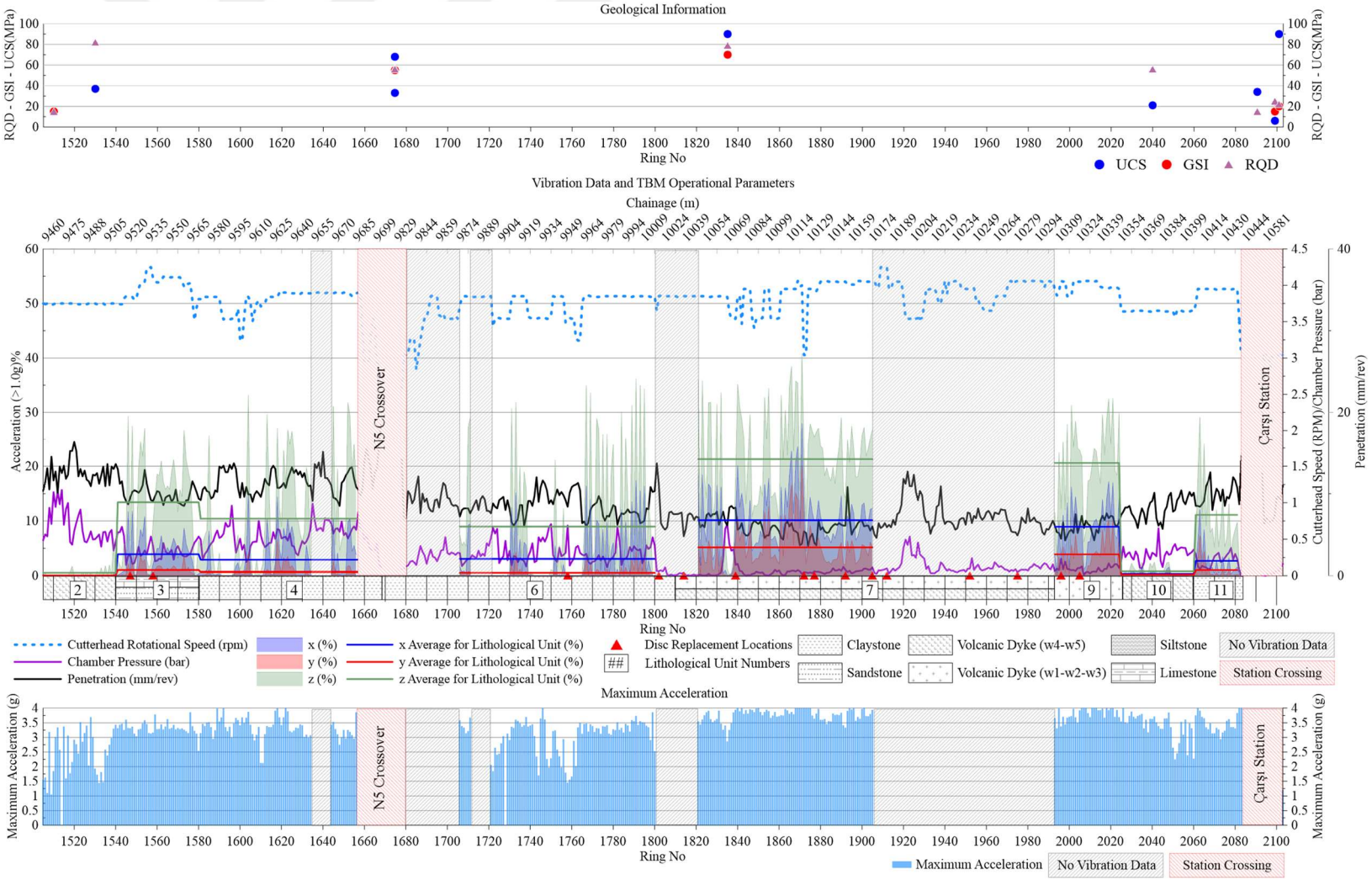

Figure 4.16 : TBM 3 top accelerometer data between rings 1500 and 2100 (Umraniye-Atasehir-Goztepe Metro Line).

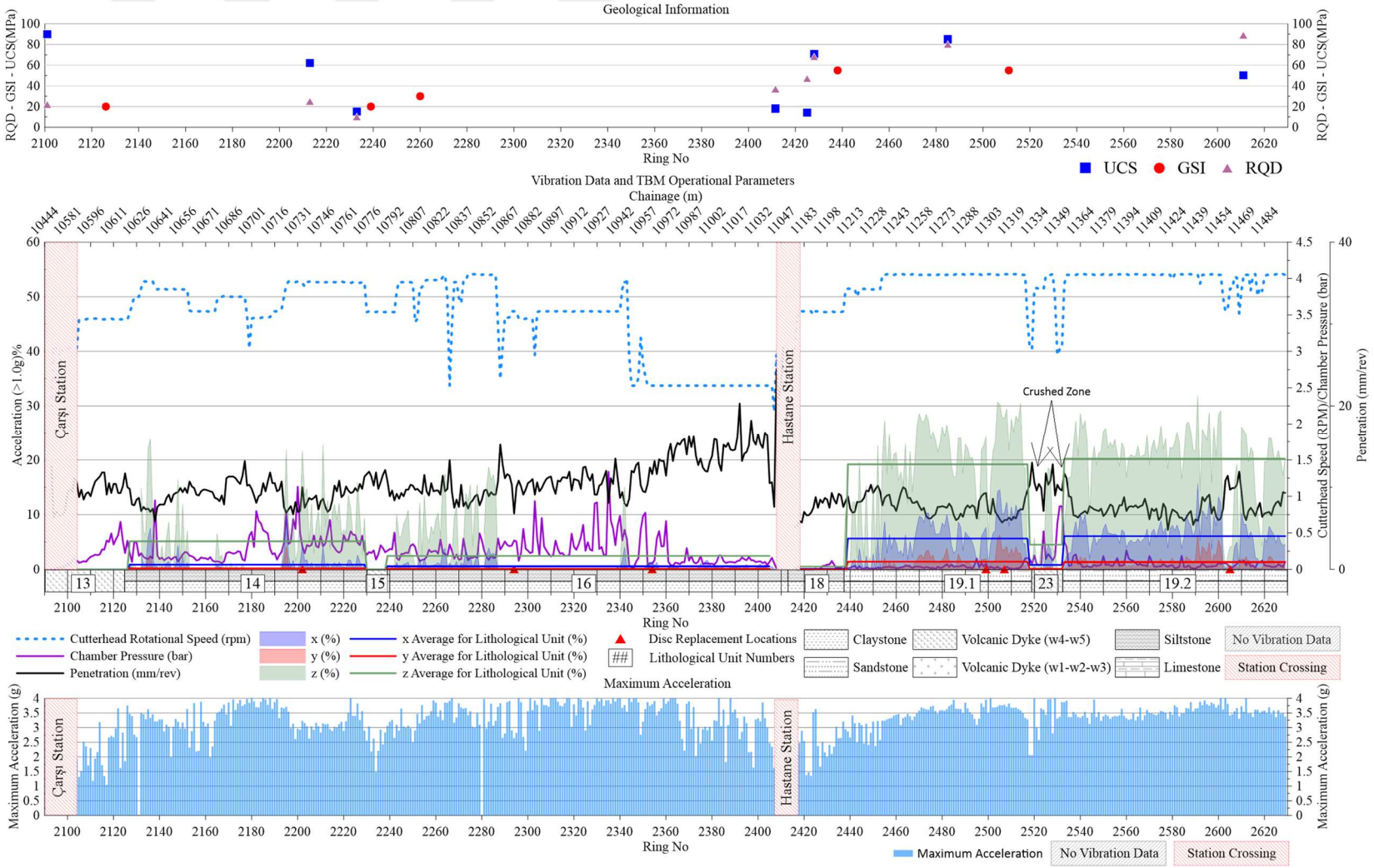

Figure 4.17 : TBM 3 top accelerometer data between rings 2100 and 2630 (Umraniye-Atasehir-Goztepe Metro Line).

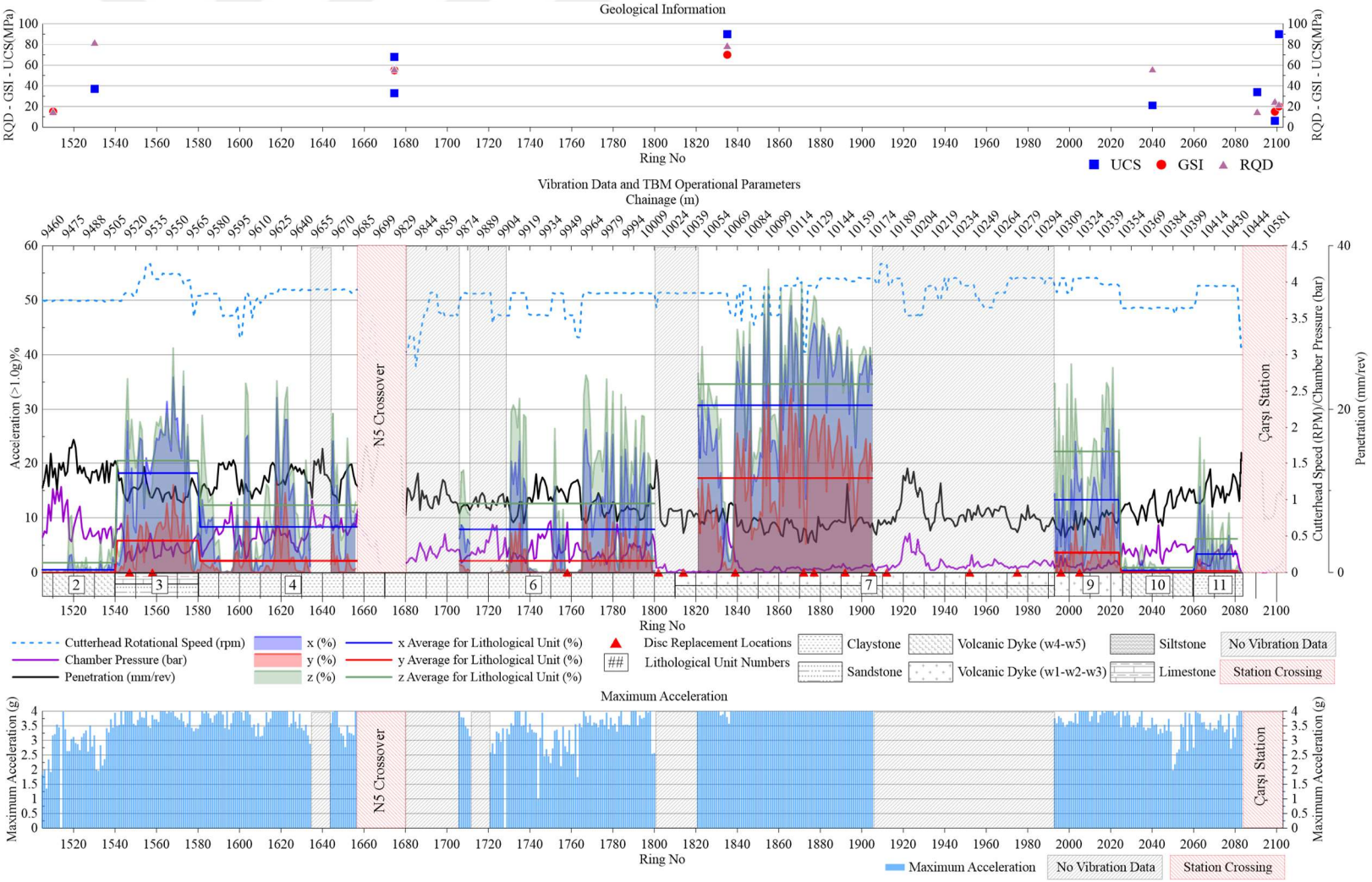

Figure 4.18 : TBM 3 bottom accelerometer data between rings 1500 and 2100 (Umraniye-Atasehir-Goztepe Metro Line).

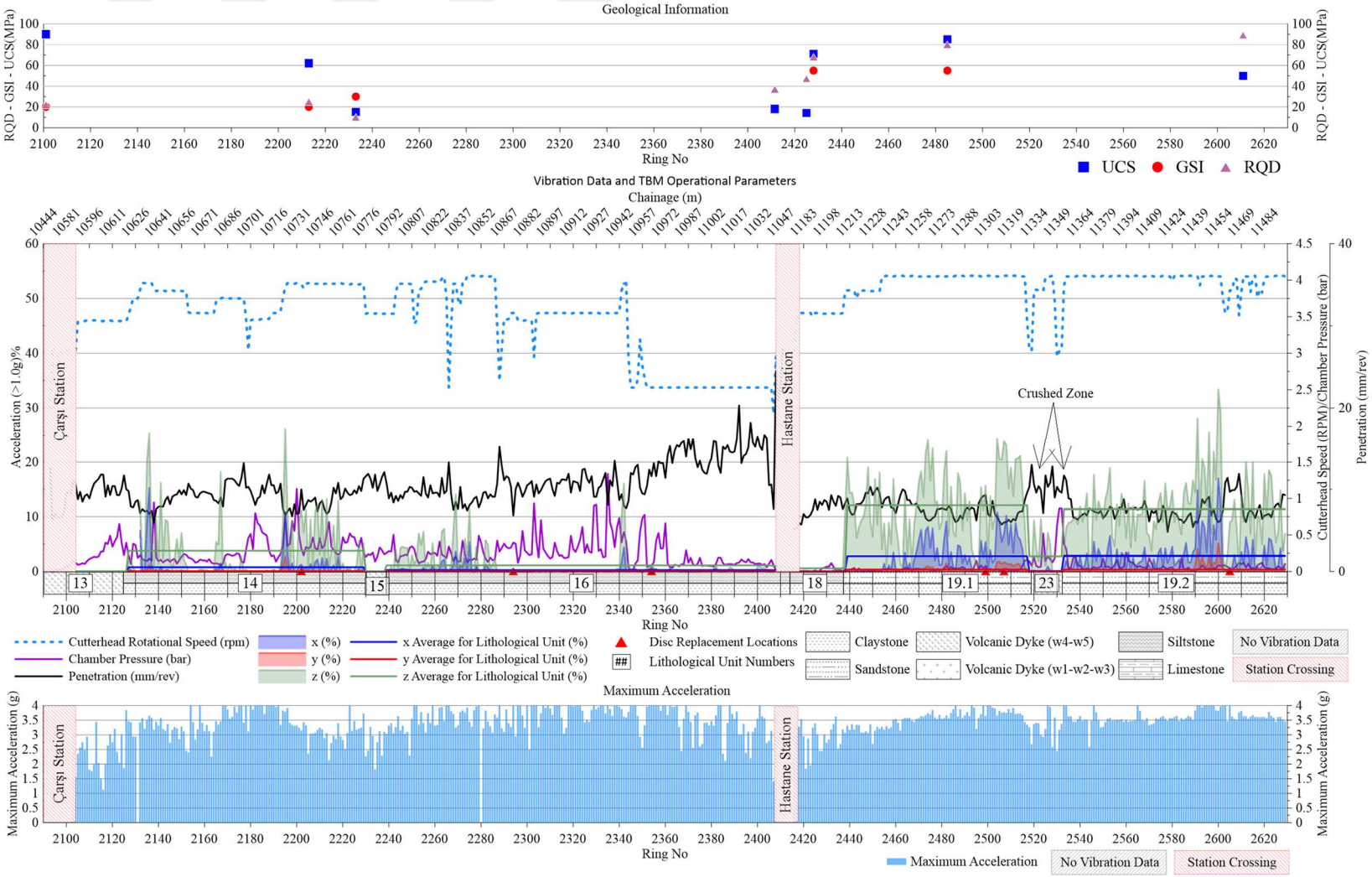

Figure 4.19 : TBM 3 bottom accelerometer data between rings 2100 and 2630 (Umraniye-Atasehir-Goztepe Metro Line).

Upon thorough analysis of the figures (Figure 4.16 to Figure 4.19), the primary findings can be summarized as follows:

- Consistent with observations from other TBMs, vibration levels were strongest on the z-axis for TBM 3. However, on TBM 2, notable distinctions between axes were apparent, while on TBM 3, x and y-axes were very close to the z-axis, particularly on the bottom accelerometer.
- The vibration amplitudes recorded on the bottom accelerometer exceeding ±1g were higher than the top accelerometer. Notably, the difference in vibration amplitudes between the top and bottom accelerometers was significantly smaller for TBM 3 compared to TBM 2. This discrepancy can likely be attributed to the limited measurement range of the accelerometers used in TBM 3. Most likely, in certain locations with high strength rocks, even the amplitudes at the bottom side were higher, both accelerometers were limited to 4g measurement range, and this difference was not reflected in the recorded data.
- The key observations regarding the geological conditions' effect on the vibrations can be summarized as;
    - The most substantial vibrations were recorded during the excavation of dyke units (#7 and #9), whereas the lowest levels are recorded in weathered dykes (#2, #10 and #15). This observation is similar with TBM 2.
    - Data acquisition commenced during the excavation of weathered dyke (#2) with a notably low percentage of vibrations exceeding ±1g threshold. As the TBM transitioned into the sandstone-limestone unit (#3) vibration levels exhibited a noticeable increase. Consistent with observations from TBM 2, no significant shocks were observed within this section. However, it is important to acknowledge the 4g measurement range of the accelerometers installed on TBM 3. As illustrated in Figure 4.20 for one ring, during the excavation in some stretches the recorded data consistently reached 4g limit. This implies the potential presence of higher amplitude shocks that exceeded the sensor's capacity and consequently, remained unrecorded.

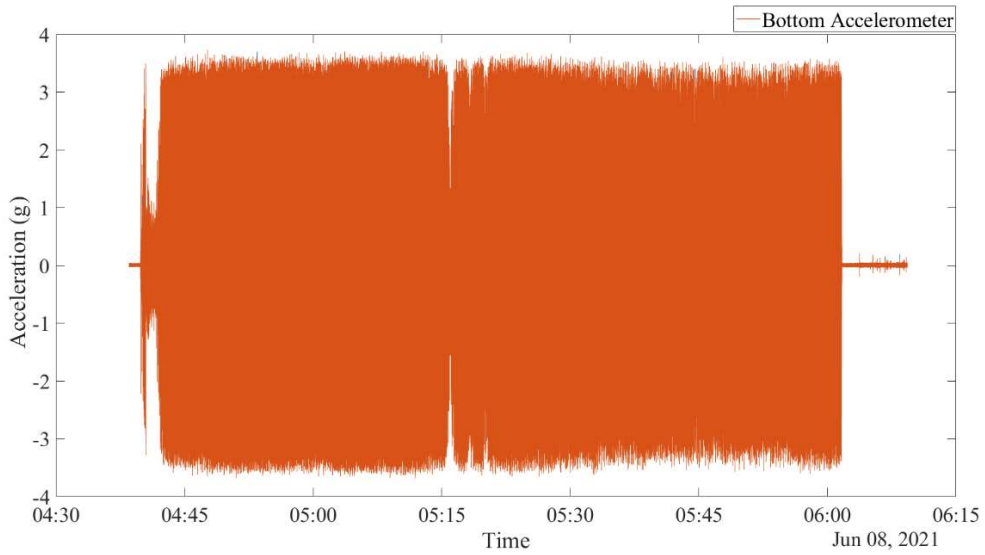

Figure 4.20 : Vibration data of ring 1860 of TBM 3 (Bottom accelerometer, z-axis).

- Subsequent to the sandstone-limestone unit (#3), the TBM excavated in claystone units (#4 and #6) between the rings 1580 and 1890 until encountering the claystone-andesite dyke (#7). In this dyke vibrations increased significantly; however, it should be noted again that accelerometers' measurement range may not have been sufficient to capture the real amplitudes. Figure 4.21 illustrates the recorded vibrations of five consecutive rings in this dyke (#7) section, showing the acceleration amplitudes of 4g throughout the excavation. Similar to the TBM 2, there were frequent cutterhead interventions for cutter replacement, which raises the possibility of the occurrence of unrecorded high amplitude shocks that exceeded the accelerometers' measurement range.

- Between ring numbers 2020 and 2060 the TBM excavated in highly weathered dyke (#10), resulting in a rapid reduction of vibration amplitudes. In this stretch, the penetration rate and face pressure were increased, while cutterhead speed was decreased. Unfortunately, there were no vibration data recorded for TBM 2 in this section, preventing direct comparison between the TBMs. However, a similar vibration profile can be seen between the rings 2230 and 2238 where TBM 3 excavated in a highly weathered dyke (#15); TBM 2, excavated in this section between ring numbers 2224 and 2240, with similar amplitude vibrations.

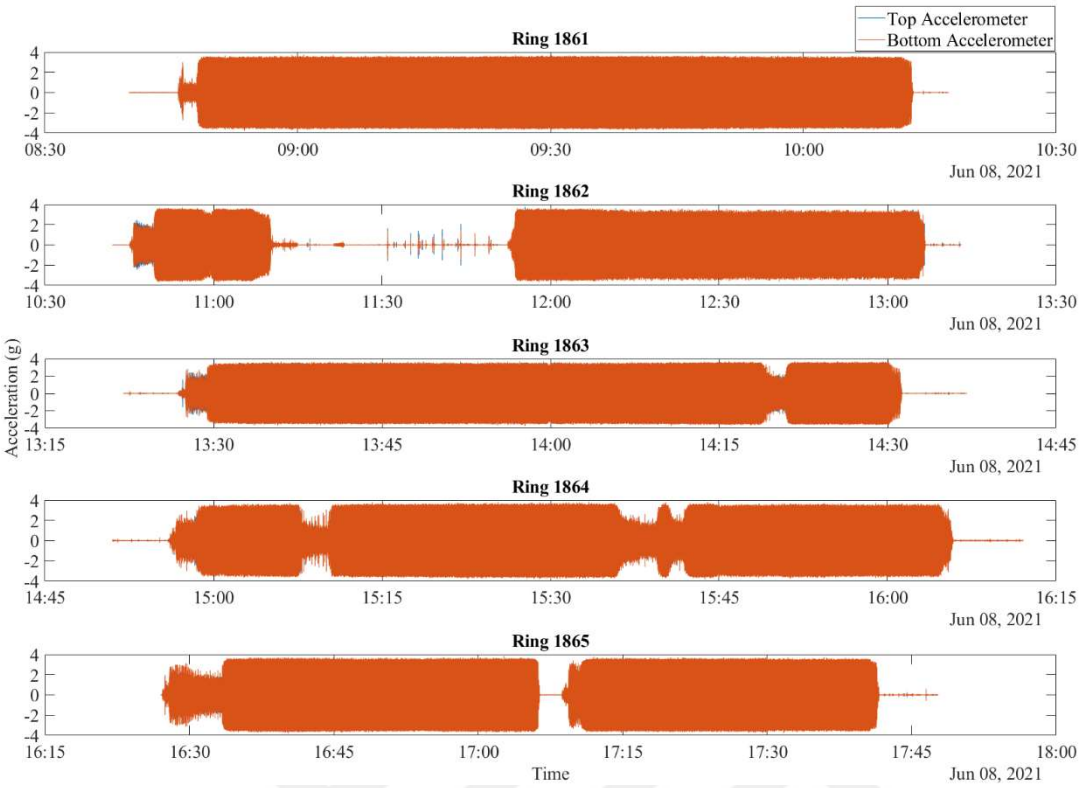

Figure 4.21 : Vibration data of ring 1861 to 1865 of TBM 3 (z-axes).

- During the excavation between Carsi Station and Hastane Station, the TBM encountered alternating siltstone-claystone (#14) units with varying degrees of strength. Notably, the section between rings 2125 and 2230 provides another good example of seeing geological conditions' influence on vibrations. In the area, TBM vibrations increased where face pressure is reduced and vice versa, proving that as the geological conditions worsen, face pressure increases and vibrations reduce.
- A crushed dyke (#23) is excavated between rings 2518 and 2532, where vibration amplitudes were reduced significantly. Notably, this unit was fresh on the TBM 2 side, where higher vibration amplitudes were observed.

4.2.2.1 Probability analyses

Weibull analyses were conducted with the acceleration data obtained from the top and bottom accelerometers, following a similar approach as with the other TBMs (Table 4.6.). Cumulative probability distributions for each lithological unit are presented on Figure 4.22. According to the analyses encountering higher amplitude vibrations in high strength rocks are more probable, as expected.

Figure 4.23. provides a more comprehensive illustration of the influence of weathering on vibrations by presenting cumulative probability distributions for fresh and weathered dykes. The distinction between the probability distributions is very clear in the figure. For example, the probability of observing 0.4g acceleration changes between 2% and 25% for weathered dyke units while, it is between 49% and 55% for fresh dykes.

To further highlight the influence of rock strength on vibration characteristics, Weibull cumulative probability distributions are presented for sandstone-claystone and siltstone-claystone units (#16, #18, and #19) with varying geomechanical properties in Figure 4.24. As detailed previously, units #19.1 and #19.2, represent the same lithological unit separated by a dyke intrusion. The figure shows that the probability curves for #19.1 and #19.2 are nearly identical, with a higher likelihood of encountering high-amplitude vibrations compared to the other units. This observation shows that, in case of having same geomechanical properties, very similar probabilities can be expected for rock units.

Table 4.6 : Average Weibull parameters per lithological unit (TBM 3).

Ring No (Start)	Ring No (End)	Lithological Unit	Top Accelerometer						Bottom Accelerometer					
			x		y		z		x		y		z	
			α	β	α	β	α	β	α	β	α	β	α	β
1505	1540	(2) Dyke (w4-w5)	1.15	0.16	1.17	0.11	1.12	0.24	1.11	0.23	1.14	0.16	1.12	0.31
1541	1580	(3) Sandstone-Limestone	1.06	0.34	1.08	0.26	1.04	0.49	1.03	0.56	1.05	0.37	1.03	0.61
1581	1657	(4) Claystone	1.04	0.28	1.06	0.21	1.02	0.42	1.00	0.39	1.03	0.26	1.01	0.46
1706	1800	(5) N5 Crossover (6) Claystone	1.00	0.24	1.03	0.17	0.97	0.35	0.97	0.34	1.01	0.23	0.96	0.42
1821	1905	(-) No Data (7) Claystone-Dyke (w1-w2) (-) No Data	0.88	0.40	0.91	0.32	0.86	0.55	0.86	0.71	0.88	0.50	0.85	0.79
1993	2024	(9) Dyke (w1-w2)	0.93	0.40	0.95	0.32	0.90	0.56	0.92	0.46	0.96	0.31	0.90	0.59
2025	2060	(10) Dyke (w4-w5)	1.01	0.14	1.02	0.10	0.99	0.20	1.01	0.15	1.04	0.10	1.00	0.20
2061	2081	(11) Claystone (12) Carsi Station	0.97	0.30	1.00	0.24	0.93	0.44	0.97	0.28	1.03	0.17	0.96	0.35
2103	2126	(13) Dyke (w4-w5)	1.13	0.07	1.15	0.06	1.10	0.10	1.14	0.07	1.17	0.05	1.11	0.11
2127	2229	(14) Siltstone-Claystone	1.03	0.20	1.05	0.15	1.00	0.30	1.03	0.19	1.08	0.11	1.01	0.29
2230	2238	(15) Dyke (w4-w5)	1.13	0.10	1.15	0.07	1.11	0.15	1.14	0.09	1.17	0.07	1.12	0.15
2239	2405	(16) Siltstone-Claystone (17) Hastane Station	1.01	0.18	1.03	0.14	1.01	0.21	1.02	0.14	1.06	0.10	1.02	0.18
2416	2438	(18) Siltstone-Claystone	1.15	0.11	1.16	0.08	1.12	0.17	1.14	0.12	1.17	0.09	1.11	0.23
2439	2517	(19.1) Sandstone-Claystone	1.05	0.38	1.07	0.27	1.03	0.59	1.06	0.30	1.08	0.19	1.04	0.49
2518	2532	(23) Dyke (w4-w5)	1.10	0.19	1.12	0.14	1.08	0.28	1.12	0.15	1.15	0.10	1.10	0.26
2533	2629	(19.2) Sandstone-Claystone	1.04	0.39	1.06	0.28	1.01	0.59	1.04	0.31	1.07	0.18	1.02	0.47

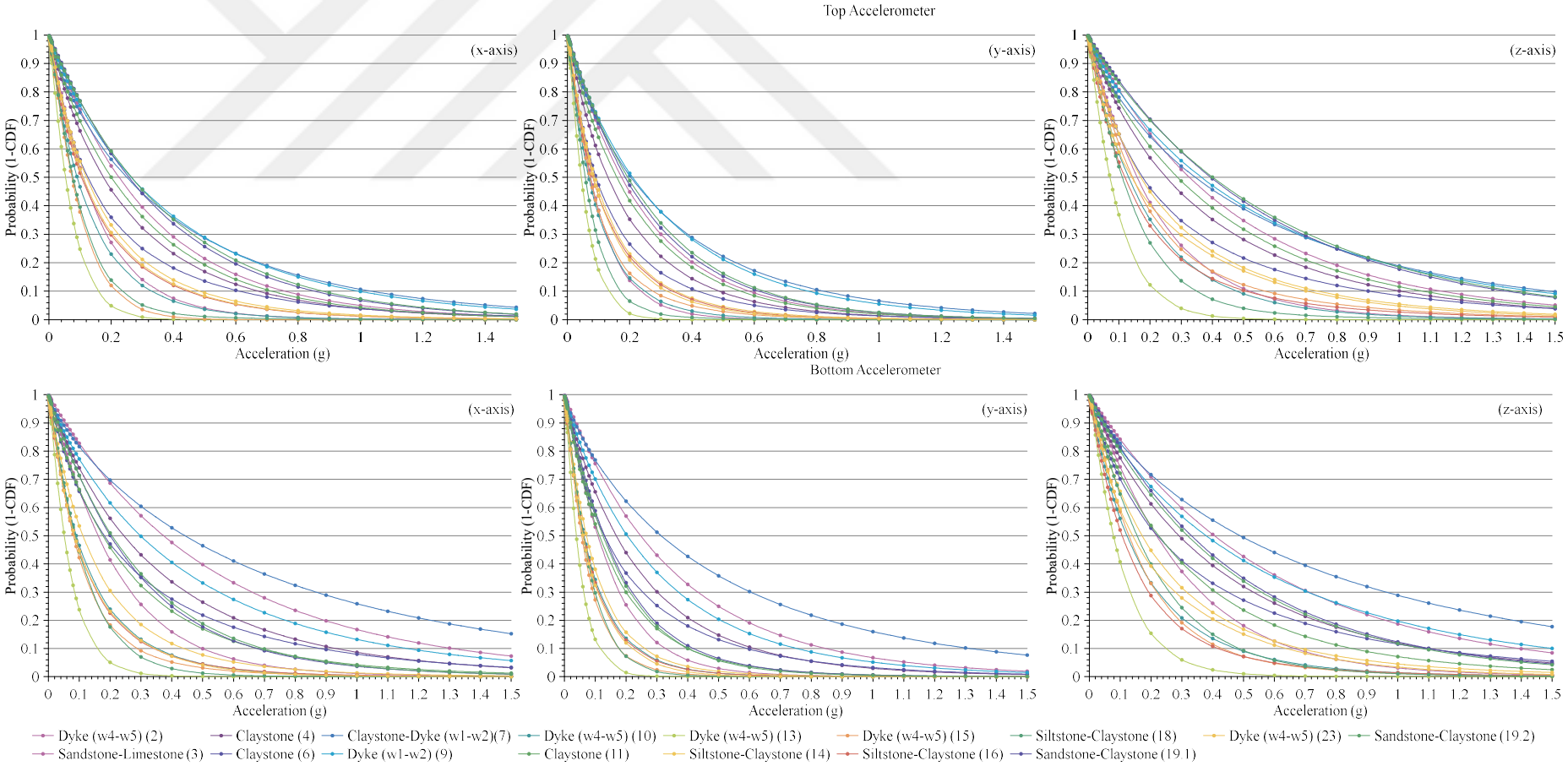

Figure 4.22 : Probability graphs obtained by using Weibull distribution for top and bottom accelerometers for TBM 3.

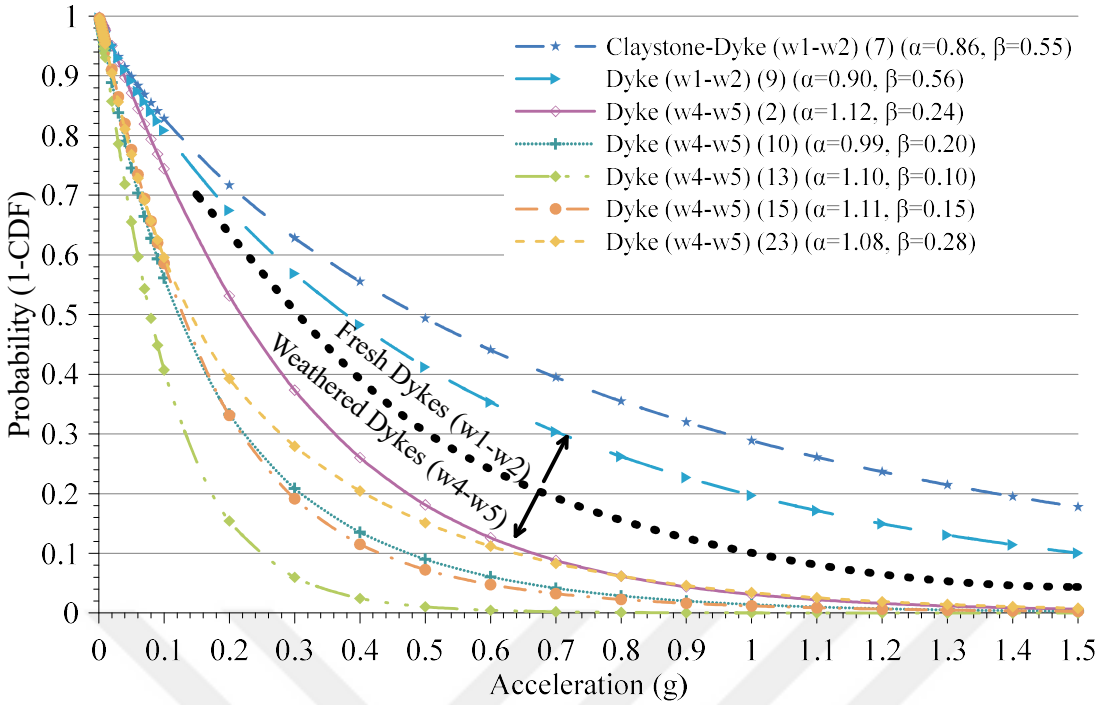

Figure 4.23 : Weibull probability distributions for dykes with different weathering degrees (TBM 3, top accelerometer z-axis).

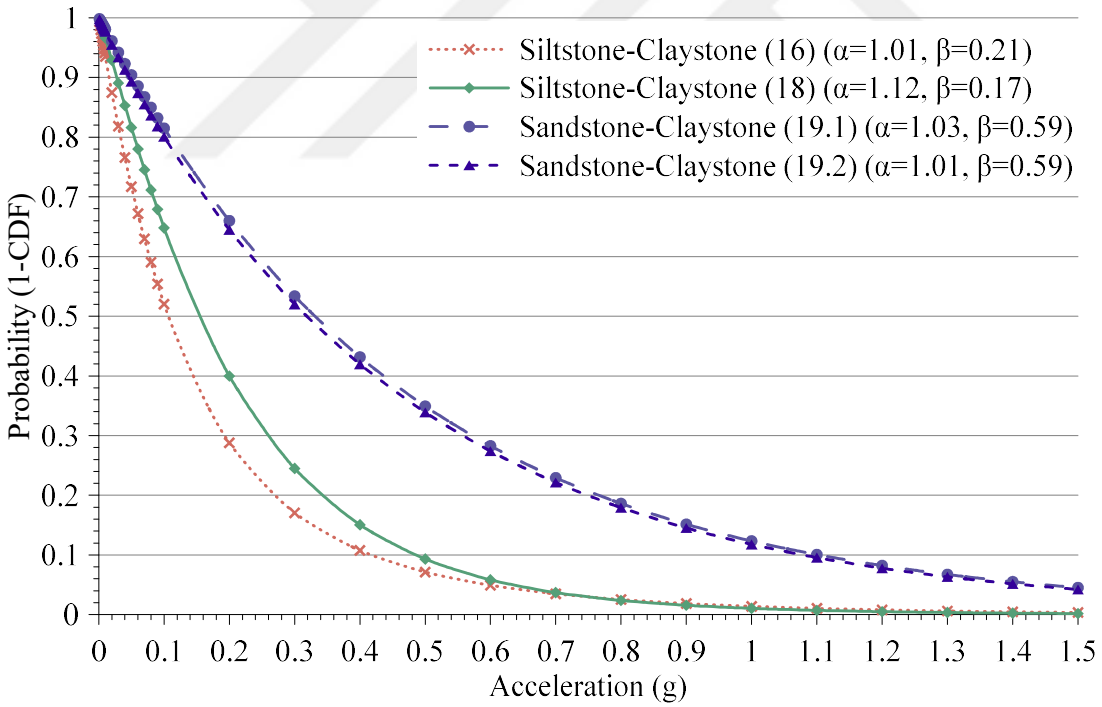

Figure 4.24 : Weibull probability distributions for siltstone-claystone and sandstone-claystone units (TBM 3, top accelerometer z-axis).

4.3 European Region Potable Water Transmission Tunnel Project (TBM 4)

The TBM 4 holds particular significance within the scope of this research in terms of diversity by having a different excavation diameter than the other TBMs. In addition, the studied area's geological conditions include both soil and rock units. Even a direct comparison with the other TBMs would be misleading due to TBM size and the presence of soils; these differences make the project important for comprehending the general vibration trends associated with TBM diameter and geological conditions.

The TBM operational parameters along with the lithological units and ring number intervals are provided in Table 4.7.

Figure 4.25 to Figure 4.28 present rock mass properties obtained from the boreholes and point load tests, top and bottom accelerometer data as the percentage of the points per ring exceeding ±1g threshold including their average per geological unit, disc replacement locations, selected of the TBM operating parameters, and maximum acceleration levels recorded on the accelerometer.

Upon thorough analysis of the data presented between Figure 4.25 and Figure 4.28, the primary findings can be summarized as follows;

- The vibrations are most significant on the z-axis, however, consistent to other TBMs utilizing MEMs type accelerometers the difference between z-axis and the other axes are minimal.
- Vibration recordings exceeding the ±1g threshold on the bottom accelerometer were consistently higher compared to those on the top accelerometer.
- The vibration levels change in accordance with the geological conditions;
    - The highest acceleration amplitudes recorded in the fresh sandstone units (#12, #14, and #16), whereas the lowest amplitudes are observed in the alluvium units (#5, #6, #19, and #30).

Table 4.7 : Geological units seen on the alignment with identification numbers and TBM 4's operational parameters.

Ring No (Start)	Ring No (End)	Lithological Unit	Cutter Speed (RPM)	Cutter Torque (kNm)	Average Face Pressure (bar)	Total Thrust (kN)	Penetration Rate (mm/rev)	Thrust / Cutter (kN)	Boreability Index (kN/cutter)/(mm/rev)	P (kW)	SE (kWh/m^3)	ICR (m^3/h)
0	23	(1) Sandstone	2.83	870	0.05	5564	15.34	179	12.20	258	5.69	47.04
24	37	(2) Sandstone-Claystone	2.74	920	0.02	5267	22.30	170	7.67	264	4.03	66.25
38	70	(3) Sandstone	2.96	1012	0.00	4855	19.14	157	8.51	314	5.30	61.70
70	220	(4) No Data										
221	265	(5) Alluvium	2.70	1269	1.84	11982	22.59	387	19.08	363	5.83	65.40
266	440	(6) Alluvium-Siltstone	2.92	1444	0.69	10475	22.21	338	16.57	439	6.76	69.76
441	573	(7) Claystone-Siltstone	3.24	1343	0.13	8590	19.39	277	14.66	456	6.77	68.26
574	618	(8) Sandstone	3.22	1092	0.04	9018	13.79	291	22.30	370	7.93	48.45
619	645	(9) Sandstone-Siltstone	3.27	1168	0.11	7890	19.92	255	13.45	400	5.85	70.81
646	673	(10) Sandstone	3.08	1352	0.08	9294	17.27	300	19.43	434	8.73	57.28
674	683	(11) Siltstone	3.24	1502	0.16	9545	18.43	308	17.11	508	8.04	64.98
684	755	(12) Sandstone	3.27	1186	0.06	9333	13.70	301	24.28	405	8.82	48.48
756	860	(13) Sandstone-Siltstone	3.33	1028	0.08	6830	20.31	220	11.24	359	5.01	73.62
861	914	(14) Sandstone	3.33	1097	0.03	8495	14.10	274	21.18	382	8.00	51.01
915	928	(15) Siltstone	3.24	1273	0.04	8357	16.16	270	17.90	430	8.01	56.84
929	975	(16) Sandstone	3.24	1308	0.04	8726	14.82	281	19.87	443	8.77	52.18
976	1028	(17) Sandstone-Siltstone	3.06	1179	0.11	8212	16.46	265	16.70	376	7.01	54.32
1029	1220	(18) Siltstone	3.29	1079	0.15	7370	18.52	238	11.75	372	5.63	66.10
1221	1230	(19) Alluvium	3.31	984	0.18	9033	24.90	291	12.08	340	3.91	89.59
1231	1313	(20) Siltstone-Claystone	3.30	1116	0.46	10135	16.99	327	20.58	384	6.71	60.66
1314	1325	(21) Sandstone-Siltstone	3.35	1139	0.12	7792	16.29	251	16.44	400	7.03	59.27

Table 4.7 (continues) Geological units seen on the alignment with identification numbers and TBM 4's operational parameters.

Ring No (Start)	Ring No (End)	Lithological Unit	Cutter Speed (RPM)	Cutter Torque (kNm)	Average Face Pressure (bar)	Total Thrust (kN)	Penetration Rate (mm/rev)	Thrust / Cutter	Boreability Index (kN/cutter)/(mm/rev)	P (kW)	SE (kWh/m^3)	ICR (m^3/h)
1326	1400	(22) Siltstone-Claystone	3.27	1498	0.89	11337	18.67	366	20.94	513	8.13	66.47
1401	1502	(23) Sandstone-Siltstone	3.30	1392	0.29	8898	17.08	287	17.31	482	8.09	61.12
1503	1514	(24) S3 Shaft										
1515	1600	(25) Siltstone-Claystone	3.13	1086	0.32	7793	22.61	251	11.74	355	4.78	76.38
1601	1652	(26) Sandstone-Siltstone	3.10	1178	0.18	7010	21.47	226	11.17	382	5.50	72.00
1653	1737	(27) Siltstone-Claystone	3.14	1042	0.26	6448	20.38	208	10.48	342	5.01	69.49
1738	1760	(28) Sandstone-Siltstone	3.17	1149	0.25	7278	21.86	235	11.17	384	5.33	75.09
1761	1800	(29) Siltstone-Claystone	3.14	1172	0.17	7226	21.83	233	11.17	387	5.35	74.13
1800	1849	(30) Alluvium	3.18	1074	0.21	8465	23.85	273	12.11	358	4.67	82.20
1850	1961	(31) Siltstone-Claystone	3.15	1156	0.29	11408	21.21	368	18.20	381	5.45	72.22
1962	1965	(32) Sandstone-Siltstone	3.06	1158	0.18	7594	18.36	245	13.47	372	6.12	61.05
1966	1999	(33) Siltstone-Claystone	3.11	927	0.16	7139	19.30	230	12.30	302	4.77	64.77
		Average	3.15	1167	0.24	8302	19.01	268	15.26	386	6.36	64.74
		Minimum	2.70	870	0.00	4855	13.70	157	7.67	258	3.91	47.04
		Maximum	3.35	1502	1.84	11982	24.90	387	24.28	513	8.82	89.59

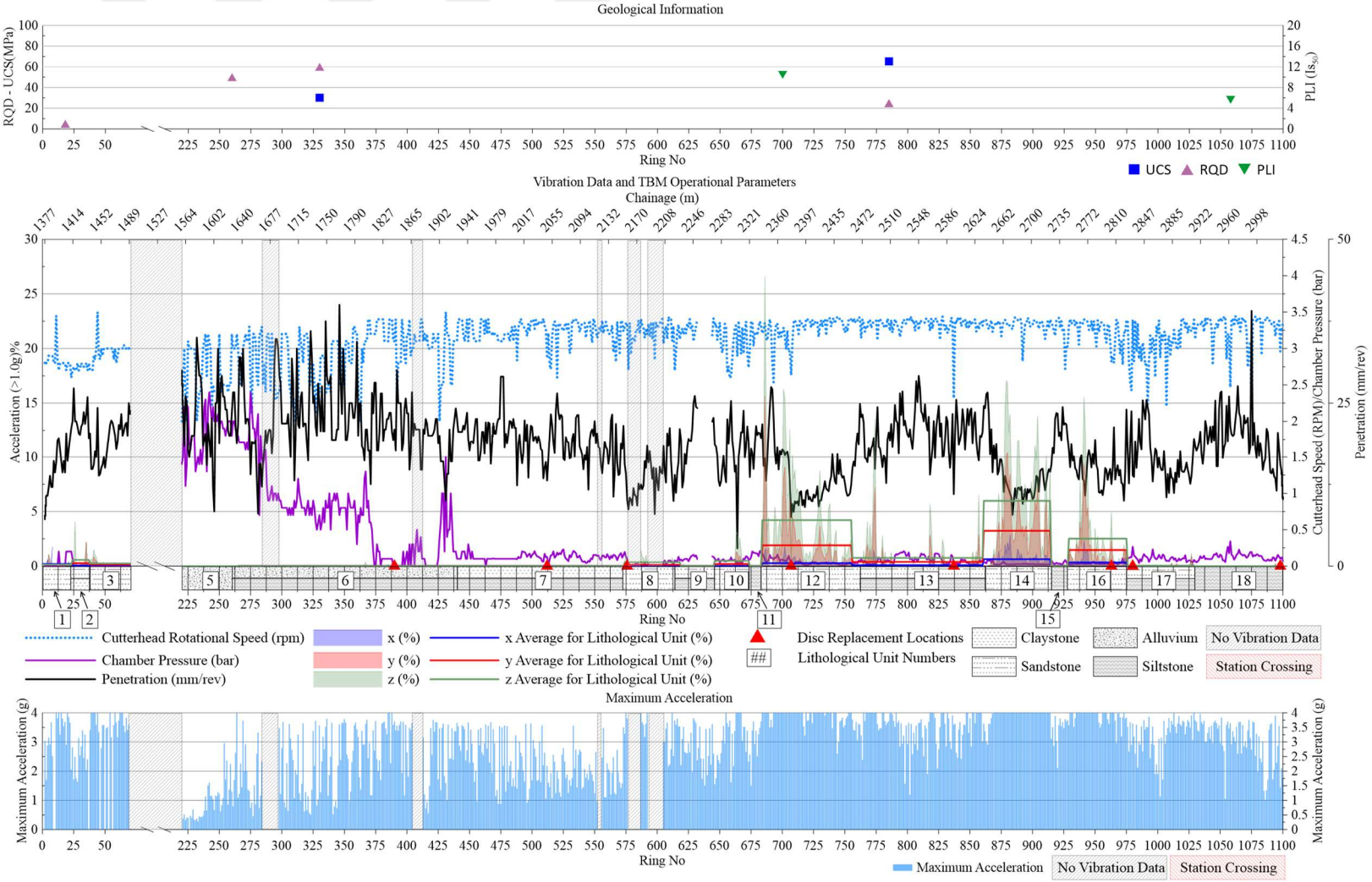

Figure 4.25 : TBM 4 top accelerometer data between rings 1 and 1100 (European Region Potable Water Transmission Tunnel Project).

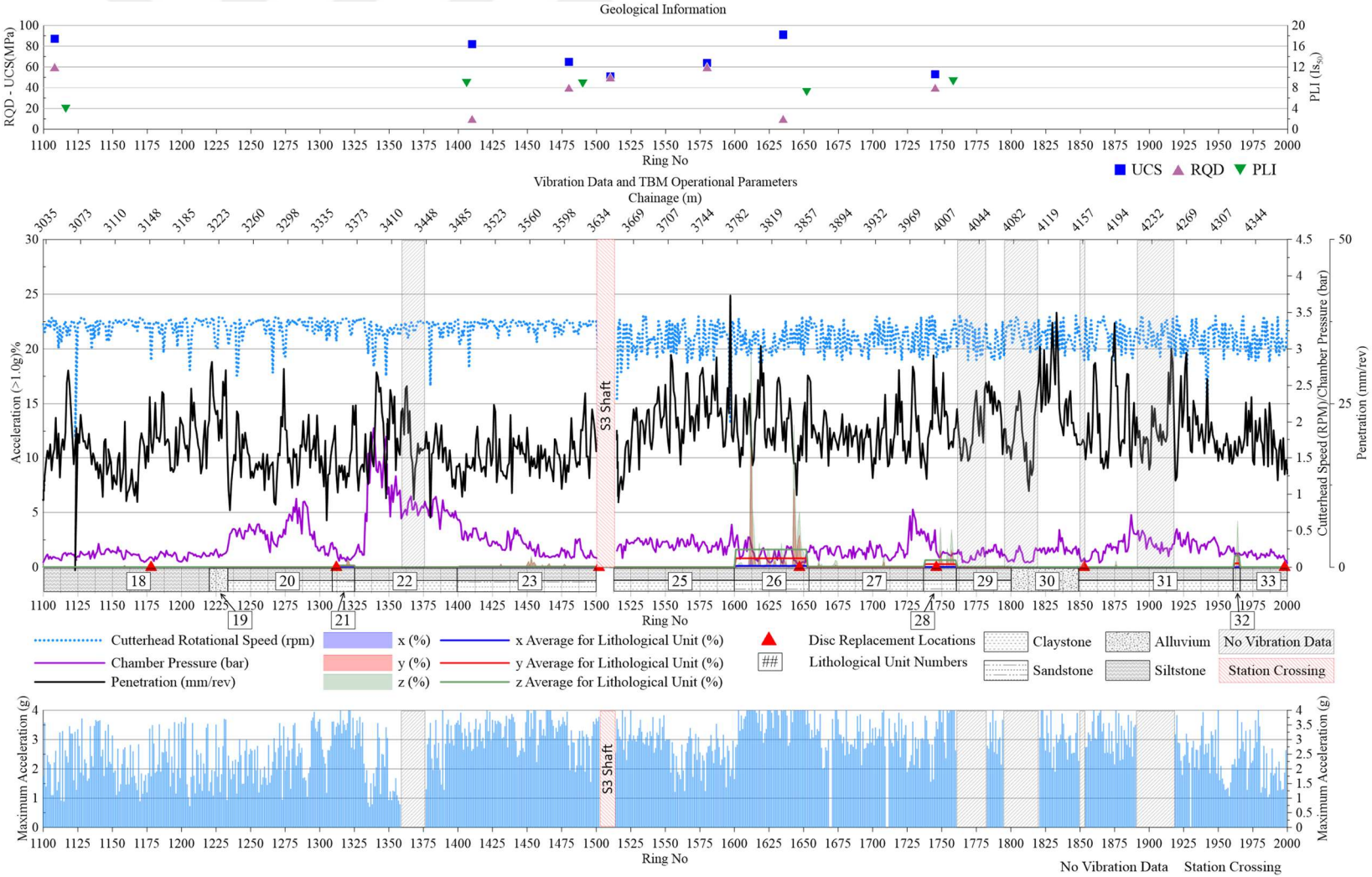

Figure 4.26 : TBM 4 top accelerometer data between rings 1100 and 2000 (European Region Potable Water Transmission Tunnel Project).

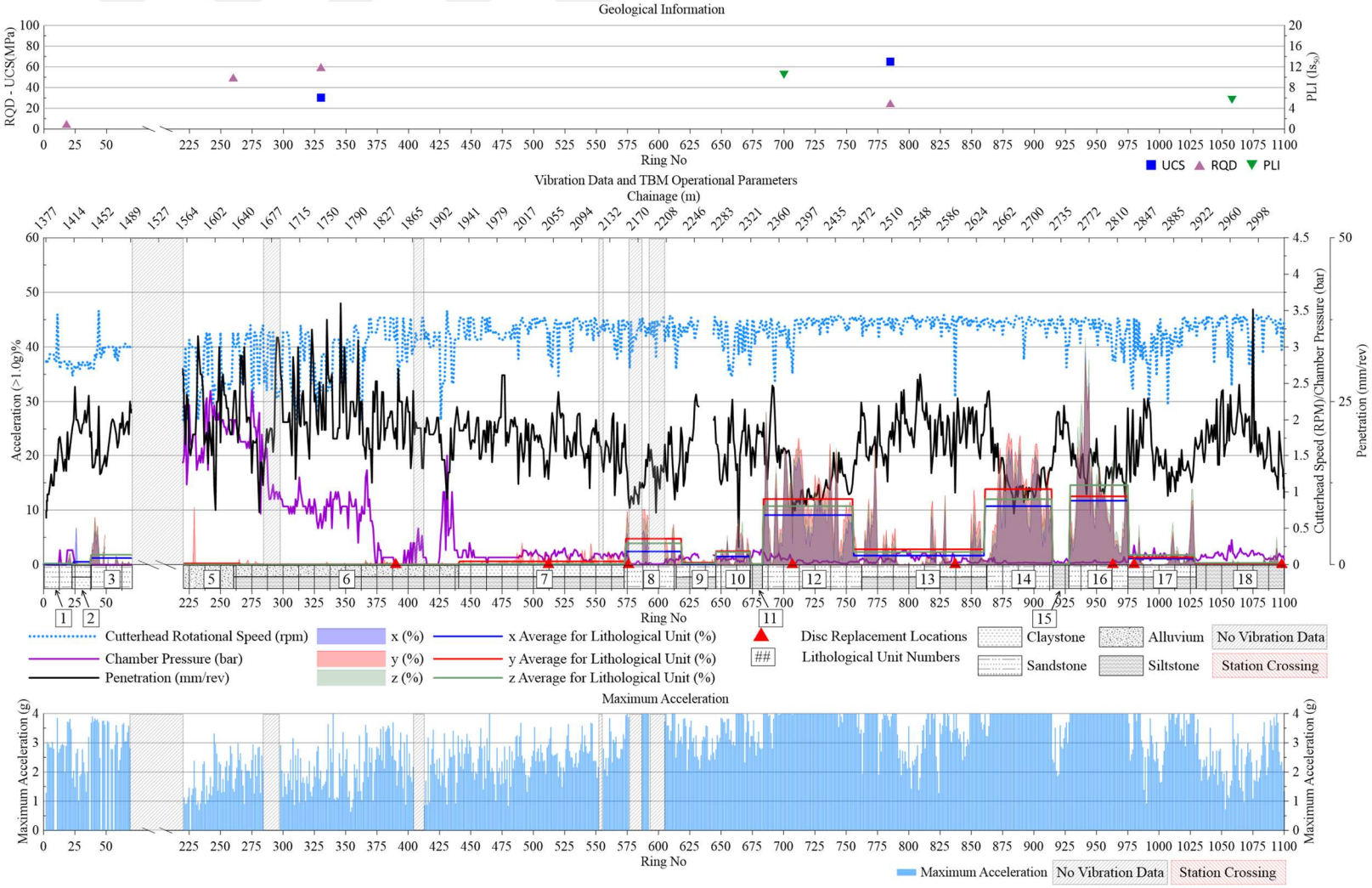

Figure 4.27 : TBM 4 bottom accelerometer data between rings 1 and 1100 (European Region Potable Water Transmission Tunnel Project).

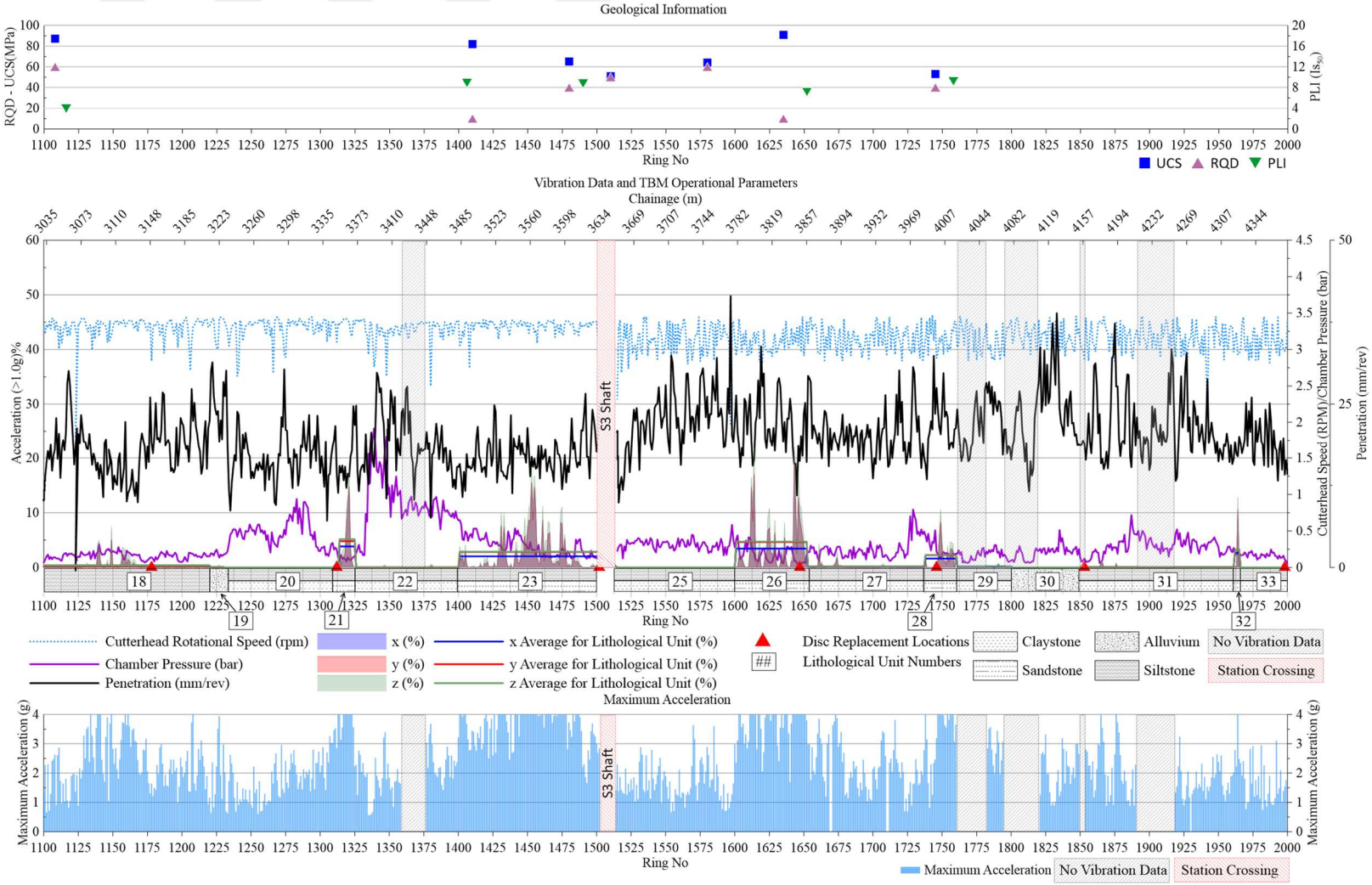

Figure 4.28 : TBM 4 bottom accelerometer data between rings 1100 and 2000 (European Region Potable Water Transmission Tunnel Project).

- The TBM excavated in the alteration of claystone-siltstone-sandstone units (#7 to #10) which can be classified as weak rock, where the vibrations stayed at minimal level. Upon reaching the fresh sandstone (#12) an increase in the vibration amplitudes were observed and the high strength of the sandstone (#12) was justified with the point load tests applied to the rock samples taken from this location (Table 2.10). With some gaps this unit continued until the ring no 975 (#14 and #16).
- The vibration recordings exhibit significant variations corresponding to the geological transitions from fresh sandstone units to altered rock units (#12 to #17).
- The observed vibration characteristics between the units #20 to #28 further proves the effectiveness of vibration monitoring as an indicator of the lithological variations. Within this section, TBM excavated in siltstone-claystone units (#20, #22, #25, and #27) where face pressure was increased due to unstable ground conditions, and correspondingly, exhibited very low levels of vibrations exceeding 1g. In comparison, at the adjoining siltstone-sandstone units (#21, #23, #26 and #28), which were comparatively stronger, the amount of vibrations exceeding 1g threshold were approximately 3% in average. To illustrate the aforementioned variations in vibration characteristics, the vibration profiles of selected rings are presented in Figure 4.29.

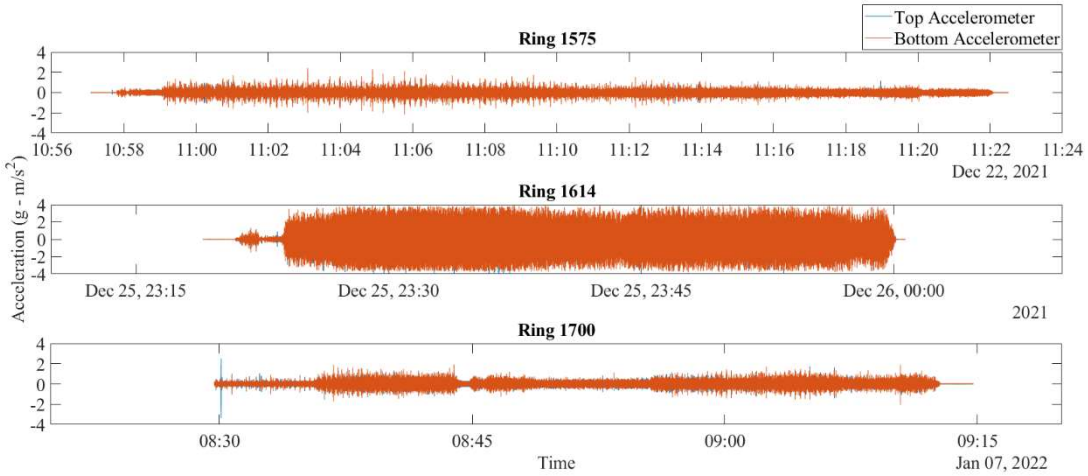

Figure 4.29 : Vibration data of rings 1575 (#25), 1614 (#26) and 1700 (#27) for TBM 4.

4.3.1 Probability analyses

The Weibull parameters obtained from the vibration data are presented in Table 4.8, averaged according to the corresponding lithological units. Figure 4.30 presents resulting Weibull cumulative probability distributions for each lithological section, utilizing the calculated average α and β parameters. Consistent with observations from other TBMs, this figure illustrates a distinction in the probability of vibration levels across the various geological units.

Figure 4.31 presents the Weibull cumulative probability distribution for the vibration data recorded on TBM 4 between rings 674 and 1220. This particular section is characterized by alternating lithological units between siltstone (#11, 15, 18) and sandstone (#12, 14, 16), while on some stretches (#13, 17), both siltstone and sandstone were present at the excavation face. Siltstone unit (#18) in this section has PLI of 5.62 and 3.91, while sandstone unit (#12) has a PLI of 10.44 as detailed in Table 2.10. The probability distribution distinctly illustrates the contrast between these units. The β parameter exhibits a positive correlation with increasing rock strength, while α parameter shows a slight decrease.

Table 4.8 : Average Weibull parameters per lithological unit (TBM 4).

Ring No (Start)	Ring No (End)	Lithological Unit	Top Accelerometer						Bottom Accelerometer					
			x		y		z		x		y		z	
			α	β	α	β	α	β	α	β	α	β	α	β
0	23	(1) Sandstone	1.05	0.16	1.04	0.14	1.04	0.14	1.06	0.07	1.05	0.10	1.05	0.10
24	37	(2) Sandstone-Claystone	1.02	0.14	0.97	0.16	1.01	0.20	1.10	0.11	1.04	0.08	1.06	0.08
38	70	(3) Sandstone	1.03	0.14	1.00	0.12	0.99	0.13	0.92	0.14	0.94	0.17	0.94	0.17
70	220	(4) No Data												
221	265	(5) Alluvium	1.09	0.05	1.18	0.03	1.14	0.04	1.10	0.05	0.98	0.11	1.05	0.07
266	440	(6) Alluvium-Siltstone	1.06	0.05	1.15	0.04	1.10	0.04	1.11	0.04	0.93	0.09	1.04	0.06
441	573	(7) Claystone-Siltstone	1.02	0.08	1.07	0.05	1.04	0.06	0.99	0.08	0.88	0.16	0.97	0.11
574	618	(8) Sandstone	0.97	0.12	0.91	0.11	0.90	0.13	0.84	0.19	0.85	0.27	0.85	0.23
619	645	(9) Sandstone-Siltstone	1.01	0.09	1.01	0.06	0.98	0.07	0.92	0.09	0.90	0.16	0.93	0.11
646	673	(10) Sandstone	0.97	0.10	0.89	0.09	0.88	0.11	0.82	0.15	0.82	0.21	0.84	0.18
674	683	(11) Siltstone	0.99	0.08	0.98	0.06	0.97	0.07	0.90	0.09	0.87	0.17	0.91	0.12
684	755	(12) Sandstone	0.93	0.17	0.86	0.21	0.85	0.25	0.81	0.34	0.82	0.39	0.82	0.36
756	860	(13) Sandstone-Siltstone	0.98	0.12	0.94	0.10	0.94	0.11	0.88	0.14	0.87	0.17	0.88	0.16
861	914	(14) Sandstone	0.89	0.19	0.82	0.23	0.80	0.27	0.78	0.34	0.78	0.39	0.79	0.36
915	928	(15) Siltstone	0.97	0.12	1.02	0.07	1.00	0.08	0.99	0.09	0.96	0.11	0.98	0.11
929	975	(16) Sandstone	0.97	0.18	0.90	0.19	0.90	0.22	0.85	0.38	0.85	0.39	0.85	0.42
976	1028	(17) Sandstone-Siltstone	1.08	0.11	1.04	0.08	1.06	0.08	0.96	0.14	0.98	0.16	0.97	0.17
1029	1220	(18) Siltstone	1.09	0.10	1.10	0.06	1.11	0.06	1.03	0.09	1.05	0.10	1.04	0.11
1221	1230	(19) Alluvium	1.10	0.07	1.12	0.04	1.12	0.05	1.03	0.06	1.04	0.08	1.03	0.08
1231	1313	(20) Siltstone-Claystone	0.69	0.59	0.78	0.60	1.14	0.60	0.65	0.59	0.63	0.59	0.66	0.59
1314	1325	(21) Sandstone-Siltstone	1.07	0.14	1.00	0.12	1.01	0.12	0.93	0.23	0.93	0.25	0.93	0.26

Table 4.8 (continues) Average Weibull parameters per lithological unit (TBM 4).

Ring No (Start)	Ring No (End)	Lithological Unit	Top Accelerometer						Bottom Accelerometer					
			x		y		z		x		y		z	
			α	β	α	β	α	β	α	β	α	β	α	β
1326	1400	(22) Siltstone-Claystone	1.10	0.09	1.13	0.05	1.13	0.06	1.06	0.08	1.06	0.08	1.05	0.10
1401	1502	(23) Sandstone-Siltstone	1.05	0.12	1.00	0.09	1.02	0.09	0.90	0.18	0.90	0.20	0.91	0.21
1503	1514	(24) S3 Shaft												
1515	1600	(25) Siltstone-Claystone	1.10	0.09	1.15	0.04	1.14	0.05	1.12	0.05	1.13	0.06	1.13	0.06
1601	1652	(26) Sandstone-Siltstone	1.04	0.18	0.96	0.15	0.95	0.18	0.90	0.22	0.90	0.24	0.91	0.25
1653	1737	(27) Siltstone-Claystone	1.08	0.15	1.09	0.07	1.09	0.08	1.04	0.08	1.06	0.09	1.06	0.10
1738	1760	(28) Sandstone-Siltstone	1.08	0.15	1.01	0.11	1.00	0.13	0.95	0.15	0.97	0.18	0.96	0.18
1761	1800	(29) Siltstone-Claystone	1.07	0.14	1.02	0.08	1.03	0.09	0.96	0.09	0.98	0.10	0.98	0.11
1801	1849	(30) Alluvium	1.10	0.12	1.10	0.06	1.10	0.07	1.05	0.06	1.08	0.07	1.07	0.07
1850	1961	(31) Siltstone-Claystone	1.11	0.13	1.11	0.06	1.11	0.07	1.07	0.07	1.10	0.07	1.09	0.08
1962	1965	(32) Sandstone-Siltstone	1.11	0.18	1.07	0.13	1.06	0.15	1.00	0.17	1.01	0.18	1.02	0.19
1966	1999	(33) Siltstone-Claystone	1.10	0.16	1.13	0.07	1.13	0.08	1.11	0.05	1.14	0.06	1.13	0.06

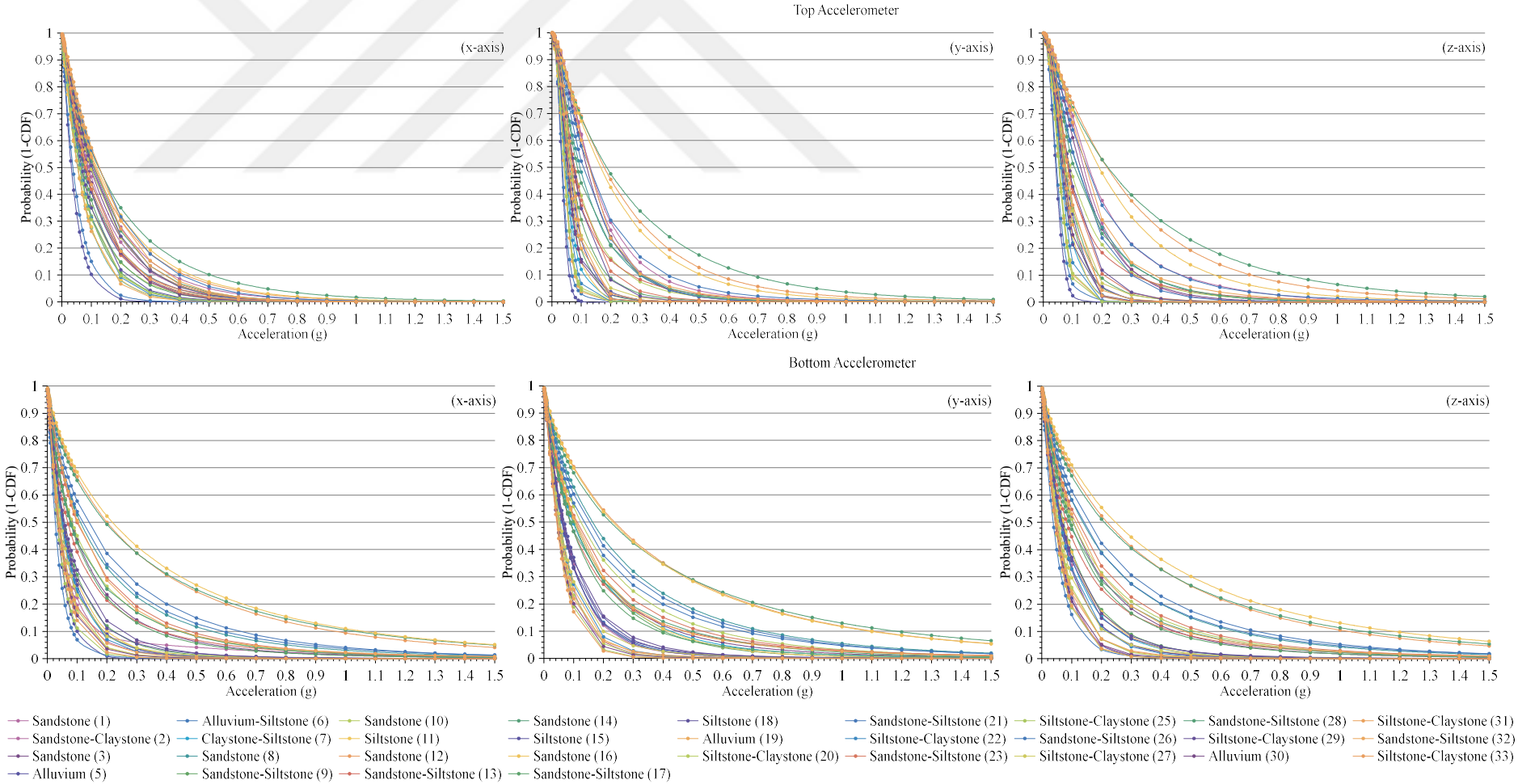

Figure 4.30 : Probability graphs obtained by using Weibull distribution for top and bottom accelerometer for TBM 4.

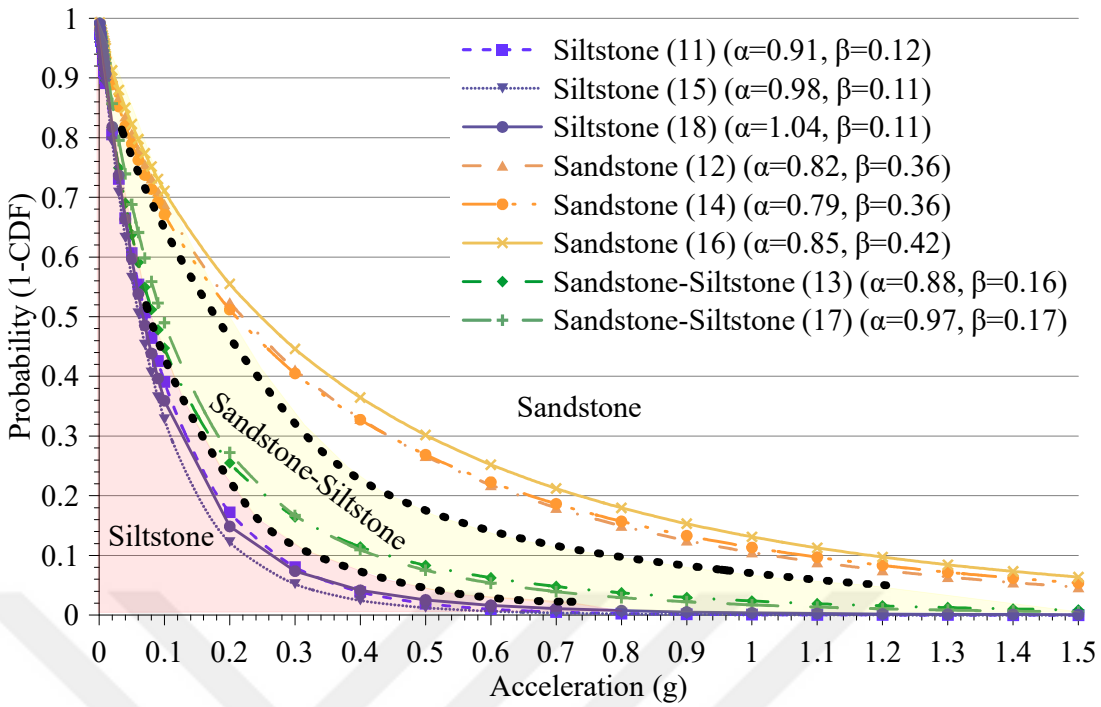

Figure 4.31 : Weibull probability distributions graphs showing siltstone, siltstone-sandstone and sandstone units (TBM 4, bottom accelerometer, z-axis).

4.4 Investigation of Variables affecting Vibrations based on Field Measurements

To gain a more comprehensive understanding of the variables influencing vibration characteristics, this section presents a combined analysis of the data obtained from the field experiments. The analyses focused on the effects of various parameters on vibrations, including geological conditions, TBM operational parameters, cutter conditions, TBM diameter, and accelerometer position.

4.4.1 Effect of geological / lithological changes on TBM vibrations

Geological conditions are considered the primary factor influencing TBM vibrations. A comparative analysis between lithological units together with their geomechanical parameters and various vibration parameters has been undertaken in this section.

Figure 4.32 visually represents the percentage of the acceleration data exceeding 1g for the bottom accelerometers of TBM 2, 3 and 4. This figure can be viewed as a summary of the detailed accelerometer data presented earlier in this section (e.g., Figure 4.6). The corresponding data for top accelerometer can be seen on Figure A.1 in Appendix A. For a better understanding, the figures also incorporate the rock parameters (UCS, GSI, RQD and PLT).

Across all TBMs, a significant correlation was observed between the percentage of acceleration data exceeding 1g and rock strength. As rock strength increases, the likelihood of exceeding the 1g threshold also increases. Furthermore, the vibration patterns on TBM 2 and TBM 3 exhibit a parallel distribution and the highest amount of vibration signals passing 1g is recorded on the sandstone-limestone (#3), claystone-andesite dyke (w1-w2) (#7) and andesite dyke (w1-w2) (#9) units. Likewise, as the TBMs excavate in highly weathered dyke (w4-w5) (#2, #10, #13 and #15) the percentages dropped significantly.

For TBM 4, the geological data provided in the reports (EMAY Uluslararası Mühendislik ve Müsavirlik A.S., 2018) did not fully represent to on-site observations. Consequently, only PLI values were included into the figure. Similar to the other TBMs, vibration values correspond to alterations in rock strength. Notably, the percentage of vibrations exceeding 1g is minimal in soil, while vibrations increase significantly in rock formations. These figures effectively demonstrate substantial potential of the vibration recording system in effectively distinguishing and differentiating geological conditions.

It is noteworthy that in all TBMs, the highest acceleration magnitudes were consistently recorded on the z-axis.

Figure 4.33 presents the average RMS levels, calculated as given in equation 3.4, for each lithological unit recorded by the bottom accelerometers of TBMs 2, 3, and 4. The corresponding data for the top accelerometers can be found in Figure A.2. The RMS vibration levels exhibit a similar pattern with acceleration percentage exceeding 1g shown previously, and RMS vibration levels increases with the rock strength.

To provide deeper insights into the relationships between the rock mass properties with vibrations, RQD, GSI, UCS and PLI values are presented alongside vibration data for each axis. The correlations between RMS accelerations and RQD values are presented in Figure 4.34 and as can be seen, for both TBMs the relationships can be classified as strong, having x-axis of TBM 2 as exception. It should also be noted that, the top accelerometers have higher coefficient of determination values on both TBMs for this relationship, thus Figure 4.34 presents the data for top accelerometers, while the data for bottom accelerometers can be found at Figure A.3 in the Appendices. The discrepancy between the top and bottom accelerometers could be attributed to the

additional noise sources at the bottom side of the TBMs, as the ones at the top side are less effected by the noise, they probably have a better relationship with the various rock parameters.

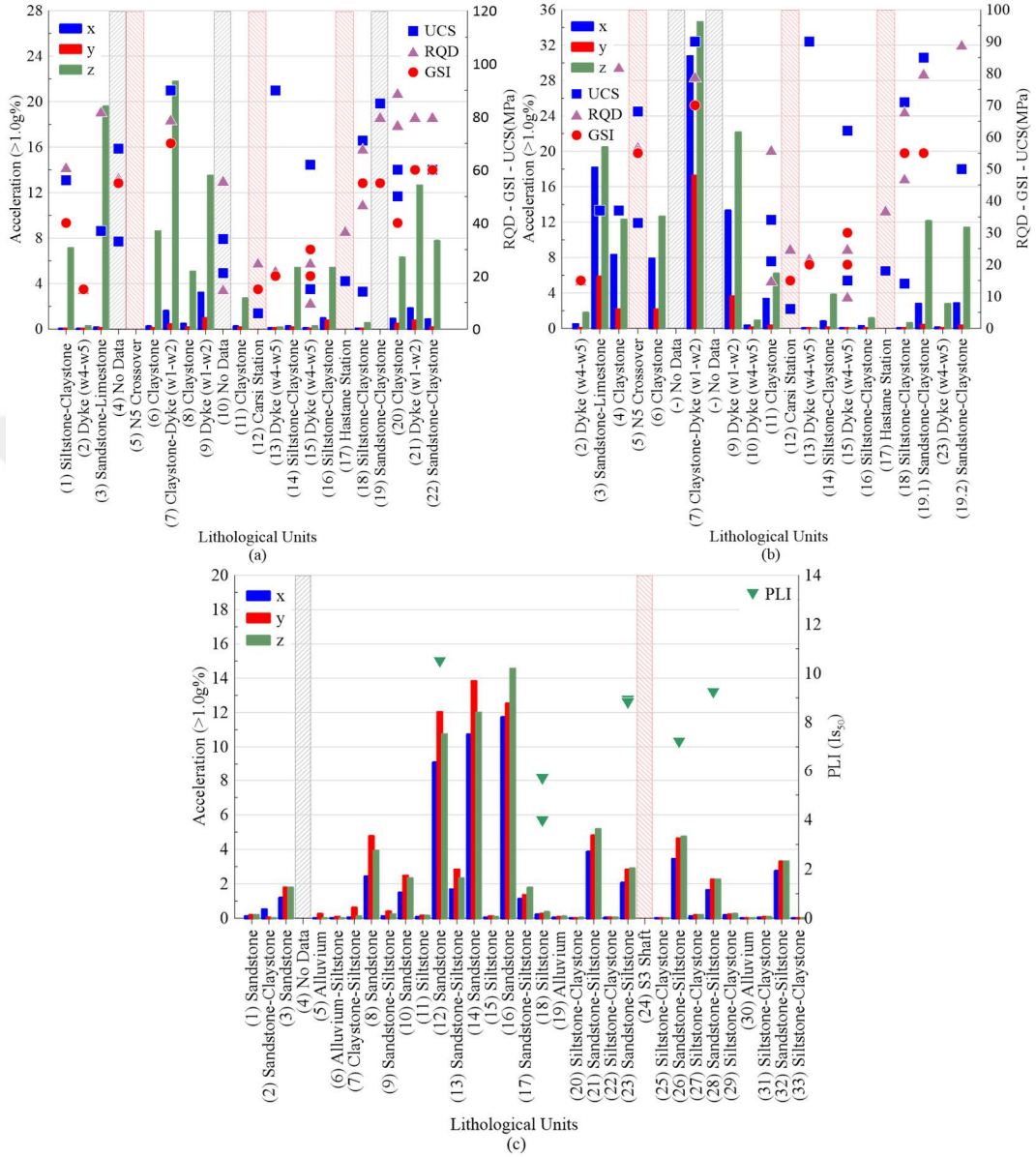

Figure 4.32 : Percentage of acceleration data higher than 1g per lithological section for bottom accelerometers of (a) TBM 2, (b) TBM 3 and (c) TBM 4.

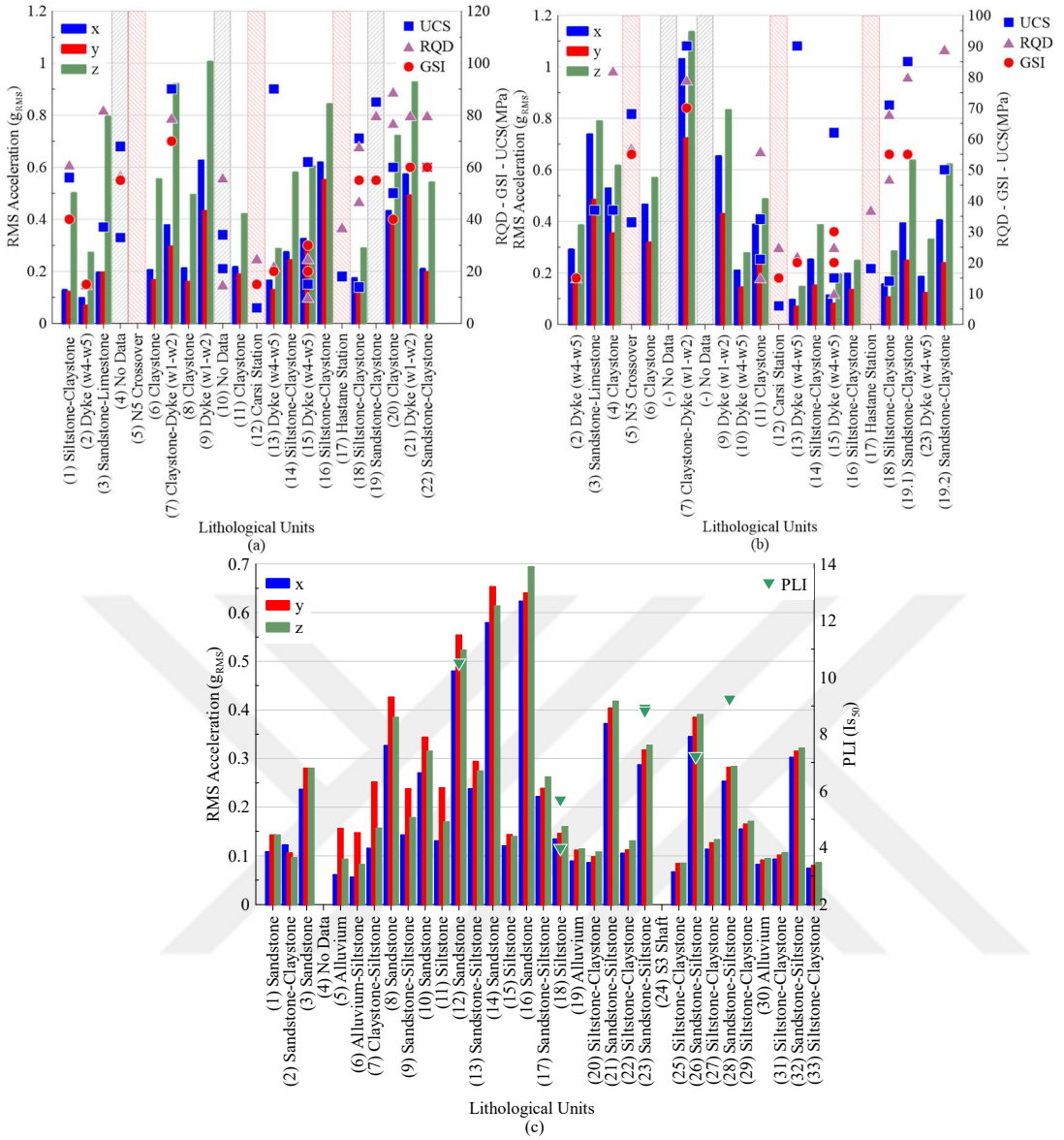

Figure 4.33 : RMS vibration data per lithological section for bottom accelerometers of (a) TBM 2, (b) TBM 3 and (c) TBM 4.

Similar to observations on the RQD, the top accelerometers have higher coefficient of determination values between GSI and RMS vibrations, as illustrated in Figure 4.35. The corresponding data for the bottom accelerometers can be found in Figure A.4 at the Appendix. For top accelerometers, these relationships can be classified as moderately strong to strong, excluding the x-axis of TBM 2. Furthermore, for TBM 2 a logarithmic function provided the best fit for the data, while a linear function yielded a better fit for TBM 3 data.

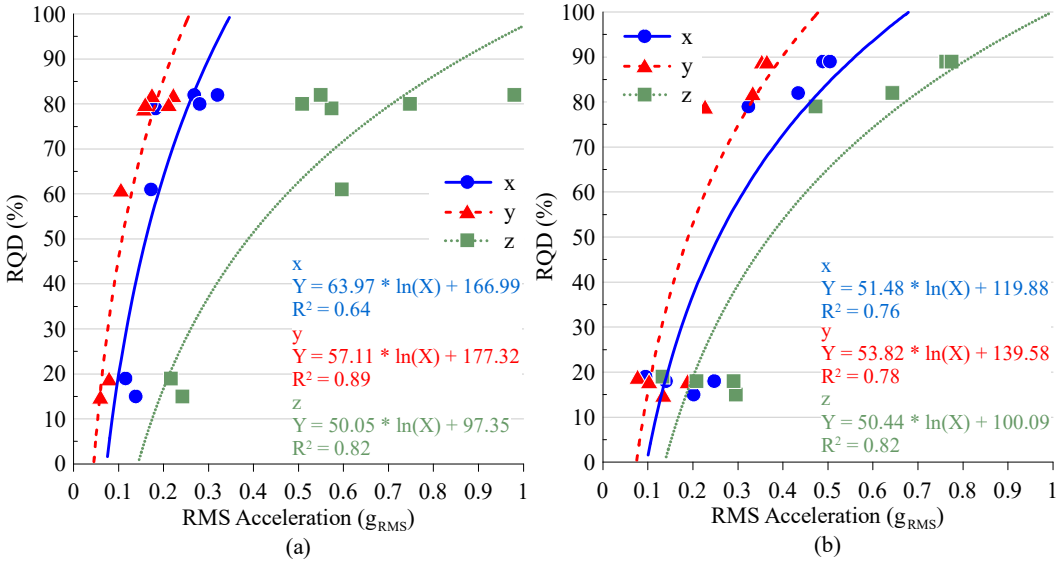

Figure 4.34 : The relationships between RMS vibration data and RQD for top accelerometers of (a) TBM 2, (b) TBM 3.

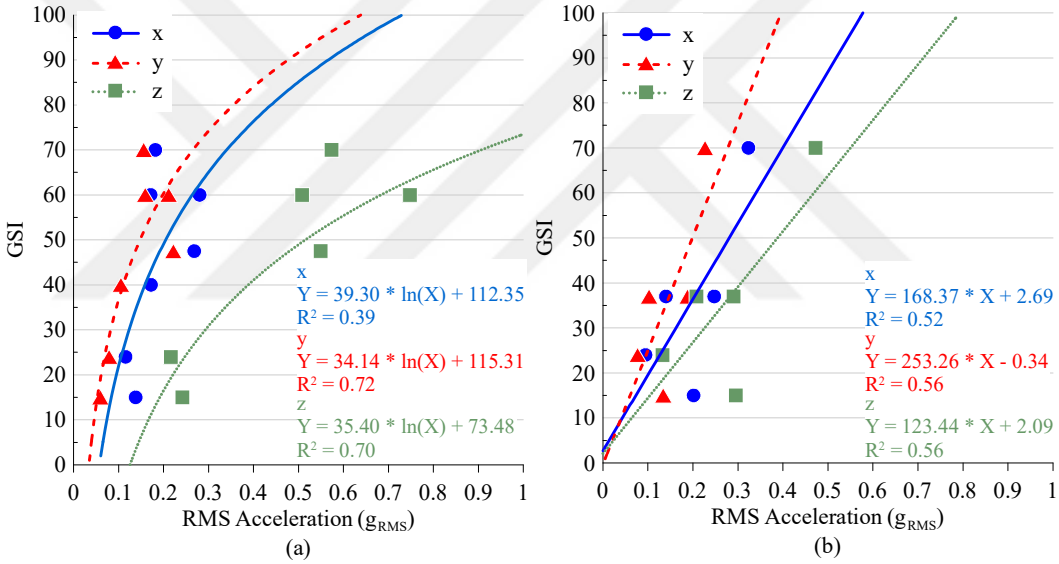

Figure 4.35 : The relationships between RMS vibration data and GSI for top accelerometers of (a) TBM 2, (b) TBM 3.

It is important to acknowledge that the uniaxial compressive strength values provided in the geological reports (Geodata Engineering S.p.A., 2016; Yüksel Proje, 2017) belong to intact rock specimens, and not the rock mass at the tunnel level. Even with this disparity, moderately strong to strong relationships were observed between RMS acceleration and UCS (Figure 4.36 and Figure A.5).

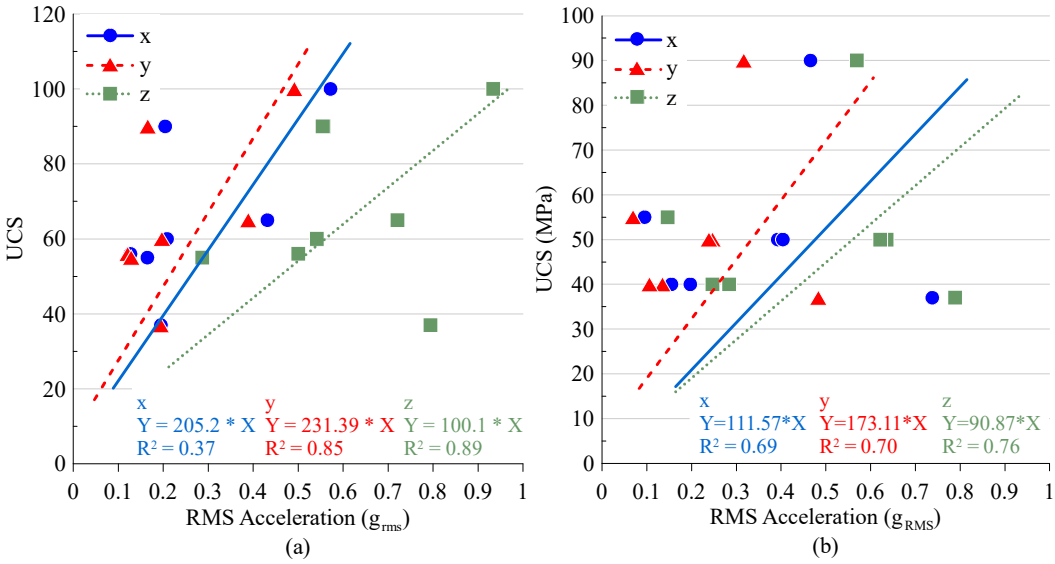

Figure 4.36 : The relationships between RMS vibration data and UCS for bottom accelerometers of (a) TBM 2, (b) TBM 3.

Interval RMS acceleration values, calculated as the square root of the sum of squared values across all axes as detailed in equation 3.5, are presented in Figure 4.37 for bottom accelerometers, and in Figure A.6 for top accelerometers. As anticipated, a positive correlation is observed between interval RMS acceleration and rock strength. Conversely, decrease with increasing weathering degree, interval RMS accelerations reduce. By incorporating all channels into the calculation, the anomalies seen on individual channels are eliminated and the effect of acceleration differences on axes between the TBMs are reduced.

Figure 4.38 to Figure 4.40 presents interval RMS values averaged per lithological unit plotted against RQD, GSI, and PLI (Is_{50}) or both top and bottom accelerometers on TBMs 2, 3, and 4. It's important to note that interval RMS values employed in these figures were solely derived from sections where borehole data present or rock sample tests were conducted to ensure data reliability of the results. Consequently, the dataset size in these graphs are limited.

As can be seen, the coefficient of determination values indicate moderately strong relationships between the interval RMS and RQD for TBM 2 and TBM 3 (Figure 4.38). The best-fit lines for the data obtained by using logarithmic function.

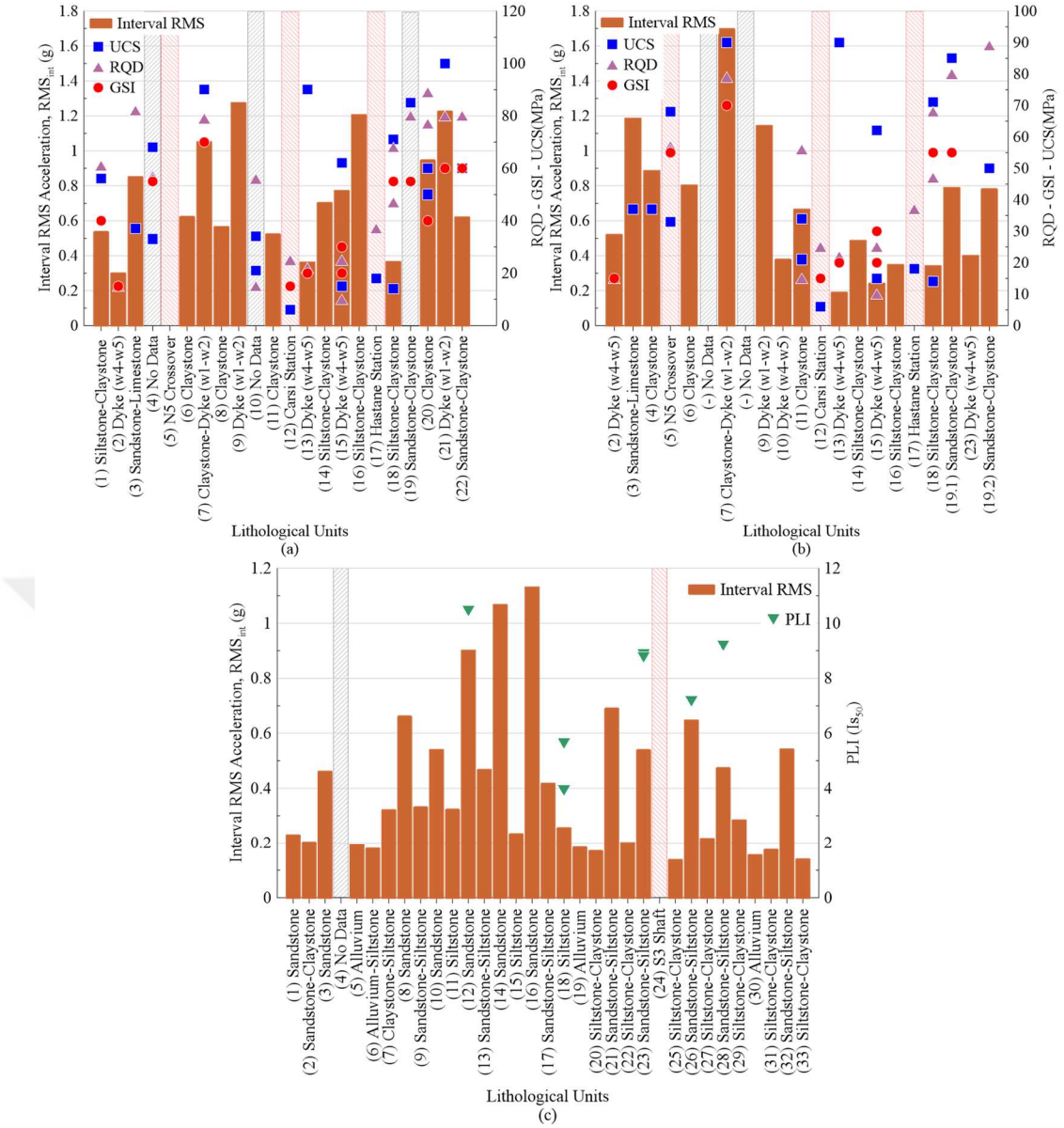

Figure 4.37 : Interval RMS vibration data per lithological section for bottom accelerometers of (a) TBM 2, (b) TBM 3 and (c) TBM 4.

The relationships between interval RMS vibrations and GSI can be classified as moderately strong which are presented in Figure 4.39 for TBM 2 and 3. A logarithmic function provided the best fit for TBM 2 data, while a linear function resulted in a higher R^2 value for TBM 3. This behavior is different from RQD relations; however, it could be attributed to the limitations in data size.

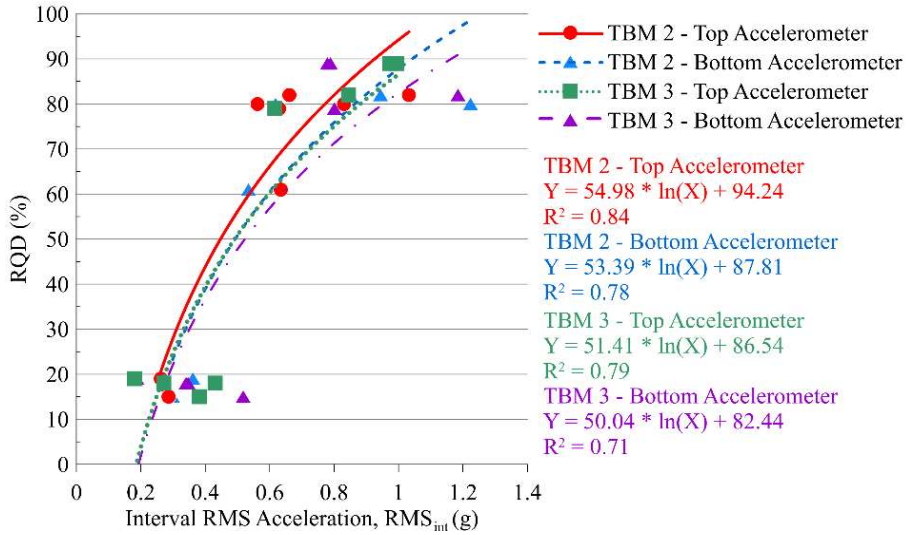

Figure 4.38 : Relationships between interval RMS vibrations and RQD for TBM 2 and TBM 3.

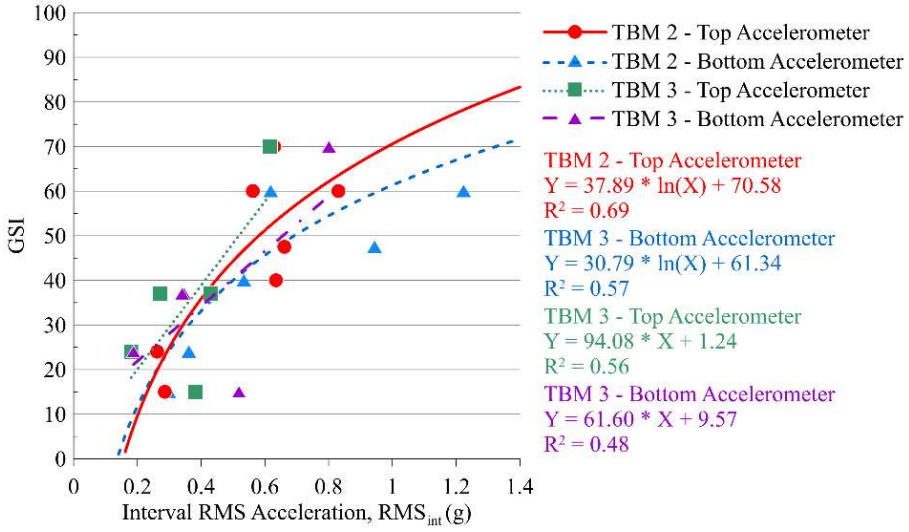

Figure 4.39 : Relationships between interval RMS vibrations and GSI for TBM 2 and TBM 3.

Despite RQD has an accumulation of around 80% and certain data gaps present (Figure 4.39), it exhibits a stronger correlation with acceleration as compared to GSI (Figure 4.40). This distinction could be attributed to GSI's reliance on engineering judgment, which can vary based on interpretation. The observed variation in interval RMS values, ranging from 0.5 to 1.3 while RQD remains relatively constant at around 80% can be explained by the difference in the UCS values of the rocks and TBM operational parameters (penetration, thrust, and cutterhead speed), since the excavation characteristics are different for each lithological unit.

Figure 4.40 illustrates the relationships between interval RMS acceleration and UCS, which can be classified as moderately strong to strong. While the inclusion of data

points below 40 MPa would strengthen the statistical significance of the relationships, a clear trend is present.

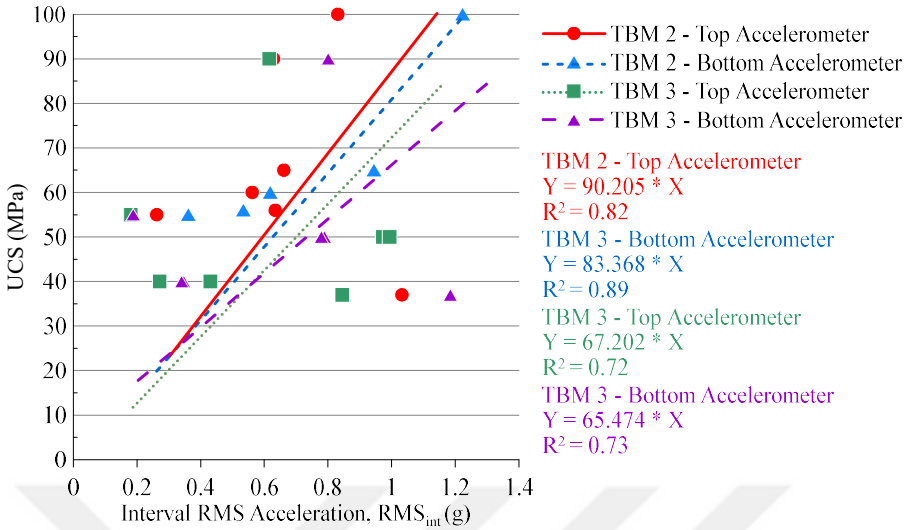

Figure 4.40 : Relationships between interval RMS vibrations and UCS for TBM 2 and TBM 3.

The relationships between interval RMS accelerations and PLI (Is_{50}) for TBM 4 are presented in Figure 4.41. These relationships can be classified as moderately strong to strong. It should be mentioned that, since it is not possible to do any point load test in the low strength sections, the related graph (Figure 4.41) shows only the samples with high strength. It is hypothesized that incorporating data from low-strength sections, which are also expected to exhibit low acceleration values, could potentially strengthen the correlations.

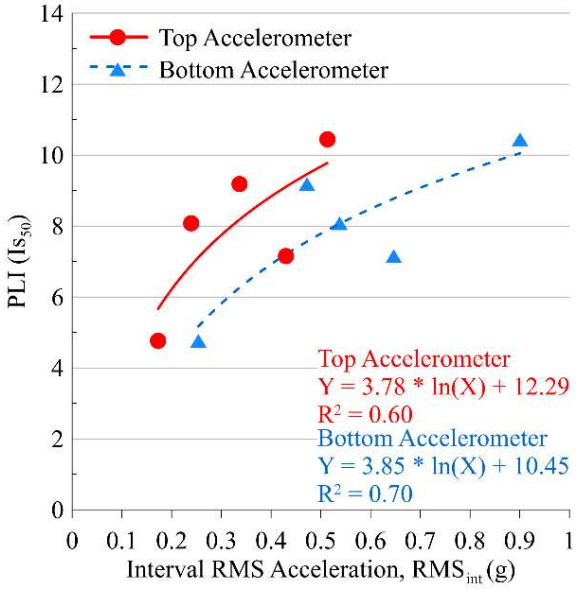

Figure 4.41 : Relationships between interval RMS vibrations and PLI for TBM 4.

The utilization of a logarithmic function consistently yields the highest R^2 values for the best-fit lines between vibrations and rock quality parameters (e.g., RQD, GSI), with one exception, as well as thrust which will be addressed in the subsequent section. This observation can be attributed to the rapid and continuous escalation of the vibrations from soil or weak rock to the hard rock conditions, whereas, RQD, GSI, and thrust do not increase after reaching their maximum. For example, RQD of a 30 MPa and a 200 MPa rock could be 100% while vibrations could be 0.5g and 2g. As acceleration values continue to rise, the logarithmic functions provide a better fit. It is also very common to use logarithmic functions for similar data types (sound and vibration as decibel, and Richter scales).

Figure 4.42 presents the crest factor for the bottom accelerometers of TBMs 2, 3, and 4. The crest factor, as defined by equation 3.6, serves as a measure of the peakiness of the data. The corresponding data for the top accelerometers can be found in Figure A.7.

The analyses conducted in this study suggest that the crest factor may be a useful indicator for identifying mixed face conditions, where the TBM excavates both soil and rock together. For example, during the construction of the Umraniye-Atasehir-Goztepe Metro Line, the sandstone-limestone units between rings 1550 and 1600 (#3) exhibited high amount of vibration measurements exceeding ±1g, while the maximum acceleration levels rarely reach ±10g, showing that almost no shocks were present. In this section, the average crest factor across all axes for TBM 2 was 14.98 (Figure 4.42a). Conversely, the sandstone-claystone units between rings 2240 and 2440 (#16 and #18) displayed a lower percentage of vibration levels exceeding ±1g. However, the maximum vibrations in this section nearly reached ±10g in almost all rings, suggesting the presence of continuous shocks. The average crest factor for all axes in this section was significantly higher at 37.85 (Figure 4.42a). This contrasting behavior is attributed to the frequent alternation of lithological units at the excavation face, supporting the potential application of the crest factor as an indicator of mixed face conditions. Figure 4.43 illustrates the vibration data for two representative rings from these sections.

The crest factor values for TBM 3 display a similar pattern to those observed for TBM 2, with the values reaching its peak between Carsi and Hastane Stations (Figure 4.42b). This trend suggests a positive correlation between crest factor and decreasing rock

strength. In other words, lower strength sections exhibit higher crest factors, whereas stronger rock sections are associated with lower crest factors. This behavior can likely be explained by the presence of a more homogeneous excavation face in stronger rock formations. The crest factor values are demonstrably higher in the weathered dyke sections (w4-w5) compared to the fresh dykes (w1-w2), supporting the statement further.

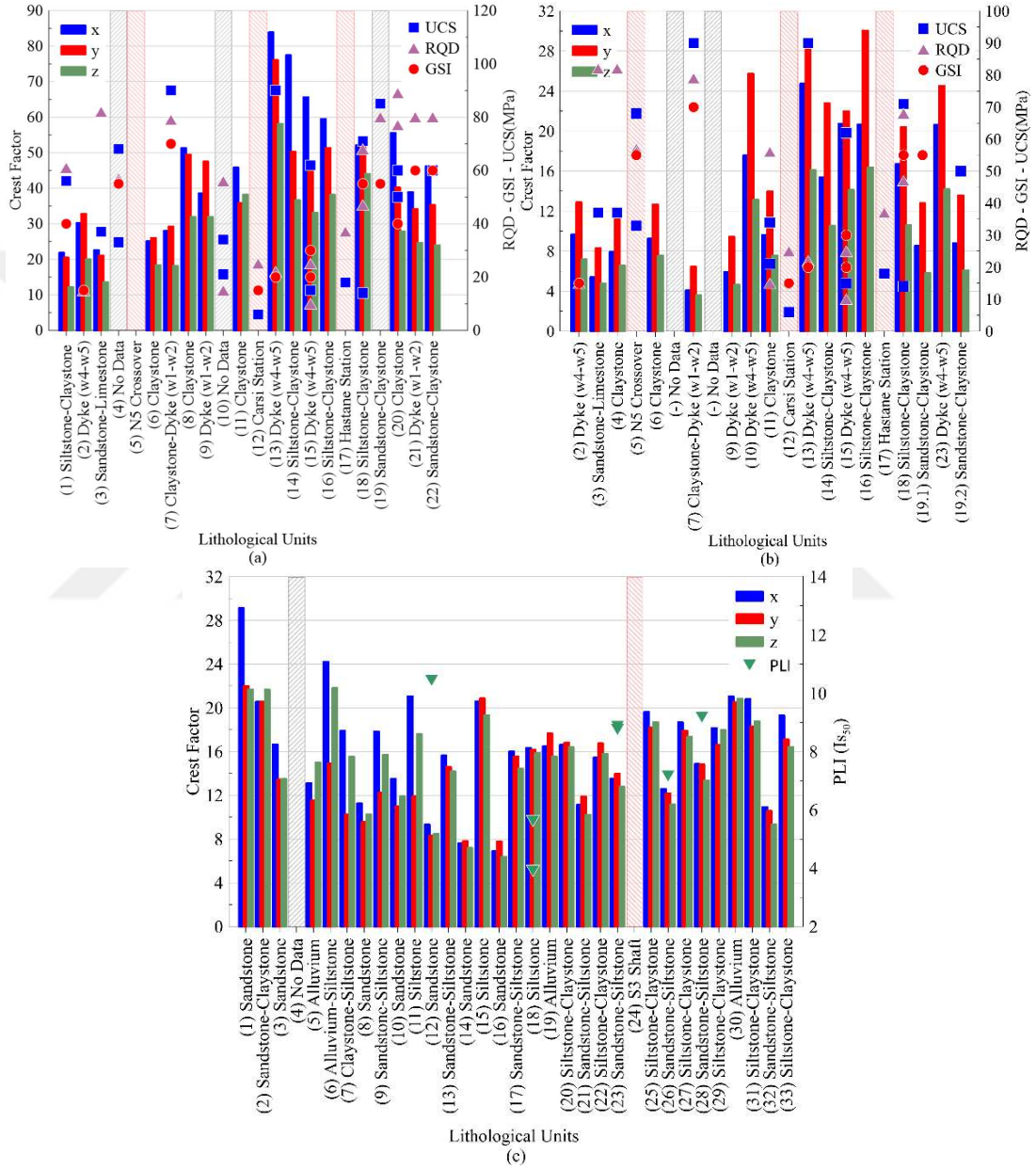

Figure 4.42 : Crest factor per lithological section for bottom accelerometers of (a) TBM 2, (b) TBM 3 and (c) TBM 4.

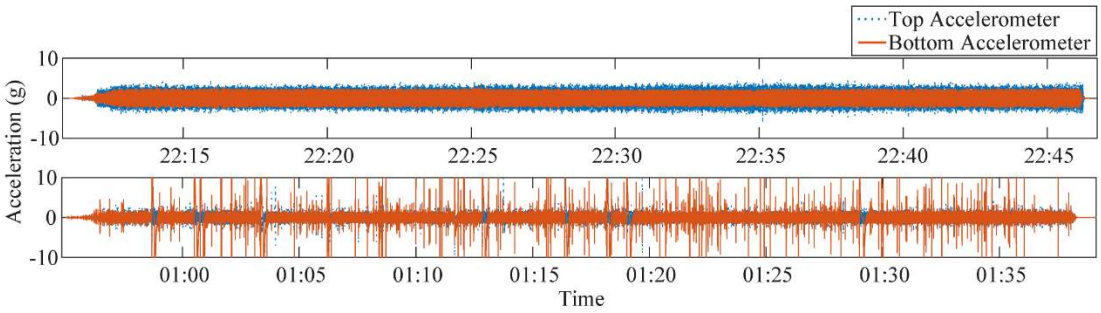

Figure 4.43 : Vibration data of the z-axes for the top and bottom accelerometers on TBM 2 belonging to the rings 1561 (top) and 2303 (bottom).

An attention should be paid to the differences on the crest factor values between TBM 2 and 3. This divergence can be attributed to the variance in the measurement range of the accelerometers, since higher peak values (±10g) could be recorded on TBM 2, that could increase peakiness in comparison with ±4g accelerometers on other TBMs.

The skewness of the vibration data for TBM 2, 3 and 4 are shown in Figure 4.44 for bottom accelerometers (and in Figure A.8 for top accelerometers). The distribution of vibration data for TBMs 3 and 4 appears relatively symmetrical, whereas TBM 2 exhibits a positive skew, particularly evident in high-strength rock sections. As skewness shows the signal's asymmetrical spread from its mean value, this difference between the TBMs believed to be caused by difference in the accelerometer types and measurement range. The piezoelectric accelerometers on TBM 2 were susceptible to saturation during high impact events generally observed in hard rock sections, due to their measurement range. These saturation events likely resulted in an overrepresentation of high vibration values, thus causing the positive skew in the data. An example of saturation instances in the data from TBM 2 is presented in Figure 4.45.

Kurtosis values of the vibration data for TBM 2, 3 and 4 are presented in Figure 4.46 (and Figure A.9) per lithological section. As previously discussed, the data exhibits leptokurtic behavior, suggesting that Weibull distributions are more appropriate for accurately representing the probability distribution. Leptokurtic distributions are characterized by heavier tails, indicating a higher probability of extreme values compared to normal distributions. A notable distinction was observed between TBM 2 and the other TBMs in terms of kurtosis values, which can again be attributed to the accelerometers' measurement range, and it is likely that the higher peak values recorded on TBM 2 caused this difference.

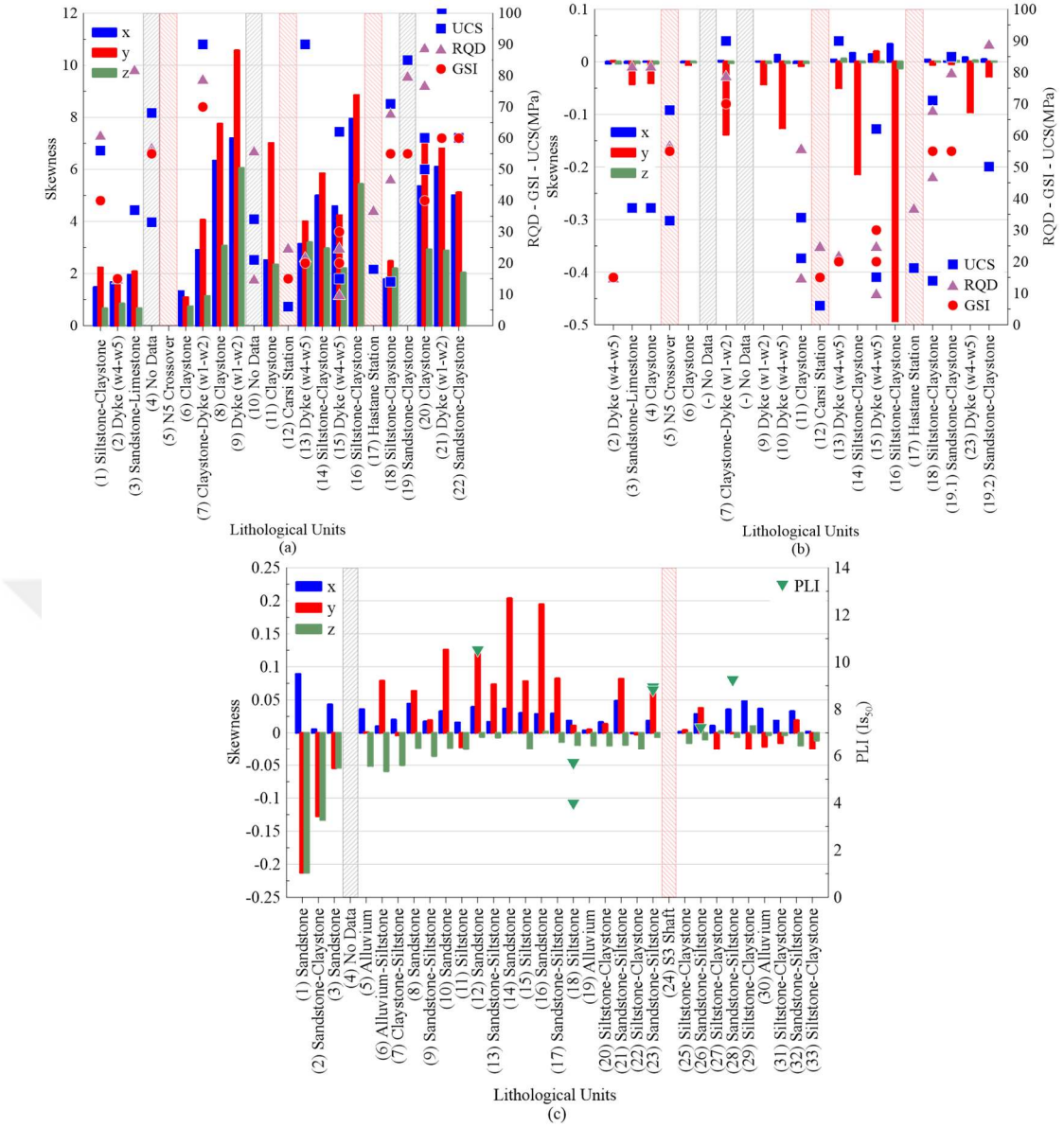

Figure 4.44 : Skewness of the data per lithological section for bottom accelerometers of (a) TBM 2, (b) TBM 3 and (c) TBM 4.

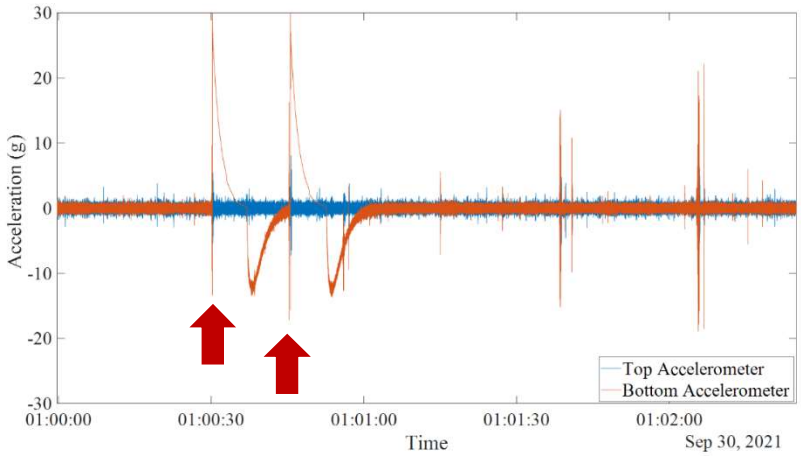

Figure 4.45 : Saturation seen on piezoelectric accelerometers of TBM 2.

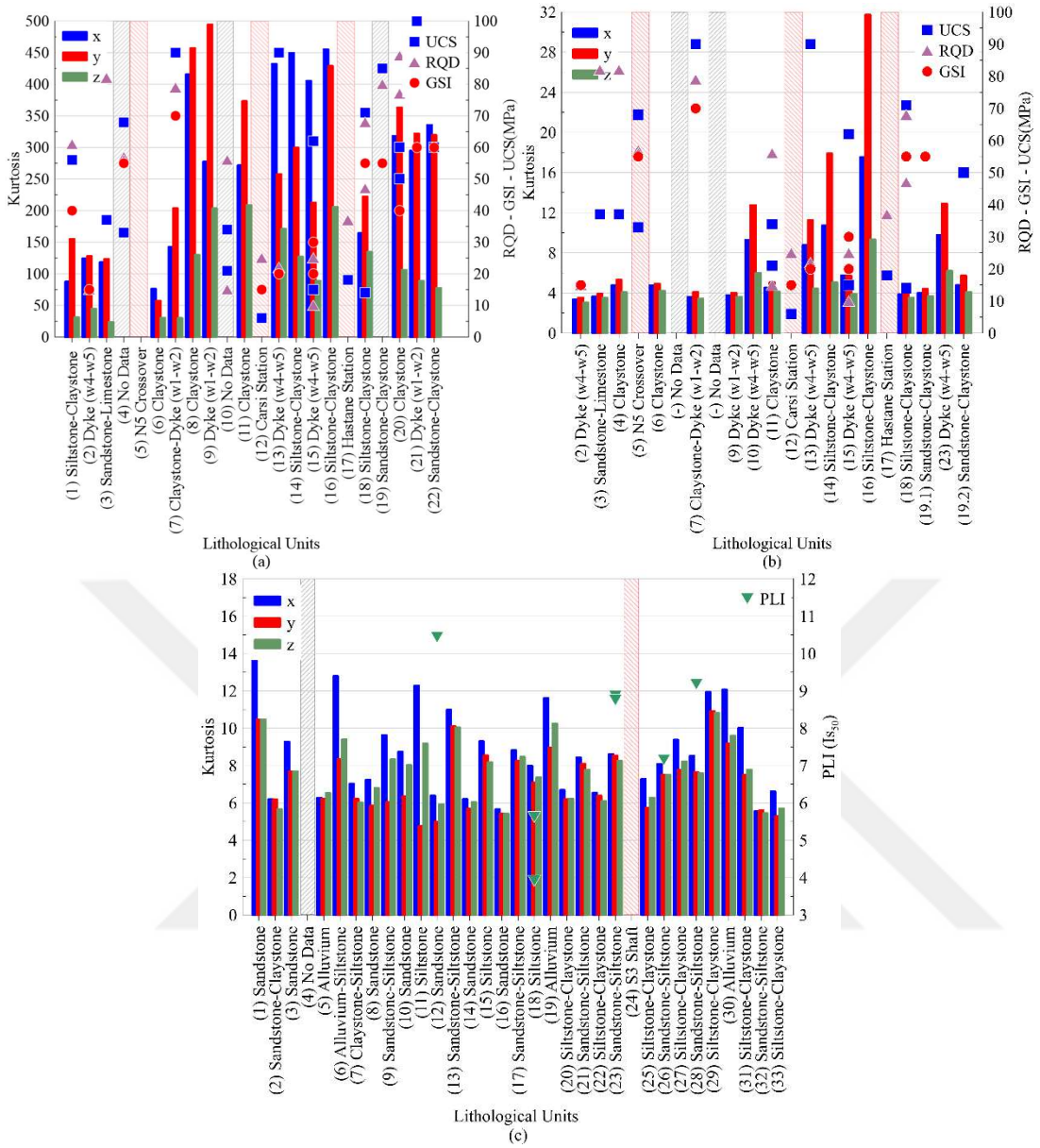

Figure 4.46 : Kurtosis of the data per lithological section for bottom accelerometers of (a) TBM 2, (b) TBM 3 and (c) TBM 4.

The boreability index of a TBM is defined as the thrust per cutter and per unit penetration rate. In a specialized context, Gong et al. (2007) introduced the Specific Rock Mass Boreability Index (SRMBI) which evaluates the boreability of the rock mass. In Figure 4.47 relationship between boreability index and interval RMS acceleration is presented for the TBMs 2, 3, and 4. As evident from the figure, a positive correlation exists between the boreability index and the vibration level.

As the boreability index is mostly independent from the effect of the operational factors, TBM 2 and TBM 3, which shared same specifications and operated side by side, exhibited very close trendlines. No statistically significant correlations were

observed for TBM 4, which can be attributed to the coexistence of soil and soil-like conditions along with rock formations, resulting in a large dispersion of data. These conditions were different from the other TBMs, and the effect of these mixed conditions can also be seen in some of the other relations presented in this study.

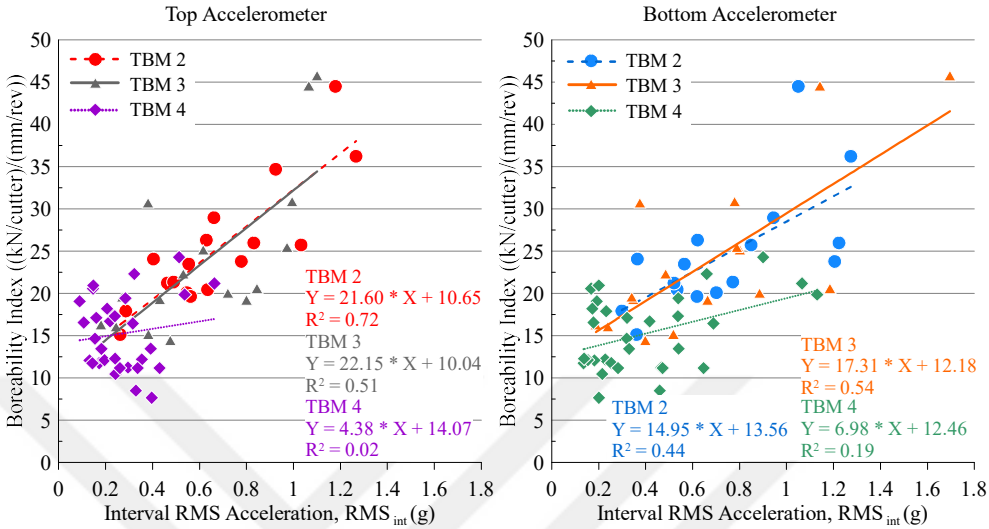

Figure 4.47 : Relationships between interval RMS acceleration and Boreability Index for TBM 2, 3 and 4.

As demonstrated in previous sections, the Weibull cumulative probability distribution is sensitive to variations in lithological units. This implies that changes in rock properties, and consequently vibration characteristics, are reflected in the probability of recorded acceleration levels, consequently, in the shape and scale parameters.

The Weibull distributions in both TBM 2 and TBM 3 show similar results, in terms of useability to distinguish different lithological units. Furthermore, TBM 4 clearly demonstrates that even with a smaller excavation diameter and different geological conditions, Weibull distributions yield valuable outcomes.

Since both “α” and “β” parameters are affected by the geological conditions, there are some correlations exists between them and rock quality parameters. To investigate these relationships, the RQD values are plotted against the Weibull parameters in Figure 4.48 for bottom accelerometers and in Appendix A (Figure A.10) for top accelerometers. While a clear correlation is not evident for the “α” parameter, trends suggest that the “α” parameter tends to decrease with increasing RQD. In contrast, moderately strong to strong positive correlation exists between the “β” parameter and RQD, where “β” parameter increases with increasing RQD values.

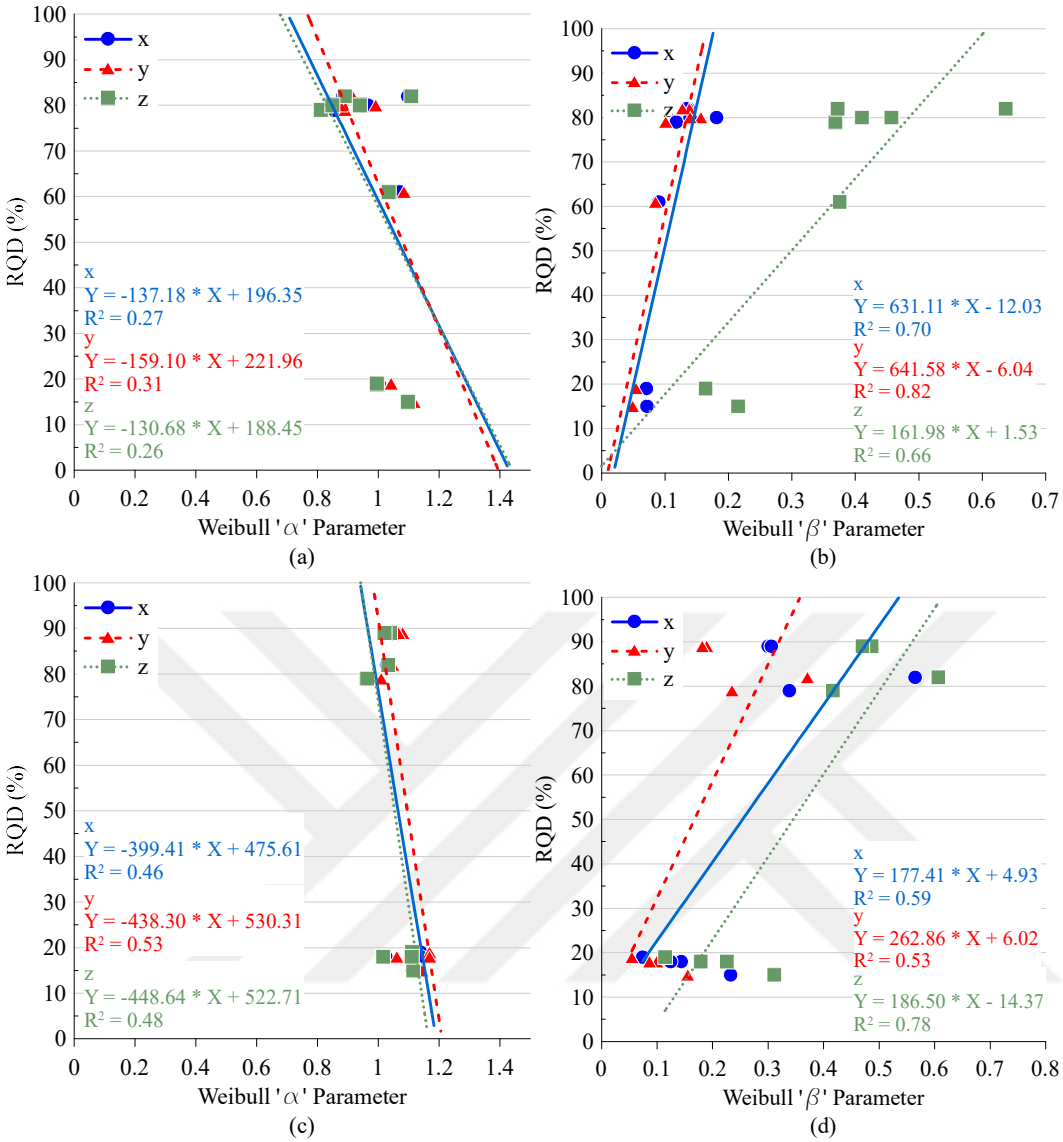

Figure 4.48 : The relationships between RQD and Weibull parameters for bottom accelerometers, (a) and (b) for TBM 2, (c) and (d) for TBM 3.

The influence of rock mass quality on the Weibull distribution parameters was further investigated by analyzing the relationships between the GSI and these parameters. Figure 4.49 presents these relationships for data collected from bottom accelerometers, while the corresponding plots for top accelerometers can be found in Appendix A (Figure A.11). Similar to the trends observed with RQD, GSI exhibits a negative correlation with the "α" parameter and a positive correlation with the "β" parameter of the Weibull distribution. However, the correlations between the "α" parameter and GSI are moderately strong to strong, contrasting with the weaker trend observed for RQD, while a slight reduction on the coefficient of determination values observed for the relationships between GSI and "β" parameter.

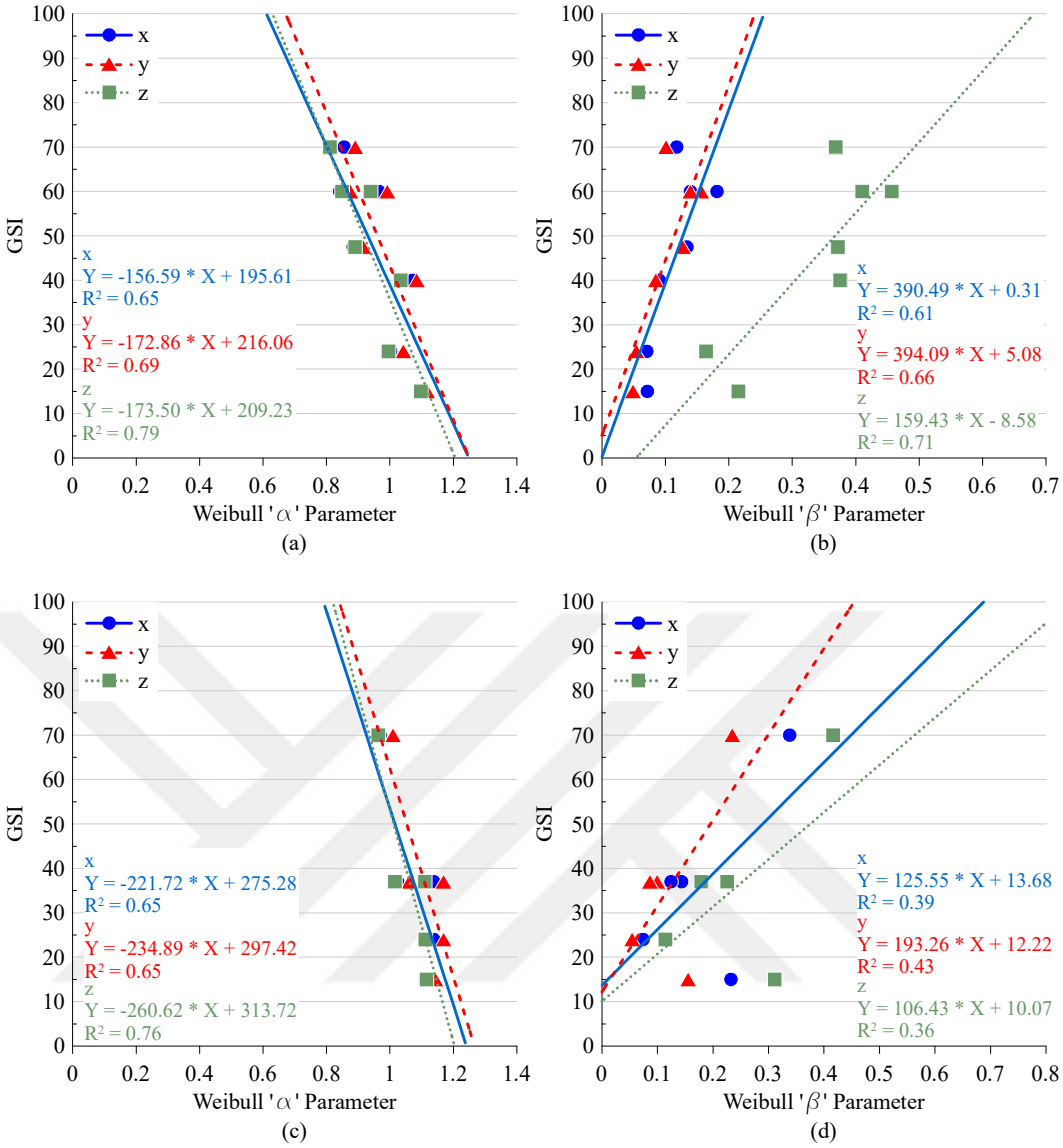

Figure 4.49 : The relationships between GSI and Weibull parameters for bottom accelerometers, (a) and (b) for TBM 2, (c) and (d) for TBM 3.

The relationships between point load index values and Weibull parameters obtained from the data of TBM 4 are presented in Figure 4.50 for bottom accelerometer while the relationships for the top accelerometer can be found in Appendix A (Figure A.12). A moderately strong correlation is observed between point load index and both “α” and “β” parameters. Similar to the other relationships, “α” parameter increases with reducing PLI, while “β” parameter has a positive correlation with PLI.

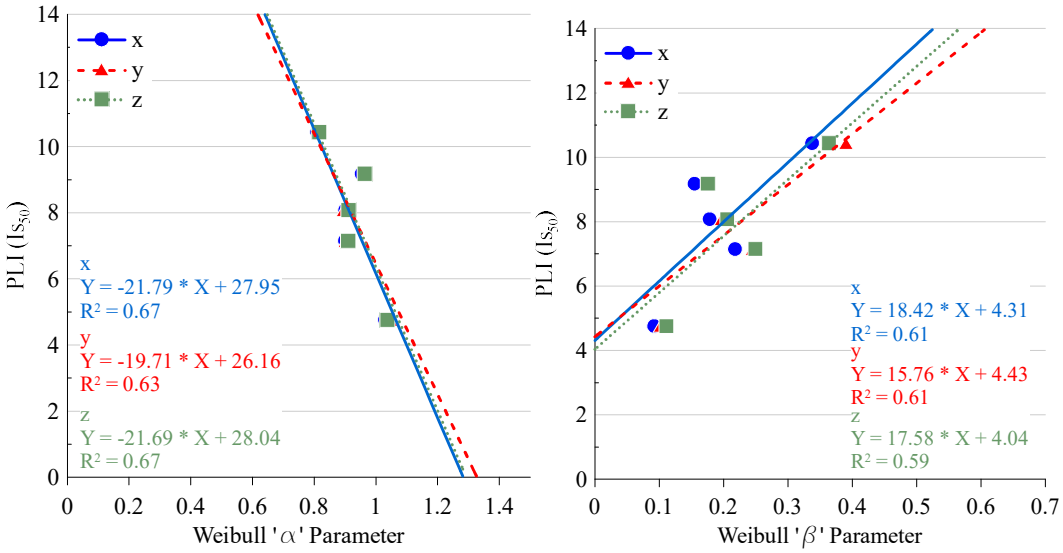

Figure 4.50 : The relationships between PLI and Weibull parameters for bottom accelerometer of TBM 4.

Taking both RQD, GSI and PLI relationships into consideration, it can be concluded that there is minimal difference in terms of coefficient of determination values between the axes. Given that the Weibull parameters are influenced by geological conditions, they can serve as valuable indicators to detect geological conditions in real time. Fluctuations in these parameters could indicate the presence of stronger or weaker rock during excavation, providing operators with valuable insights into the changing geological environment.

The influence of rock strength can also be visualized in the frequency domain. Figure 4.51 presents the power spectral densities of weathered (#2) and fresh (#9) dykes excavated by TBM 2. Excavations with similar cutterhead speeds were deliberately selected to minimize the influence of external variables on the power spectral densities. As presented, in the fresh dyke, which can be considered as hard rock, the vibration data contains more energy in all frequency ranges and the dominant frequencies are less apparent after 1000 Hz. Conversely, the weathered dyke displays more clearly defined peaks in the PSD, containing less energy. Even the peaks are not distinct after 1000 Hz in hard rock conditions, it observed that all data share similar dominant frequencies across the entire spectrum. This observation was further supported by analyzing the PSDs of other lithological units. As the dominant frequencies are not distinguishable between the lithological formations, it could be said that the usability of frequency domain analyses is limited for detecting geological variances.

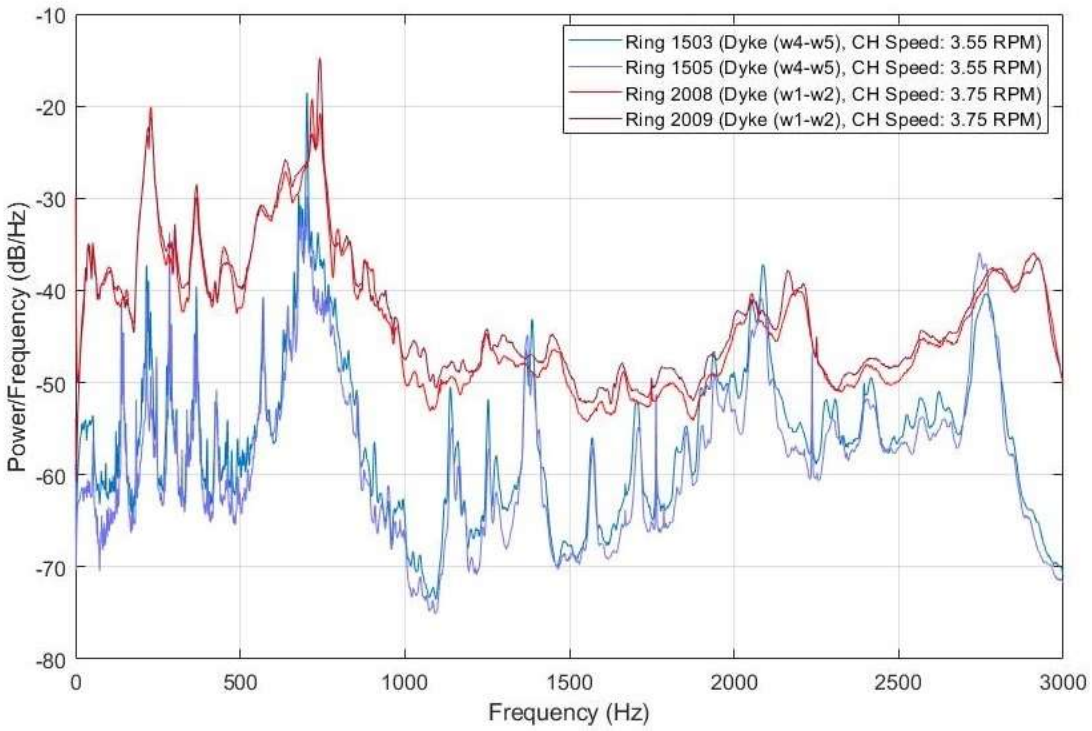

Figure 4.51 : Power spectral densities for fresh and weathered dykes obtained from the data of TBM 2 (bottom accelerometer, z-axis).

4.4.2 Effect of TBM operational and performance parameters on vibration

The relationships between various TBM operational parameters (thrust, torque, cutterhead rotational speed, face pressure), performance parameters (penetration rate, specific energy), and TBM vibrations were investigated to gain a better understanding of their effects on vibrations. Interval RMS values averaged per lithological unit for TBMs 2, 3, and 4 were used for the investigations.

Figure 4.52 shows the relationships between thrust force and interval RMS accelerations for TBMs 2, 3, and 4. It is observed that TBM 2 and TBM 3 exhibit similar trends of increasing acceleration with increasing thrust. However, TBM 4 has an opposing trend to the other TBMs. Since the data of TBM 4 obtained in both soil and rock conditions, the internal RMS accelerations exhibit significant variability for a given thrust value. Thrust increase for this TBM in some sections was related to face pressure increase (due to soil conditions), which resulted a decrease on vibrations, while some related with increased thrust due to the hard rock. During the tunneling, the thrust in soil conditions could easily match and exceed the ones in rock conditions, and subtracting the thrust amount caused by face pressure for eliminating the effect

due to soil conditions did not enhance relationships. This heterogeneity made it challenging to establish a clear relationship between thrust and vibrations for TBM 4.

Additionally, for TBM 4, it was observed that some thrust values were lower compared to the rest of the data, as marked with red circles in the figure. Further analysis of these points revealed that the mentioned values corresponded to the first 70 rings of excavation, which could be interpreted as a learning curve. During this period the crew get used to work with TBM and generally excavation is done in a more cautious way. As the other TBMs had already commenced excavation before the accelerometers were installed, they do not have similar data.

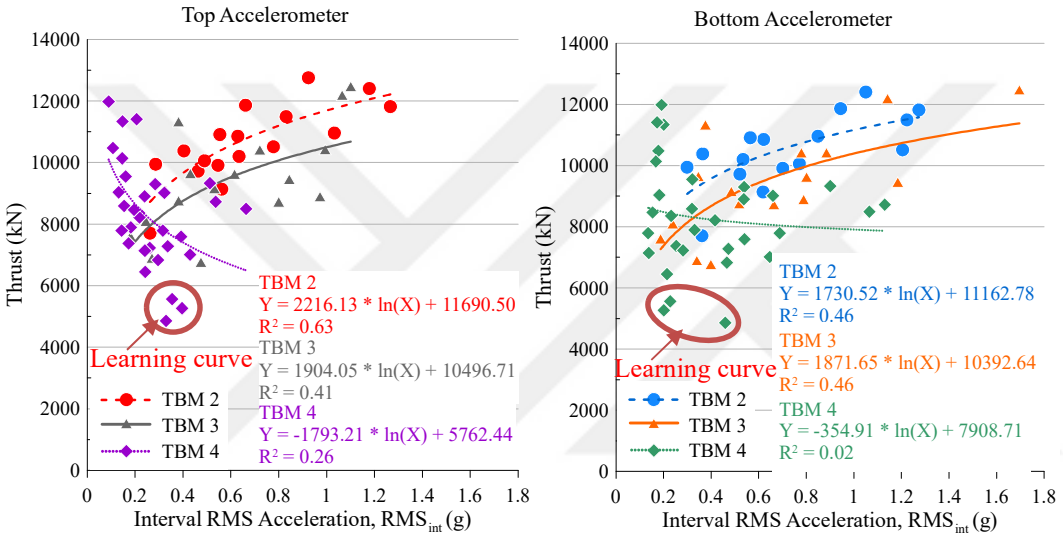

Figure 4.52 : Relationships between interval RMS acceleration and thrust for TBM 2, 3 and 4.

The relationships between cutterhead speed and vibrations are presented in Figure 4.53, which shows moderately strong positive correlation for TBM 2 and 3. No statistically relevant correlations could be observed TBM 4. The cutterhead speed maintains a relatively narrow range of approximately 3.5 to 4 RPM across the majority of recorded sections, rendering its statistical interpretation challenging due to this limited variability and the difference between the TBM 4 and other TBMs can be explained by the soil presence in this TBM's stretch.

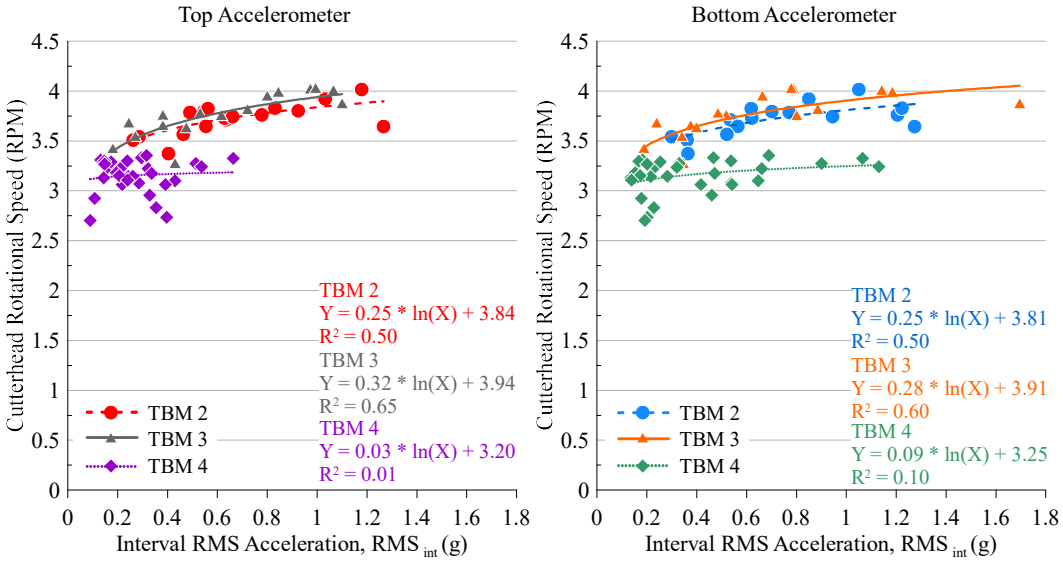

Figure 4.53 : Relationships between interval RMS acceleration and cutterhead speed for TBM 2, 3 and 4.

The influence of cutterhead speed on vibration characteristics is apparent in the frequency domain. Figure 4.54 presents power spectral densities for four consecutive rings excavated by TBM 2 with varying cutterhead speeds. Analyzing consecutive rings excavated in similar geological conditions minimizes the influence of geological variability on the frequency content. As observed in the figure, the peak frequencies in the PSDs shift towards higher values with increasing cutterhead speed, while the energy content remains mostly unchanged.

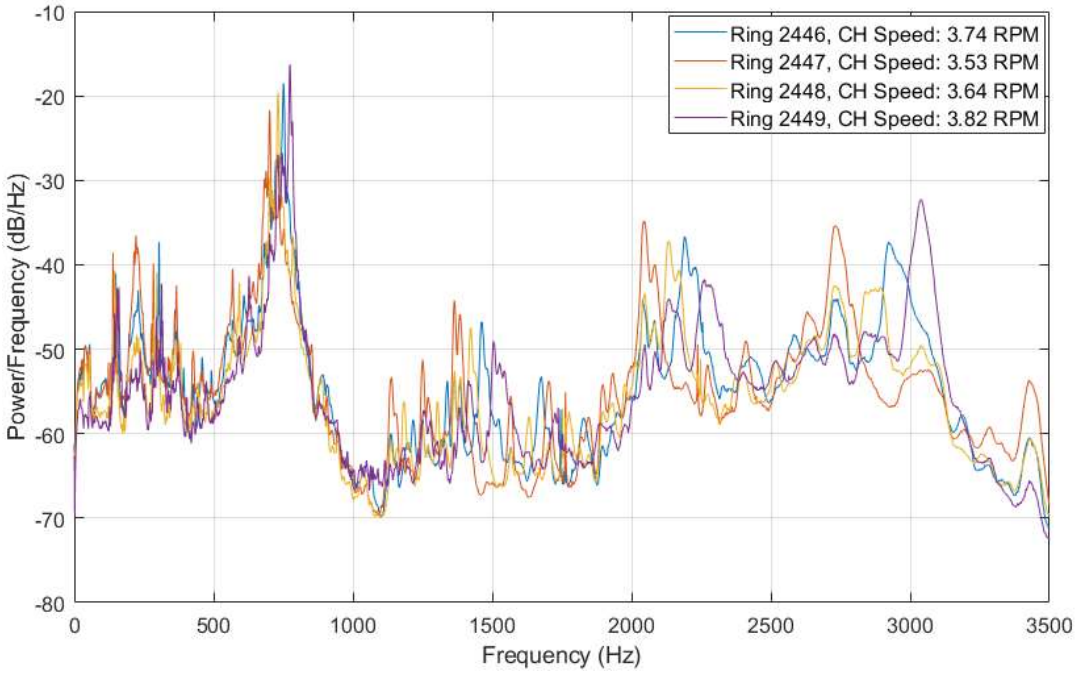

Figure 4.54 : Power spectral densities for consecutive rings with different cutterhead speeds obtained from TBM 2 (bottom accelerometer, z-axis).

The relationships between penetration rate and interval RMS accelerations are presented in Figure 4.55. For EPB TBMs, it is expected that the penetration rate would decrease when encountering harder rocks and cohesionless soils (Ates et al. 2016, 2017). While the second case is not present for TBMs in this study, it can be inferred that the reduction in penetration rate is primarily attributable to the increase in rock strength, subsequently leading to increased TBM vibrations. TBMs 2 and 3, which share identical specifications and excavated adjacent tunnels with similar geological conditions, exhibit a very close trend. The TBM 4 also has a similar trend with the other ones. While some of the relationships demonstrate low R^2 values, the overall trends are noticeable.

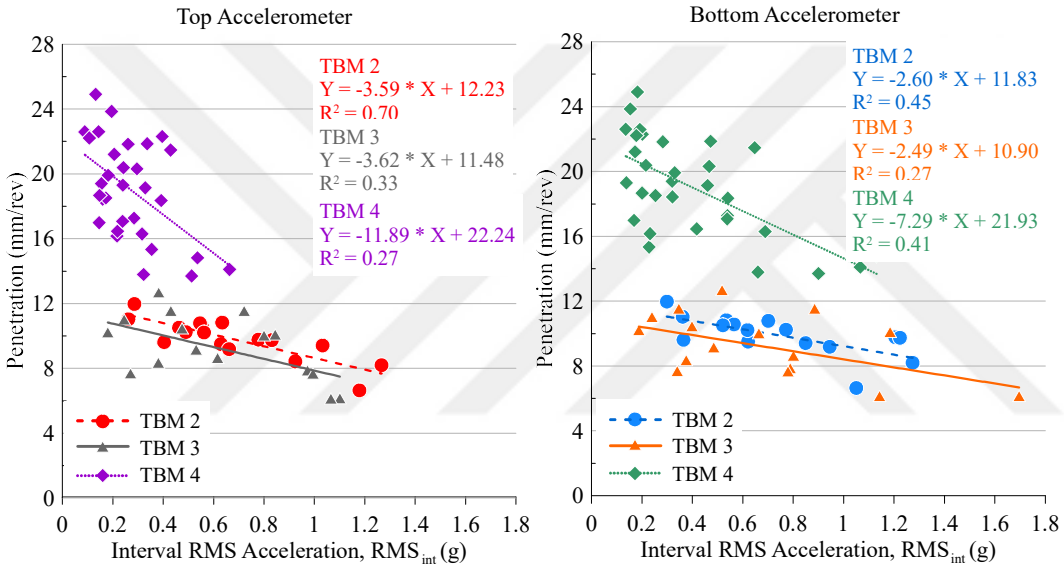

Figure 4.55 : Relationships between interval RMS acceleration and penetration for TBM 2, 3 and 4.

Specific energy is a crucial parameter for assessing excavation system efficiency and it represents power consumption per unit volume of excavation (Avunduk & Copur, 2018). Its relationship with interval RMS acceleration is presented in Figure 4.56 for TBMs 2-4. Coefficient of determination values between specific energy and TBM vibrations show weak relationships for TBM 2 and TBM 4, while TBM 3's bottom accelerometer exhibit a moderately strong correlation. Despite the low R^2 values for TBM 2, a trend with a positive correlation can be observed. The scattered data points for TBM 4 can be explained by varying face conditions, given that the energy spent per unit volume is affected by a range of parameters such as torque, face pressure, excavated soil material, etc.

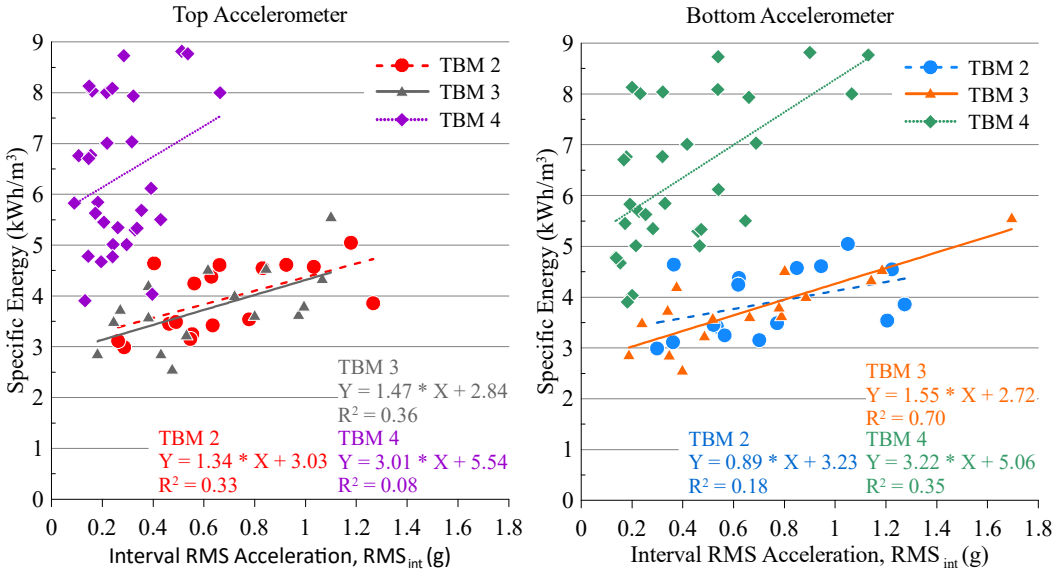

Figure 4.56 : Relationships between interval RMS acceleration and specific energy for TBM 2, 3 and 4.

A statistically significant relationship can not be identified between face pressure, torque and interval RMS accelerations, despite observing a trend indicating that interval RMS acceleration increase as face pressure decreases. The recorded maximum face pressures remain below 1.5 bar, which is at the lower end of the 4-5 bar capacity applicable by EPB TBMs potentially resulting in an inability to establish a significant relationship. Nonetheless, the observed trend aligns with expectations; when the lithological units are stronger and more stable, the face pressure requirement reduces, and the vibration levels increase.

In summary, the analyses suggest that, while the relationships between vibrations and TBM operational parameters might not be strong, a correlation or general trend does exist.

4.4.3 Effect of cutter conditions on TBM vibrations

In recent years, several monitoring systems have been developed to monitor the condition of disc cutters during excavation (Shanahan, 2010; Mosavat, 2017). These systems typically installed within the disc housing and often costly due to the complexity of the cutterhead. The vibration monitoring system developed particularly for the present study is not directly equivalent to these systems; however, certain anomalies in the vibration data recorded in hard rock conditions appear to be associated with cutting tool damages.

The initial detection of vibration differences attributed to broken disc cutters were observed through the test system implemented on TBM 1. It is important to note that the vibration recording system installed on this TBM served as a proof of concept, and the amount of collected data was relatively limited.

While the information gained from TBM 1 provided an initial indication of the potential for vibration monitoring to detect broken disc cutters, the limited dataset necessitated additional investigations. The TBM 2 provided a good opportunity to further study the relationship between cutterhead vibrations and cutter damages. In the andesite dyke (#7) encountered with this TBM, a significant number of broken rings had reported by the site crew. Correlating this data with the cutterhead vibrations unveiled a trend; as the number of damaged discs increases, there is a concurrent increase in cutterhead vibrations. Furthermore, it has been observed that instances of high amplitude shocks align with automatic conveyor belt stops due to the metal sensors detecting the broken disc ring pieces. While definitive verification and a complete understanding of the underlying mechanism remain challenging, it is hypothesized that when a disc ring gets broken, some parts of it fall in front of the cutterhead. Subsequently, these fragments get squeezed between the other cutting tools and the rock surface, thereby generating high-amplitude shocks.

The vibration data of the ring 1886 of TBM 2 is a good example of these shocks (Figure 4.57), even the accelerometers' measurement range is ±10g, and measurements beyond this amplitude are not reliable due to the saturation of data.

Following the excavation of the ring 1886 (Figure 4.57), the cutterhead inspected was conducted, revealing damaged disc cutters. During the inspection of the vibration data, it was seen that high amplitude shocks were present on all channels. Another similar occurrence took place during the excavation of ring 1895 located in a very short distance from the first example, where the excavation was stopped due to a broken disc ring found on the conveyor belt. Again, high amplitude shocks were present on all channels of the accelerometers (Figure 4.58).

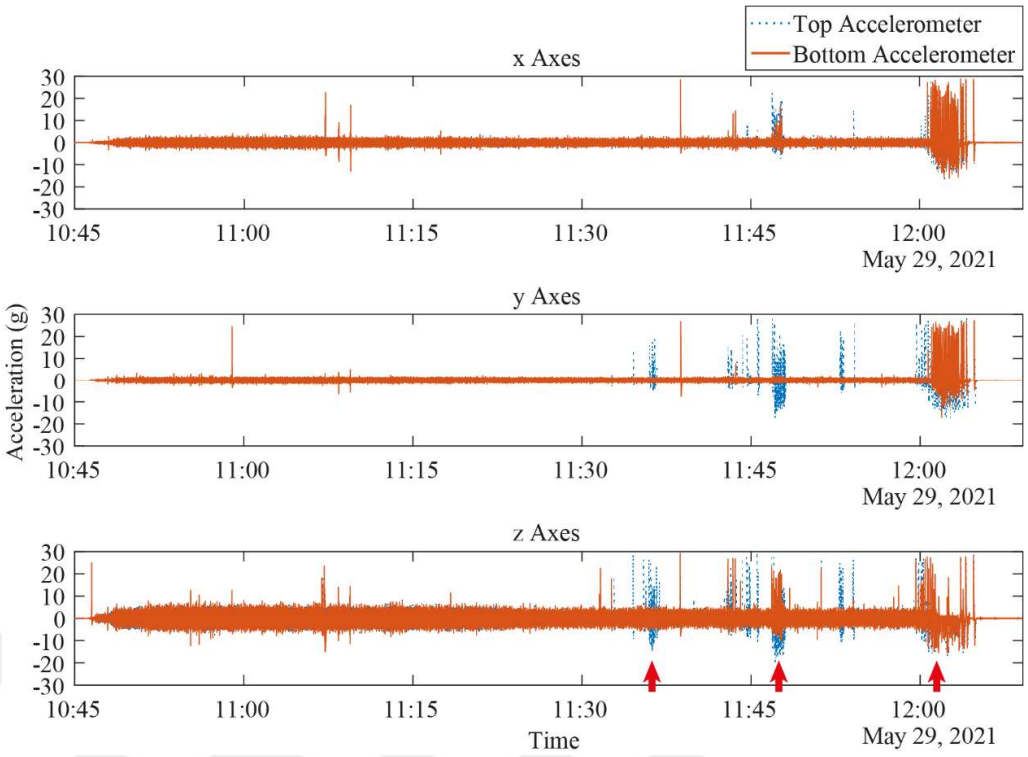

Figure 4.57 : Vibration data of the ring 1886 (x, y and z-axes, top and bottom accelerometers, TBM 2).

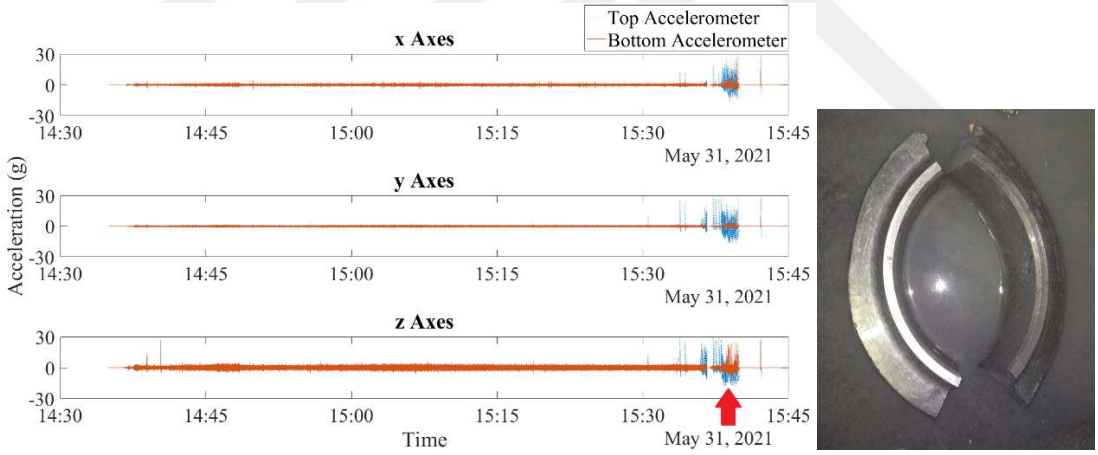

Figure 4.58 : Vibration data of the ring 1895 and the broken disc ring (x, y and z-axes, top and bottom accelerometers, TBM 2).

A waterfall FFT plot for excavation of the ring 1985 is presented in Figure 4.59 focusing on the last 900 seconds and sub 50 Hz frequency range, where very high amplitude vibrations observed. It should also be noted that these vibrations happened in a very short timeframe. As can be seen from the figure, most of the high amplitude vibrations are below 10 Hz.

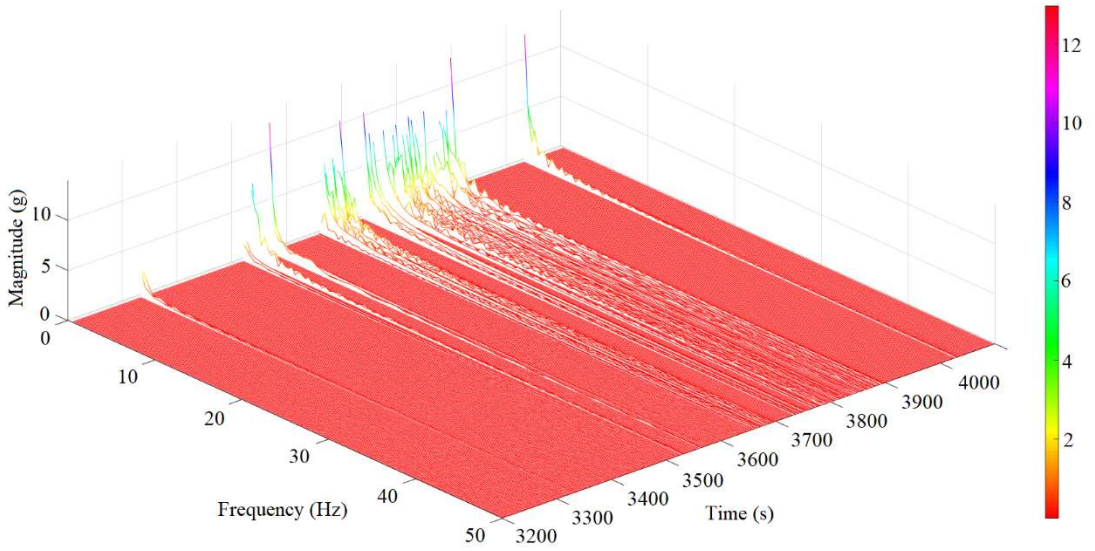

Figure 4.59 : Waterfall FFT graph of the ring 1895 (z-axis of bottom accelerometer).

Figure 4.60 presents the vibration data of z-axes for three consecutive excavations, ring 2329 to 2331. During the excavation of ring no 2329, the shocks recorded were not too strong and frequent. However, on the next ring, there were some long-lasting peaks (marked with red) very similar to the ring no 1895 of the previous case. A post-excavation inspection of the cutterhead revealed broken disc cutters. The vibration data for ring 2331, following disc cutter replacement, still displays some peaks. However, none of these peaks reach the same extended duration as those observed during the excavation of rings 1895 or 2330.

Waterfall FFT plots are presented in Figure 4.61 for the rings 2330 and 2331. Similar to the previous example, on ring 2330, in a short timeframe, high amplitude sub 10Hz vibrations were observed and it is believed that some of the cutter damages occurred in this section. In contrast, during the subsequent excavation, although similar amplitude vibrations were seen, they distributed across a more extended time period.

Due to the limited measurement range (±4g) of the accelerometers on the TBM 3 and TBM 4, these shocks were often indistinguishable, as the actual vibration levels encountered during excavation tend to surpass the measurement range of the accelerometers.

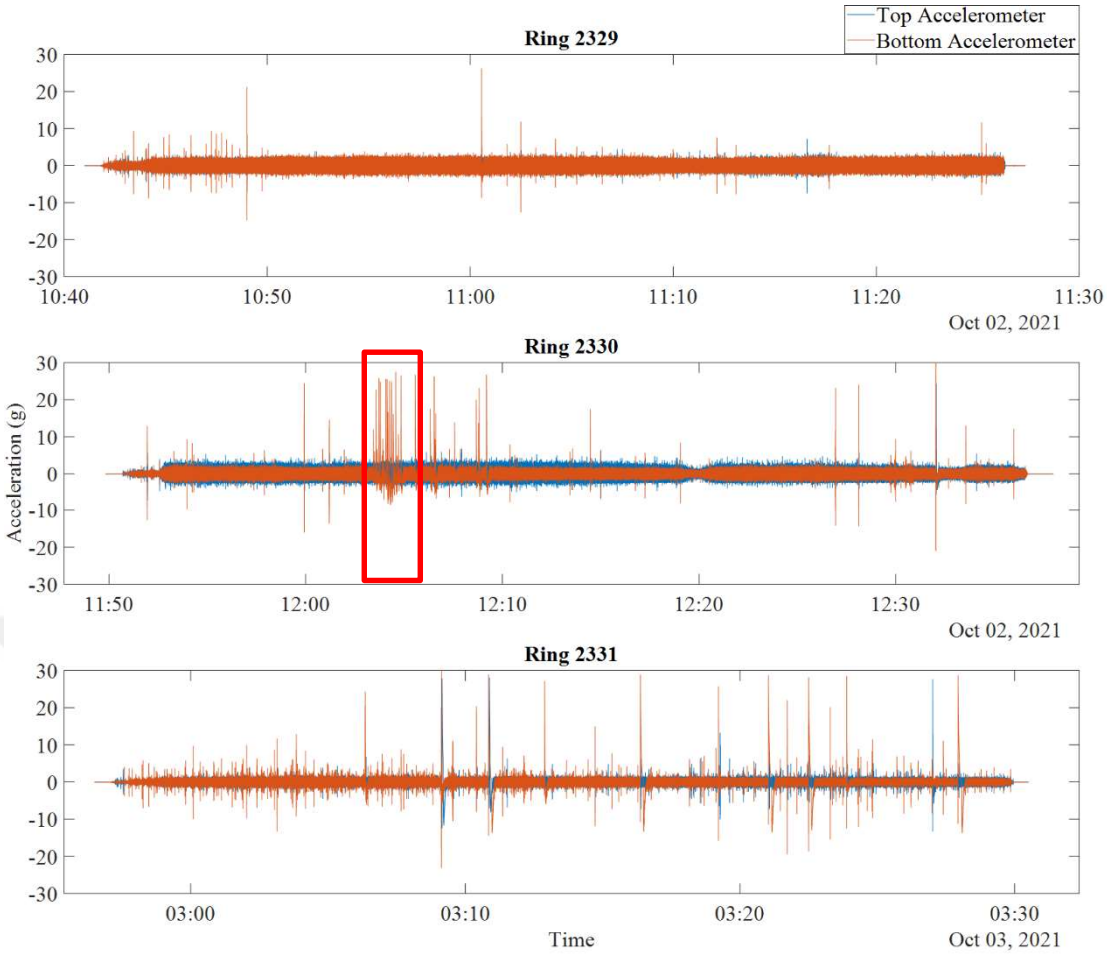

Figure 4.60 : Vibration data of the rings 2329 to 2331 (z-axes, top and bottom accelerometers, TBM 2).

It is evident that long-lasting high amplitude vibrations could serve as an indicator of damaged cutting tools. However, as previously discussed, these indications are typically observable solely in hard rock conditions, and their presence is not consistent. Most probably, to create a distinguishable vibration pattern from the regular one, the broken tool needs to be squeezed between the cutterhead and rock, or components within the cutterhead.

While the vibration recording system might not consistently enable immediate identification of damaged cutting tools, in cases of observing similar long-lasting high amplitude vibrations in hard rock formations, a prompt cutterhead inspection could help to minimize the damages on the cutterhead. The positive feedback received from the site crew operating TBM 2 underscores the value of the information provided by the system.

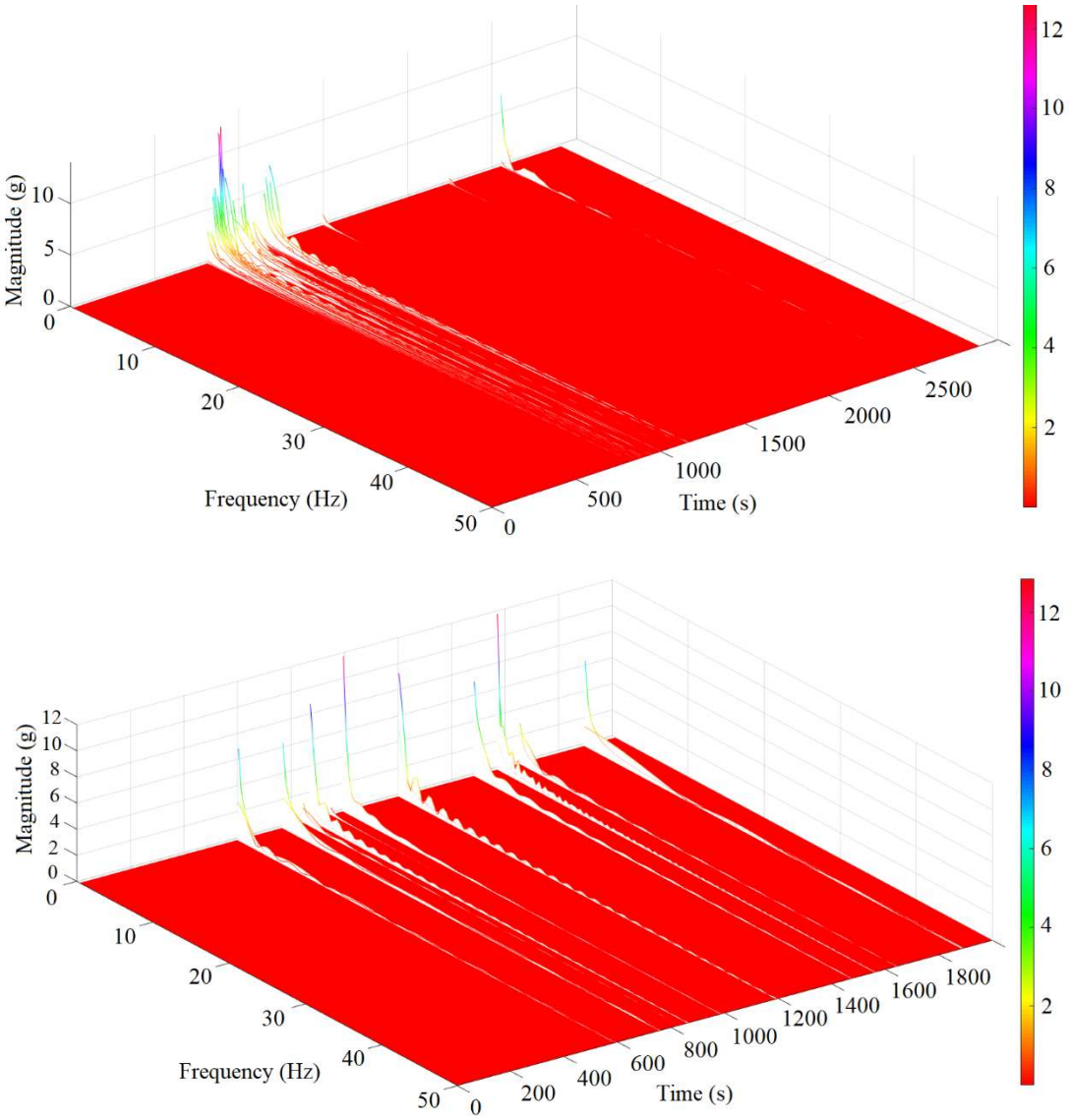

Figure 4.61 : Waterfall FFT graphs of the of rings 2330 (top) and 2331 (bottom) of TBM 2 (z-axis of bottom accelerometer).

4.4.4 Effect of accelerometer positions on vibration

The analysis of vibration data revealed variations in acceleration amplitudes between the top and bottom accelerometer positions on the TBMs. However, despite these variations, general trends in the vibration characteristics remained consistent across both locations. The positions of the accelerometers on the TBMs are presented in Figure 4.62 in a transverse cross-section.

Table 4.9 presents the average RMS vibration ratios between the top and bottom accelerometers for all TBMs across the entire dataset. The data reveal that vibration magnitudes were consistently higher at the bottom accelerometer, with the exception of the z-axis on TBM 1.

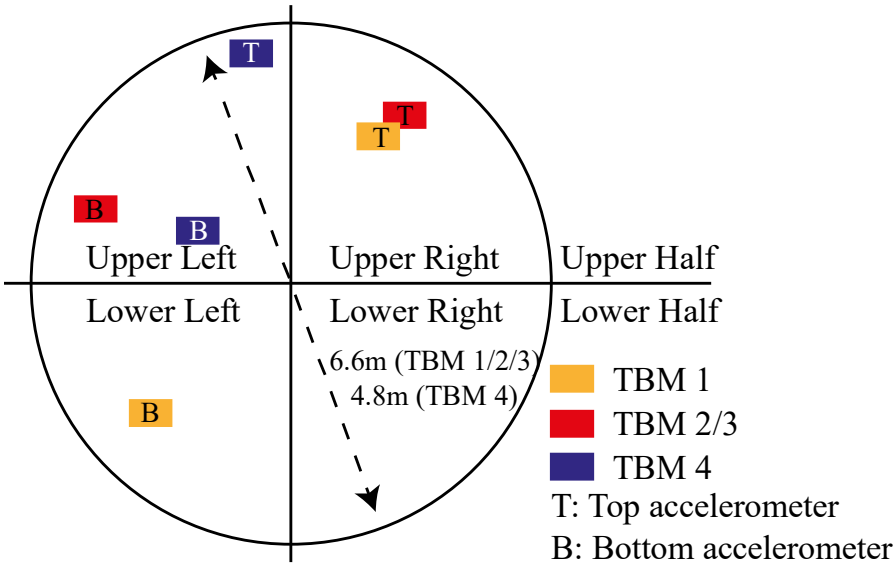

Figure 4.62 : Accelerometer installation positions in TBMs.

Table 4.9 : Average RMS vibration ratios of top to bottom accelerometers for all TBMs and measurement axes.

TBM No	Measurement Axes		
	x	y	z
TBM 1	0.93	0.49	1.06
TBM 2	0.85	0.71	0.93
TBM 3	0.87	0.98	0.97
TBM 4	0.63	0.63	0.64

The difference between top and bottom accelerometers can likely be attributed to TBM operation and equipment layout within the shield. A common practice in TBMs involves maintaining higher thrust levels in the lower half of the TBM to prevent sinking of cutterhead and overcoming the friction between bottom of part of the TBM and ground (caused by mass of cutterhead and shield seating on the ground). As a consequence, the transmission of vibrations through the TBM structure might be more effective in the lower half of the TBM.

Additionally, it is worth noting that certain equipment, such as the screw conveyor, positioned within the shield and typically located at the lower part of the TBM, might introduce additional vibrations during excavation. It should also be noted that in TBM 1, cutterhead motors were hydraulic and some of the hydraulic pumps (thrust pump, erector pump etc.) were located within the shield area as opposed to other TBMs. These components may have contributed to the differences in vibration characteristics observed in TBM 1.

The selection of an optimal accelerometer placement location on the pressure bulkhead is challenged by variations in vibration transmission through the TBM structure. These variations can be attributed to differences in structural and mechanical designs, as well as the presence of internal noise sources such as motors and pumps. The implementation of two accelerometers per TBM has proven to be a practical solution. This redundancy mitigates the effects of potential accelerometer malfunctions and ensures the uninterrupted collection of vibration data. As demonstrated during the study, when one accelerometer encountered issues, the other continued to function, preserving data continuity.

4.4.5 Effect of accelerometer types on vibration

Two distinct accelerometer types were utilized during the study, which are MEMS type accelerometers and piezoelectric accelerometers. As detailed in previous sections, MEMS type accelerometers measure static gravity, while piezoelectric type excludes static gravity. Consequently, the influence of static gravity should be considered and deducted from the acceleration values recorded by MEMS type accelerometers. On the other hand, piezoelectric accelerometers do not record lower frequencies (below 0.5 Hz in this study), which might result in data losses if the data has frequency content below the lower range of the accelerometer. Nonetheless, no discernible disparities were observed regarding the applicability of these accelerometer types within the TBM vibration recording system, and considering cost considerations, MEMS type accelerometers might be good enough for these kinds of systems.

4.4.6 Effect of EPB TBM diameter on vibration

Larger diameter TBMs are theoretically expected to generate higher vibration levels due to their larger excavation cross-section area with potentially leading to greater ground inhomogeneity, a higher number of cutters, and higher TBM operational parameters. A notable distinction among the TBMs in this study is the excavation diameter, with one of them (TBM 4) having a smaller diameter (4.8 m) compared to the others (6.56 m). This discrepancy presented an opportunity to explore the impact of TBM diameter on vibrations.

While a direct comparison of vibration differences solely based on the TBM diameter was not possible due to different geological conditions encountered by each machine, analysis revealed that the vibration differences between the lithological units were also

distinguishable on the small diameter TBM. This observation suggests the potential applicability of the measurement system for pipe jacking and micro tunneling machines, where operator's cabin is typically located outside the tunnel for allowing remotely controlled operation.

5. LABORATORY EXPERIMENTS

There are numerous influencing factors and sources of noise present that impact TBM vibrations, highlighting the necessity for a more thorough understanding of vibrations generated during the rock cutting process. With this objective, a full-scale linear rock cutting machine was equipped with accelerometers and rock cutting tests were conducted on three different rock samples with a 17" disc cutter. Forces acting on the cutting tool and vibrations generated during cutting simultaneously recorded in three orthogonal directions. Peak, root mean square (RMS), and interval RMS accelerations were calculated from the recorded vibration data. Subsequently, the relationships between vibrations, cutting performance parameters (e.g., average and maximum normal, rolling and side forces etc.), cutting geometry, and geomechanical properties of rocks were investigated. Weibull cumulative probability distributions were also generated to analyze the vibration characteristics.

5.1 Equipment, Procedures and Parameters

5.1.1 Physical and geomechanical property test equipment and procedures

The physical and geomechanical properties of the rock blocks employed in the FLCM experiments were determined through laboratory analyses conducted on core samples directly extracted from the blocks.

These analyses included unit weight, uniaxial compressive strength, indirect tensile strength, elasticity modulus, and Schmidt hammer tests in accordance with ISRM (2007) suggestions, point load tests in accordance with ASTM D5731-02 (ASTM, 2016), seismic wave velocity tests in accordance with ASTM D2845 (2008) and Shore sclerescope tests in accordance with McFeat-Smith (1977). To ensure consistency in the results, at least three core samples were tested for each rock type unless otherwise indicated.

5.1.2 Full-scale linear rock cutting test equipment and accelerometers

The full-scale linear cutting test measures the forces acting on a cutter while cutting a block of rock sample, cast in a sample box. The results of this test can be used as input for selection, designing, and predicting/optimizing the costs and performance of mechanical miners (Bilgin et al., 2013).

The tests carried out by using the full-scale linear cutting machine (FLCM) at Istanbul Technical University, Mining Engineering Department's laboratory. Together with a strain-gauge based load cell to measure the cutting tool forces, five accelerometers were also attached to FLCM, which features a large stiff reaction frame that the cutter and load cell assembly are mounted. A block sample up to 0.6 × 0.8 × 1.0 m in size is cast within a sample box with concrete at a certain dip angle, parallel or perpendicular to the bedding planes in order to simulate the real cutting conditions of the site. A hydraulic cylinder moves the sample box through the cutter at a present penetration (p), a line of spacing (S_L), and a constant velocity. These parameters can be adjusted as desired. A triaxial load cell located between the cutter and the frame measures the orthogonal forces acting on the cutter. After each cut, the cut length is measured; the cut materials (muck) are collected, weighed, and sieved. Then the rock box is moved sideways by the desired spacing to duplicate the action of the multiple cutters on the cutterhead of a mechanical excavator, and the experiment is repeated (Copur et al., 2017).

Specific energy is one of the most important factors for defining the optimum cutting geometry for a given rock sample which is calculated as (Pomeroy, 1963; Roxborough, 1973);

$$SE = \frac{FC}{Q} \tag{5.1}$$

where; SE is specific energy (MJ/m^3), that can be converted to (kWh/m^3) by dividing the result by 3.6, FC is cutting force acting on the tool (kN), and Q is the yield or rock volume cut in unit cutting length (m^3/km). Following the tests, specific energy is calculated using equation 5.1, and used for estimating and comparing the cutting efficiency.

A schematic of the machine is given in Figure 5.1 and the forces acting on the disc cutter during rock cutting are shown in Figure 5.2.

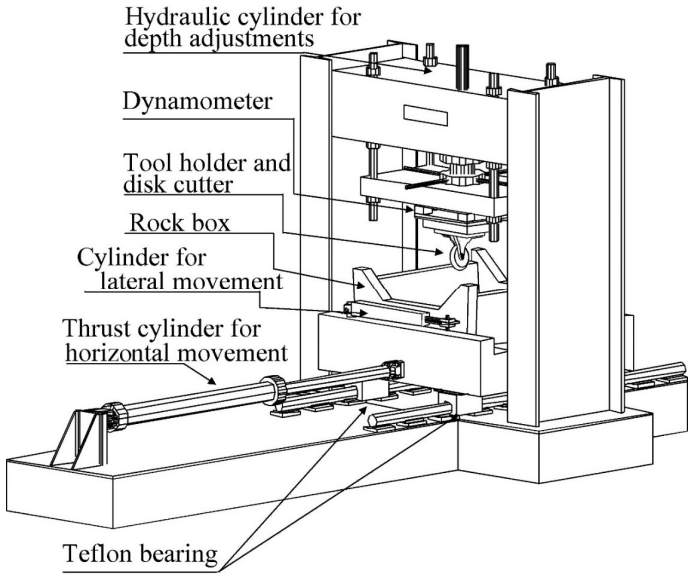

Figure 5.1 : Schematic view of full-scale linear cutting machine.

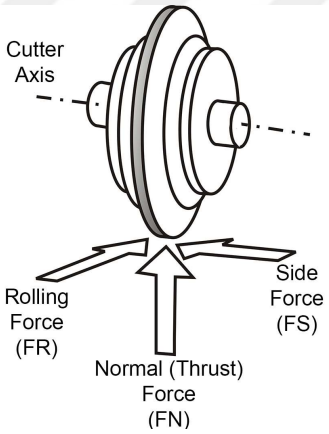

Figure 5.2 : Forces acting on a CCS disc cutter.

The initial testing configuration employed four accelerometers; two pairs of model 356A17 (10g) from PCB Electronics and model ADXL354BZ (4g) from Analog Devices (PCB Electronics, 2008; Analog Devices, 2017). However, due to the unexpectedly high acceleration values following the first tests (siltstone, line spacing of 70 mm), accelerometer placement was changed, and a 5th accelerometer from Analog Devices model number ADXL356CZ with a measurement range of 40g (Analog Devices, 2020) was added to the system. The specifications of the accelerometers are detailed in Table 3.1.

The accelerometer placement, their identification numbers used throughout the study, the axes and the cutting sequence are presented in Figure 5.3.

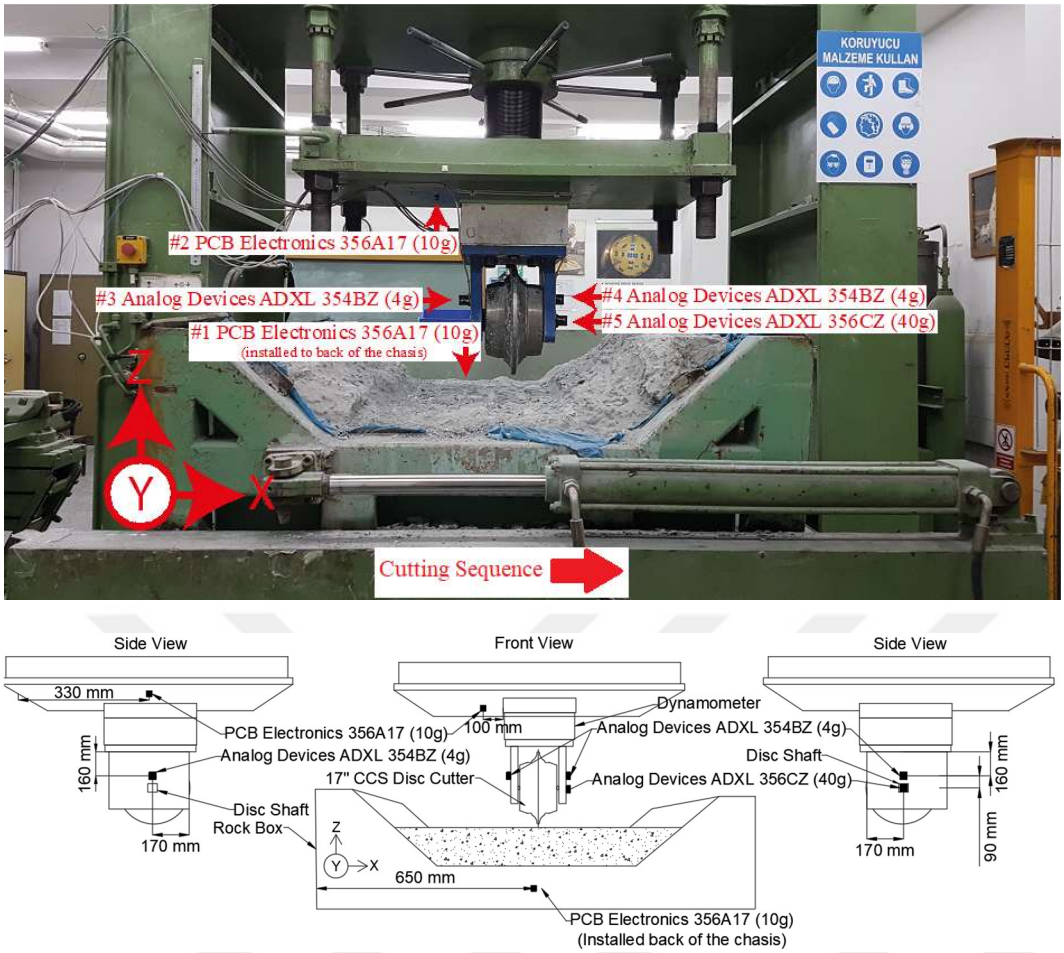

Figure 5.3 : Accelerometer numbers (#) and placements on FLCM.

Preliminary data analysis revealed discrepancies in the acceleration levels recorded by accelerometers 3 and 4. While the definitive cause remains unclear, it is hypothesized that, these differences were related to the cutting sequence direction. Throughout the tests, the accelerometer 3 was placed on the freshly cut (relieved) side of a cut on the cutting tool, whereas the accelerometer 4 was positioned on the opposite (unrelieved) side. Although the side forces were not significantly different, the chipping of the rock on the unrelieved side (accelerometer 4) could potentially lead to higher vibrations. In light of the varying vibration levels between accelerometers 3 and 4, their data was averaged to achieve a more representative measure of overall acceleration during rock cutting. These averaged values used to calculate the interval RMS based on equation 3.5. The accelerometer 5 with 40g measurement range was installed on the unrelieved side of the cutting tool to capture the maximum vibrations as much as possible.

Pairs of USB-6009 and 9230 BNC model analog-digital converters from National Instruments (National Instruments, 2008; National Instruments, 2015) were used for

digitizing the signal. NI USB-6009 was used with MEMS-type accelerometers, whereas NI 9230 BNC was used with piezoelectric accelerometers.

5.2 Rock Samples used During the FLCM Experiments

Two rock blocks (mudstone of the Pendik Formation and siltstone of the Kurtkoy Formation) from Goztepe-Umraniye-Atasehir Metro Line along with a beige marble sample from a quarry, were utilized for the full-scale linear rock cutting tests. The mudstone and siltstone samples had bedding planes, whereas the beige marble did not.

5.2.1 Pendik Formation (mudstone)

This rock sample is from the Pendik Formation's Kartal Member. The formation shows intercalation of micaceous shales, mudstones, and siltstones with rare micaceous sandstone of 5-10 cm thick, and bioclastic limestone with thickness of 5 - 10 cm to 40 - 50 cm at various ratios (Geodata Engineering S.p.A., 2016). The sample used during the rock-cutting tests were belongs to mudstone units of this formation (Figure 5.4).

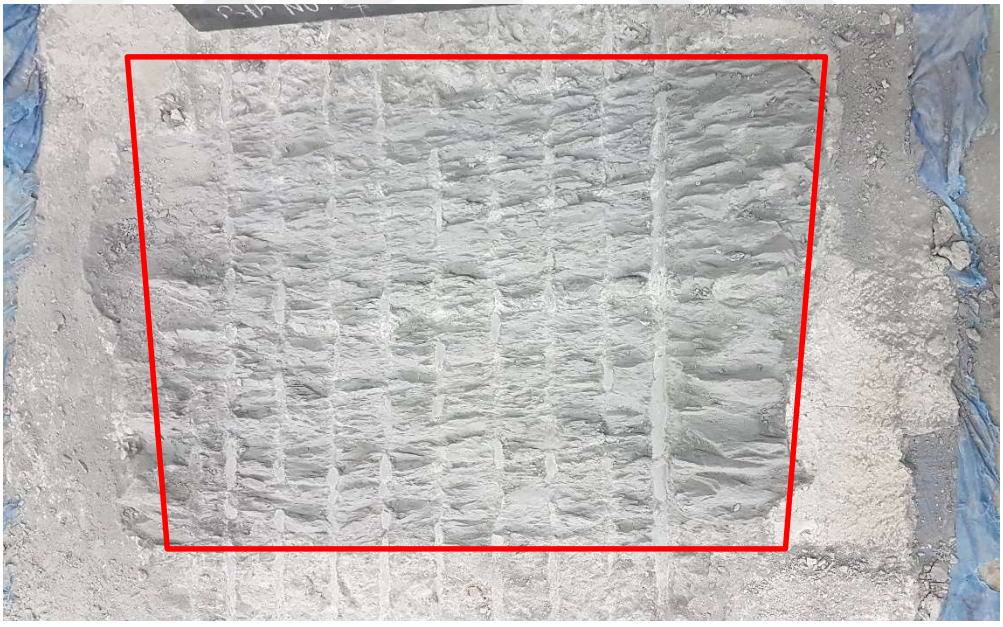

Figure 5.4 : The view of the concreted mudstone sample in the FCLM box.

5.2.2 Kurtkoy Formation (siltstone)

Bakacak Member of the Kurtkoy Formation is dominant in the area where the rock block was obtained. This lithological unit is characterized by thin to medium bedded, parallel, and cross-laminated siltstone and sandstone. The lower parts show purple to

brown color banding; upwards in the sequence the purple color becomes dominant, and the grain size increases (Geodata Engineering S.p.A., 2016). The view of the sample in the FCLM box can be seen on Figure 5.5.

Figure 5.5 : The view of the concreted siltstone sample in the FCLM box.

5.2.3 Beige marble

The beige marble (sparitic limestone) sample was not homogenous in terms of strength and cuttability features, and one side of the sample was much harder to cut during the FLCM tests than the other side. Thus, the data was evaluated in two different sections which are difficult cuttability (DC) and easy cuttability (EC). The sample can be seen on Figure 5.6.

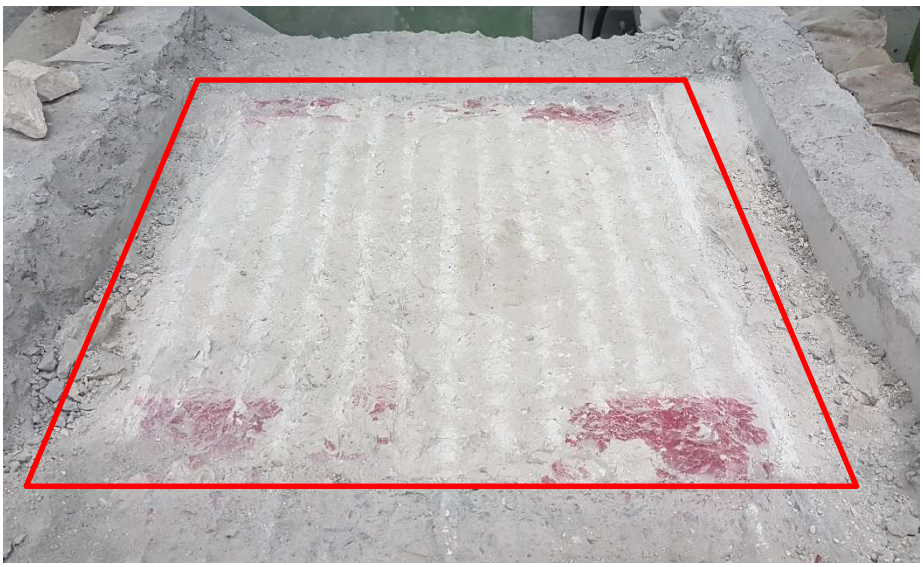

Figure 5.6 : The view of the concreted marble sample in the FCLM box.

To better understand the distinction between the easy and difficult cuttability sections, petrographic analyses were performed on the thin sections. The ratio of intraclasts to pellets is observed to be the most significant difference between the two samples, as the intraclast ratio rises, the rock gets more difficult to cut and requires a greater tool force. It was also observed that the smaller pellet size requires a greater tool force.

5.2.3.1 Difficult cuttability section (DC)

This section is described as “Fossilized Intra Pel Sparite or Fossilized Pel Intra Sparite”. It includes sparitic cemented limestone, which consists of intraclasts, pellets (35-40%), and a slight amount of fossils. Intraclastic parts composed of micritic limestone fragments. Mostly fractured with calcite fillings. Pellet size is between 0.1 and 0.4 mm.

5.2.3.2 Easy cuttability section (EC)

This section is characterized as “Fossilized Intra Pel Sparite". Sparitic cemented limestone includes more calcite fillings than the other section (DC). Pellets are larger in size (0.3-0.6 mm) and occupy more space (50%). Intraclast size and ratio are lower and include a little amount of microfossils. Mostly fractured with calcite fillings.

5.2.4 Physical and geomechanical properties of the rock samples

The physical and geomechanical properties of the rock samples are summarized in Table 5.1. The rocks have a wide range of properties, changing between 21 and 82 MPa for uniaxial compressive strength, 5 and 26 GPa for static elasticity modulus, while Brazilian tensile strength values are between 5 and 7 MPa. The determined rock properties will serve as key variables in the forthcoming investigation of factors influencing vibration levels during rock cutting.

Table 5.1 : Physical and geomechanical properties of the rock samples used in linear cutting experiments.

	Siltstone (Kurtkoy Formation)	Mudstone (Pendik Formation)	Beige Marble (EC)	Beige Marble (DC)
Density (gr/cm^3)	2.73	2.52	2.68	2.69
Uniaxial compressive strength (MPa)	46.50*	21.55	81.58	77.57
Indirect tensile strength (MPa)	6.94	4.95	5.83	6.51
Static Poisson's ratio	0.31	0.11	0.19	0.11
Dynamic Poisson's ratio	0.32	0.08	0.16	N/A
Static elastic modulus (GPa)	14.52	4.93	26.34	19.97
Dynamic elastic modulus (GPa)	29.38	19.33	17.29	17.03
P-Wave velocity (m/s)	3903	2744	2695	2517
S-Wave velocity (m/s)	2022	1850	1672	1784
Schmidt hammer hardness (L-Type)	32.95	23.11	39.42	41.03
Shore sclerescope hardness	53.2	31.2	48.6	52
Brittleness (B1)**	6.62	4.35	13.99	11.91
Brittleness (B2)***	0.73	0.62	0.86	0.84

* Only one core sample was available for uniaxial compressive strength test; the results of point load test were used for calculation of average uniaxial compressive strength.

** $B1 = {}^{\sigma_c}/_{\sigma_t}$ by Hucka and Das (1974)

*** $B2 = {}^{(\sigma_c - \sigma_t)}/_{(\sigma_c + \sigma_t)}$ by Andreev (1995)

5.3 Full-Scale Linear Cutting Test Procedures and Parameters

During the single spiral pattern cutting tests, a 17" CCS disc cutter possessing a tip width of 18 mm was employed, and the cutting speed of 12.7 cm/s was used. Before the experiments surface conditioning procedures defined by Copur et al. (2017) were implemented.

It should be noted that, due to the very high cutting forces experienced during the experiments with the difficult cuttability section of the beige marble sample, only 4 mm and 6 mm penetration values were applied to this section. Furthermore, the limited size of this rock block prevented the execution of tests with a line spacing of 70 mm.

Selected line spacing and penetration configurations along with the cutting sequence are presented in Table 5.2 and Figure 5.7.

Table 5.2 : Rock cutting configuration (experimental matrix).

Formation	Siltstone	Mudstone	Beige Marble (EC)	Beige Marble (DC)
Line Spacing (S_L) (mm)	Penetration (p) (mm)			
70	5	5	-	-
	7	7	-	-
85	4	4	4	4
	6	6	6	6
	8	8	8	-
	-	10	-	-

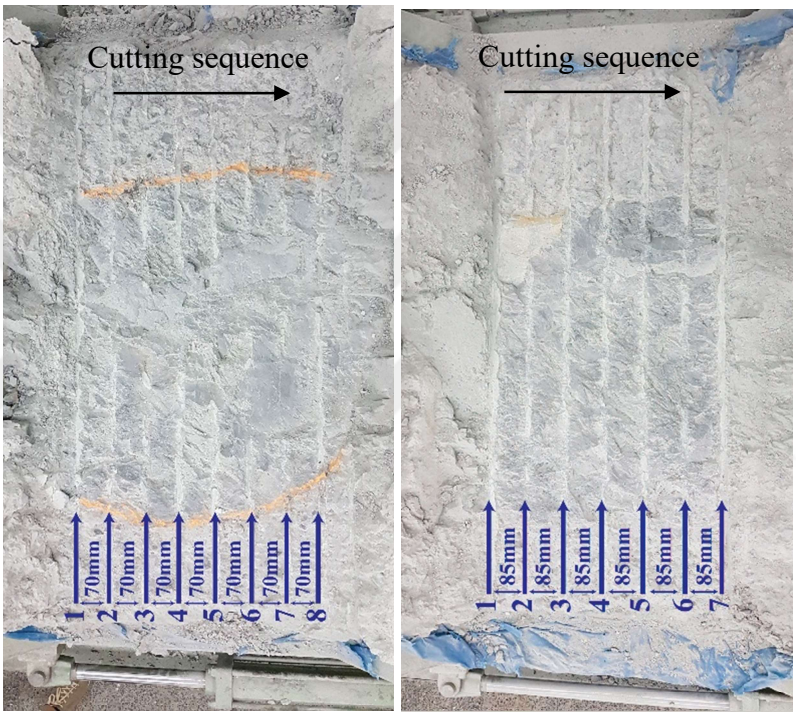

Figure 5.7 : Rock cutting paths (Siltstone of Kurtkoy Formation).

The cutting direction was aligned parallel to the bedding planes for the siltstone sample, while it was 45° angled for mudstone, as illustrated in Figure 5.8. No bedding planes or foliation were present on the beige marble sample.

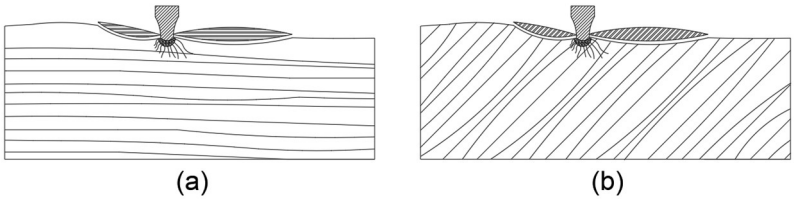

Figure 5.8 : Bedding planes (a for siltstone and b for mudstone).

Sieve analyses were conducted on the muck samples collected after each cut to determine the coarseness index. This index is the sum of cumulative weight percentages of the muck retained on a set of sieves and is characterized as a dimensionless parameter (Barker, 1964; Tuncdemir et al., 2008). As the coarseness index gets higher, the amount of coarse material increases, indicating more efficient cutting (Copur et al., 2017).

The forces acting on the cutting tool during the course of the cutting experiments were sampled at 2 kHz, while the data from piezoelectric accelerometers and MEMS type accelerometers were sampled at 12.8 kHz and 6 kHz, respectively. Video recording was also carried out during the experiments for a better understanding of the reasons of vibrations. The recorded vibration data was analyzed both in time and frequency domains utilizing custom Matlab scripts, using the analysis techniques outlined in Section 3. The process began with synchronization of the raw vibration data with the corresponding force data acquired from the FLCM for each cutting test. This was followed by statistical calculations (peak acceleration, RMS acceleration, interval RMS acceleration), obtaining Weibull shape (α) and scale (β) parameters through distribution fitting, and frequency domain analyses. Accelerometers 3 and 4 ($\pm$4g) were predominantly utilized during analyses, which were installed directly on the cutter's holder. Meanwhile, accelerometer 5 ($\pm$40g), positioned at the disc cutter's shaft axis, was utilized to obtain the maximum acceleration values.

Following the calculation of the cutting parameters individually for each cut, the results were averaged for each combination of line spacing and penetration to establish a representative value. For instance, if the siltstone sample has five cutting with a line spacing of 85 mm and a penetration of 4 mm, the corresponding force and acceleration data from these trials were averaged to create a single data point.

Figure 5.9 presents vibration data from accelerometers 3 and 4 (denoted by x3, y3, z3 and x4, y4, z4, respectively) alongside the corresponding cutting force data. The figure reveals a clear correlation, where instances of high amplitude vibrations measured by the accelerometers coincide with increases in cutting forces. This observation is further supported by photo showing the rock surface following the cutting experiment. Periods of elevated vibration and force also corresponded to the occurrence of larger rock chips during the cutting process. The boundaries of the analyzed rock section are denoted by yellow markings for clarity.

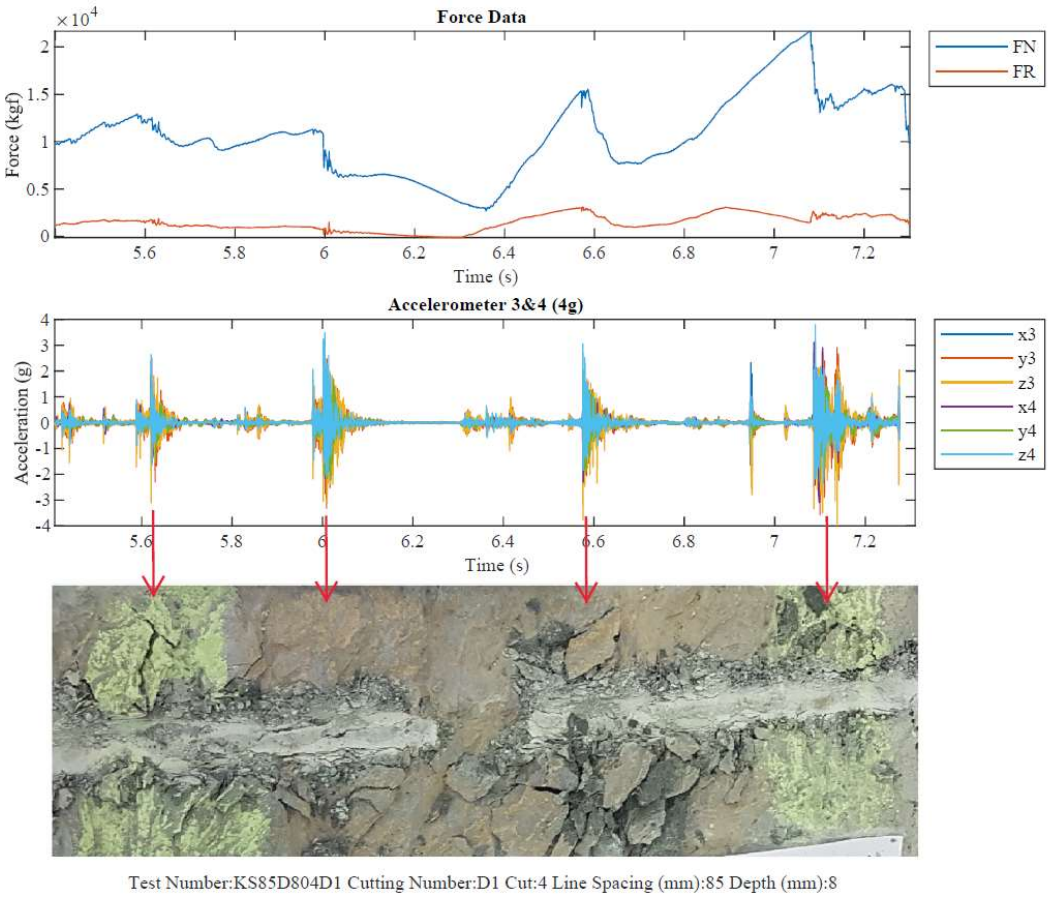

Figure 5.9 : Force and vibration data recorded during one of the cutting tests.

5.4 Experimental Results

During the rock cutting experiments, a total of 55 individual cuts were performed and subsequently analyzed. Table 5.3 summarizes the parameters obtained and calculated following the rock cutting tests.

Figure 5.10 shows that both average normal (a) and average rolling forces (b) increase with increasing penetration, as expected based on rock cutting science. Beige marble's difficult cuttability (DC) section required the greatest average normal force in all penetrations compared to the other rocks, while its easy cuttability (EC) section required the lowest normal force. Similarly, the beige marble's easy cuttability (EC) section also exhibited the lowest average rolling force; however, in contrast with the normal force, the siltstone sample exhibited the highest average rolling force for 85 mm line spacing.

Table 5.3 : Results of full-scale linear rock cutting tests.

Sample	S_L (mm)	p (mm)	S_L/p (-)	SE (kWh/m^3)	FN (kN)	F'N (kN)	F'N/FN (-)	FR (kN)	F'R (kN)	F'R/FR (-)	FR/FN[1] (%)	FS (kN)	CI (%)	+25mm (%)	RMS_{int}[2] (g)	Max. Acc.[3] (g)
Siltstone	70	5	14.0	6.1	99.5	182.6	1.84	7.6	15.5	2.04	7.68	13.30	414.4	11.1	0.36	7.65
	70	7	10.0	7.0	137.9	190.8	1.38	13.2	25.0	1.89	9.59	15.03	423.2	12.6	0.48	10.00
	85	4	21.3	5.6	130.4	191.0	1.46	8.0	16.5	2.06	6.10	2.95	455.7	17.4	0.18	10.96
	85	6	14.2	5.3	129.6	222.4	1.72	10.2	24.0	2.35	7.88	0.70	501.6	46.7	0.33	7.87
	85	8	10.6	6.5	123.1	205.3	1.67	14.4	29.5	2.05	11.69	13.72	459.5	29.4	0.48	16.41
Mudstone	70	5	14.0	6.5	86.1	130.6	1.52	5.3	11.4	2.15	6.13	0.16	410.7	2.9	0.03	0.75
	70	7	10.0	5.6	105.0	155.1	1.48	8.8	15.4	1.75	8.41	2.41	361.7	7.4	0.07	1.46
	85	4	21.3	4.6	76.3	132.1	1.73	4.7	11.9	2.53	6.18	0.93	429.3	4.9	0.04	1.14
	85	6	14.2	4.5	82.1	135.2	1.65	6.4	12.6	1.97	7.82	0.30	434.9	12.4	0.03	3.29
	85	8	10.6	3.7	94.9	153.0	1.61	9.0	16.9	1.88	9.45	1.73	456.8	19.7	0.05	1.08
	85	10	8.5	4.7	105.1	152.8	1.45	14.4	25.7	1.78	13.68	1.80	451.5	23.6	0.15	7.27
Beige Marble (EC)	85	4	21.3	7.1	56.0	139.6	2.49	3.6	12.8	3.56	6.49	0.49	430.2	12.6	0.16	3.89
	85	6	14.2	6.3	74.4	160.3	2.15	5.1	12.5	2.45	6.90	0.48	413.2	10.7	0.21	9.4
	85	8	10.6	3.7	82.9	164.2	1.98	8.4	19.4	2.31	10.16	2.11	450.4	17.0	0.35	12.09
Beige Marble (DC)	85	4	21.3	9.4	163.0	241.1	1.48	6.2	23.9	3.85	3.81	1.41	426.2	7.8	0.37	12.76
	85	6	14.2	5.5	182.2	267.6	1.47	9.8	26.9	2.74	5.36	5.32	489.5	40.6	0.74	20.15

S_L: Line spacing, p: Penetration (depth of cut), SE: Specific energy, FN: Mean (average) normal force, F'N: Peak (maximum) normal force, FR: Mean (average) rolling force, F'R: Peak (maximum) rolling force, FS: Side force, CI: Coarseness index, RMS_{int}: Interval RMS acceleration.

[1] FR/FN = Cutting coefficient (CC)

[2] Interval RMS acceleration was calculated by averaging the accelerometers 3 and 4 data.

[3] Maximum acceleration values show the highest recorded acceleration in z direction of accelerometer 5 (40g). For siltstone's 70 mm line spacing cuts, maximum acceleration values from accelerometer 1 (10g) are used.

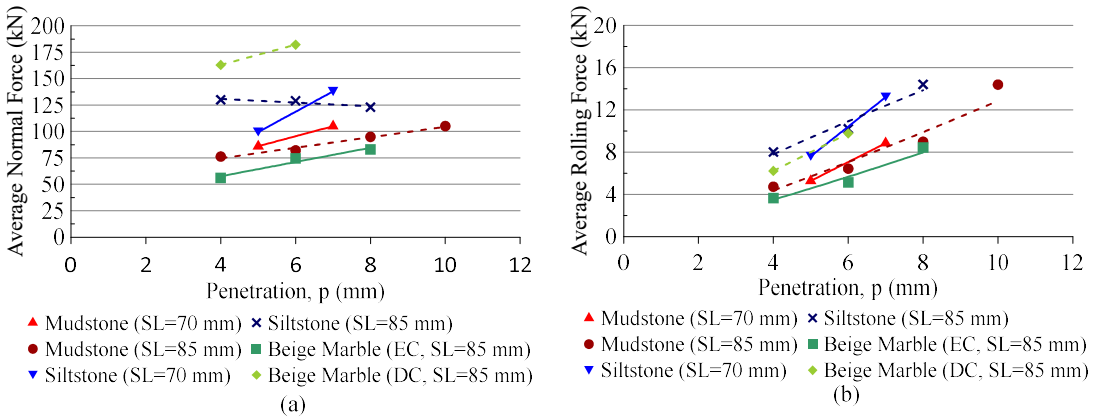

Figure 5.10 : Variations of average normal force (a) and average rolling force (b) with penetration.

It is noteworthy that the average normal force recorded on the siltstone sample exhibits minimal variation across the tested penetration rates. This observation can be attributed to the orientation of the sample's bedding planes, which were perpendicular to the disc cutter (Figure 5.8). In this specific configuration, the same level of normal force appears to be sufficient to achieve rock fracture within the 4-8 mm penetration range. However, it is reasonable to expect an increase in the average normal force if the tests extended to include higher penetration depths.

The normal force typically exhibits a relationship with a rock's uniaxial compressive strength. However, the results of the experiments did not follow the same order as the uniaxial compressive strength of the rocks. Moreover, despite the relatively minor difference in uniaxial compressive strength values between the difficult cuttability (DC) and easy cuttability (EC) sections of beige marble, the former exhibited greater cutting forces. These observations underscore the substantial influence of the petrographic attributes of rocks on their cutting characteristics.

Figure 5.11 illustrates the relationship between specific energy and the ratio of line spacing to penetration. The analysis reveals that the optimum S_L/p ratio for mudstone and beige marble (EC) is approximately 11, while it is 14 for siltstone and beige marble (DC). However, for a more accurate assessment of the optimal SL/p ratio for the difficult cuttability section of beige marble, it would be advantageous to have at least a third data point.

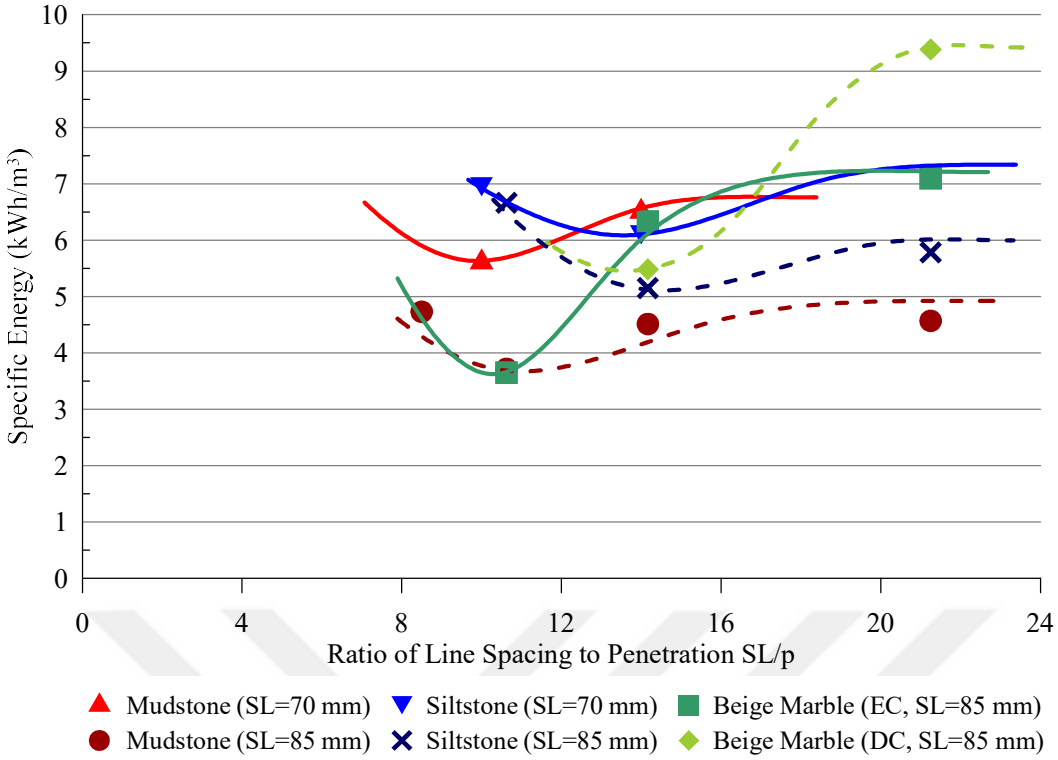

Figure 5.11 : Variations of specific energy with S_L/p ratio.

The relationships between peak tool forces and penetration are presented in Figure 5.12. Similar to the trend observed in average normal force, the difficult cuttability section of beige marble (DC) exhibited the highest peak normal force, while mudstone had the lowest.

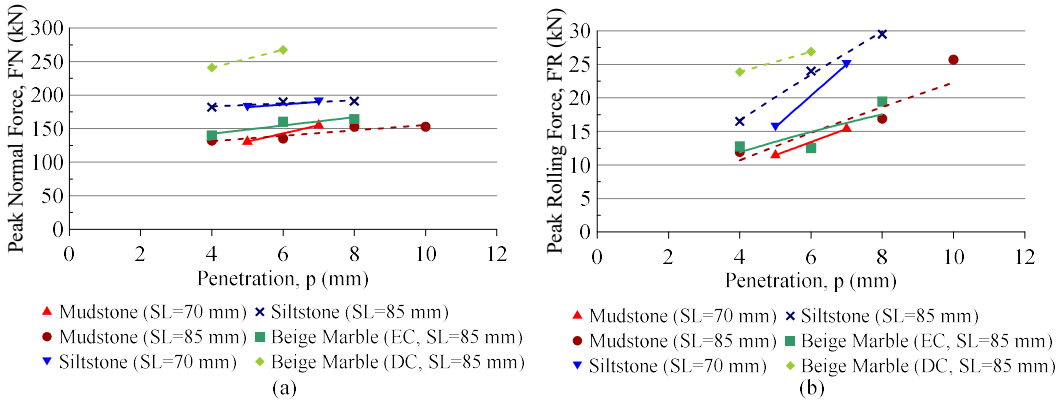

Figure 5.12 : Variations of peak normal force (a) and peak rolling force (b) with penetration.

The observed trends (Figure 5.10, Figure 5.12 and Table 5.3) reveal that as penetration increase, the average force exhibit a more substantial increase than the corresponding peak force across all rock types, excluding the beige marble's difficult cuttability (DC) section. For instance, the increase was 46% for average normal force while it was only

17% for peak normal force of beige marble's easy cuttability (EC) section when the penetration increased from 4 mm to 8 mm. Similarly, for both the average and peak rolling forces of the same sample, the values exhibited respective increments of 133% and 52%. In connection with this observation, Figure 5.13 illustrates the variations in ratios of peak to average normal force and peak to average rolling force with penetration. Generally, both ratios exhibited a decline as penetration increased across all rock types, with a minor exception observed in the case of siltstone (line spacing of 85 mm). These results align with prior investigations (Gertsch, 1993; Gertsch et al., 2007; Cho et al., 2013) while diverging from the findings of Balci (2009), which reported an increase in peak forces relative to average forces with rising penetration. It is also important to acknowledge that the rates of change in these peaks to average force ratios with respect to penetration depth also differ among the various rock types. This observed decrease in ratios can be attributed to the higher increase in average cutting forces with penetration, with respect to increase in peak forces.

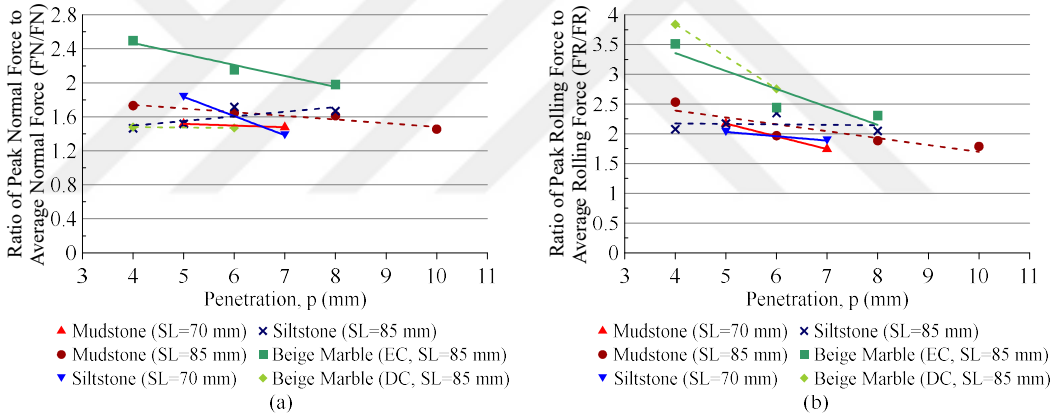

Figure 5.13 : Variations of peak to average normal force (a) and peak to average rolling force (b) with penetration.

5.5 Investigation of Variables Affecting Vibrations Based on FLCM Tests

The laboratory experiments provided a valuable opportunity to explore the influence of rock cutting parameters and the rock properties on the vibrations. This section presents the key findings regarding the relationships between these factors and the vibrations produced during rock cutting.

5.5.1 Effect of mineralogical and geomechanical properties on vibrations

The rock cutting experiments yielded results that align with established principles in rock cutting science, demonstrating a correlation between the mineralogical and

geomechanical properties of the rocks and the resulting cutting forces. As these parameters influence the cutting forces, they can be expected to also have an influence on the vibration characteristics generated during the cutting process. To investigate these relationships, the interval RMS acceleration (equation 3.5) and maximum acceleration (equation 3.3) values were compared to the geomechanical properties of the rocks presented in Table 5.1, such as uniaxial compressive strength, tensile strength, Schmidt hammer hardness etc.

The samples that have been tested with the same line spacing and penetration values are represented together in graph form to highlight the effect of the rock's geomechanical properties on vibrations. An example of this representation is shown in Figure 5.14. Each figure's legend section includes correlation coefficients for the respective best-fit lines. It is important to note that when the number of data points is less than three, the correlation coefficient is indicated as "N/A".

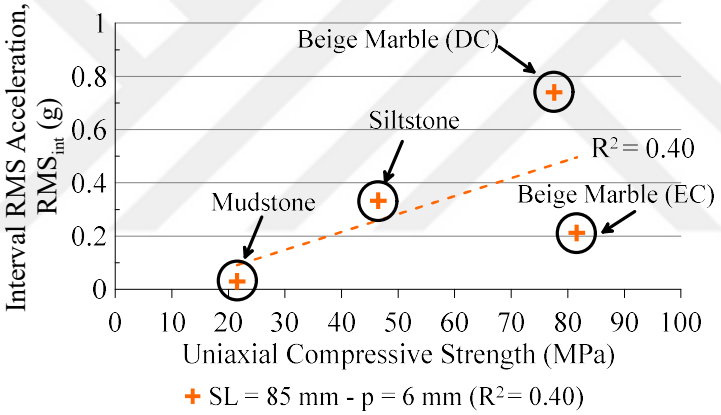

Figure 5.14 : An example representation of the relationships between vibrations and rocks geomechanical properties.

The effect of selected geomechanical properties on the vibration levels are presented in Figure 5.15, while the rest presented in Figure B.1 and B.2 in Appendix section. A close examination of these figures reveals that there is a positive correlation between rock strength, penetration and vibration magnitudes. This trend is observable across various geomechanical properties, including uniaxial compressive strength, Schmidt hammer hardness, Shore sclerescope hardness, indirect tensile strength, dynamic elasticity modulus, dynamic Poisson's ratio, and brittleness. However, any clear patterns can not be identified for static Poisson's ratio, as well as P and S wave velocities. Notwithstanding the observable trends, it is worth mentioning that the coefficients of determination vary across distinct geomechanical properties. For

instance, Schmidt hammer hardness shows moderately strong correlations with interval RMS accelerations, while UCS only reach R^2 of 0.52 (for SL = 85 mm, p = 4 mm). There are also differences present between coefficients of determination values depending on the penetration levels for the same geomechanical property. For example, the R^2 values for the relationship between tensile strength and interval RMS accelerations are 0.45, 0.49, and 0.91 for penetration depths of 4 mm, 6 mm, and 8 mm, respectively. A more in-depth analysis revealed that the presence of a difficult cuttability section of the beige marble sample significantly impacted the coefficient of determination values due to its exceptionally high acceleration readings. When this particular rock (in the case for SL = 85 mm, p = 4 and 6 mm) was included in the dataset, the coefficient of determination values remained generally low. However, its exclusion from the experiments (SL = 85 mm, p = 8 mm) resulted in statistically more robust correlations. Another good example of this phenomena can be seen on the relationships between interval RMS accelerations and Shroe sclerescope hardness (Figure 5.15 g), where the coefficient of determination values for penetration depths of 4 mm, 6 mm, and 8 mm are 0.55, 0.51, and 0.99, respectively.

Similar to the TBM vibration data, the Weibull distribution is suitable for representing the cumulative probability of the vibrations observed during the FLCM experiments. The Weibull shape (α) and scale (β) parameters obtained through distribution fitting are presented in Table 5.4. The effect of varying rock geomechanical properties and cutting configurations on the Weibull cumulative distributions were investigated during the analyses. To effectively illustrate these variations, separate Weibull distribution graphs are prepared for each combination of rock type and cutting geometry.

Figure 5.16 presents Weibull cumulative probability distribution of vibrations recorded by accelerometer 3 on all three axes (x, y, and z), derived using the shape and scale parameters obtained from the data analysis. This figure clearly illustrates the effect of penetration depth on vibration probability. As the penetration increases, the probability of encountering high amplitude vibrations increases and probability of high amplitude vibrations directly corresponds to the penetration values. It is important to highlight that the penetration depths of 5 mm and 7 mm were applied with a 70 mm line spacing, while the depths of 4 mm, 6 mm, 8 mm and 10 mm were applied with an 85 mm line spacing.

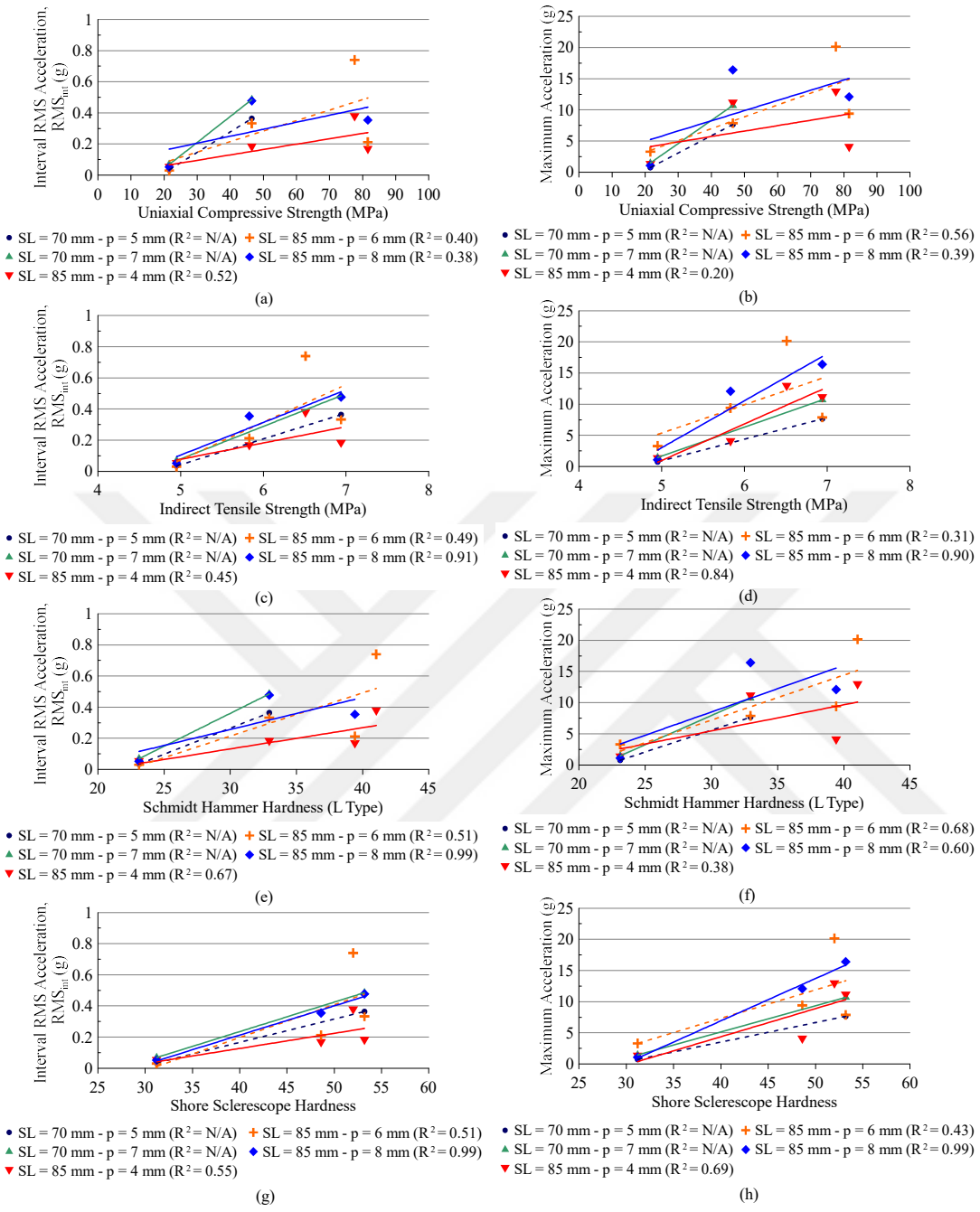

Figure 5.15 : Variations of interval RMS acceleration and maximum acceleration with uniaxial compressive strength (a,b), tensile strength (c,d), Schmidt Hammer hardness (e,f), Shore Sclerescope hardness (g,h).

Table 5.4 : Average Weibull parameters obtained from laboratory experiments for Accelerometer 3 and 4.

Rock Sample	Experiment Setup		Accelerometer 3						Accelerometer 4					
			x		y		z		x		y		z	
	SL (mm)	p (mm)	α	β	α	β	α	β	α	β	α	β	α	β
Siltstone	70	5	0.64	0.03	0.62	0.09	0.60	0.07	0.63	0.03	0.63	0.05	0.64	0.05
	70	7	0.67	0.07	0.68	0.18	0.62	0.14	0.68	0.06	0.73	0.13	0.67	0.09
	85	4	0.70	0.02	0.65	0.04	0.61	0.03	0.73	0.02	0.69	0.03	0.66	0.02
	85	6	0.70	0.05	0.73	0.12	0.66	0.10	0.72	0.04	0.78	0.08	0.70	0.06
	85	8	0.71	0.08	0.74	0.17	0.67	0.14	0.69	0.07	0.76	0.12	0.69	0.10
Mudstone	70	5	1.05	0.01	0.91	0.01	0.88	0.01	1.06	0.01	1.01	0.01	0.96	0.01
	70	7	0.91	0.01	0.84	0.03	0.79	0.02	0.94	0.01	0.90	0.02	0.82	0.01
	85	4	1.04	0.01	0.86	0.01	0.86	0.01	1.06	0.01	0.92	0.01	0.92	0.01
	85	6	1.15	0.01	1.02	0.02	0.99	0.01	1.14	0.01	1.08	0.02	1.05	0.01
	85	8	0.91	0.01	0.87	0.02	0.85	0.01	0.91	0.01	0.88	0.02	0.86	0.01
	85	10	0.81	0.02	0.80	0.05	0.71	0.03	0.81	0.02	0.85	0.04	0.71	0.02
Beige Marble (EC)	85	4	0.76	0.02	0.69	0.03	0.69	0.03	0.83	0.02	0.83	0.02	0.77	0.02
	85	6	0.70	0.03	0.65	0.04	0.63	0.04	0.70	0.02	0.68	0.03	0.68	0.03
	85	8	0.63	0.04	0.62	0.07	0.61	0.07	0.64	0.03	0.66	0.04	0.62	0.04
Beige Marble (DC)	85	4	0.63	0.03	0.61	0.04	0.57	0.04	0.64	0.02	0.68	0.03	0.60	0.03
	85	6	0.57	0.08	0.58	0.13	0.57	0.13	0.56	0.08	0.60	0.08	0.55	0.08

The probability distributions for mudstone are presented in Figure 5.17 while those for the beige marble sample can be found in Appendix B (Figure B.3 to Figure B.4). A clear trend of increasing vibration levels with increasing penetration depth is observed across all rock samples, with the exception of mudstone. The probability distributions for mudstone (Figure 5.17) exhibit minimal variation at the lower penetration depths (SL = 85 mm, p = 4 mm and p = 6 mm). This contrasting behavior in mudstone compared to other rock types is likely attributable to its lower rock strength.

Cumulative probability distributions of vibrations observed in different rock types for varying penetration rates are presented in Figure 5.18. The data reveals a clear trend, where the likelihood of encountering high amplitude accelerations is demonstrably highest for the difficult cuttability section of beige marble, followed by siltstone, the easy cuttability section of beige marble, and lastly mudstone. This pattern is consistent across all penetration rates. As an example, at a line spacing of 85 mm and a penetration depth of 6 mm, the probability of exceeding 0.2g is approximately 0% for mudstone, 2% for beige marble (EC), 11% for siltstone and 22% for beige marble (EC). The observation underscores the fact that each rock type exhibits a unique vibration probability due to different rock strengths. Furthermore, the beige marble exemplifies the significant influence of mineralogical composition on vibration characteristics. Even within a single rock type, variations in mineral composition can contribute to distinct vibration patterns.

An analysis of the relationships between Weibull parameters (Table 5.4) and various rock properties (Table 5.1) also revealed a statistically significant trend. The “α” parameter exhibits a slight decrease with increasing rock strength, while the “β” parameter demonstrates a corresponding increase. This trend is observed across numerous rock characteristics, including uniaxial compressive strength, Schmidt hammer hardness, Shore scleroscope hardness, indirect tensile strength, dynamic elasticity modulus, dynamic Poisson's ratio, and brittleness (both for B1 and B2 as given in Table 5.1), However, no clear trends were identified for static Poisson's ratio, P wave velocity, or S wave velocity. As an illustrative example Figure 5.19 presents the relationship between uniaxial compressive strength and the Weibull parameters derived from accelerometer 4’s data.

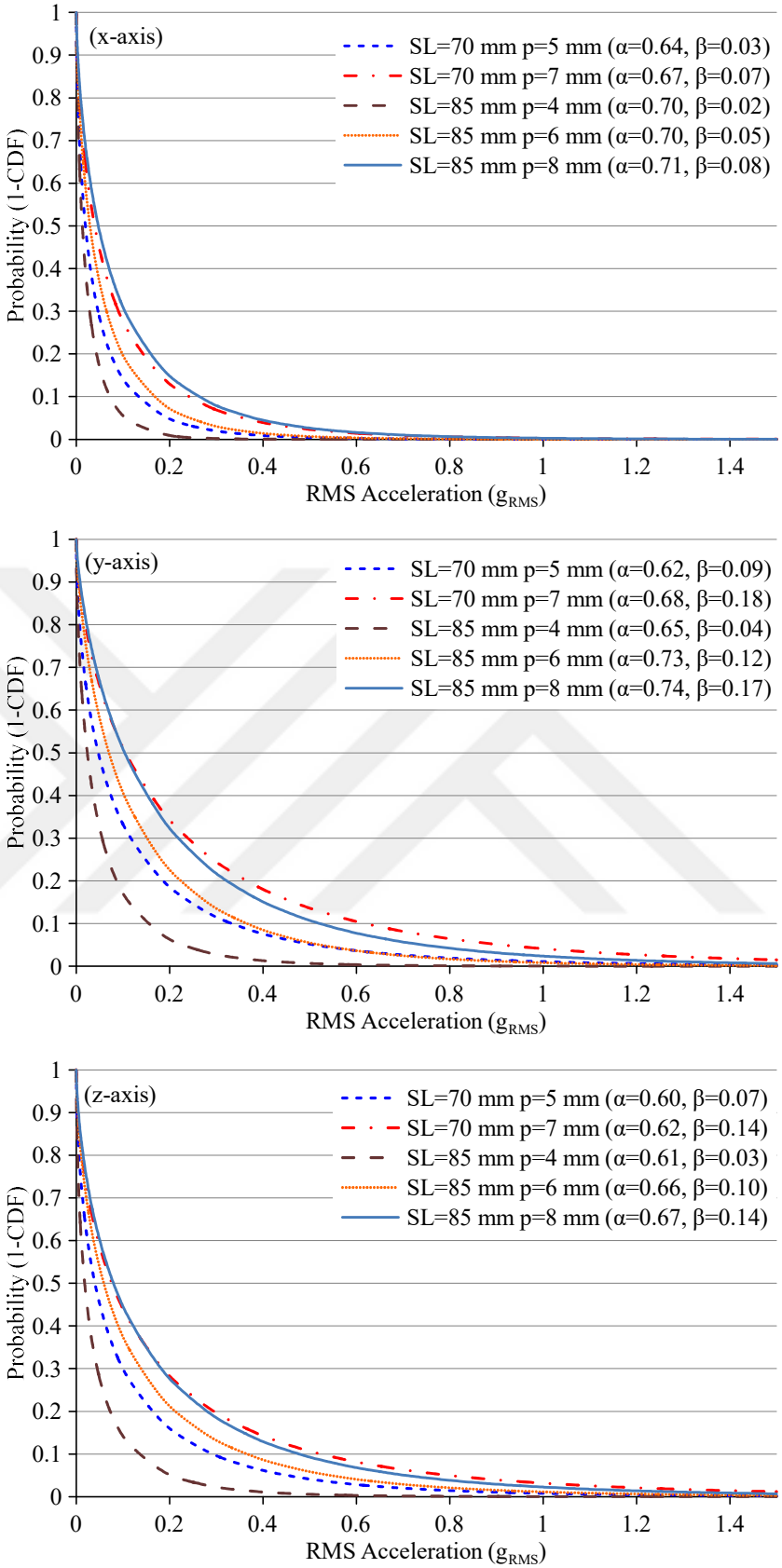

Figure 5.16 : Weibull distribution for siltstone calculated from accelerometer 3.

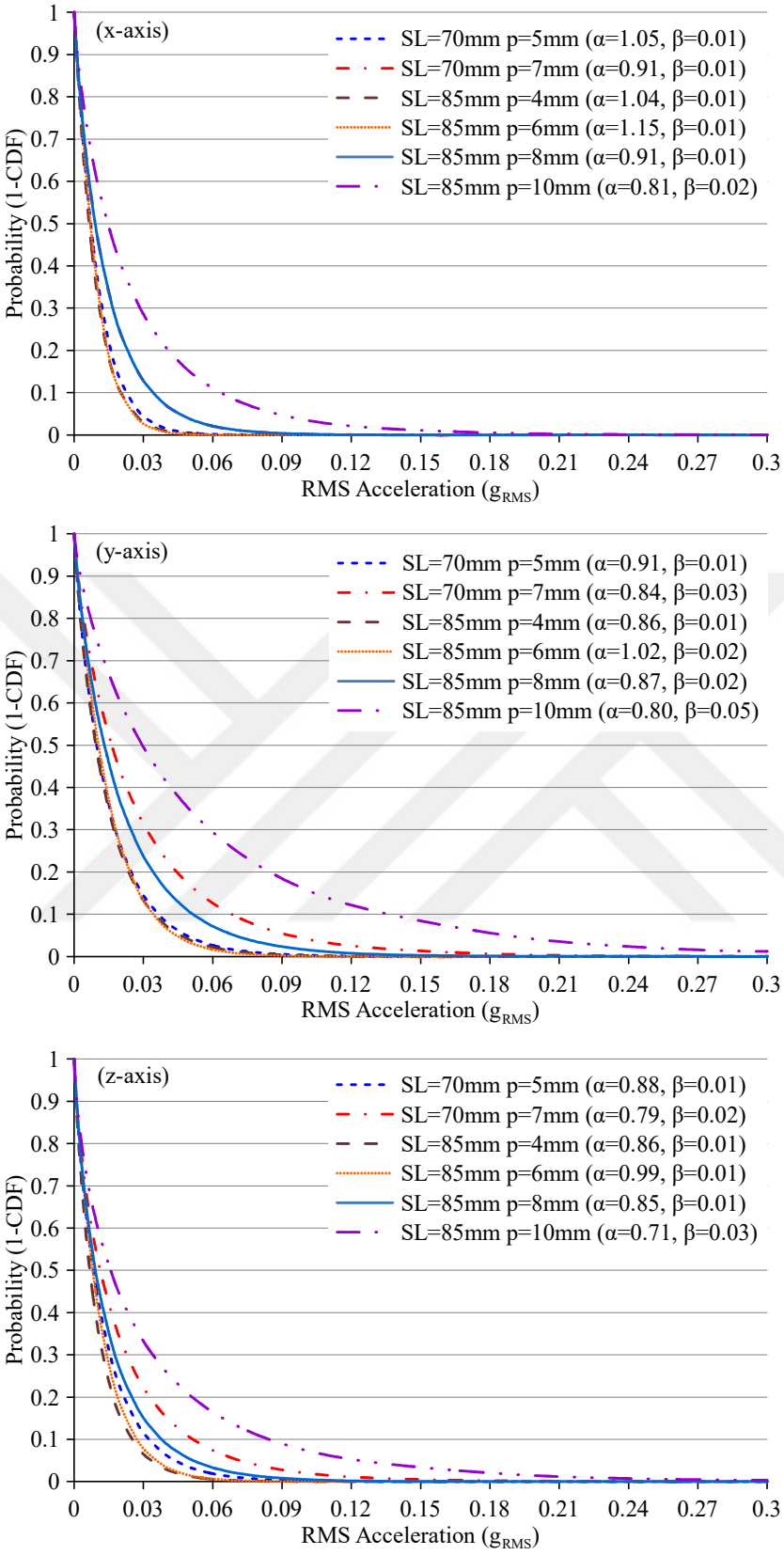

Figure 5.17 : Weibull distribution for mudstone calculated from accelerometer 3.

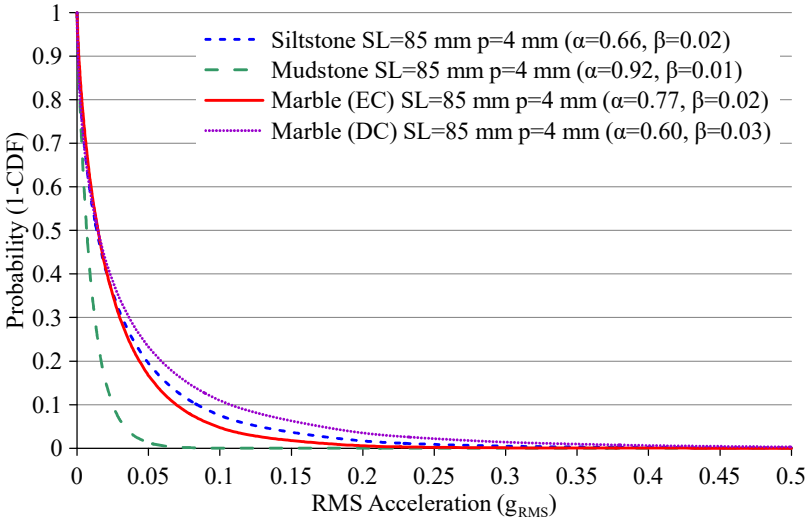

(a)

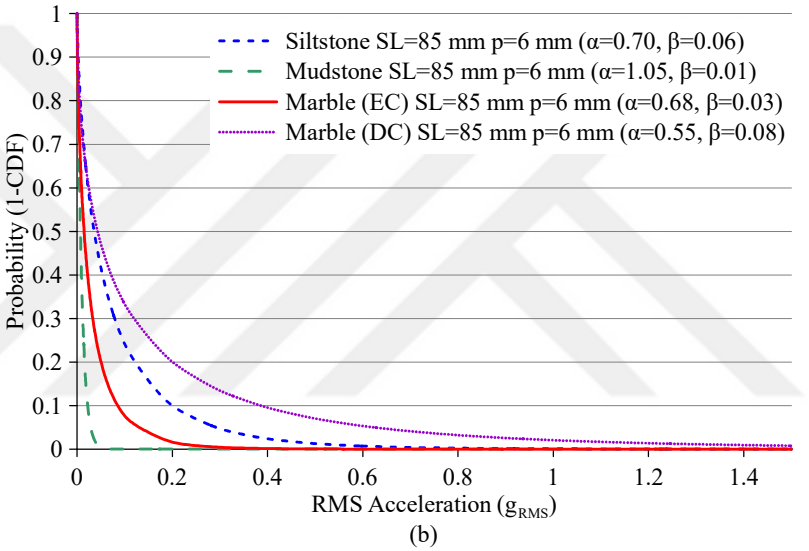

(b)

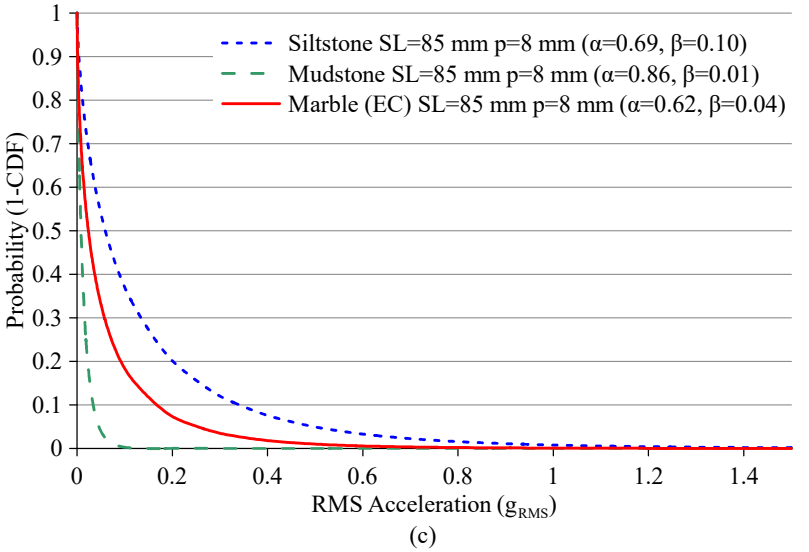

(c)

Figure 5.18 : Weibull distribution for all rock samples calculated from z-axis of accelerometer 4 for different penetration values (a) 4 mm, b) 6 mm and c) 8 mm.

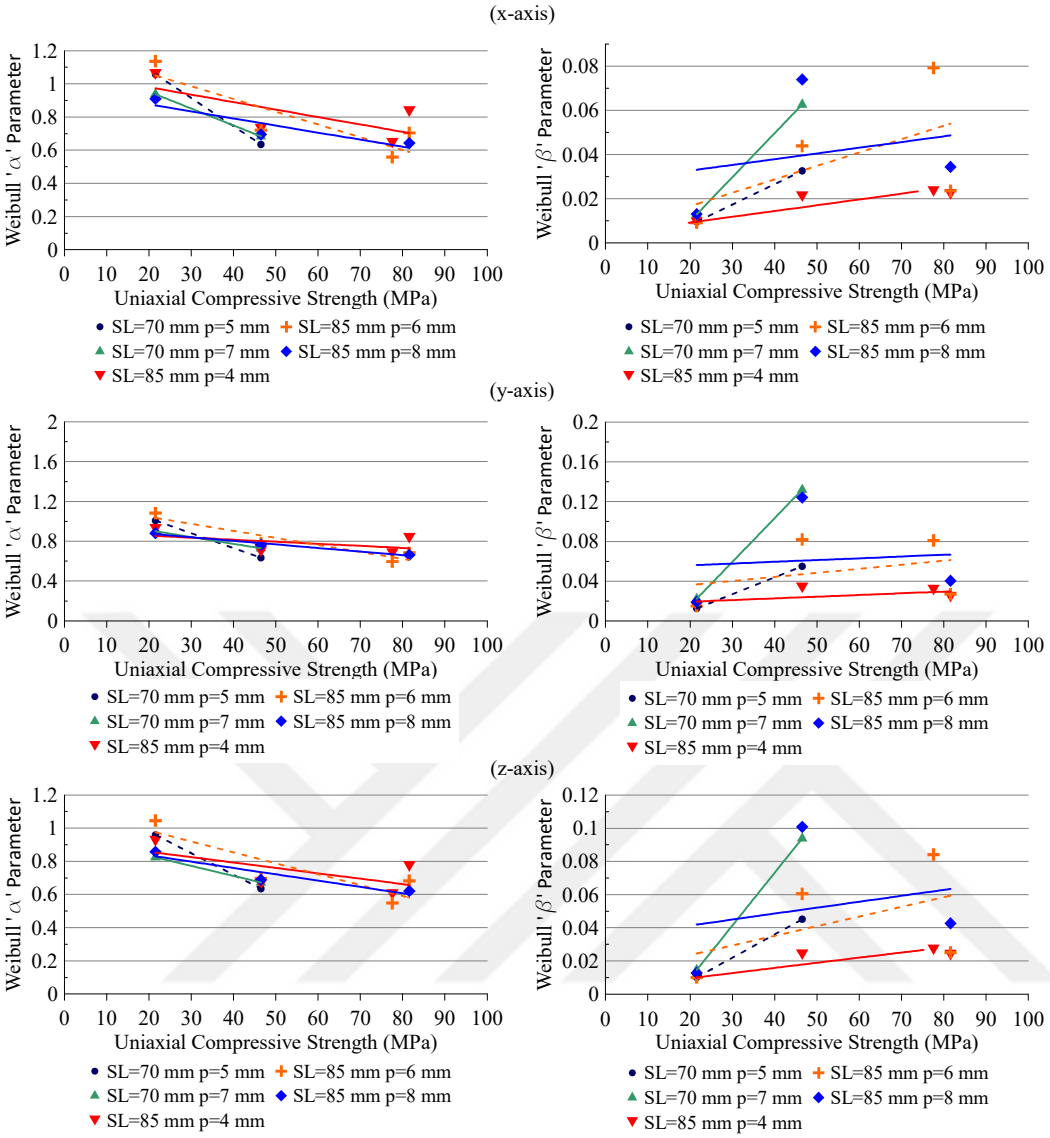

Figure 5.19 : Variations of Weibull parameters with uniaxial compressive strength for x, y and z-axis of accelerometer 4.

Since there is a relationship between rock properties and the Weibull parameters exists, these parameters could be used to develop a real-time rock identification system. As one of the key rock parameters is uniaxial compressive strength, equations 5.1 and 5.2 present the relationships between UCS, "α" and "β" parameters derived from z-axis of accelerometer 4, employing a line spacing of 85 mm and a penetration of 4 mm.

$$\sigma_c = -130.77\alpha + 153.33 \quad (R^2 = 0.43) \tag{5.1}$$

$$\sigma_c = 3237.60\beta - 11.18 \quad (R^2 = 0.73) \tag{5.2}$$

While acknowledging the limitations of the current data set in establishing definitive correlations, the findings presented in this study suggest that vibration analysis holds significant promise for enabling real-time estimations of rock properties.

5.5.2 Effect of rock cutting parameters on vibrations

It is crucial to recognize that cutting parameters, particularly cutting forces obtained through FLCM experiments, are directly utilized as key input parameters during TBM design. In addition, vibrations are also an important consideration for the design of any mechanical system. Since TBMs experience continuous vibrations during operation, understanding the specific vibration profiles associated with different rock types could offer valuable insights for optimizing TBM design. By establishing relationships between these cutting parameters and vibration characteristics, the TBM industry could potentially benefit by tailoring the TBMs according to the anticipated rock formations, ultimately enhancing performance and durability.

As the prior section explored the influence of rock properties on vibration profiles, it is essential to consider this section in conjunction with it, as cutting forces are demonstrably impacted by both cutting configuration and geomechanical properties.

To understand effect of rock cutting parameters on vibrations, Figure 5.20 presents the relationships between average normal force, average rolling force, penetration, cutting coefficient and interval RMS acceleration. The cutting coefficient (CC) presented in Figure 5.20 is defined as the ratio of average rolling force to average normal force, serves as an indicator of the torque requirement for a given thrust during excavation. A higher cutting coefficient signifies the higher torque demands for mechanical excavation. The established principles in rock cutting science indicate a positive correlation between the cutting coefficient and penetration depth, as demonstrated previous studies (Gertsch et al., 2007). The data reveals a general trend, where vibrations increase across all rock types as these parameters increase. Since these parameters are known to correlate positively with rock strength, the observed increase in vibrations aligns with the expectation of higher vibration with rising rock strength. A noteworthy exception is observed for siltstone at a line spacing of 85 mm. In this case, vibrations decrease with increasing average normal force, however, the fluctuation of the average normal force was minimal. This distinct behavior can be attributed to the bedding plane angle of the siltstone (as shown in Figure 5.8). As

discussed earlier, it is reasonable to expect that if the tests were extended to include higher penetration depths beyond 8 mm, a corresponding increase in normal force thus, vibrations would be observed.

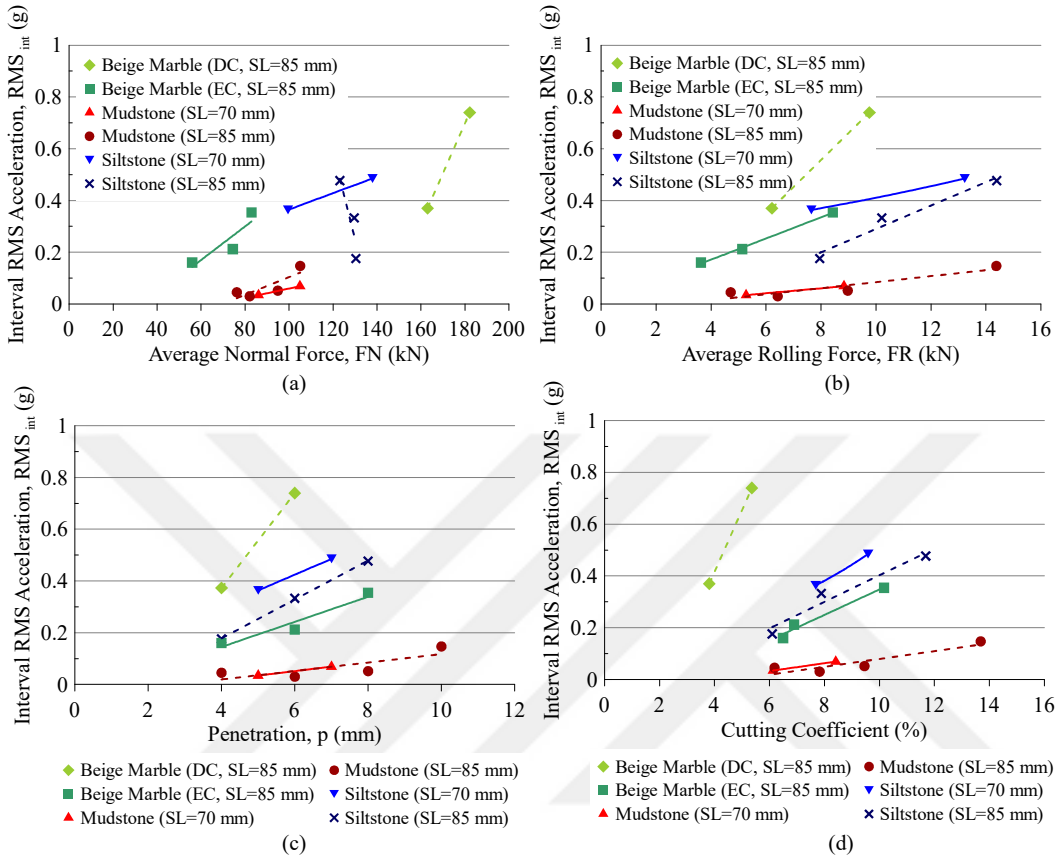

Figure 5.20 : Variation of interval RMS acceleration with normal force (a), rolling force (b), penetration (c) and cutting coefficient (d).

Figure 5.21 illustrates the relationships between interval RMS accelerations and peak forces, where best-fit lines were calculated by incorporating all available data points. The results revealed a strong correlation between peak normal force and interval RMS acceleration, while the correlation between peak rolling force and interval RMS acceleration can be classified as moderately strong. These findings align with established principles in rock cutting science, which indicates that locations within the rock sample requiring the most energy for chip formation are expected to experience the highest peak forces. Thus, these locations have the highest vibrations, as the energy required to remove the chip from the main rock is very high.

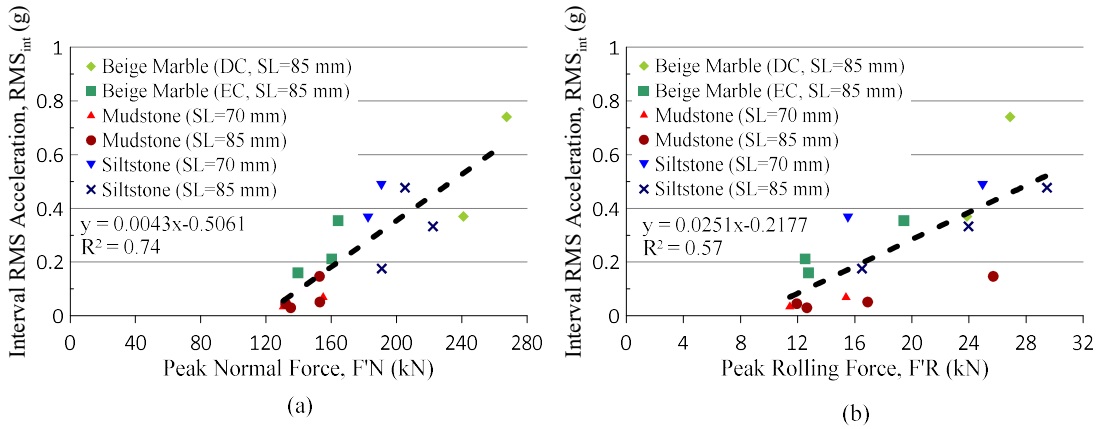

Figure 5.21 : Variation of interval RMS acceleration with peak normal force (a) and peak rolling force (b).

As the tunnelling machinery needs to withstand constant vibrations, the peak acceleration information is particularly significant, and together with the tool force data this information can be used during the design stage. The equation 5.3 formulizes relationship between interval RMS acceleration and peak normal force. Considering the strong correlation established between these two parameters, a real-time prediction of the peak normal force through the real-time measurement of interval RMS acceleration values can be achieved.

$$F'N = 171.43RMS_{int} + 133.12 \qquad (R^2 = 0.74) \qquad (5.3)$$

Figure 5.22 illustrates the relationships between interval RMS acceleration and the ratio of peak to average cutting forces. While the vibrations tend to increase with both average and peak forces individually (as observed in Figure 5.20 and Figure 5.21), they decrease with an increasing peak to average force ratio. This behavior can be attributed to the observed difference in the rates of increase between these forces. Across all samples (except for siltstone with a line spacing of 85 mm), the average forces demonstrate a higher increase compared to the peak forces. Although the cutting tool types are different, these findings are in contrary with Copur et. al. (2011 and 2017), which reported a reduction in vibrations with an increasing ratio of peak to average forces.

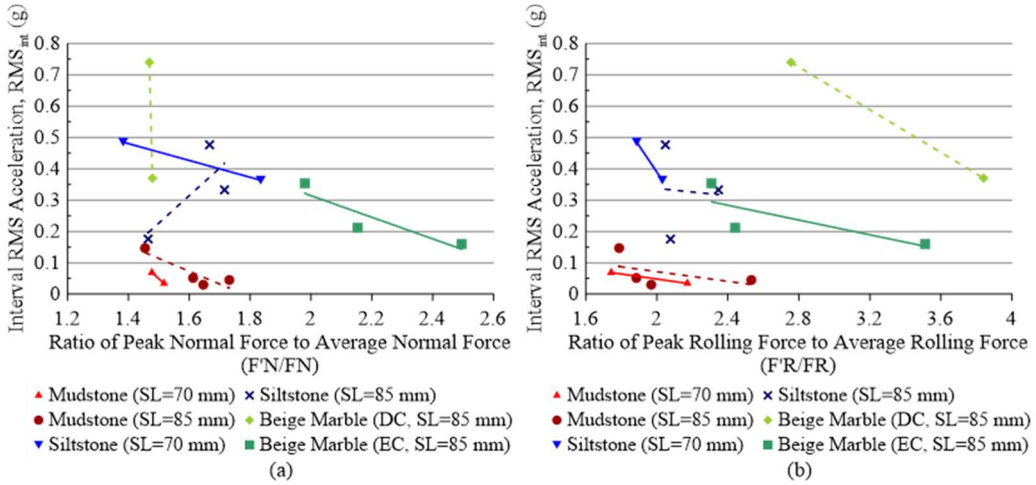

Figure 5.22 : Variation of interval RMS acceleration with ratio of peak normal force to average normal force (a) and peak rolling force to average rolling force (b).

The relationships between coarseness index, chip (muck) size over 25 mm as a percentage of the total and the interval RMS acceleration values are presented in Figure 5.23. While a clear relationship between interval RMS acceleration and the coarseness index itself is not apparent (Figure 5.23a); stronger positive correlations can be observed for the chip size >25 mm (Figure 5.23b). This finding suggests that, larger chips lead to higher tool forces and subsequently greater vibrations and it was further proved with the video recordings that captured instances of vibration surges following the detachment of large rock fragments.

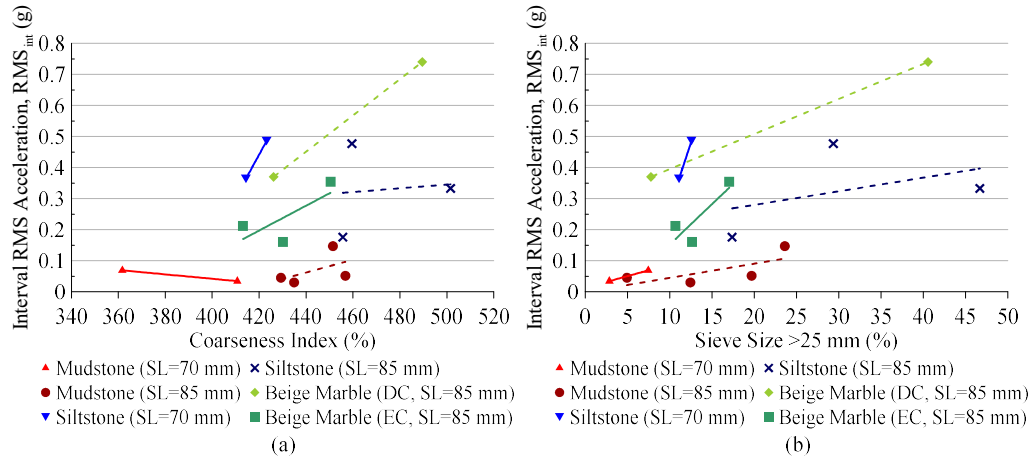

Figure 5.23 : Variation of interval RMS acceleration with coarseness index (a) and sieve size (>25 mm) (b).

Figure 5.24 illustrates the relationships between normalized optimum forces, optimum specific energy, normalized optimum coarseness index and interval RMS values. These normalized values were obtained by dividing the corresponding optimum values (forces and coarseness index) by the penetration depth measured at the optimum SL/p

ratio. As the values are normalized, they are unaffected by penetration. Since the beige marble sample was solely tested on an 85 mm line spacing, only the data corresponding to this line spacing were included in the analysis. The data reveals clear trends, with increasing acceleration values observed as forces, specific energy, and coarseness index increase. However, the strength of these relationships varies; a moderately strong correlation is present for both optimum normal force and optimum specific energy, while the correlations with optimum rolling force and coarseness index can be classified as weak. The development of a comprehensive database incorporating a wider range of data points would enable a more robust investigation of these relationships and their potential for integration into machinery design considerations.

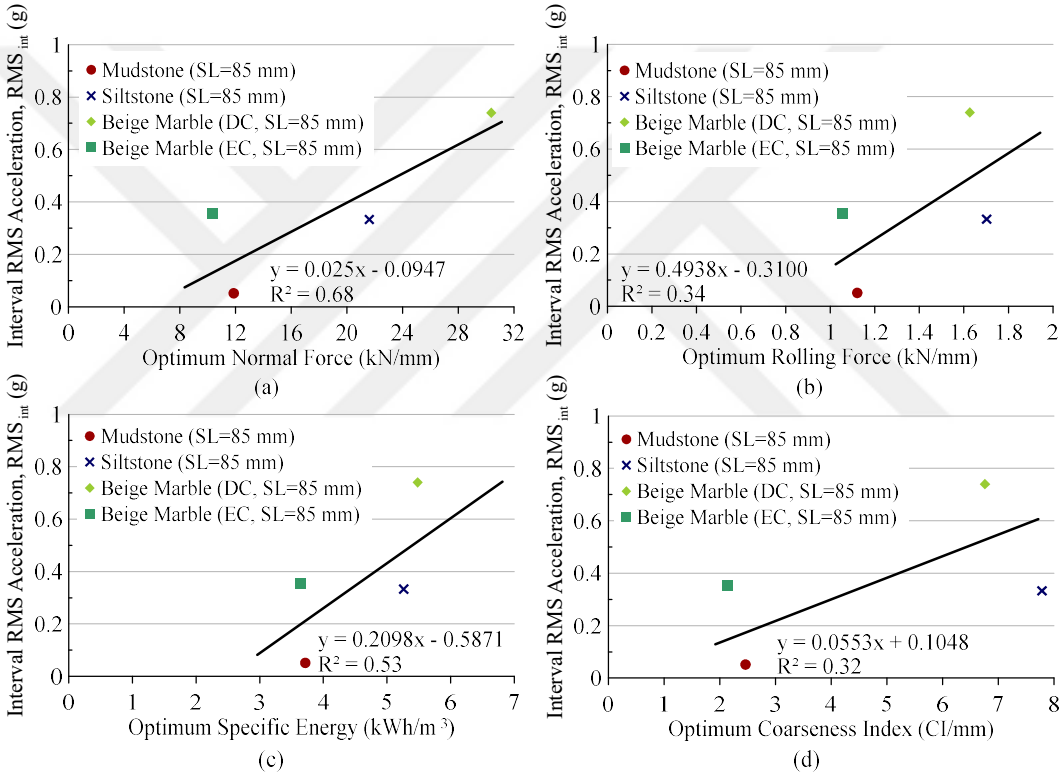

Figure 5.24 : Interval RMS acceleration versus normalized optimum normal force (a), normalized optimum rolling force (b), optimum specific energy (c), normalized optimum coarseness index (d).

Figure 5.25 illustrates relationships between peak forces (normal (a) and rolling (b)) and maximum acceleration, demonstrating that maximum accelerations rise with increasing peak forces and that there is a moderately strong correlation between these variables. As previously indicated, peak forces typically occur before a major chip breaks off from the rock, and high amplitude vibrations are created during this break-off, which explains the moderately strong relationships observed between peak forces and maximum accelerations. Through the conducted analyses, equation 5.4 has been

derived, offering a potential to predict peak normal force in real-time by employing maximum acceleration.

$$F'N = 5.85\, Max.Acc. + 130.06 \quad (R^2 = 0.69) \tag{5.4}$$

The variations in maximum acceleration with respect to penetration depth and cutting coefficient are illustrated in Figure 5.25c and Figure 5.25d. While a general trend of increasing acceleration with these parameters was observed, the data exhibit considerable scatter depending on the rock type. As a result, best fit lines are presented separately. The maximum acceleration exhibits a rising trend with increasing penetration depth, with a slight deviation observed for siltstone and mudstone at the 85 mm line spacing. Similarly, a scatter is present for cutting coefficient of siltstone 85 mm and beige marble 85 mm. It is important to emphasize that penetration depth is a critical parameter alongside cutter spacing in the design of TBMs.

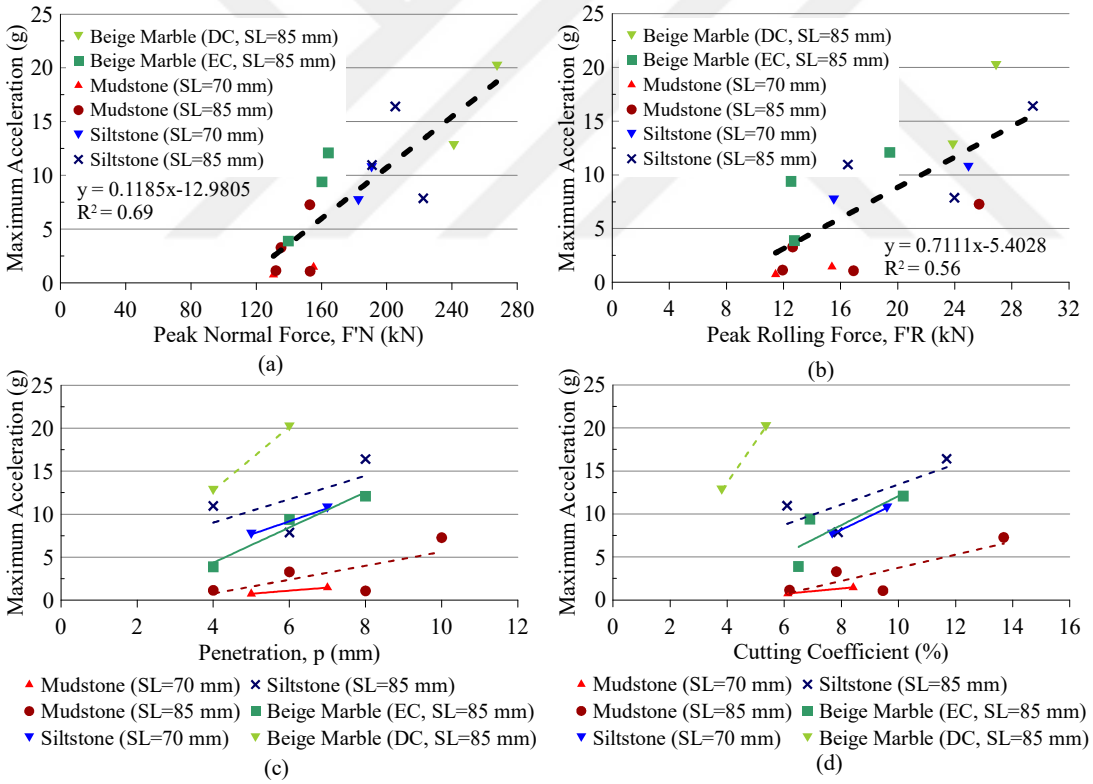

Figure 5.25 : Variation of maximum acceleration with peak normal force (a), peak rolling force (b), penetration (c) and cutting coefficient (d).

No statistically significant correlation can be identified between the coarseness index and maximum accelerations. Additionally, it was observed that, similar to interval RMS acceleration, changes in the ratio of peak to average cutting forces also lead to a decline in maximum vibrations.

The influence of cutting forces on vibrations was further investigated by analyzing changes in Weibull shape (α) and scale (β) parameters with respect to variations in cutting tool forces. Figure 5.26 and Figure 5.27 illustrate the relationships between Weibull parameters and cutting tool forces, obtained from accelerometer 4.

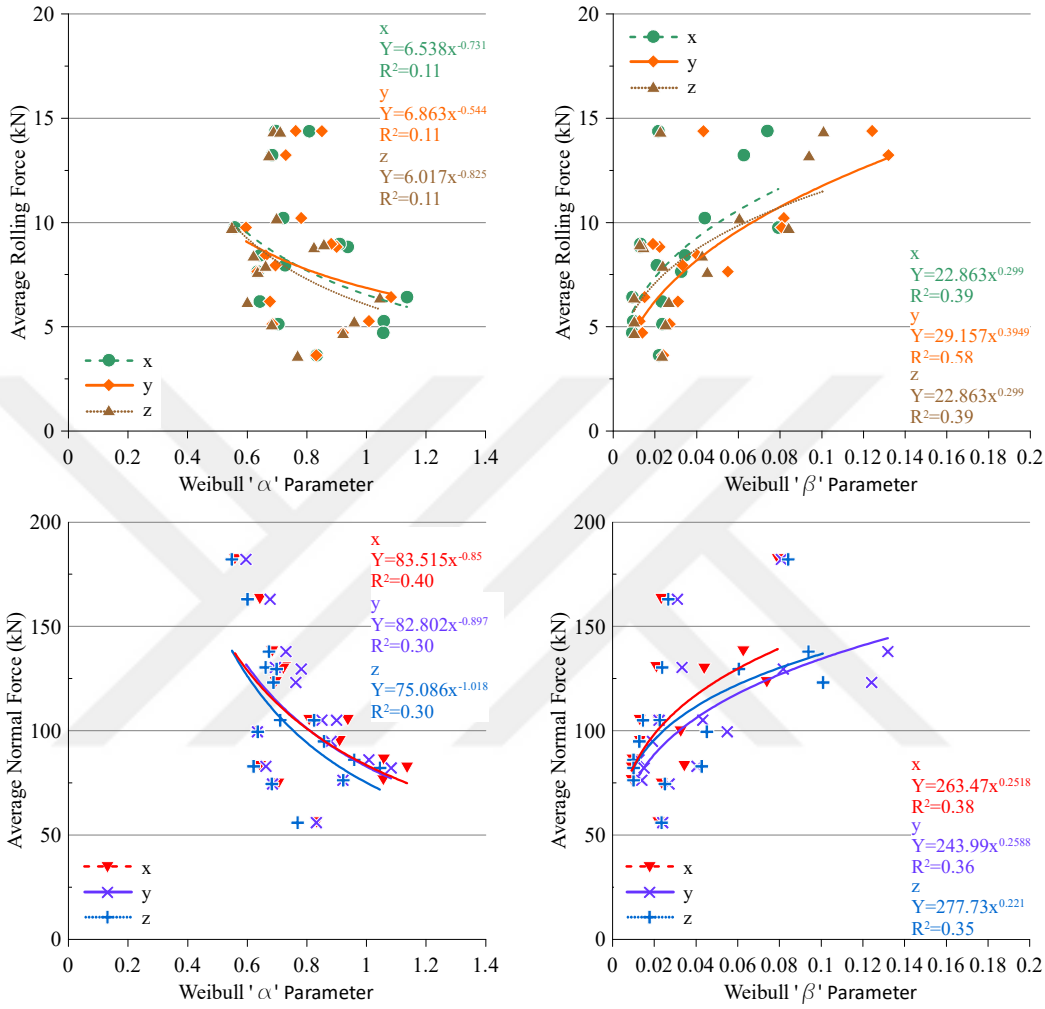

Figure 5.26 : The variations on the Weibull parameters with normal forces obtained from accelerometer 4 during laboratory experiments.

The analyses for accelerometer 3 also revealed similar results, thus they will not be presented. Analyzing these relationships reveals that the “β” parameter increases with both peak and average rolling and normal forces while the “α” parameter decreases. The strength of the relationships between average forces and the Weibull parameters can be characterized as low, whereas the relationships are moderately strong for peak forces (excluding peak rolling force with the "α" parameter). These patterns are similar to the ones presented in Section 5.5.1, where it was demonstrated that the "β" parameter exhibits an increasing trend as the rock strength increases, whereas the "α" parameter demonstrates a decreasing trend.

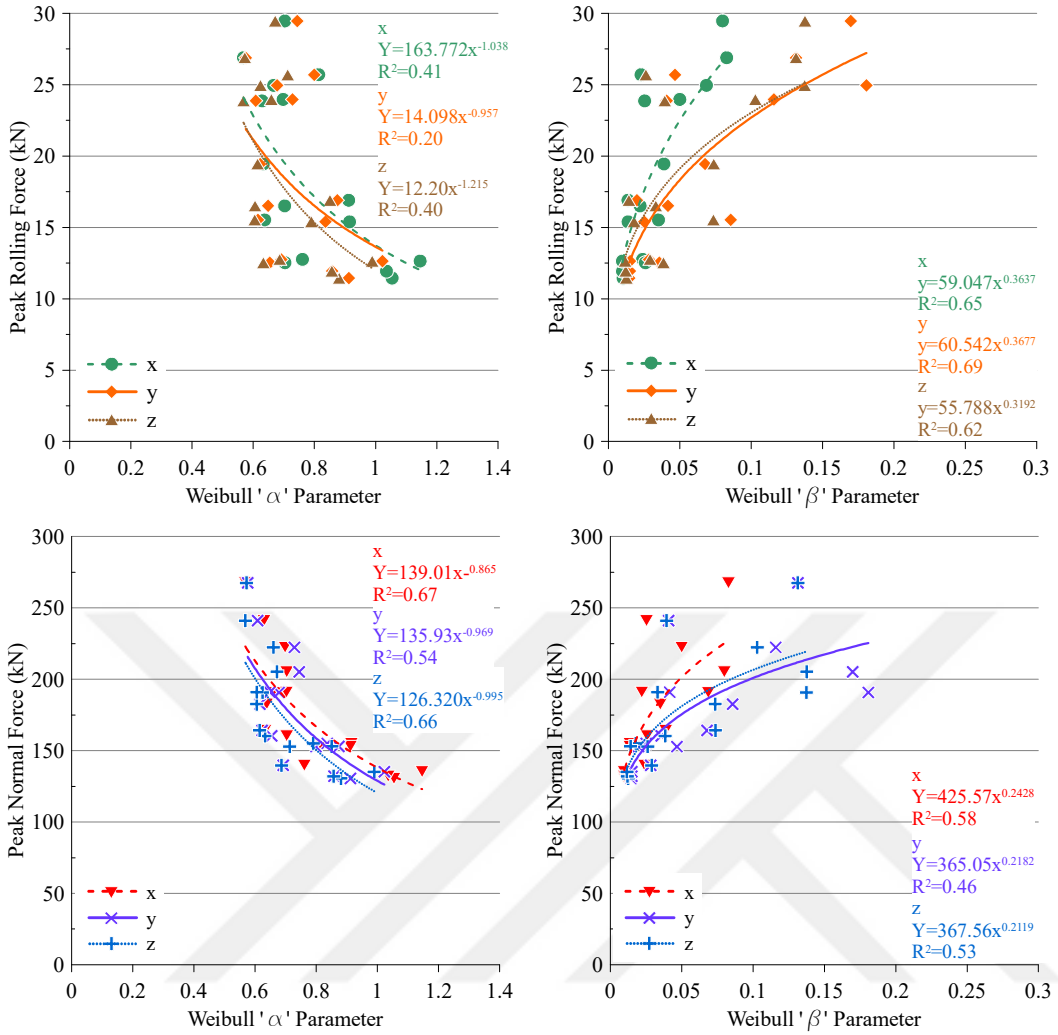

Figure 5.27 : The variations on the Weibull parameters with peak forces obtained from accelerometer 4 during laboratory experiments.

Figure 5.28 and Figure 5.29 further illustrate the correlations between Weibull parameters and tool forces, focusing on the optimum cutting geometry (SL/p). Both rolling and normal forces at the optimum SL/p exhibit moderately strong correlations with the β parameter, while only a general negative trend can be observed for the "α" parameter. In the case of the peak rolling forces at the optimum SL/p (Figure 5.29), it is observed that both the "α" and "β" parameters demonstrate a stronger correlation compared to the optimum rolling force. The correlation strength is classified as strong for the β parameter and moderately strong for the α parameter. For both peak normal force and peak normal force at the optimal SL/p, both Weibull parameters exhibit similar relations. It is important to acknowledge that the distinction between the optimum forces and the other measurements could potentially be attributed to the variation in sample numbers, as the dataset for optimum forces notably comprises a lower sample count.

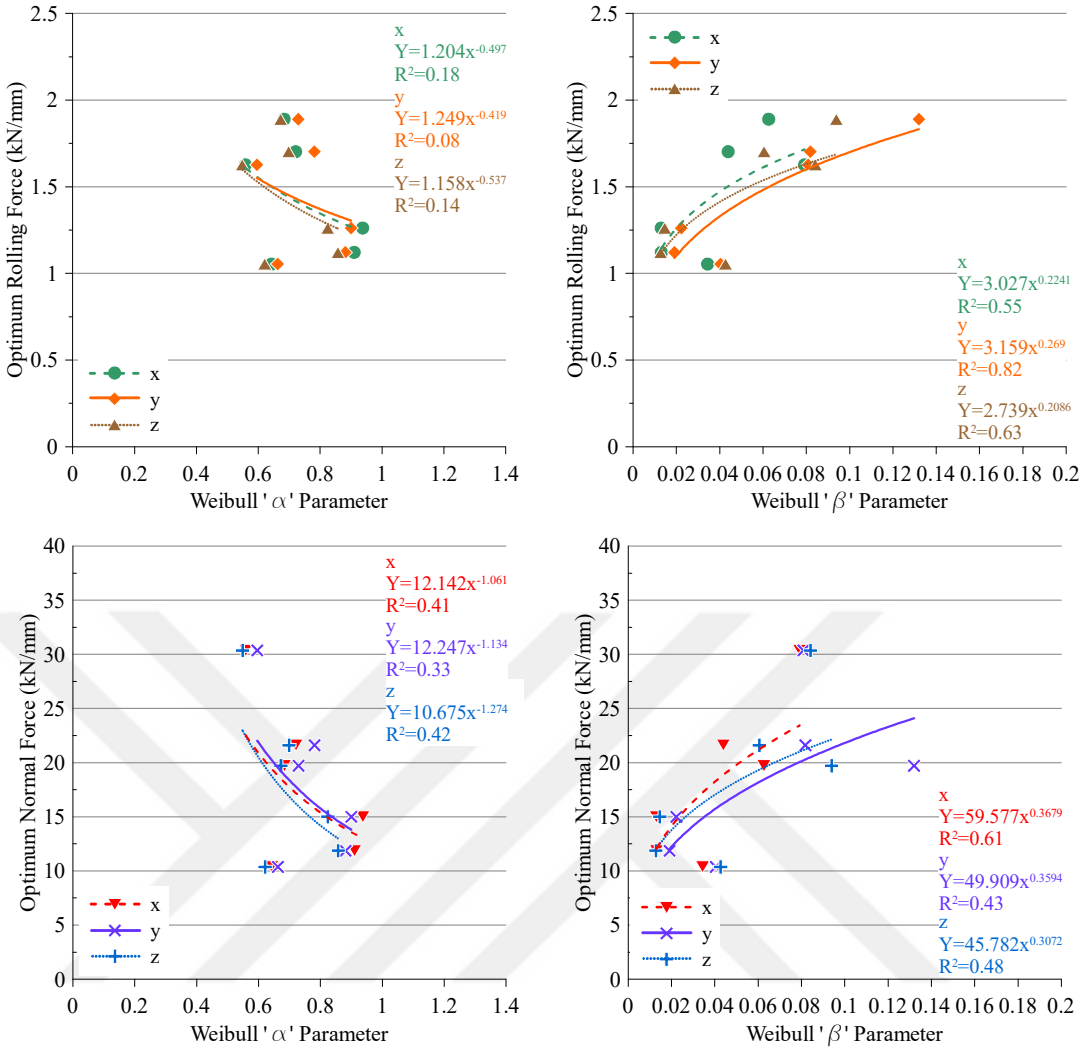

Figure 5.28 : The variations on the Weibull parameters with optimum normal forces obtained from accelerometer 4 during laboratory experiments.

5.5.3 Frequency analyses of FLCM vibration data

In order to gain a deeper understanding of the dynamic interactions between the cutting process and the resulting vibrations, frequency analyses were performed on the FLCM vibration data. Figure 5.30 presents an illustrative example for a siltstone cut (cut no. 3) with a line spacing of 85 mm. This figure includes the raw vibration data, cutting force data, spectrogram, and PSD analysis. As discussed previously, high amplitude vibrations were observed during rock break-off events, coinciding with reductions in cutting forces, indicating a stress relief on the rock. This relationship between the forces and vibrations can specifically be seen on 1, 1.5, 2, 2.4 and 2.8 seconds. The frequency content of these high amplitude vibrations can be classified as broadband, and the PSD analysis does not reveal any dominant frequencies within the data.

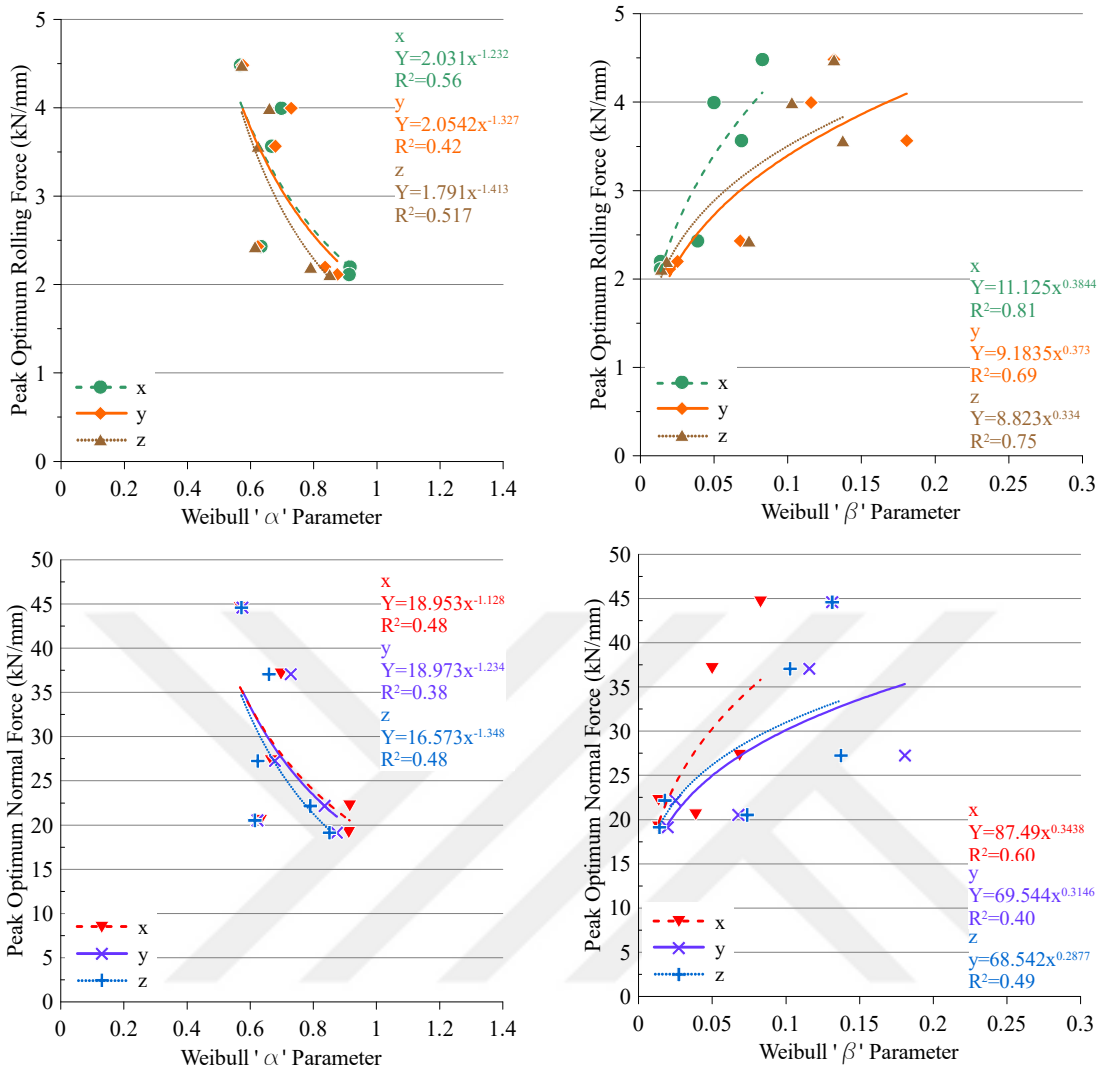

Figure 5.29 : The variations on the Weibull parameters with peak optimum forces obtained from accelerometer 4 during laboratory experiments.

The observed broadband frequency content and the absence of dominant frequencies within the power spectral density limit the applicability of the frequency domain for detailed analysis of the vibration characteristics, while aligning with the observations reported by Walter et al. (2012) and Walter (2013).

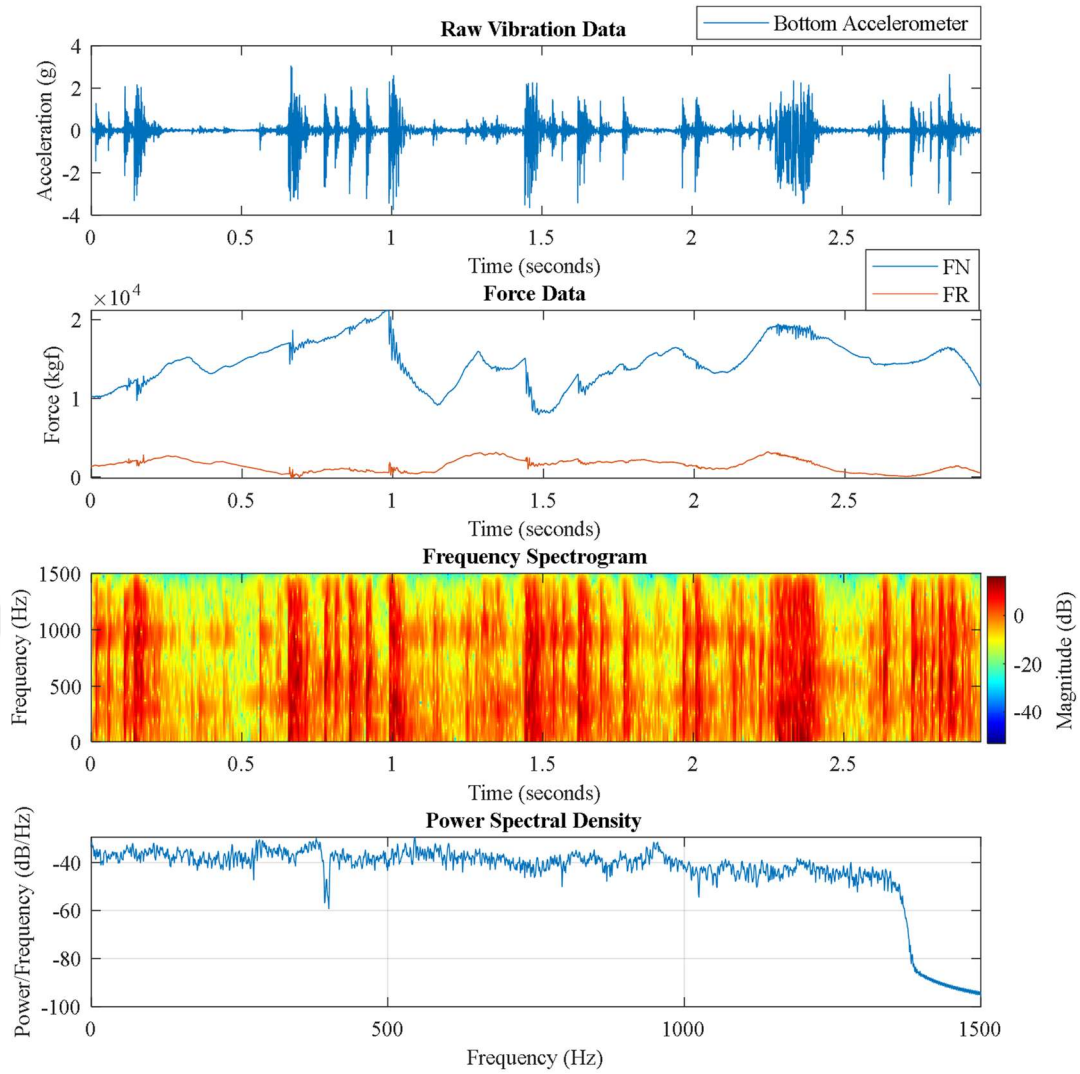

Figure 5.30 : Raw acceleration data from z-axis of accelerometer 3, cutting force data, spectrogram and PSD of the vibration data.

6. DISCUSSION

This research distinguishes itself from prior studies through its unique combination of TBM vibration data analyses and laboratory analyses. By integrating these two approaches, a more comprehensive understanding of the vibration characteristics and their underlying factors were achieved. In this section, the differences with the previous research will be discussed and shortcomings of the study will be explained with some recommendations for the future studies.

The analysis of TBM vibration data reveals that the vibrations generated during excavation change depending on to geological conditions, which aligns with the findings of previous studies (Walter et al., 2012; Walter, 2013; Mooney et al., 2014; Buckley, 2015; Hunt & Frank, 2021 and Liu et al., 2022). Notably, this study distinguishes itself from the previous ones with capturing vibration data belongs to 6 km of tunnel excavation across four EPB TBMs. This extensive dataset addresses the limitations of previous research, which often relied on a limited amount of data. By utilizing this rich dataset, it was possible to identify significant correlations between vibrations and rock mass parameters such as RQD, GSI as well as geomechanical properties such as point load index.

During the study it was observed that the most significant vibrations being recorded along the z-axis, which is in the direction of excavation. The observation is consistent with prior studies conducted by Walter (2013), Buckley (2015), Huang et al. (2018), Wu et al. (2021) and Liu et al. (2022).

This present study introduces a unique aspect by considering the TBM diameter as a distinguishing factor. A majority of prior studies, with the exception of Huang et al. (2018), concentrated on TBMs larger than or approximating 6.5m in diameter (Walter, 2013; Mooney et al., 2014; Buckley, 2015; Liu et al., 2021 and Wu et al., 2021). The inclusion of TBM 4, with its comparatively small size provided an opportunity to understand that, similar to larger TBMs vibration changes are also distinguishably affected from the geological conditions on smaller ones. This feature renders the

vibration recording system suitable for use on micro tunneling machines, where the operator's cabin is positioned externally, impeding the operator's ability to perceive alterations in vibration within TBM and subsequently identify geological variations. However, a more comprehensive understanding of the relationship between TBM diameter and vibration requires data from a broader range of TBM diameters operating under similar geological conditions. Obtaining such data can be challenging, and future research efforts may be directed towards addressing this challenge.

While mounting the accelerometers directly on the cutterhead yields more precise measurements, installing them behind the pressure bulkhead also provides satisfactory results. This placement strategy mitigates the well-documented challenges associated with the harsh cutterhead environment, including limitations in power supply, data transfer capabilities, and overall sensor reliability as discussed by Shanahan (2010), Mosavat, (2017), Huang et al. (2018) and Wu et al. (2021).

While evaluating the TBM vibrations to understand the geological conditions, the effect of TBM operational parameters on the vibrations should also be taken into account. A prominent study on the impact of TBM operational and performance parameters on TBM vibrations was conducted by Wu et al. (2021), and cutterhead vibrations using various combinations of thrust, torque, penetration rate, and cutterhead speed in a controlled environment were investigated. Wu et al. (2021) observed minimal influence of these parameters on vibration until a critical thrust threshold was reached. Beyond this threshold, vibrations associated with penetration substantially escalated. Unfortunately, their study was limited to a 3 mm/rev penetration rate which is relatively low compared to actual TBM excavation. This prevents direct comparison with the current study where penetration rates usually exceed 6 mm/rev. Furthermore, Wu et al. (2021) established a correlation between the boreability index and TBM vibrations, aligning with the observations presented in this study. Huang et al. (2018) reported that following the entrapment of the TBM, there was a significant increase in the break-out torque of the cutterhead, leading to increased vibrations of the cutterhead. This suggests a potential link between torque and vibrations under extreme operational conditions. In the present study, however, no significant correlations between torque and vibrations were observed, which is potentially related with the mostly stable geological conditions differing from the challenging conditions encountered by Huang et al. (2018). Mooney et al. (2014)

reported a correlation between cutterhead speed and TBM vibrations, while Walter (2013) emphasized the relationship between specific energy and vibrations. These findings align with the observations of the present study, where despite generally exhibiting weak or moderate strengths, several correlations have been identified. The key TBM operational factors influencing vibrations were found to be the thrust, boreability index, cutterhead rotational speed, penetration rate, and specific energy. Notably, the examination of similar conditions involving TBMs of the same size, such as TBMs 2 and 3, revealed remarkably close and sometimes even nearly identical trends between these operational parameters and vibrations. However, a distinctive behavior observed in TBM 4, which can be attributed to variations in geological conditions encompassing soil and rock compositions.

Interpreting correlations between vibrations, TBM operational parameters, and geological conditions necessitates a holistic approach. For instance, in rock environments, when all other parameters are held constant, a reduction in penetration rate indicates a stronger rock, consequently leading to increased vibrations. In contrast, for soil conditions, decreased penetration rate might be caused by factors like squeezing, cutterhead clogging, or the presence of cohesionless material, and so on. Given that vibrations are not distinct in soil as they are in rock, significant reductions in penetration rate might not be accompanied by evident vibration changes.

Understanding the complex relationships between geological conditions, TBM operational parameters, and resultant vibrations holds the potential to effectively mitigate surface vibrations. This becomes particularly crucial for tunnels in proximity to the surface, where the presence of sensitive structures necessitates a consideration of vibration control measures.

The vibration measurement system also has a potential for detecting cutter tool damages during excavation. However, as previously noted by Shanahan (2010), pinpointing the exact timing of such damage requires additional cutter monitoring systems. Analysis of the data suggests that, high amplitude vibrations sustained across all accelerometer axes during hard rock excavation may serve as a preliminary indicator of potential cutter tool damages. While it is acknowledged that the system might yield certain instances of false positives, the site crew finds the provided information helpful for identifying potential cutter damages.

The present study primarily focused on time domain analyses, but also employed frequency domain analyses for a more comprehensive understanding of the vibrations. Huang et al. (2018) and Wu et al. (2021) utilized the FFT for frequency domain analysis in their respective studies. However, this approach might not be correct due to the inherent random nature of TBM vibrations. Spectrograms or PSD are considered more appropriate methods for converting time domain data to the frequency domain, as demonstrated by various researchers (Walter et al., 2012; Walter, 2013; Buckley, 2015). Additionally, Liu et al. (2022) employed CWT as a viable technique. The findings of the present research in the frequency domain align with previous studies (Walter et al., 2012; Walter, 2013; Buckley, 2015; Liu et al., 2022), where the broadband nature of the frequency content was identified and the influence of cutterhead speed on the dominant frequencies observed as Walter (2013) and Buckley (2015) also highlighted.

While concentrating on TBM vibrations, the need for a more comprehensive understanding of vibrations directly linked to rock cutting processes is crucial. The mineralogical properties of the rock could vary over a very short distance, and it would be impossible to distinguish their influence on the vibrations from TBM data. Furthermore, the TBM operational parameters have an influence on the vibrations, which could mask the difference caused by the mineralogical changes, consequently, this underscores the importance of conducting laboratory analyses within a controlled environment. However, it is imperative to recognize that since linear cutting tests in this study were conducted in a controlled laboratory setting, they are not directly representative of the actual stress conditions in the field.

The process of rock breakage is recognized as a three-dimensional phenomenon influenced by three-dimensional field stresses. In linear rock cutting tests, the rock sample is encased within a concrete cast material, introducing a passive confining pressure. Consequently, it is acknowledged that laboratory cutting tests may not accurately mirror the exact field stress conditions. To identify the difference between laboratory and field stress conditions Bilgin et al. (2000) conducted an experimental and numerical study involving linear cutting tests with a chisel tool. It was revealed that a critical lateral stress threshold (in two-dimensional stress in atmospheric conditions) is equivalent to 20–25% of the rock's compressive strength. Beyond this threshold, lateral stress ceased to impact cutter forces and specific energy. Prior to

reaching the critical lateral stress, cutter forces experienced an escalation of up to 20–30% under relieved cutting mode. Moreover, their investigation demonstrated a 1.3-fold increase in specific energy under stressed conditions, compared to unstressed conditions. Another study in this topic was conducted by Balci et al. (2020), who arrived at the conclusion that the optimum specific energy for hyperbaric deep-sea floor mining escalated by 1.30~1.35 times in comparison to atmospheric excavation conditions, a finding similar to the outcomes of Bilgin et al. (2000). These collective studies underscore the influence of stress conditions on rock breakage via mechanical cutting tools, and this difference should be kept in mind while evaluating the outcomes of laboratory experiments in the present research since these conditions have an effect also on the vibrations. Therefore, if vibration data is to be utilized for TBM design, a safety factor of 1.35 may be considered.

The present study's findings on FLCM tool forces (normal and rolling force) are consistent with previous work in rock cutting science. Tool forces (both average and peak) increase and the ratio of peak to average cutting forces decrease with increasing penetration. In their respective studies, Gertsch (1993), Gertsch et al. (2007) and Cho et al. (2013) observed a consistent trend in rock cutting experiments with CCS disc cutters: the decline of peak-to-average force ratios with increasing penetration; however, a statistically significant correlation between these parameters could not be found. Those findings are consistent with the outcomes of this study. Furthermore, Copur et al. (2017) stated that reducing the ratio of peak to average tool forces for a conical drag tool would reduce the vibrations, as well as machine damages. However, the present study contradicts this by demonstrating an increase in vibrations for the employed CCS type disc cutter as the ratio decreases. The reason for this contradiction is considered to be the difference between the increase ratios of peak to average forces for disc cutters and conical drag cutters. Throughout this study, the average force exhibited a more significant increase compared to the peak force as penetration depth increases. Consequently, this leads to a reduction in the ratio of peak to average tool forces.

Fitting a full-scale linear rock cutting machine with accelerometers to measure vibrations during rock cutting tests has not been performed before, which is one of the unique aspects of this study; therefore, any direct comparison with previous studies in terms of vibrations is not possible. An important finding of the present research is the

observed trend of increasing vibrations with rising penetration, peak, and mean tool forces. Furthermore, moderately strong to strong correlations were established between tool forces and vibration levels. These observations suggest that despite a decrease in the peak-to-average force ratio, the overall vibration amplitude may still escalate due to the combined rise in both peak and average forces as penetration depth increases.

The assumption in the field of rock cutting science is that the ideal cutting condition yields the highest excavation rate while minimizing machine vibrations. However, during the laboratory experiments, it was observed that the vibrations have a positive correlation with penetration and increases as the penetrations increase.

The FLCM experiments conducted in this study revealed that the accelerations generated during rock cutting exhibit random characteristics, with peak values reaching up to 20g. These findings align with the observations reported by Huo et al. (2015), who created a multi-degree-of-freedom model for disc cutters and modelled vibrations using the tool force data from another study. However, any information on the used rock properties were not provided by Huo et al. (2015), making any direct comparison very difficult. It was reported that vibration amplitudes reduce from disc ring to the disc shaft, however, it was not possible to verify this finding in the present study since the used disc cutter itself was not equipped with accelerometers.

Yang et al. (2020) employed a Multi-Mode Boring Test System to investigate the vibrational characteristics of rock cutting within three distinct geological environments under controlled laboratory conditions. The research stands out as a rare instance, where accelerations were measured during rock cutting in a controlled laboratory environment. Notably, their testing system utilized a cutterhead equipped with multiple cutters, which is the main difference from the present study. The authors reported that both rock strength and the ratio of soil to rock influenced the measured vibrations. These findings well align with the observations of both laboratory and field experiments of the current study.

The developed vibration recording system yielded valuable results that encourage further research on TBM vibrations, despite its certain limitations. Notably, the accelerometers' measurement range presented a challenge, particularly in hard rock formations, as it was observed that on a 6.6m TBM, the accelerations can exceed 10g.

This amplitude is equivalent to, or even surpasses, the ranges utilized in a majority of the adjacent studies (Walter, 2013; Buckley, 2015; Huang et al.; 2018 and Liu et al., 2022) with a sole exception, where ±16g accelerometers that were employed by Wu et al. (2021). The utilization of ±4g accelerometers on TBM 3 and 4 introduced a limitation in accurately capturing the precise accelerations during the excavation time to time. However, it is important to emphasize that despite this constraint, the acquired data remains informative and valuable for the study's objectives, with the exception of detecting broken cutting tools, which requires higher precision.

The relationship between vibrations (including both interval RMS and maximum), and tool forces, particularly peak normal force, suggests that vibration data can be utilized for designing TBMs and cutters to make them more robust against the impact of vibrations. Moreover, in hard rock formations where TBMs are vulnerable to vibration induced damages, knowledge of anticipated maximum vibration levels could also help for optimizing the cutterhead design (changing disc spacing). Integrating vibration data within the TBM design process holds promise for reducing vibration levels and consequently mitigating potential damage to TBM itself.

During the course of the study data losses encountered time to time due to malfunctions of the data recording computers. The primary cause of this problem was computers' placement within the TBM shield, where high vibration intensity compromised their stability and led to data loss.

The relatively slow pace of data analysis, which was conducted manually on different computers was created constraints on the timely identification of the geological conditions. To mitigate this limitation, it is advised to integrate automated data processing capabilities into the software to enable real-time ground identification in the future projects so that the tunneling industry could benefit. Furthermore, establishing data communication between the vibration recording system and the TBMs' programmable logic controller (PLC) would be highly valuable in integrating TBM data into the vibration analyses.

The developed software exhibited satisfactory performance and did not present any issues during the course of the study; besides, the majority of the problems were linked to hardware. The implemented trigger and e-mail functionalities proved valuable by promptly notifying relevant parties in the case of detecting an anomaly. Future

refinements should focus on enhancing the software's predictive capabilities for geological conditions. Additionally, incorporating visual information messages would further improve user experience.

Time constraints, financial resources, and logistical challenges restricted the laboratory experiments to only three rock samples. This limited sample size has hindered the generalizability of the findings and the ability to fully explore variations on the vibrations according to different rock types and cutting parameters. Future studies should aim to overcome this limitation by acquiring a larger and more diverse set of rock samples to ensure more robust and comprehensive experimental results. While one of the initial objectives of this study involved acquiring rock samples directly from TBM excavation sites for FLCM experiments, this objective ultimately proved unfeasible during the course of the research.

As data collection spanned three separate projects, finding Contractors who were willing to permit the installation of vibration recording systems in their TBMs was challenging. This process was further complicated by the additional delays caused by the ongoing pandemic, that prevented access to construction sites and restricted data collection activities. As a result, the acquisition of site data experienced significant delays, impacting the overall schedule of the study.

Insufficient geological information poses a common obstacle in numerous research as acknowledged in prior studies (Walter, 2013 and Buckley, 2015). While this study successfully identified general vibration trends, a key limitation lies in the inability to obtain muck samples from every location where vibration characteristics changed. Increased muck sampling frequency during tunnel excavation could potentially mitigate the limitations associated with insufficient geological information.

It is acknowledged that further FLCM experiments are necessary given the constrained sample numbers of this study for establishing better relationships between rock properties and vibrations. However, the patterns found with both FLCM tests and TBM vibration recordings yields similar results validating the observations. Despite these acknowledged limitations, the study presents valuable findings and can serve as a significant reference for future research. Continuous vibration monitoring, as demonstrated in this study, holds significant promise for real-time identification of geological variations, rock properties (both intact and mass), and potential

broken/damaged disc cutters during TBM excavation. The outcomes of this study contribute to addressing certain limitations inherent in prior research efforts. Additionally, vibration anomalies detected during monitoring could serve as early warning indicators of developing mechanical problems within the TBM, which can be investigated in the future.

7. CONCLUSIONS

A vibration data recording system was developed specifically for this research and installed on four EPB TBMs operating across three project sites, with the objective of capturing and analyzing the vibrations generated during TBM excavation. To complement these field measurements and gain a deeper understanding of the vibrations generated during the rock cutting process, laboratory experiments were conducted using a full-scale linear cutting machine (FLCM) equipped with accelerometers. The FLCM experiments utilized three rock samples, allowing for the analysis of vibration characteristics under controlled conditions for different rocks.

The first phase of the study focused on field experiments to establishing correlations between vibrations generated by EPB TBMs and the geological conditions encountered during excavation. Accordingly, TBM vibration data had been collected and analyzed, creating a large dataset. The vibration data recording system was successfully implemented on TBMs excavating the Mecidiyekoy-Mahmutbey Metro Project, Umraniye-Atasehir-Goztepe Metro Project, and European Region Potable Water Transmission Line Project. Utilizing the system in different projects ensured the dataset include a wide range of geological conditions. Following the initial deployment, the vibration data recording system underwent significant enhancements to optimize its performance and functionalities. Supplementary data including geological reports, shift reports, TBM operational parameters, and cutter replacement records were also obtained from the sites. To better characterize rock properties, additional muck samples were collected from the conveyor belt whenever deemed necessary and tested in the laboratory to identify their geomechanical properties.

The acquired vibration data was processed on a ring-by-ring basis, resulting in individual vibration data files for each segment ring. Custom Matlab scripts were then employed to analyze this data alongside the corresponding TBM operational parameters per ring.

Analysis of the vibration data revealed that the accelerations measured on the EPB TBMs can exceed ±10g, particularly during excavation of hard rock formations. Furthermore, it was possible to identify the geological/lithological variations through the utilization of vibration measurements. A positive correlation was observed between vibrations and rock strength. As example to this positive correlation, the average interval RMS acceleration measured on TBM 2's top z-axis accelerometer was 0.27g for a weathered dyke with a low UCS of 15 MPa while, a significantly stronger fresh dyke with a UCS of 210 MPa exhibited an interval RMS acceleration exceeding 1.0g.

The identification of short, weathered zones within dykes was possible through the analysis of vibration data, rendering the measurement system effective for the purpose of providing early warnings. A vibration threshold of 1g, representing the percentage of data points exceeding this threshold, emerges as a proficient criterion for differentiating lithological units and used throughout the study. Notably, the crest factor serves as a reliable gauge of face homogeneity. For example, sandstone-limestone units with different weathering/homogeneity degrees have crest factor values ranging between 15 and 38, as the rock becomes more homogenous the crest factor reduces. Interval RMS acceleration value proves to be a good indicator of the fluctuations in geomechanical and TBM operational variables. In particular, moderately-strong to strong correlations are observed between interval RMS acceleration and rock mass parameters such as RQD and GSI. Interval RMS acceleration of 0.2g correspond to rock masses with 20% RQD, whereas the average value increases to 0.8g for rock masses with 80% RQD. Although not as robust as the RQD correlation, the link between interval RMS accelerations and GSI remains informative, and this difference can be attributed to the GSI’s dependence on engineering judgement. Uniaxial compressive strength and point load index were another rock geomechanical variables that have a relationship between interval RMS, 0.2g corresponds to UCS of 15 MPa and PLI of 4, while 1g corresponds to UCS of 75 MPa and PLI of 10. These relationships can also be utilized for real-time ground prediction on TBMs.

The increase in thrust of TBM due to the rock strength, demonstrates a corresponding increase in interval RMS acceleration. This trend is consistent with the observations made during laboratory experiments (between normal force and vibrations). Notably,

a general trend of increasing interval RMS acceleration with increasing specific energy was also found.

The Weibull distribution employed for constructing probability plots, and clearly indicate the difference between fresh and weathered rocks, as well as between soils and rocks for all TBMs. In alignment with the findings from laboratory analyses, Weibull shape (α) and scale (β) parameters varies in accordance with the geological conditions. Notably, while a distinct pattern for "α" could not be recognized, the "β" parameter exhibits an upward trajectory correlated with rock strength.

The TBM vibration measurements could serve as a valuable tool in detecting potential cutter tool damages, offering the advantage of cost and time savings. Although the distinctive vibration pattern is not consistently observed, the broken cutters resulted long-lasting high amplitude vibrations.

While the primary focus of this study is within the time domain analysis of vibration signals, spectrogram and power spectral density were employed to gain insights into the frequency content of these signals. The analyses revealed that the TBM vibrations have broadband characteristics. It was observed that rock weathering changes the energy content of the signals, while cutterhead speed is one of the factors that affect the dominant frequencies. However, due to the broadband nature of the vibration signals observed in this study, limited information could be obtained in the frequency domain.

The laboratory experiments undertaken during the study showed that the vibrations generated during full-scale linear rock cutting tests are influenced by various factors, including the cutting configuration (line spacing and penetration), cutting performance (particularly peak tool forces), mechanical properties of the rock, and the mineral composition of the rock. It was observed that tool forces and vibration levels tend to increase as the penetration increases. Furthermore, it can be generally concluded that both vibrations and forces exhibit an increasing trend with increasing rock strength. Most notably, a strong correlation having coefficient of determination value of 0.79 was identified between interval RMS acceleration and peak normal force. Similarly, a noteworthy relationship, with a coefficient of determination value of 0.69, was observed between maximum acceleration and peak normal force. Strong relationships were also observed between interval RMS accelerations and two other variables:

optimum normal force and optimum specific energy, in addition, as the percentage of the chips over 25 mm increases, vibrations rise. These findings provide compelling evidence that the vibrations generated during rock cutting are predominantly influenced by the penetration, which in turn leads to an increase in the normal forces during cutting. With the objective of facilitating in real-time prediction applications the preliminary equations for forecasting peak tool forces and uniaxial compressive strength of the excavated rock based on acceleration measurements were presented.

The laboratory analyses also indicate the occurrence of significant vibration shocks following the breakage of a major rock chip, resulting in acceleration levels reaching up to 20g. The magnitude of these maximum accelerations is influenced by various factors, including penetration depth and the mechanical and mineralogical properties of the rock.

This study also underscores the significant impact of the rocks' mineralogical properties on cutting forces and vibrations. Notably, even within rock samples exhibiting comparable strength characteristics, variations in mineralogical composition can lead to distinct vibration patterns and cutting forces. The beige marble sample in this study is a very good example for observing the effect of mineralogical properties on vibrations.

The Weibull probability distributions provide clear insights into the relationship between penetration, rock strength (and/or cuttability), and vibration levels for the FLCM experiments. Specifically, the "β" parameter exhibits an increasing trend with higher rock strength, while the "α" parameter shows a decreasing trend. These parameters hold a potential for rock characterization and can be utilized for predicting rock strength. These results remain consistent with the field data.

Similar to the ones recorded in the TBMs, the vibration signals recorded during the rock cutting experiments exhibited a broadband frequency content. Notably, at locations where large rock chips detached from the sample, high amplitude signals were observed across the entire frequency spectrum. In these specific locations, a decrease in vibration levels was observed alongside a reduction in cutting tool forces, indicating stress relief on the rock in conjunction with chipping.

Incorporating vibration tests as a part of full-scale linear cutting experiments can offer valuable insights to TBM manufacturers, aiding in the design of TBMs and their

components, especially for the cutters and main bearing by providing essential information about expected vibration levels.

The accelerometer type, whether MEMS or piezoelectric, does not significantly impact data usability. While recorded acceleration values may exhibit variations based on accelerometer placement, overall trends remain consistent for both top and bottom accelerometer positions. The average vibration amplitudes were greater on the bottom accelerometers compared to the top ones. Furthermore, the recorded vibration data along the z-axis, which corresponds to the excavation direction, exhibited highest amplitudes compared to the data recorded along other axes. Therefore, for potential cost reduction, the utilization of single-axis accelerometers could be a future consideration.

Despite certain limitations in terms of equipment and rock sample availability, many of the intended objectives have been successfully attained throughout the study. It has been proven that the vibrations generated during TBM excavation and rock cutting experiments are linked with rock characteristics and operational parameters.

For future studies, several recommendations can be made to enhance the outcomes of the research and improve the accuracy of results;

- Increasing the number of FLCM tests: A broader dataset would yield a more comprehensive understanding of the complex relationships between rock properties, cutting configurations, cutting performance, and resulting vibrations.
- Accelerometer measurement range: To capture high amplitude vibration peaks, employing accelerometers with a measurement range of at least ±20g is advisable.
- Software enhancements: Improving both the recording and analysis software can lead to more streamlined and efficient data processing. Incorporating visual notifications and integration with the TBM's PLC would substantially enhance its usability and practicality in real-time monitoring and decision-making processes.

- TBM diameter variability: Deploying the measurement system in different diameter TBMs excavating similar lithological units could provide insights into the impact of TBM diameter on vibrations.
- Improved muck sampling procedure at the site: Improving the muck sampling procedure could yield more robust correlations between vibrations and the intact and rock mass properties.
- Mechanical problem detection for TBMs: Exploring the utilization of TBM vibrations for the detection of mechanical issues within TBM components should be a subject of investigation. This approach could provide valuable information on the early identification of potential mechanical problems, contributing to proactive maintenance and minimizing downtime during tunneling operations.
- Machine learning applications: Given the complexity of the factors influencing vibrations and their relationships, it is advisable to explore the application of machine learning techniques in future studies. Employing machine learning algorithms could enable the identification of complex patterns and correlations within the data, potentially leading to more accurate predictions.
- Real-time geological information: For future research, development of the systems that provide real-time geological information to the site crew should be a priority. Such a system would enable the crews to adapt their decisions based on the current geological conditions.

The implementation of these recommendations in future studies has the potential to enhance the comprehension of vibrations generated during rock cutting and TBM excavation, in addition to the real-time prediction of the geological conditions ahead the machine.

REFERENCES

Andreev, G.E. (1995). *Brittle failure of rock materials: Test results and constitutive models.* Rotterdam : A.A. Balkema.

Analiz Engineering and Cons. (2018). European Region Drinking Water Tunnel – Laboratory Analyses (in Turkish, Unpublished).

Analog Devices. (2017). ADXL354/ADXL355: Low Noise, Low Drift, Low Power, 3-Axis MEMS Accelerometers Data Sheet (Rev. 0).

Analog Devices. (2020). ADXL356/ADXL357: Low Noise, Low Drift, Low Power, 3-Axis MEMS Accelerometers Data Sheet (Rev. A).

Artson Geoteknik (2014). Mecidiyekoy-Mahmutbey Metro Hatti Depo, Bakım Sahasi ve Depo Bağlantı Hatları Inşaat Isleri – Jeolojik-Jeoteknik Kesit (in Turkish, Unpublished).

ASTM. (2008). *Standard test method for laboratory determination of pulse velocities and ultrasonic elastic constants of rock. American Society for Testing and Materials* (ASTM-D2845).

ASTM. (2016). *Standard test method for determination of the point load strength index of rock* (ASTM D5731-02).

Ates, U., Binen, I. S., Acun, S., Murteza, M., and Celik, Y. (2016). EPB tunneling challenges in sandy ground. *2nd International Conference on Tunnel Boring Machines in Difficult Grounds*, Istanbul, 16–18 November 2016.

Ates, U., Binen, I. S., Acun, S., and Celik, Y. (2017). TBM performance and challenges faced during excavation of Mecidiyekoy-Mahmutbey Metro Line. *International Tunneling Symposium in Turkey: Challenges of Tunneling,* Istanbul, 2–3 December 2017.

Ates, U., and Copur, H. (2023). Investigation of parameters affecting vibration patterns generated during excavation by EPB TBMs. *Tunnelling and Underground Space Technology, 138*, 105185. doi:10.1016/j.tust.2023.105185.

Avunduk, E., and Copur, H. (2018). Empirical modeling for predicting excavation performance of EPB TBM based on soil properties. *Tunneling and Underground Space Technology. 71,* 340-353. doi:10.1016/j.tust.2017.09.016.

Balci, C. (2009). Correlation of rock cutting tests with field performance of a TBM in a highly fractured rock formation: a case study in Kozyatagi-Kadikoy metro tunnel, Turkey. *Tunnelling and Underground Space Technology, 24 (4),* 423-435. doi:10.1016/j.tust.2008.12.001.

Balci, C., Copur, H., Bilgin, N., Ozdemir, L., and Jones, G.R. (2020). Cuttability and Drillability Studies towards Predicting Performance of Mechanical Miners Excavating in Hyperbaric Conditions of Deep Seafloor Mining. *International Journal of Rock Mechanics and Mining Science 130 (2020, June) 104338*.

Barker, J.S. (1964). A laboratory investigation of rock cutting using large picks. *International Journal of Rock Mechanics and Mining Sciences & Geomechanics 1 (4),* 468–476.

Bendat, J. S., and Piersol, A. G. (2011). *Random data: Analysis and measurement procedures* (4th ed.). John Wiley & Sons.

Bieniawski, Z. T., and Bernede, M. J. (1979). Suggested Methods for Determining the Uniaxial Compressive Strength and Deformability of Rock Materials: Part 1. Suggested Method for Determining Deformability of Rock Materials in Uniaxial Compression. *International Journal of Rock Mechanics and Mining Sciences & Geomechanics Abstracts. 16(2)*, 138–140. doi:10.1016/0148-9062(79)91451-7.

Bilgin, N., Tuncdemir, H., Balci, C., Copur, H., and Eskikaya, S. (2000). A model to predict the performance of tunnelling machines under stressed conditions. *In: World Tunnel Congress, Durban, South African Institute of Mining and Metallurgy*, 47-53.

Bilgin, N., Copur, H., Balci, C. (2013). *Mechanical excavation in mining and civil industries.* CRC press.

Brandt, A. (2011). *Noise and vibration analysis: signal analysis and experimental procedures*. John Wiley & Sons.

Buckley, J. (2015). *Monitoring the vibration response of a tunnel boring machine: Application to real time boulder detection.* (M.Sc. thesis). Colorado School of Mines, Department of Mechanical Engineering, Golden, COLORADO.

Cho, J. W., Jeon, S., Jeong, H. Y., Chang, S. H. (2013). Evaluation of cutting efficiency during TBM disc cutter excavation within a Korean granitic rock using linear-cutting-machine testing and photogrammetric measurement. *Tunnelling and Underground Space Technology, 35,* 37-54. doi:10.1016/j.tust.2012.08.006.

Copur, H., Balci, C., Tumac, D., and Bilgin, N. (2011). Field and laboratory studies on natural stones leading to empirical performance prediction of chain saw machines. *International Journal of Rock Mechanics and Mining Sciences, 48(2),* 269-282. doi:10.1016/j.ijrmms.2010.11.011.

Copur, H., Bilgin, N., Balci, C., Tumac, D., and Avunduk, E. (2017). Effects of different cutting patterns and experimental conditions on the performance of a conical drag tool. *Rock Mechanics and Rock Engineering, 50 (6)*, 1585-1609. doi:10.1007/s00603-017-1172-8

Dimension Engineering. (2011). DE-ACCM3D Buffered ±3g Tri-axis Accelerometer Datahseet.

EMAY Uluslararasi Mühendislik ve Müsavirlik A.S. (2018). European Region Drinking Water Tunnel - Geological and Geotechnical Investigation Report for Water Tunnel Projects between Kagithane Treatment Plant Shaft and Sefakoy Water Depot Shaft (in Turkish, Unpublished).

Fei, X., Chuanri, L., Tongmin, J., and Ahlin, K. (2014). Synthesis of running RMS-induced non-gaussian random vibration based on Weibull distribution. *Vibroengineering Procedia, 4,* 40-45.

Garcia-Romeu-Martinez, M. A., Rouillard, V., and Cloquell-Ballester, V. A. (2007). A model for the statistical distribution of road vehicle vibrations. *Proceedings of the World Congress on Engineering 2007* (Vol II, pp. 1225-1230), July 2 - 4, 2007, London, U.K.

Geodata Engineering S.p.A. (2016). Final Project Services Work of Umraniye-Atasehir-Goztepe Railway System Line, Preparatory Studies and Ground Site Investigation Final Design Phase - Report 2B2, Site, Laboratory and Geological & Geotechnical Studies Interpretative Report (Unpublished).

Gertsch, R. E. (1993). *Tunnel boring machine disk cutter vibrations.* (M.Sc. thesis). Colorado School of Mines, Department of Mining Engineering, Golden, COLORADO.

Gertsch, R., Gertsch, L., Rostami, J. (2007). Disc cutting tests in Colorado Red Granite: Implications for TBM performance prediction. *International Journal of Rock Mechanics and Mining Sciences, 44 (2)*, 238-246. doi:10.1016/j.ijrmms.2006.07.007.

Gong, Q. M., Zhao, J., and Jiang, Y. S. (2007). In Situ TBM Penetration Tests and Rock Mass Boreability Analysis in Hard Rock Tunnels. *Tunneling and Underground Space Technology. 22(3),* 303-316. doi:10.1016/j.tust.2006.07.003.

Hanly, S. (2016). *Shock & vibration overview*. Midé Technology Corporation. Retrived on: 2020-05 from: https://endaq.com/pages/handbooks.

Harris, C. M. and Piersol, A. G. (2002). *Harris' Shock and Vibration handbook* (5th ed.), New York: McGraw-Hill.

Huang, D. S., Chen, X. Y., Zhang, G. J., and Teng, L. (2008). Research on vibration monitoring and fault diagnosis for principal bearing in shield machine. *The Shanghai Yangtze River Tunnel Theory, Design and Construction* (pp. 305-209). London : Taylor & Francis Group.

Huang, X., Liu, Q., Liu, H., Zhang, P., Pan, S., Zhang, X., and Fang, J. (2018). Development and in-situ application of a real-time monitoring system for the interaction between TBM and surrounding rock. *Tunneling and Underground Space Technology, 81,* 187-208. doi:10.1016/j.tust.2018.07.018.

Hucka, V., Das, B. (1974). Brittleness determination of rocks by different methods. *Int. J. Rock Mech. Min. Sci., 11,* 389-392. doi:10.1016/0148-9062(74)91109-7.

Hunt, S.W., and Frank G.R. (2021). Abrasivity and cutter life assessment for TBM tunneling in cobbles and boulders. *Rapid Excavation and Tunneling Conference 2021 Proceedings,* 300-319.

Huo, Jz., Sun, Xl., Li, Gq., Li, T., and Sun, W. (2015). Multi-Degree-Of-Freedom Coupling dynamic characteristic of TBM disc cutter under shock excitation. *Journal of Central South University, 22(9),* 3326-3337. doi:10.1007/s11771-015-2873-3.

Irvine, T. (2019). *An Introduction to Shock & Vibration Response Spectra.*

ISRM. (2007). *The complete ISRM suggested methods for rock characterization, testing and monitoring: 1974–2006.* In: Ulusay, R., Hudson, J.A., (Eds.), Suggested methods prepared by the ISRM commission on testing methods.

Iwano, K., Hashiba, K., Nagae, J., and Fukui, K. (2020). Reduction of tunnel blasting induced ground vibrations using advanced electronic detonators. *Tunnelling and Underground Space Technology, 105, 103556.* doi:10.1016/j.tust.2020.103556.

Karadeniz, H., Saka, M. P., and Togan, V. (2013). Introduction to random vibration and stochastic analysis. *Stochastic Analysis of Offshore Steel Structures,* 121-176. doi:10.1007/978-1-84996-190-5_2.

Lindstrom, M. (2019). *What's Wrong With My Piezoelectric Accelerometer?*. PCB Electronics whitepaper.

Liu, M., Liao, S., Yang, Y., Men, Y., He, J., and Huang, Y. (2021). Tunnel boring machine vibration-based deep learning for the ground identification of working faces. *Journal of Rock Mechanics and Geotechnical Engineering. 13(6),* 1340-1357. doi:10.1016/j.jrmge.2021.09.004.

Liu, M. B., Liao, S. M., Men, Y. Q., Xing, H. T., Liu, H., and Sun, L. Y. (2022). Field monitoring of TBM vibration during excavating changing stratum: patterns and ground identification. *Rock Mechanics and Rock Engineering. 55(3),* 1481-1498. doi:10.1007/s00603-021-02714-6.

McFeat-Smith, I. (1977). Rock property testing for the assessment of tunnelling machines performance. *Tunnels and Tunnelling March 29–33.*

Montgomery, D.C., and Runger, G.C. (2018). *Applied statistics and probability for engineers* (7th ed.). John Wiley & Sons.

Mooney, M., Walter, B., Steele, J., and Cano, D. (2014). Influence of geological conditions on measured TBM vibration frequency. *G. Davidson, A. Howard, L. Jacobs, R. Pintabona, B. Zernich (Eds.), North American Tunneling 2014 Proceedings* (pp. 32-41), Englewood : Society for Mining, Metallurgy & Exploration.

Mosavat, K. (2017). A smart disc cutter monitoring system using cutter instrumentation technology. *Rapid Excavation and Tunneling Conference 2017 Proceedings,* 109-118.

National Instruments. (2008). NI USB-6008/6009 User Guide and Specifications.

National Instruments. (2015). NI 9230 Datahseet and User Manual.

National Instruments. (2016). Acquiring an Analog Signal: Bandwidth, Nyquist Sampling Theorem, and Aliasing

Nyquist, H. (1928). Certain Topics in Telegraph Transmission Theory. *Transactions of the American Institute of Electrical Engineers, 47(2)*, 617-644.

Palakci, U., and Ugur, I. (2021). *Ümraniye-Atasehir-Göztepe metro tunelinde km 7+700 – km 9+700 arasında jeolojik özelliklerle kazı performansı arasındakı ilişkinin incelenmesi* (Graduation Project), Istanbul Technical University, Mining Engineering Department, ISTANBUL (in Turkish).

PCB Electronics (2008). Triaxial, high sensitivity, ceramic shear ICP® accelerometer, 500 mV/g, 0.5 to 3k Hz, Installation and operating manual.

Polat, F. (2014). Mecidiyekoy – Mahmutbey Metro Line, Depot, Maintenance Area and Depot Connection Lines Construction Works Geological – Geotechnical Works Report for the Section Between Yenimahalle - Mahmutbey (Km 15+535 – 22+763) (Unpublished).

Polat, F. (2015). Mecidiyekoy – Mahmutbey Metro Line, Depot, Maintenance Area and Depot Connection Lines Construction Works Geological – Geotechnical Works Report for the Section Between Yenimahalle – Alibeykoy River (Km 13+780 – 10+540) (Unpublished).

Pomeroy, C.D. (1963). Breakage of coal by wedge action—Factors affecting breakage by any given shape of tool. *Colliery Guardian, November 21,* 672–677.

Ray, S., and Dauji, S. (2019). Ground vibration attenuation relationship for underground blast: a case study. *Journal of The Institution of Engineers (India): Series A, 100*, 763-775. doi: 10.1007/s40030-019-00382-y

Rinne, H. (2008). *The Weibull distribution: A handbook.* CRC Press.

Rogers, M. J. B., Hrovat, K., McPherson, K., Moskowitz, M. E., and Reckart, T. (1997). *Accelerometer data analysis and presentation techniques.* NASA Technical Memorandum, 113173.

Rouillard, V. (2007). The Synthesis of Road Vehicle Vibrations Based on The Statistical Distribution of Segment Lengths. *In Proceedings of the 5th Australasian Congress on Applied Mechanics*. Engineers Australia.

Rouillard, V., and Sek, M. A. (2010). Synthesizing nonstationary, non-Gaussian random vibrations. *Packaging Technology and Science, 23(8),* 423-439.

Roxborough, F.F. (1973). Cutting rocks with picks. *The Mining Engineer, June,* 445–455.

Samuel, A. E., and L. P. Seow. (1984). Disc force measurements on a full-face tunnelling machine. *International Journal of Rock Mechanics and Mining Sciences & Geomechanics Abstracts, vol. 21, no. 2,* 83-96. doi:10.1016/0148-9062(84)91176-8.

Shanahan, A. (2010). Cutter instrumentation system for tunnel boring machines. *North American Tunneling 2010 Proceedings*, 110-115.

Sinha, S., Shakya, S., Mukhiya, R., Gopal, R., and Pant, B. D. (2014). Design and simulation of MEMS differential capacitive accelerometer. *Proceeding of ISSS international conference on smart materials, structures and systems,* 08-11 July 2014, Bangalore, India

Steinberg, D.S. (2000). *Vibration Analysis for Electronic Equipment* (3rd ed), John Wiley and Sons.

Tuncdemir, H., Bilgin, N., Copur, H., Balci, C. (2008). Control of rock cutting efficiency by muck size. *Int J Rock Mech Min Sci, 45(2),* 278–288. doi:10.1016/j.ijrmms.2007.04.010.

Turkish Standards Institution. (1975). *Determination of Elastic Module and Poissons Ratio of Rocks in Uniaxial Compression* (TS 2030).

Turkish Standards Institution. (2006a). *Methods of Testing Soils for Civil Engineering Purposes in the Laboratory* (TS 1900).

Turkish Standards Institution. (2006b). *Methods of Testing Soils for Civil Engineering Purposes in the Laboratory – Part 1: Determination of mechanical properties* (TS 1900-1).

Turkish Standards Institution. (2006c). *Methods of Testing Soils for Civil Engineering Purposes in the Laboratory – Part 2: Determination of mechanical properties* (TS 1900-2).

Turkish Standards Institution. (2007). *Natural Stone Test Methods - Determination of uniaxial compressive strength* (TS EN 1926).

Yang, Z., Pan, D., Zhou, J., Chen, J., Sun, Z., and Liu, H. (2020). Vibration characteristics of cutter-head in soft-hard mixed stratum: An experimental case study on Su'ai Tunnel. *KSCE Journal of Civil Engineering, 24(4),* 1338-1347. doi:10.1007/s12205-020-0966-5.

Yu, Z., Shi, X., Zhou, J., Chen, X., and Qiu, X. (2020). Effective assessment of blast-induced ground vibration using an optimized random forest model based on a Harris hawks optimization algorithm. *Applied Sciences, 10(4), 1403*. doi:10.3390/app1004140.

Yüksel Proje. (2017). Umraniye – Atasehir – Goztepe Metro Hattı Jeolojik – Jeoteknik Arastirma Raporu (Cilt 1/3 to 3/3), Ankara, (in Turkish, Unpublished).

Walter, B. W., Alavi Gharahbagh, E., Frank, G., DiPonio, M., and Mooney, M. (2012). Extending TBM Reliability by Detecting Boulders. *In the Proceedings of* North *American Tunneling Conference,* Indianapolis.

Walter, B. W. (2013). *Detecting changing geologic conditions with tunnel boring machines by using passive vibration measurements*. (Doctoral dissertation) Colorado School of Mines, College of Engineering and Computational Science, Golden, COLORADO.

Wu, F., Gong, Q., Li, Z., Qiu, H., Jin, C., Huang, L., and Yin, L. (2021). Development and application of cutterhead vibration monitoring system for TBM tunnelling. *International Journal of Rock Mechanics and Mining Sciences. 146, 104887*. doi:10.1016/j.ijrmms.2021.104887.

APPENDICES

APPENDIX A: Additional figures for TBM vibration data.
APPENDIX B: Additional figures for laboratory vibration data.

APPENDIX A: Additional figures for TBM vibration data.

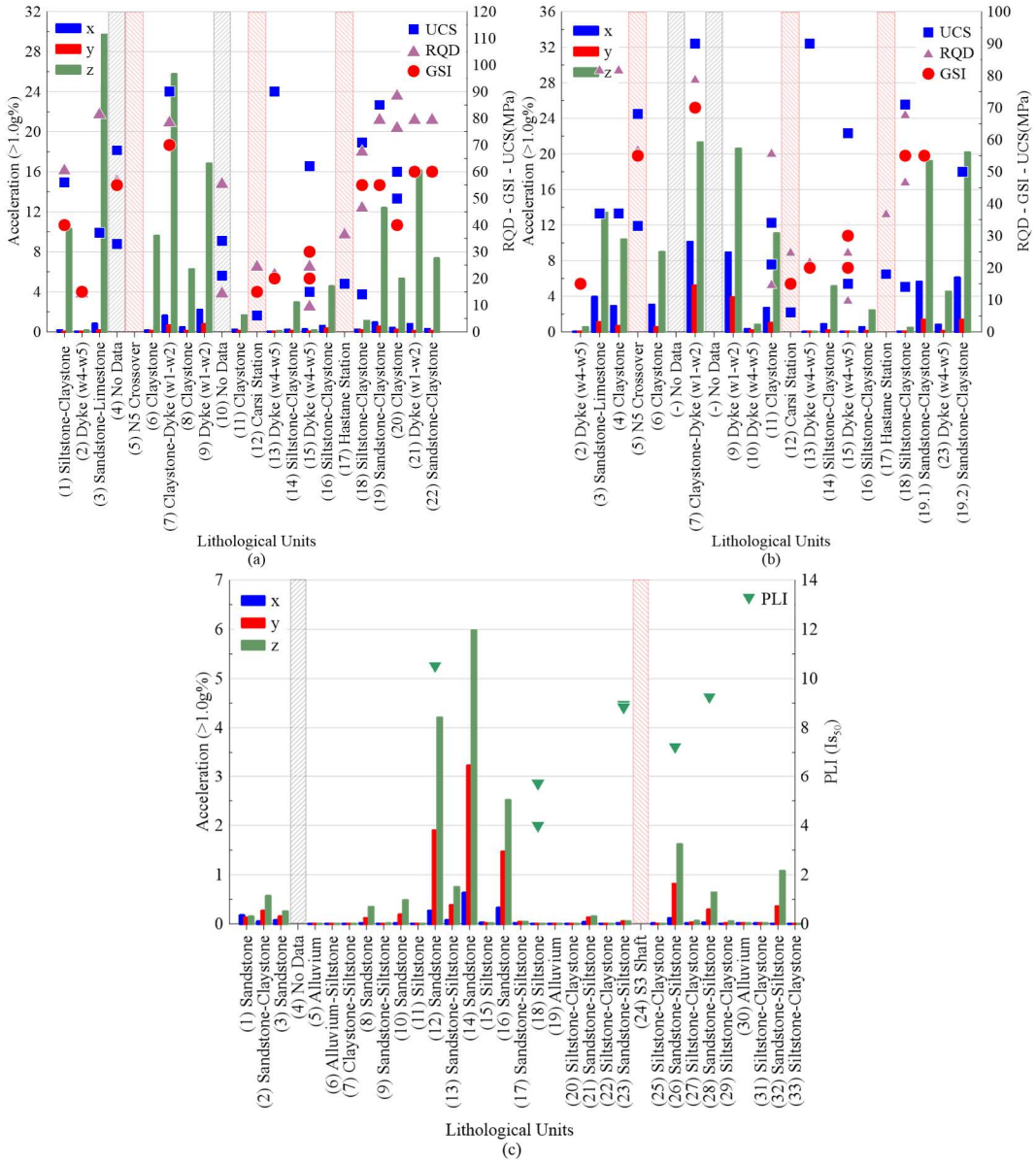

Figure A.1 : Percentage of acceleration data higher than 1g per lithological section for top accelerometers of (a) TBM 2, (b) TBM 3 and (c) TBM 4.

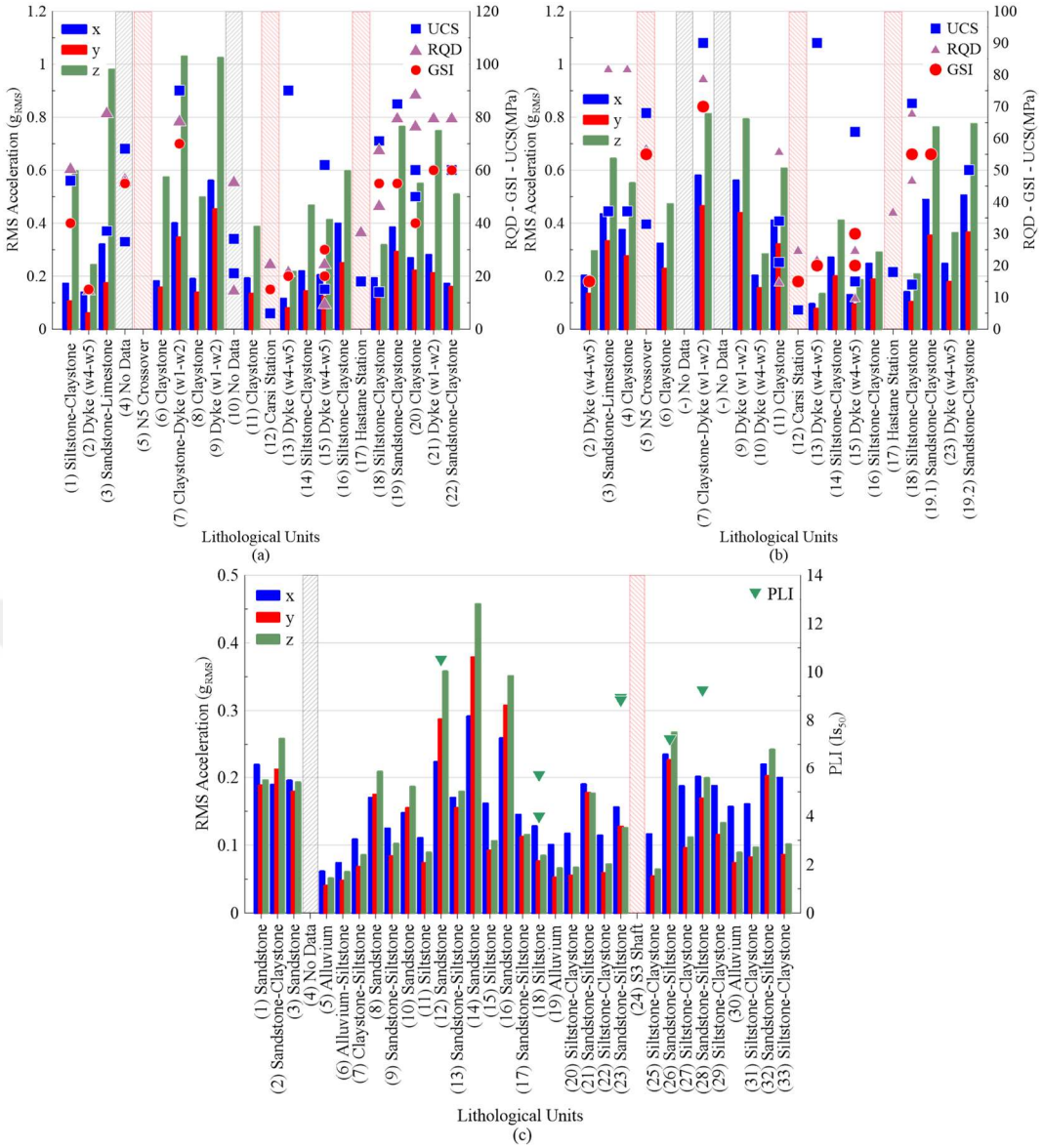

Figure A.2 : RMS vibration data per lithological section for top accelerometers of (a) TBM 2, (b) TBM 3 and (c) TBM 4.

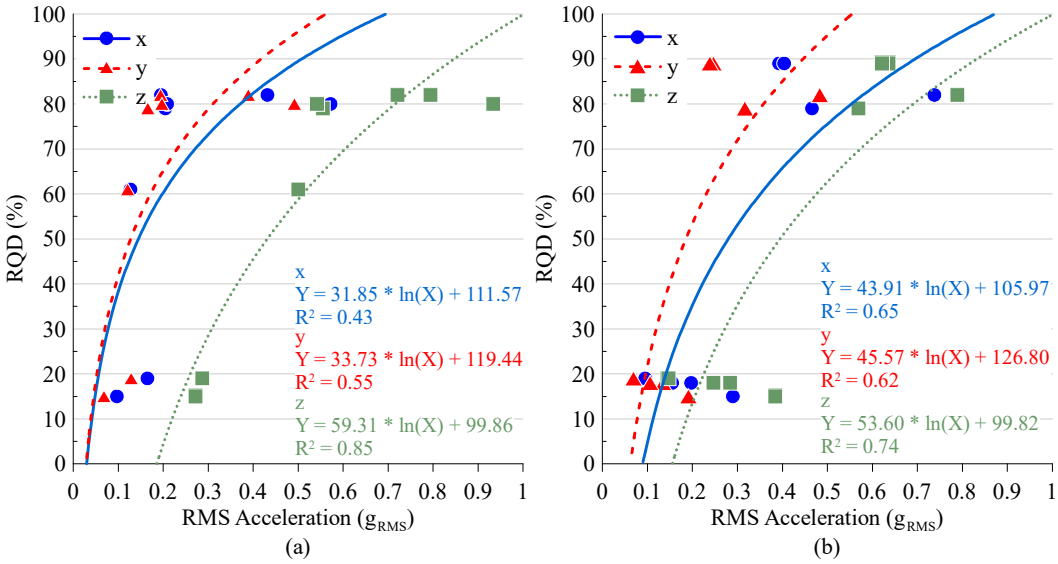

Figure A.3 : The relation between RMS vibration data and RQD for bottom accelerometers of (a) TBM 2, (b) TBM 3.

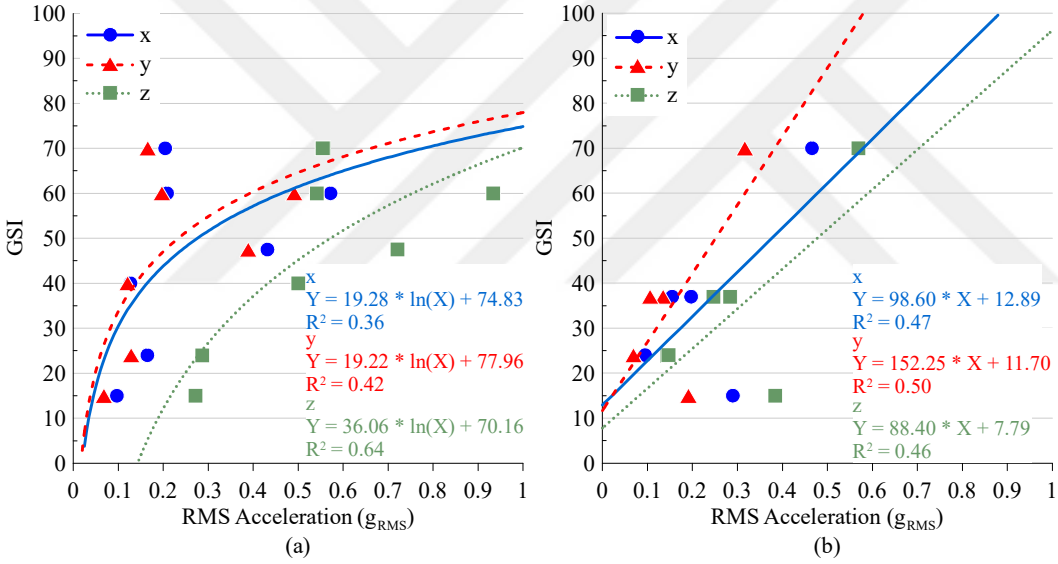

Figure A.4 : The relation between RMS vibration data and GSI for bottom accelerometers of (a) TBM 2, (b) TBM 3.

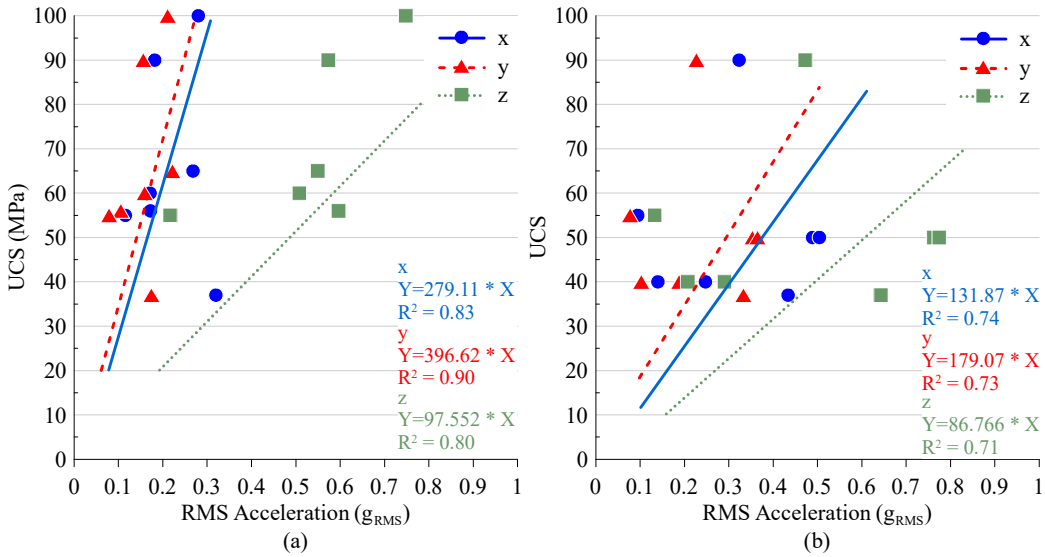

Figure A.5 : The relation between RMS vibration data and UCS for top accelerometers of (a) TBM 2, (b) TBM 3.

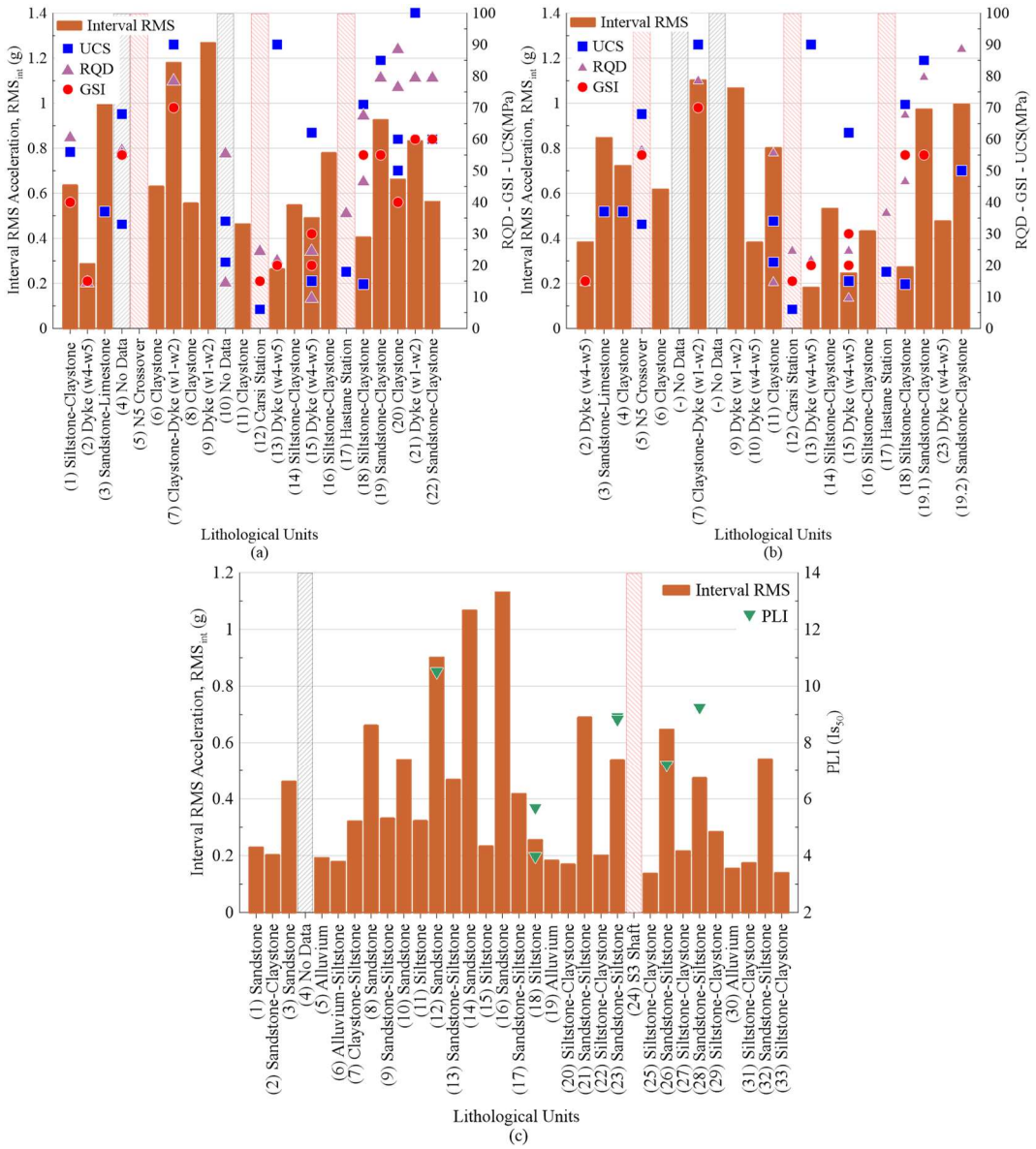

Figure A.6 : Interval RMS vibration data per lithological section for top accelerometers of (a) TBM 2, (b) TBM 3 and (c) TBM 4.

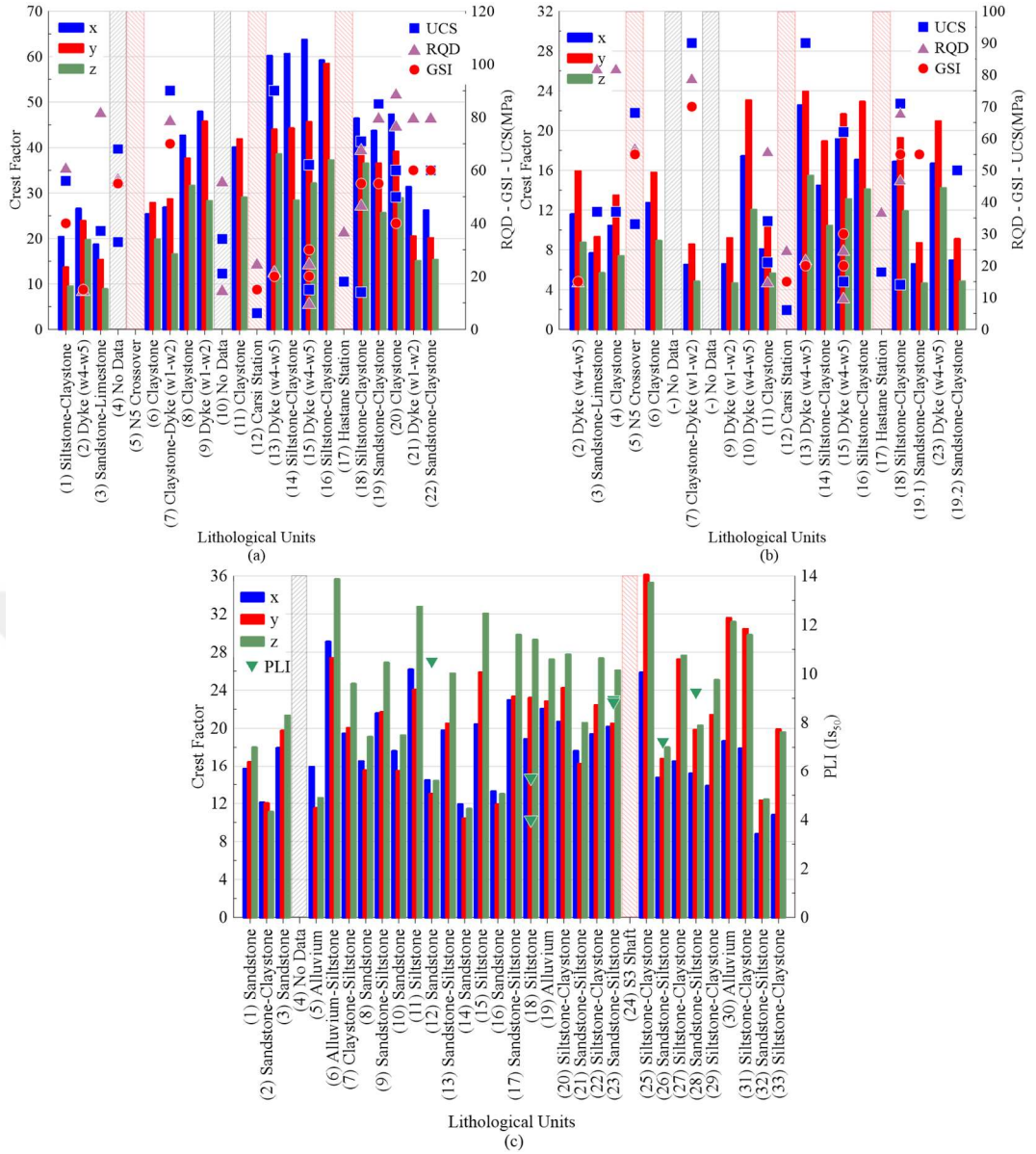

Figure A.7 : Crest factor per lithological section for top accelerometers of (a) TBM 2, (b) TBM 3 and (c) TBM 4.

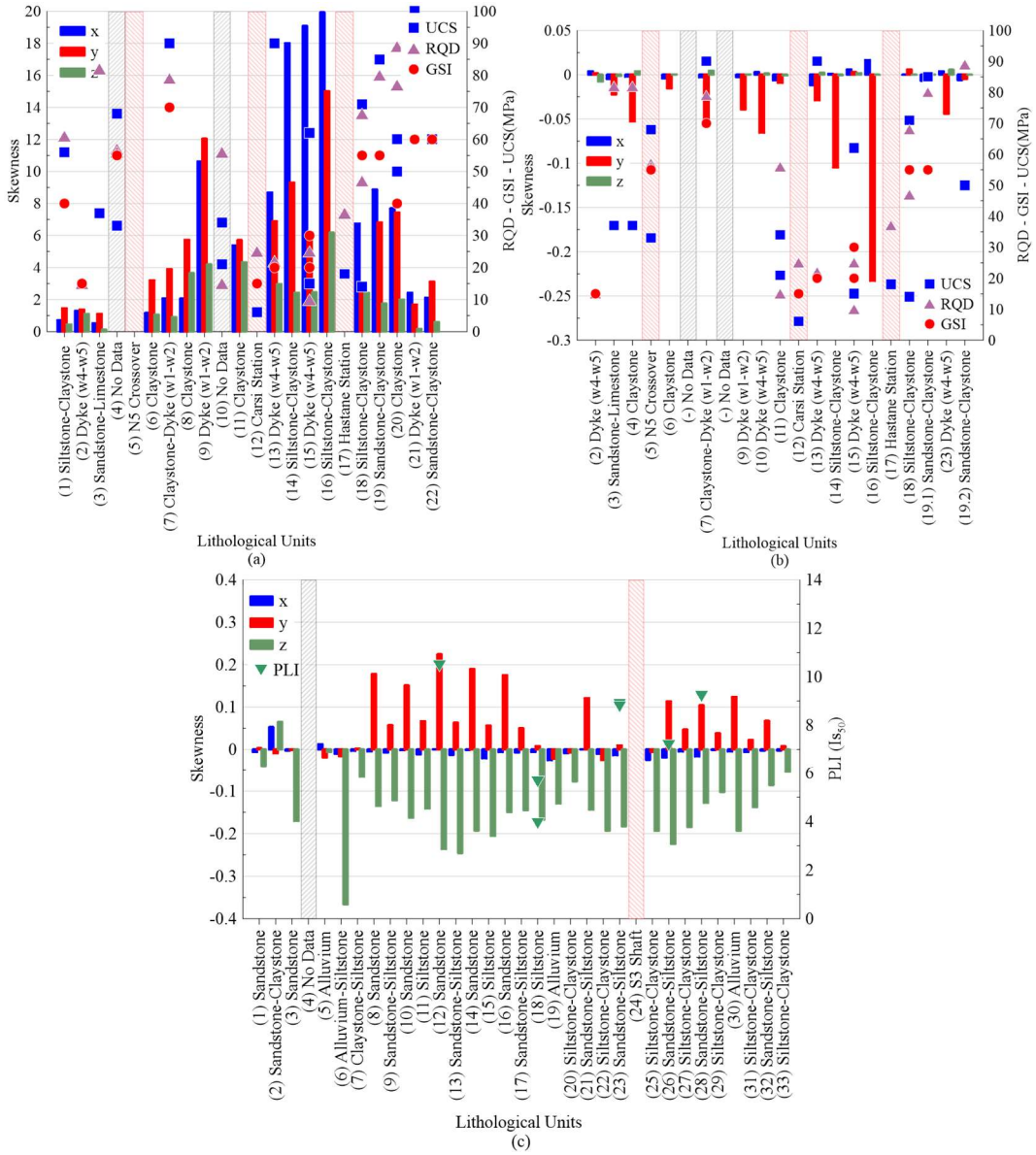

Figure A.8 : Skewness of the data per lithological section for top accelerometers of (a) TBM 2, (b) TBM 3 and (c) TBM 4.

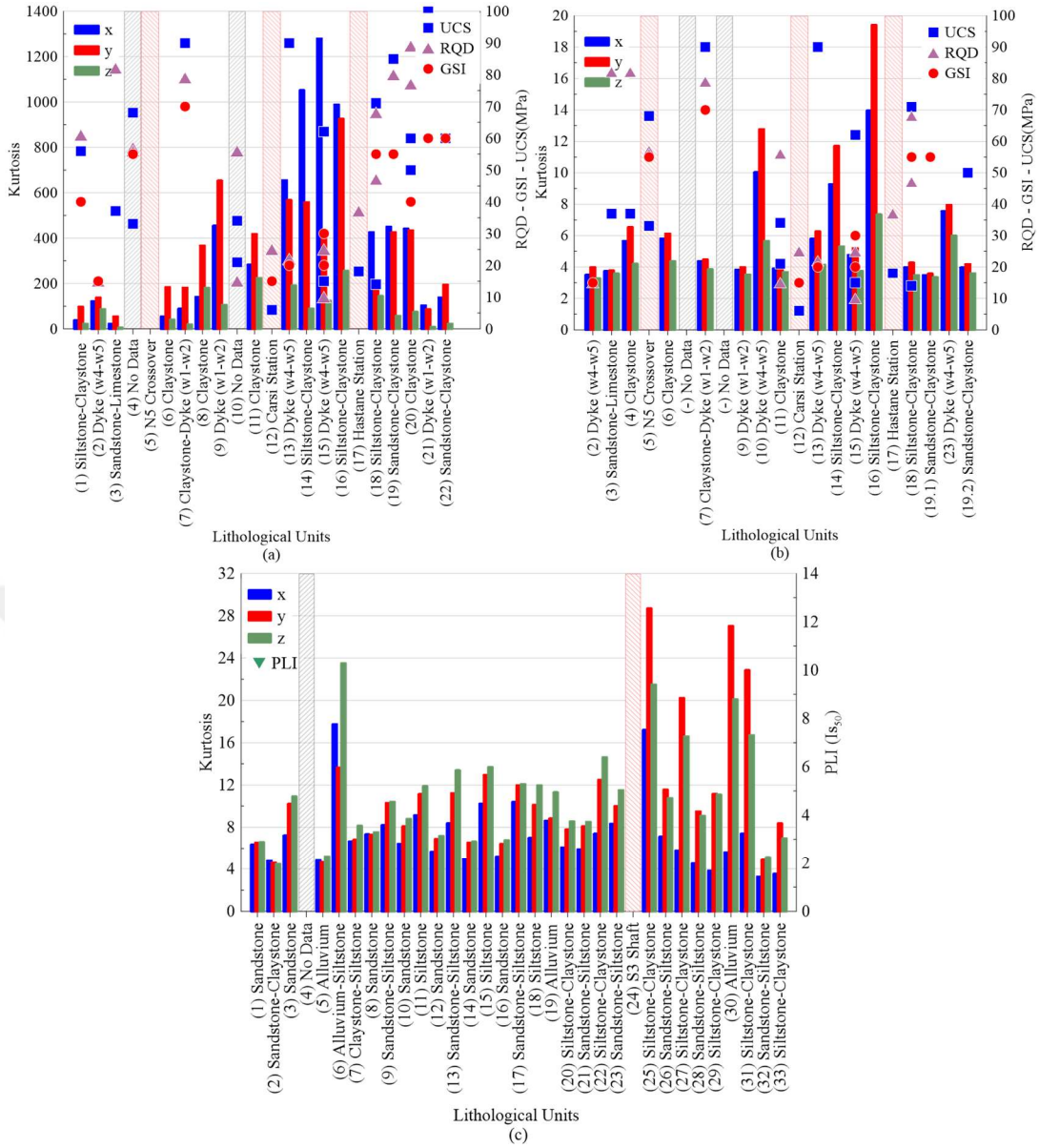

Figure A.9 : Kurtosis of the data per lithological section for top accelerometers of (a) TBM 2, (b) TBM 3 and (c) TBM 4.

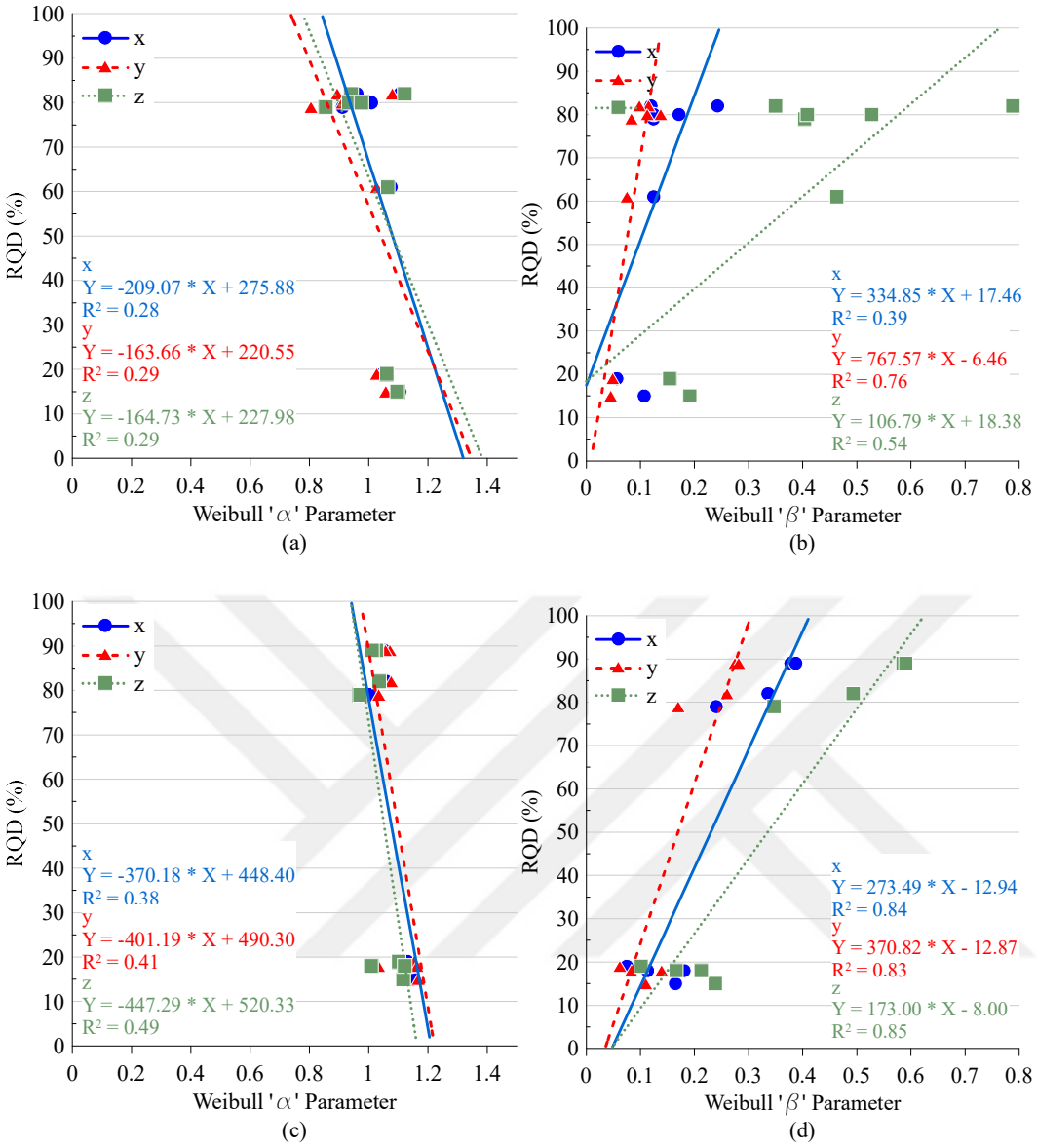

Figure A.10 : The relationships between RQD and Weibull parameters for top accelerometers, (a) and (b) for TBM 2, (c) and (d) for TBM 3.

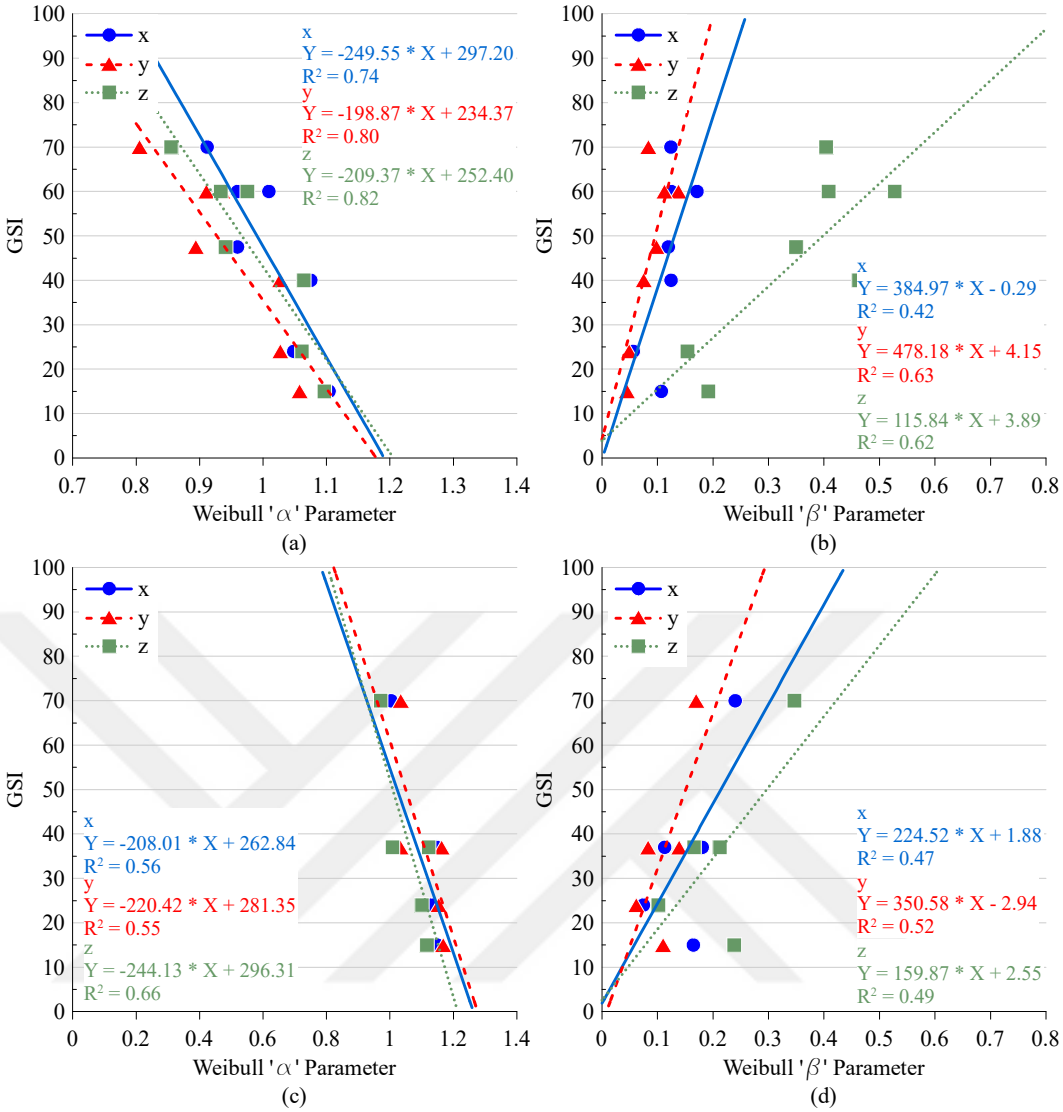

Figure A.11 : The relationships between GSI and Weibull parameters for top accelerometers, (a) and (b) for TBM 2, (c) and (d) for TBM 3.

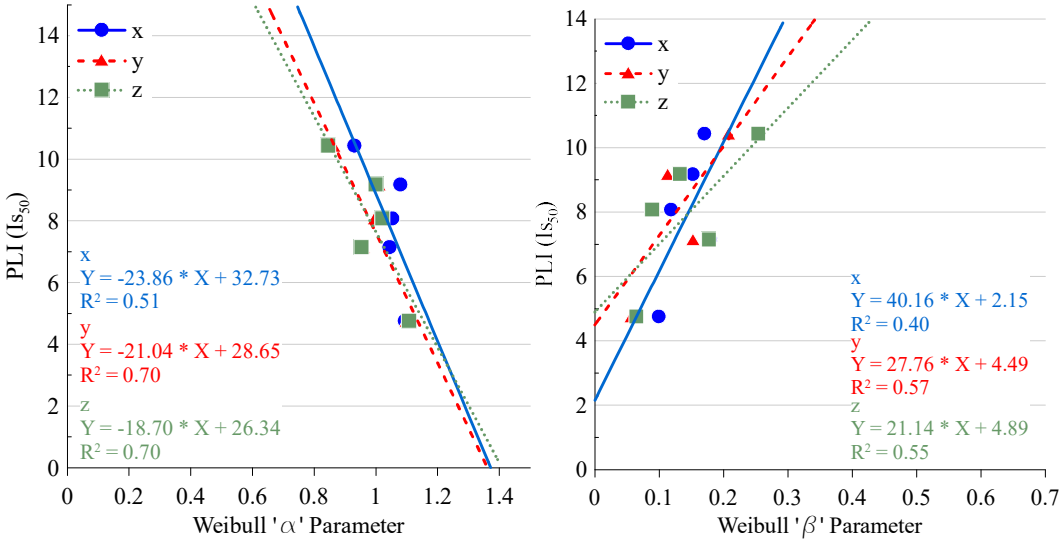

Figure A.12 : The relationships between PLI and Weibull parameters for top accelerometer of TBM 4.

APPENDIX B: Additional figures for laboratory vibration data.

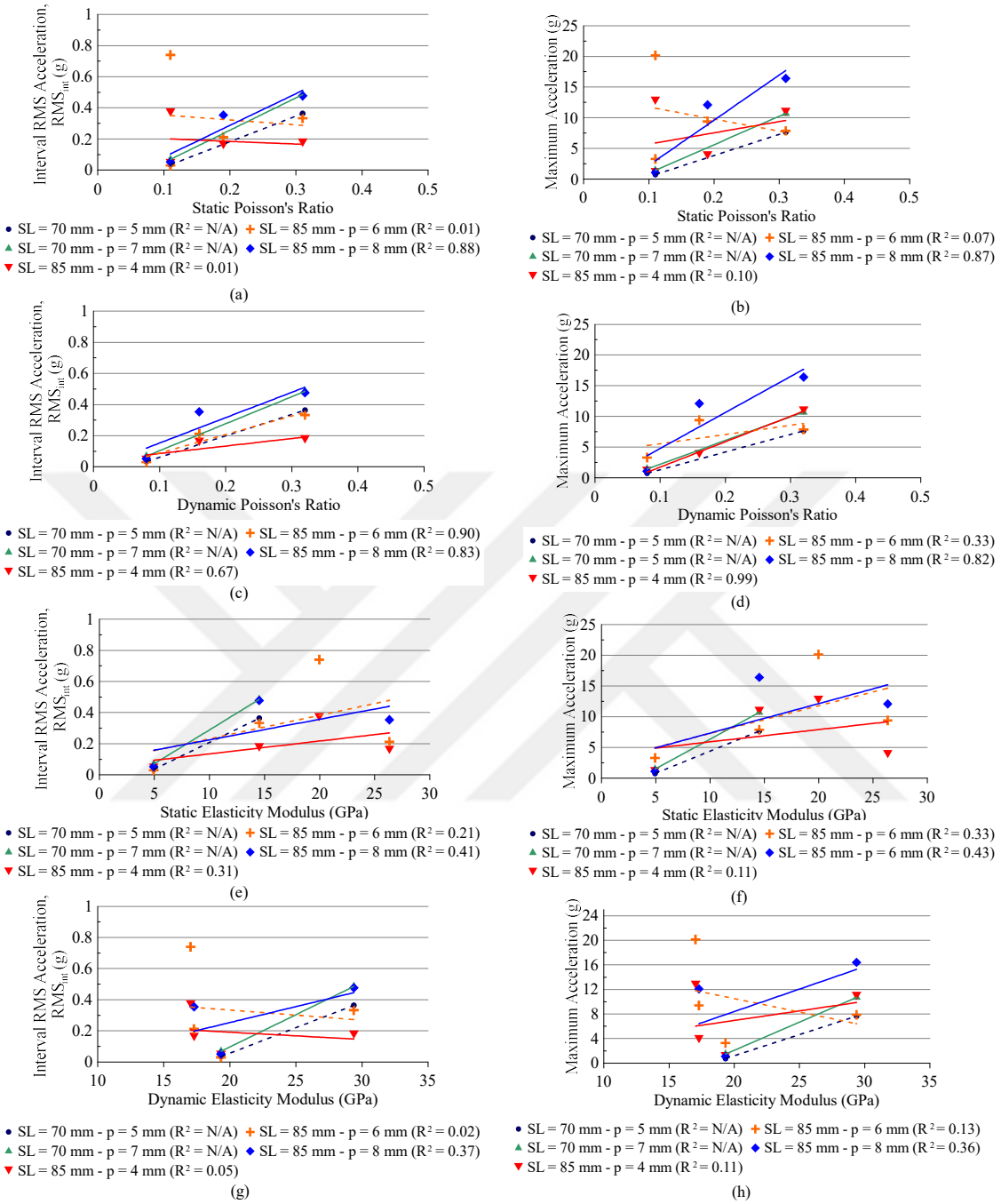

Figure B.1 : Variations of interval RMS acceleration and maximum acceleration with static Poisson's ratio (a,b), dynamic Poisson's ratio (c,d), static elasticity modulus (e,f), dynamic elasticity modulus (g,h).

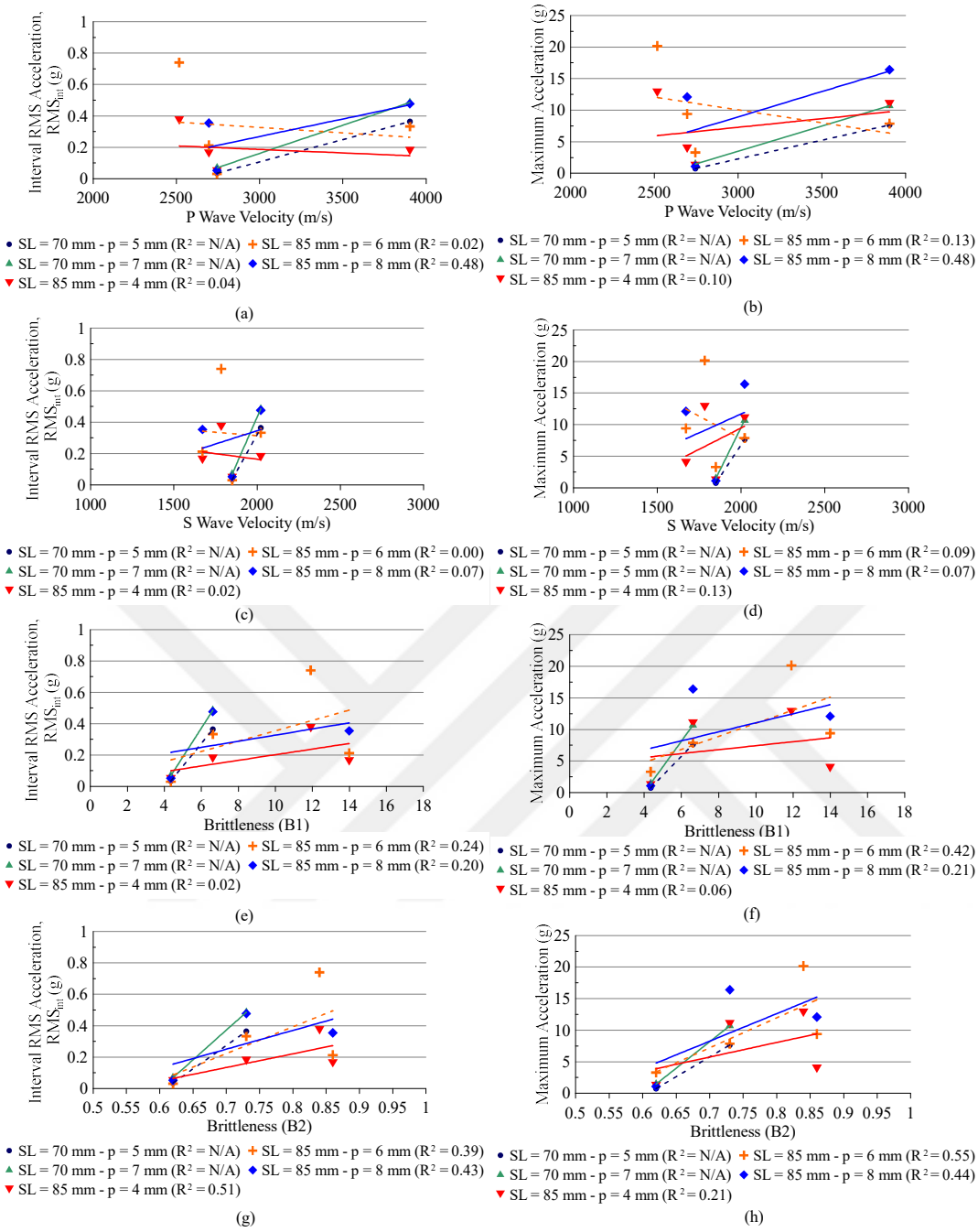

Figure B.2 : Variations of interval RMS acceleration and maximum acceleration with P wave velocity (a,b), S wave velocity (c,d), brittleness (B1) (e,f), brittleness (B2) (g,h).

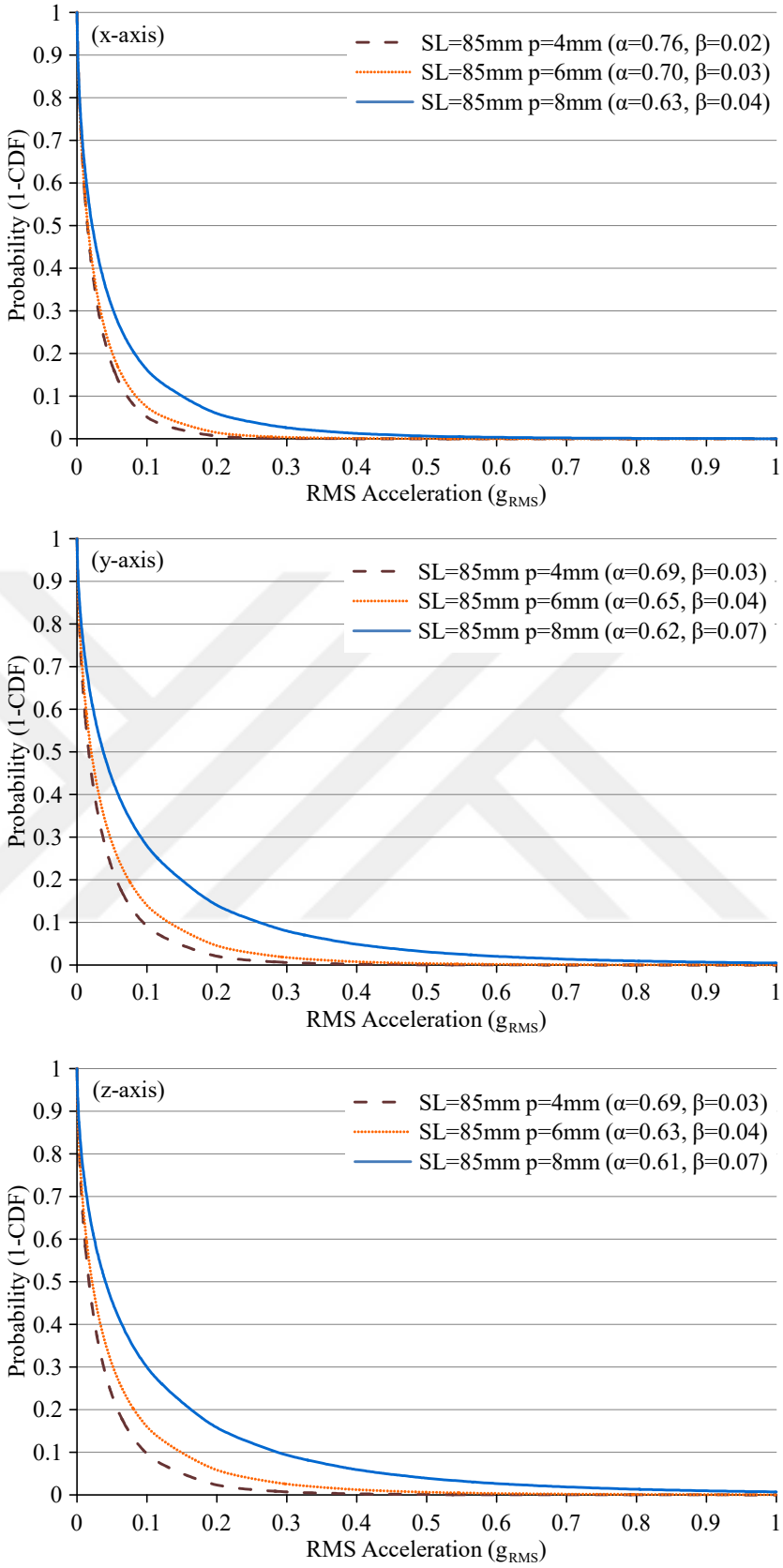

Figure B.3 : Weibull distribution for beige marble (EC) calculated from accelerometer 3.

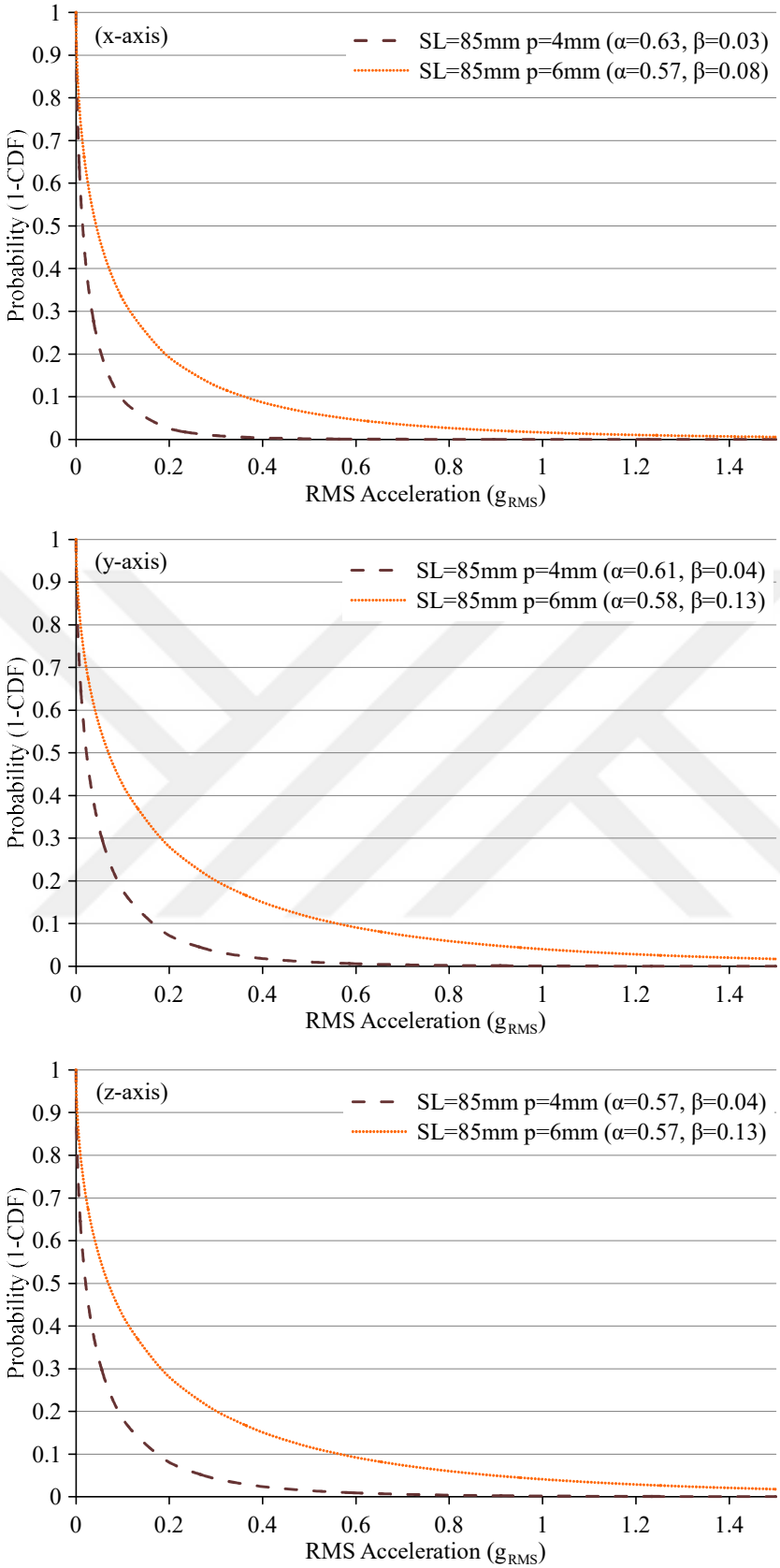

Figure B.4 : Weibull distribution for beige marble (DC) calculated from accelerometer 3.

CURRICULUM VITAE

Name Surname **:** Uğur ATEŞ

EDUCATION **:**

- **B.Sc.** **:** 2009, Istanbul University, Geophysics Engineering
- **M.Sc.** **:** 2013, Istanbul Technical University, Faculty of Mines, Mining Engineering Department

PROFESSIONAL EXPERIENCE AND REWARDS:

- 2024 – Current : TBM Expert at Pini Engineering Services LLC (United Arab Emirates)
- 2020 – 2024 : Tunnel Engineer at TunnelConsult Engineering (Turkey)
- 2019 – 2020 : Tunnel Engineer at TunnelConsult Engineering (Georgia)
- 2016 – 2018 : TBM Specialist at Statkarft (Albania)
- 2015 – 2016 : TBM Engineer at Gulermak-Kolin-Kalyon Metro Construction JV (Turkey)
- 2013 – 2015 : TBM Engineer at Gulermak Heavy Industries Construction & Contracting Co. Inc. (Turkey)

PUBLICATIONS, PRESENTATIONS AND PATENTS ON THE THESIS:

- **Ates, U.,** Copur, H and Mamaghani, A.S. (2024). Investigation of vibration patterns generated during rock cutting tests. *World Tunnel Congress 2024*, Shenzhen-China.
- **Ates, U.,** and Copur, H. (2023). Investigation of parameters affecting vibration patterns generated during excavation by EPB TBMs. *Tunnelling and Underground Space Technology*, 138, 105185. doi:10.1016/j.tust.2023.105185.
- **Ates, U.,** Copur, H., Mamaghani, A. S., and Aymir, M. E. (2023). Investigation of vibration patterns generated during rock cutting tests and TBM excavation. *World Tunnel Congress 2023*, Athens-Greece.
- **Ates, U.,** Copur, H., Kara, F., and Cinar, M. (2022). Investigation of the vibration patterns generated during TBM excavation. *World Tunnel Congress 2022*, Denmark-Copenhagen.
- **Ates, U.,** Copur, H., Mamaghani, A.S., Avunduk, E., and Binen, I.S. (2019). Investigation of vibration patterns occurred during TBM excavation and rock cutting tests. *In: Aydan, Ö., Ito, T., Seiki, T., Kamemura, K., Iwata, N. (Eds.),*

Proceedings of 2019 Rock Dynamics Summit, 7-11 May, Okinawa, Japan, pp. 704-709.

OTHER PUBLICATIONS, PRESENTATIONS AND PATENTS:

- Binen, I. S., Kara, F., Temur, M., Cinar, M., and **Ates, U**. (2023). Comparison of two identical EPB TBMs under different and complex geological conditions. *World Tunnel Congress 2023*, Athens-Greece.
- **Ates, U.,** and Binen, S. I. (2022). Artificial Neural Network Model to Predict Surface Settlements Caused by Mechanized Tunneling, *World Tunnel Congress 2022*, Copenhagen, Denmark.
- **Ates, U.,** Binen, S. I., Kara, F., Akca, M., Turker, C.B., Cinar, T., and Aciliouglu, T. (2019). The relations between surface settlements and TBM excavation parameters, *World Tunnel Congress 2019, Naples, Italy*, 3-9 May 2019.
- Binen, S. I., **Ates, U.,** Acun, S., Copur. H., and Celik, Y. (2018). Effects of Cutter Types on Cutter Consumption and TBM Performance in Different and Complex Geological Conditions, *World Tunnel Congress 2018, Dubai, United Arab Emirates.*
- Bilgin, N., Acun, S., **Ates, U.,** Murteza, M., and Celik, Y. (2017). The factors affecting the performance of three different TBMs in a complex geology in Istanbul, *World Tunnel Congress 2017, Bergen, Norway*.
- **Ates, U.,** Binen, I. S., Acun, S., and Celik, Y. (2017). TBM performance and challenges faced during excavation of Mecidiyekoy-Mahmutbey Metro Line. *International Tunneling Symposium in Turkey: Challenges of Tunneling*, Istanbul, 2–3 December 2017.
- **Ates, U.,** Binen, I. S., Acun, S., Murteza, M., and Celik, Y. (2016). EPB tunneling challenges in sandy ground. *2nd International Conference on Tunnel Boring Machines in Difficult Grounds*, *Istanbul,* 16–18 November 2016.
- Bilgin, N., and **Ates, U.** (2016). Probe Drilling Ahead of Two TBMs in Difficult Ground Conditions in Turkey, *Rock Mechanics and Rock Engineering, July 2016, (49)*, 2763–2772. doi:10.1007/s00603-016-0937-9
- **Ates, U.,** Bilgin, N., and Copur H. (2014). Estimating torque, thrust and other design parameters of different type TBMs with some criticism to TBMs used in Turkish tunneling projects, *Tunnelling and Underground Space Technology, Volume 40, 46*-63. doi:10.1016/j.tust.2013.09.004